



Role of the secretome in manganese and carbon oxidation by filamentous ascomycete fungi

Citation

Zeiner, Carolyn Alexandra. 2015. Role of the secretome in manganese and carbon oxidation by filamentous ascomycete fungi. Doctoral dissertation, Harvard University, Graduate School of Arts & Sciences.

Permanent link

<http://nrs.harvard.edu/urn-3:HUL.InstRepos:23845450>

Terms of Use

This article was downloaded from Harvard University's DASH repository, and is made available under the terms and conditions applicable to Other Posted Material, as set forth at <http://nrs.harvard.edu/urn-3:HUL.InstRepos:dash.current.terms-of-use#LAA>

Share Your Story

The Harvard community has made this article openly available.
Please share how this access benefits you. [Submit a story](#).

[Accessibility](#)

**Role of the secretome in manganese and carbon oxidation
by filamentous ascomycete fungi**

A dissertation presented

by

Carolyn Alexandra Zeiner

to

The John A. Paulson School of Engineering and Applied Sciences

in partial fulfillment of the requirements

for the degree of

Doctor of Philosophy

in the subject of

Engineering Sciences

Harvard University

Cambridge, Massachusetts

August 2015

© 2015 Carolyn Alexandra Zeiner

All rights reserved.

Role of the secretome in manganese and carbon oxidation
by filamentous ascomycete fungi

Abstract

Fungi are the primary decomposers of recalcitrant plant and animal material in terrestrial environments, thereby serving as important drivers of global carbon cycling and climate dynamics and as mediators in renewable energy production. Degradation of organic litter is achieved through secretion of a large and diverse suite of extracellular enzymes and reactive metabolites, collectively referred to as the secretome. This thesis explores the secretomes of four filamentous Ascomycete fungi that were recently isolated from field sites and have the ability to oxidize manganese (Mn)(II) to Mn(III/IV) oxides: *Alternaria alternata* SRc1lrK2f, *Stagonospora* sp. SRC1lsM3a, *Pyrenochaeta* sp. DS3sAY3a, and *Paraconiothyrium sporulosum* AP3s5-JAC2a. Mn(II)-oxidizing fungi are of engineering and industrial interest due to their utility in the remediation of metal-contaminated waters and their ability to harness Mn(II) oxidation in the breakdown of lignocellulosic plant material. While the processes of Mn(II) oxidation and carbon oxidation are mediated by the secretome in white-rot Basidiomycete fungi, comparatively little is known about the oxidative capacity of the secretomes of Ascomycetes, particularly those of environmental isolates. Using a combination of microscopy and chemical assays, this thesis identifies extracellular superoxide as the oxidant of Mn(II) in *Stagonospora* sp. and *Pyrenochaeta* sp. during growth on solid substrate and suggests a role for secreted organic

polymers in Mn(III) complexation and Mn oxide templation. Furthermore, through in-gel assays and bulk mass spectrometry, this work demonstrates that species-specific secreted enzymes confer Mn(II) oxidative capacity in the liquid, cell-free secretome of these two fungi and *P. sporulosum* and shows that Mn(II) oxidative capacity changes over time in a pattern unique to each organism. Through quantitative iTRAQ proteomics and custom bioinformatic analyses, the protein composition of the secretomes of all four filamentous Ascomycetes was fully characterized, revealing a rich and functionally diverse suite of extracellular enzymes that suggest the ability to oxidize carbon through both direct and indirect mechanisms. Although the functional diversity of the secretome was similar among the four organisms, the fungi exhibited striking differences in regulation of carbon-degrading enzymes over a three-week time course, illustrating species-specific and temporal shifts in carbon utilization strategies among the phylogenetically diverse species. Taken together, results of this thesis further our understanding of the mechanisms of Mn(II) oxidation by fungi, demonstrate the rich functional diversity and oxidative capacity of Ascomycete secretomes, and enhance our understanding of the role of filamentous Ascomycetes in recalcitrant carbon turnover in the environment.

TABLE OF CONTENTS

Abstract		iii
Acknowledgements		vi
List of tables and figures (with captions)		viii
Chapter 1	Introduction	1
Chapter 2	Fungal oxidative dissolution of the Mn(II)-bearing mineral rhodochrosite and the role of metabolites in manganese oxide formation	13
Chapter 3	Mechanisms of manganese(II) oxidation by filamentous ascomycete fungi vary with species and time as a function of secretome composition	48
Chapter 4	Comparative analysis of secretome profiles of four manganese(II)-oxidizing ascomycete fungi	92
Chapter 5	Quantitative iTRAQ-based secretome analysis reveals species-specific and temporal shifts in carbon utilization strategies among manganese(II)-oxidizing ascomycete fungi	130
Appendix 1	Supplemental Material for Chapter 2	164
Appendix 2	Supplemental Material for Chapter 3	170
Appendix 3	Supplemental Material for Chapter 4	177
Appendix 4	Supplemental Material for Chapter 5	178

ACKNOWLEDGEMENTS

This work would not have been possible without my advisor, Colleen Hansel, who has been an endless source of support, guidance, and inspiration. Colleen, you introduced me to the strange and beautiful world of fungi, and for that I will be forever grateful. Thank you for all the time and resources you have invested in me and this research and for the countless lessons in science, embarking on a career in science, and leading a life full of passion and curiosity. I am also greatly indebted to Ann Pearson, who graciously “adopted” me, welcomed me into her laboratory, and always made time to answer my questions. Ann, I cannot thank you enough for your hospitality and guidance. Thanks also to my committee members Steve Wofsy and Chad Vecitis for critical comments on this work.

One of the most valuable lessons I learned during this PhD is that a team of dedicated people can accomplish much more than any of its members could individually. As such, this work is the result of a large team of researchers whose efforts were invaluable. I cannot possibly list them all here, but to all of you who helped me along the way, whether your contributions were big or small, I offer my sincere gratitude. In particular, I am grateful to Sam Purvine, Lili Paša-Tolić, and David Hoyt at the Environmental Molecular Sciences Lab at PNNL for their enthusiastic support of this research and for sharing their expertise and resources. Thanks also to Don Pfister and Anne Pringle for sharing their knowledge of fungal biology and the many excellent vocabulary words that come along with it.

One of the many benefits of being a part of two laboratories is having twice as many knowledgeable people to turn to for support and advice. To all the current and former members of the Hansel and Pearson labs, thank you for your stimulating conversations, brilliant suggestions, and camaraderie. I am particularly grateful to Deric Learman for help getting started in the lab, Cara Santelli for a reliable stream of fungal knowledge and excitement, Wiebke Mohr, Tiantian Tang, and Sarah Sattin for a crash course in proteomics, Sarah Hurley for daily motivation in the office, and Susie Carter for keeping the lab running so smoothly that I forgot how it feels to have an instrument break. I would not have survived this PhD without the friendship and support of Julia Diaz, who cheered me on during good times, consoled me during bad times, and shared countless bits of wisdom along the way.

The Harvard community has been extremely supportive and encouraging over the past five years, pushing me to persevere and enabling my professional development. Special thanks go to the administrative staff in the SEAS Student Affairs Office and the EPS Department offices. We are all indebted to their dedication on a daily basis. I am grateful to Karen Lachmayr and the Harvard Microbial Sciences Initiative for their support of this research and for providing a stimulating forum for microbiology enthusiasts on campus. Thank you to Josh Girash, Karena McKinney, and Jessica Garrett for nourishing my love of teaching and providing invaluable mentorship, and to the students of ES164 for their curiosity and excitement. My dedication to communicating science and the joy I receive from it have flourished through our many collaborations.

To Mom and Dad, thank you for your unending and unconditional love and support. Your tireless dedication every single day for the past 35 years to my education and well-being is truly unbelievable, and I can never repay you for everything you have done for me. Finally, to John, thank you for being a constant source of delight throughout the many ups and downs of this PhD, and in particular, for tolerating my endless stream of comments. I would not be here without you.

To Mom and Dad
who encouraged me to “Go for the Gold”

LIST OF TABLES AND FIGURES

Tables

- Table 2.1.** Mn(III/IV) oxide location, morphology and structure based on linear combination fitting (LCF) results for six fungal species. 25
- Table 4.1.** Summary of identified CAZymes in secretomes of four Ascomycete fungi. 104
- Table 4.2.** Number of shared and unique identified proteins in glycoside hydrolase families among the four fungal secretomes. *A. alt.* = *A. alternata*; *P. spor.* = *P. sporulosum*; *Pyreno.* = *Pyrenochaeta* sp.; *Stago.* = *Stagonospora* sp. Percent shared = total number of proteins shared between 2-4 fungi divided by total number of proteins identified. 111
- Table 5.1.** Identified proteins with significantly changing relative abundance over time in the *A. alternata* secretome. Only proteins classified in the CAZy or MEROPS databases are shown, in addition to the protein with the highest and lowest fold change for each time point transition (in bold). Proteins that were significantly regulated in more than one time point transition are indicated with an asterisk. Refer to the text for an explanation of significance cutoffs and to Table S5.2 for the full list of significantly changing proteins for this organism. 139
- Table 5.2.** Identified proteins with significantly changing relative abundance over time in the *P. sporulosum* secretome. Only proteins classified in the CAZy or MEROPS databases are shown, in addition to the protein with the highest and lowest fold change for each time point transition (in bold). Proteins that were significantly regulated in more than one time point transition are indicated with an asterisk. Refer to the text for an explanation of significance cutoffs and to Table S5.3 for the full list of significantly changing proteins for this organism. 140
- Table 5.3.** Identified proteins with significantly changing relative abundance over time in the *Pyrenochaeta* sp. secretome. Only proteins classified in the CAZy or MEROPS databases are shown, in addition to the protein with the highest and lowest fold change for each time point transition (in bold). Proteins that were significantly regulated in more than one time point transition are indicated with an asterisk. Refer to the text for an explanation of significance cutoffs and to Table S5.4 for the full list of significantly changing proteins for this organism. 141

Table 5.4. Identified proteins with significantly changing relative abundance over time in the *Stagonospora* sp. secretome. Only proteins classified in the CAZy or MEROPS databases are shown, in addition to the protein with the highest and lowest fold change for each time point transition (in bold). Proteins that were significantly regulated in more than one time point transition are indicated with an asterisk. Refer to the text for an explanation of significance cutoffs and to Table S5.5 for the full list of significantly changing proteins for this organism.

142

- Table S4.1.** All proteins identified in secretomes of four Ascomycete fungi.
Submitted electronically
- Table S4.2.** Proteins unique to *A. alternata* (412 proteins).
Submitted electronically
- Table S4.3.** Proteins unique to *P. sporulosum* (578 proteins).
Submitted electronically
- Table S4.4.** Proteins unique to *Pyrenochaeta* sp. (381 proteins).
Submitted electronically
- Table S4.5.** Proteins unique to *Stagonospora* sp. (562 proteins).
Submitted electronically
- Table S5.1.** All identified proteins in secretomes of four Ascomycete fungi, including relative abundance data.
Submitted electronically
- Table S5.2.** Identified proteins with significantly changing relative abundance over time in the *A. alternata* secretome.
Submitted electronically
- Table S5.3.** Identified proteins with significantly changing relative abundance over time in the *P. sporulosum* secretome.
Submitted electronically
- Table S5.4.** Identified proteins with significantly changing relative abundance over time in the *Pyrenochaeta* sp. secretome.
Submitted electronically
- Table S5.5.** Identified proteins with significantly changing relative abundance over time in the *Stagonospora* sp. secretome.
Submitted electronically

Figures (with captions)

Figure 2.1. (A) Concentration and (B) percentage of Mn(II) and Mn(III, IV) oxides of the total initial Mn added as MnCO₃ at day 22 for rhodochrosite reacted with fungal species A – F (see Table 2.1 for species name).

24

Figure 2.2. Energy-specific synchrotron μ -X-ray fluorescence (μ -XRF) maps showing Mn(II) (red color) and Mn(IV) (green color) distribution in thin sections of rhodochrosite reacted with (A) *Phoma* sp. DS1wsM30b, (B) *Pyrenochaeta* sp. DS3sAY3a, and (C) *Stagonospora* sp. SRC11sM3a. Scale bar represents 10 mm. (D) μ -XANES spectra taken at the white circled areas in (C) (black lines), including a transect from bulk MnCO₃ to the Mn oxide rind and a Mn oxide hot spot. Also shown are the spectra of Mn(II) and Mn(IV) reference compounds (MnCO₃ and δ -MnO₂, respectively; dotted lines) and their peak positions (gray lines).

28

Figure 2.3. Light and electron microscopy images showing the morphology and location of Mn(II) oxides on rhodochrosite reacted with six fungal species (A – F; see Table 2.1 for species name). The brown/black color in light microscope images represents precipitated fungal Mn(III/IV) oxides.

30

Figure 2.4. Distribution of superoxide for *Pyrenochaeta* sp. DS3sAY3a (A) and *Stagonospora* sp. SRC11sM3a (B and C). Images show circular fungal mycelia on AY agar plates after approximately 2 weeks of growth starting from a center inoculation point (indicated by a black dot). (A, B) Lower portions of mycelia (below dotted lines) were stained with NBT. Blue color indicates the presence of O₂⁻. Cells were grown without added Mn(II). Scale bars are 1 cm. (C) Higher magnification image of the leading hyphal edge of *Stagonospora* sp. SRC11sM3a (as indicated in boxed region in (B)) indicating the distribution of superoxide at the hyphal tip. Scale bar = 50 mm.

33

Figure 2.5. Impact of chemical/enzyme inhibitors on Mn oxide formation by *Pyrenochaeta* sp. DS3sAY3a (A to D) and *Stagonospora* sp. SRC11sM3a (E to H). (A,E) AY agar controls amended with 200 μ M Mn(II). Brown color indicates mycogenic Mn oxides. (B,F) Cells grown with 200 μ M Mn(II) and 25 μ M (B) or 10 μ M (F) DPI, an inhibitor of NADPH oxidases. (C,G) Cells grown with 200 μ M Mn(II) and 200 μ M Cu(II), a scavenger of superoxide. (D,H) Cells grown with 200 μ M Mn(II) and 200 μ M Zn(II). Zn(II) imparts a similar level of toxicity as Cu(II) but does not react with superoxide. All scale bars are 1 cm.

34

Figure 2.6. SEM images of the Mn oxides formed by (A – C) *Pyrenochaeta* sp. DS3sAY3a and (D – F) *Stagonospora* sp. SRC11sM3a grown on rhodochrosite. Images illustrate

structurally unique Mn oxides with visible unknown filaments (see arrow in B) within the oxides. Hyphae are not in the field of view for images B through E.

37

Figure 2.7. TEM images of whole mounts (A – C) and cross-section (D) of Mn oxides produced by *Stagonospora* sp. SRC11sM3a grown in liquid AY medium. (A) An aggregate of extracellular, thread-like Mn oxides. (B) Magnified view of boxed area in (A). (C) An individual thread-like Mn oxide filament with a ball-like feature at the tip. (D) Cross-section of a ball-like feature (modified from Santelli et al., 2011).

38

Figure 3.1. Mn(II) oxidation by cell-free fungal secretomes. All experiments conducted with 500 μM Mn(II) and 200 $\mu\text{g mL}^{-1}$ fungal protein. Samples were incubated with Mn(II) for 1 hour prior to Mn oxide quantification. Within each organism, letters indicate significant differences by a Tukey-Kramer test with $P < 0.05$. All error bars represent ± 1 standard deviation over 4 biological replicates.

62

Figure 3.2. Native PAGE of selected secretome samples from *Stagonospora* sp. (A, D), *Pyrenochaeta* sp. (B, E), and *P. sporulosum* (C, F). Left (L): Pre-stained blue molecular mass markers with sizes in kDa to left of image. Center panel: Secretome samples after staining with Coomassie G-250 for 1 hour. Right panel: Replicate gel of the same secretome samples after incubation with 400 μM Mn(II) for 2 hours followed by staining with Leucoberberlin blue, which turns blue in the presence of Mn(III/IV) oxides. Images shown are representative of 4 biological replicates of each of 3 time points.

64

Figure 3.3. Proteins detected in Mn(II)-oxidizing gel bands (via LC/MS/MS) and their associated relative abundance in whole secretome samples (via iTRAQ proteomics) from *Stagonospora* sp. Proteins are displayed in descending order of number of gel band peptide observations for the time point during which maximum Mn(II) oxidative capacity was measured (7d; inset). EC numbers were derived from JGI genome annotations (regular text) or assigned manually (italics). Redox-active proteins are shown in bold. • Redox-active proteins that are detected in all Mn(II)-oxidizing gel bands (here, all 3 time points). * Proteins that exhibit relative abundance patterns over time that correlate with Mn(II) oxidation pattern (inset). Scale bar indicates relative abundance (\log_2 transformed).

65

Figure 3.4. Proteins detected in Mn(II)-oxidizing gel bands (via LC/MS/MS) and their associated relative abundance in whole secretome samples (via iTRAQ proteomics) from *Pyrenochaeta* sp. Proteins are displayed in descending order of number of gel band peptide observations for the time point during which maximum Mn(II) oxidative capacity was measured (21d; inset). EC numbers were derived from JGI genome annotations (regular text) or assigned manually (italics). Redox-active proteins are shown in bold. • Redox-active proteins that are detected in all Mn(II)-oxidizing gel bands (here, 14d and

21d). * Proteins that are detected in all Mn(II)-oxidizing gel bands and exhibit relative abundance patterns over time that correlate with Mn(II) oxidation pattern (inset). Scale bar indicates relative abundance (\log_2 transformed).

68

Figure 3.5. Proteins detected in Mn(II)-oxidizing gel bands (via LC/MS/MS) and their associated relative abundance in whole secretome samples (via iTRAQ proteomics) from *P. sporulosum*. Proteins are displayed in descending order of number of gel band peptide observations for the time point during which maximum Mn(II) oxidative capacity was measured (14d; inset). EC numbers were derived from JGI genome annotations (regular text) or assigned manually (italics). Redox-active proteins are shown in bold. • Redox-active proteins that are detected in all Mn(II)-oxidizing gel bands (here, all 3 time points). * Proteins that are detected in all Mn(II)-oxidizing gel bands and exhibit relative abundance patterns over time that correlate with Mn(II) oxidation pattern (inset). Scale bar indicates relative abundance (\log_2 transformed).

70

Figure 4.1. Distribution of proteins identified via iTRAQ proteomics in secretomes of 4 Ascomycete fungi grown on AY+Mn medium. For each fungus, proteins are shown if they were identified in any time point. Total number of proteins identified for each fungus, inclusive of all time points, is indicated in center of circles. Abbreviations from CAZy database: AA = auxiliary activities; CBM = carbohydrate-binding module; CE = carbohydrate esterase; GH = glycoside hydrolase; GT = glucosyltransferase; PL = polysaccharide lyase.

103

Figure 4.2. Distribution of proteins identified via iTRAQ proteomics in fungal secretomes among protein families according to the CAZy and MEROPS databases. (A) CAZy glycoside hydrolase families. (B) MEROPS peptidase families. (C) CAZy auxiliary activity families. (D) Other CAZyme families. For each fungus, proteins are counted if they were identified in any time point. Abbreviations as in Figure 4.1.

106

Figure 4.3. Venn diagram showing number of unique and shared proteins identified by iTRAQ proteomics in secretomes of 4 Ascomycete fungi. For each fungus, proteins were counted if they were identified in any time point. Total number of proteins identified for each fungus, inclusive of all time points, is indicated outside of diagram. Diagram generated with Venny 2.0 (Oliveros, J.C. (2007-2015) Venny. An interactive tool for comparing lists with Venn's diagrams. <http://bioinfogp.cnb.csic.es/tools/venny/index.html>).

109

Figure 4.4. Distribution of proteins (A) unique to each fungus based on amino acid sequence (as determined by JGI protein ID) and (B) unique to each fungus based on predicted function (evaluated manually). Proteins identified via iTRAQ proteomics. For each fungus, proteins are included if they were identified in any time point. Total number of unique

proteins identified for each fungus, inclusive of all time points, is indicated in center of circles. Abbreviations as in Figure 4.1.

113

Figure 5.1. Distribution of proteins identified via iTRAQ proteomics in secretomes of 4 Ascomycete fungi after 7 days, 14 days, and 21 days of growth. Total number of proteins identified for each fungus, at each time point, is indicated in center of circles. Abbreviations from CAZy database: AA = auxiliary activities; CBM = carbohydrate-binding module; CE = carbohydrate esterase; GH = glycoside hydrolase; GT = glucosyltransferase; PL = polysaccharide lyase.

136

Figure 5.2. Distribution of identified proteins in fungal secretomes that exhibited (A) significantly increasing or (B) significantly decreasing relative abundance with increasing secretome age. Refer to text for explanation of significance cutoffs. Plots include 32, 35, 30, and 36 proteins (corresponding to the top or bottom 2.5th percentile) for *A. alternata*, *P. sporulosum*, *Pyrenochaeta* sp., and *Stagonospora* sp., respectively. Only proteins that were identified in all 3 time points were evaluated. Abbreviations as in Figure 5.1.

138

Figure 5.3. Temporal changes in relative abundance of identified proteins common to all four fungal secretomes. (A) All identified proteins; each fungus plotted individually. (B) All 4 fungi plotted together; marker shapes and colors as in (A). 1st row: Selected glycoside hydrolases. 2nd row: Selected peptidases. 3rd row: Selected redox-active and ROS-generating oxidoreductases, and hypothetical proteins. 4th row: Other selected proteins and legend. Legend: Top left quadrant of each plot represents identified proteins whose relative abundance decreased from the 7d sample to the 14d sample, and then increased from the 14d sample to the 21d sample. Other quadrants as noted in legend. Only proteins that were identified in all 3 time points in all 4 fungi are shown. Abbreviations as in Figure 5.1.

148

Figure S2.1. SEM images showing the surface features of rhodochrosite crystals after reaction with (A) no fungi (control sample), (B) *Pyrenochaeta* sp. DS3sAY3a, and (C-D) *Stagonospora* sp. SRC1lsM3a. In contrast to the control sample, in the presence of fungi, extensive surface etching of the MnCO_3 surface is evident both within dissolution pits and on basal surfaces.

164

Figure S2.2. SEM images showing *Stagonospora* sp. SRC1lsM3a hyphae growing into cracks (A-B) and dissolution pits (C) on the surface of rhodochrosite crystals.

165

Figure S2.3. SEM images showing organic coatings on rhodochrosite crystals after reaction with (A-B) *Pithomyces chartarum* DS1bioJ1b and (C) *Pleosporales* sp. AP3s5JAC2b.

166

Figure S2.4. Bulk EXAFS of Mn oxides formed following Mn(II) oxidation of MnCO₃ by fungal species A – F (see Table 2.1 for species name). Three reference compounds needed to reconstruct the mycogenic oxides by linear combination fitting (LCF) are included in gray. Data are shown in solid lines and fits in dotted lines. Fitting results and parameters are listed in Table 2.1.

167

Figure S2.5. Stereomicroscope images showing the impact of chemical/enzyme inhibitors on Mn oxide formation by *Pyrenochaeta* sp. DS3sAY3a (A-D) and *Stagonospora* sp. SRC11sM3a (E-H). All images depict fungal hyphae and Mn oxides on AY agar plates after approximately 2 weeks of growth. (A, E) AY agar controls amended with 200 μM Mn(II). Brown color indicates mycogenic Mn oxides. (B, F) Cells grown with 200 μM Mn(II) and 25 μM (B) or 10 μM (F) DPI, an inhibitor of NADPH oxidases. (C, G) Cells grown with 200 μM Mn(II) and 200 μM Cu(II), a scavenger of superoxide. (D, H) Cells grown with 200 μM Mn(II) and 200 μM Zn(II). Zn(II) imparts a similar level of toxicity as Cu(II) but does not react with superoxide.

168

Figure S2.6. Mycogenic Mn oxide samples were analyzed with micro-Fourier transform infrared spectroscopy (μFTIR). Mn oxide clusters in cultures of *Pyrenochaeta* sp. DS3sAY3a. The Mn oxides were not associated with any cellular materials. Clusters were gently removed from the medium with sterile wooden inoculation sticks, washed six times in distilled water, and dissolved with 20 mM ascorbic acid to liberate organics from Mn oxides prior to analysis. Samples were analyzed on a μ-FTIR at Bruker Optics, Inc. (Billerica, MA) in reflectance mode. These preliminary μ-FTIR data are promising in that they indicate the presence of organics directly associated with cell-free Mn oxide clusters.

169

Figure S3.1. Fungal cultures of *Stagosospora* sp., *Pyrenochaeta* sp., and *P. sporulosum* in liquid AY + Mn medium at time of secretome harvest. Dark brown color indicates presence of biogenic Mn oxides. Images are representative of 4 biological replicates.

172

Figure S3.2. (A-C) Mn(II) oxidation normalized to protein mass in the untreated secretome (white bars), after boiling at 100°C for 30 minutes (gray bars), and after incubation with 1 mg mL⁻¹ proteinase K for 2 hours (black bars). All error bars represent +/- 1 standard deviation over 4 biological replicates. (D) *Stagonospora* sp. mycelium growing on a 0.2 μm filter on solidified AY medium without Mn(II) (left). Cells and filter were removed, and metabolites in agar either untreated (center) or heated at 70°C for 30 minutes (right). Plates in center and right images were then flooded with 200 μM Mn(II) for 1 hour and stained with LBB. Blue color indicates presence of Mn(III/IV) oxides.

173

Figure S3.3. Native PAGE of secretome samples from all 3 time points for *Stagonospora* sp. (A), *Pyrenochaeta* sp. (B), and *P. sporulosum* (C). (L) Pre-stained blue molecular mass

markers with sizes in kDa to left of images. (Center panels) Gel stained with Coomassie G-250 for 1 hour. (Right panels) Replicate gel of the same secretome samples after incubation with 400 μM Mn(II) for 2 hours followed by staining with Leucoberbelin blue, which turns blue in the presence of Mn(III/IV) oxides. Images shown are representative of 4 biological replicates.

174

Figure S3.4. (A) *Pyrenochaeta* sp. secretome sample dropped onto solidified AY medium supplemented with 200 μM Mn(II). Secretome from 500 mL culture aged 17 days. (B) Same secretome sample incubated with 75 μM *o*-phenanthroline in 8% ethanol for 2 hours prior to dropping sample on plate. (C) Same sample incubated with 8% ethanol only prior to dropping on plate. Entire plate was stained with LBB; blue color indicates presence of Mn(III/IV) oxides.

175

Figure S3.5. Mn(II) oxidation normalized to protein mass in the unamended cell-free secretome (white bars) and in the presence of 50 kU L^{-1} superoxide dismutase (gray bars) for (A) *Stagonospora* sp., (B) *Pyrenochaeta* sp., and (C) *P. sporulosum*. All error bars represent \pm 1 standard deviation over 4 biological replicates. * The Mn+SOD treatment is significantly different from the Mn treatment by a paired t-test with $P < 0.05$.

176

CHAPTER 1

Introduction

Fungi are the primary decomposers of recalcitrant plant and animal material in terrestrial ecosystems. As such, they are an important driver of global carbon cycling and climate dynamics, as well as a mediator in the production of renewable energy from plant-based substrates. Degradation of organic litter and subsequent release of CO₂ to the atmosphere is achieved through extracellular digestion, a process by which fungi release a large and diverse suite of extracellular enzymes and reactive metabolites into the environment to breakdown recalcitrant material into more easily digestible compounds from which they can obtain carbon, energy, and nutrients. This suite of secreted proteins and metabolites, collectively referred to as the *secretome* (Tjalsma et al., 2000; Agrawal et al., 2010), is utilized by fungi not only for oxidative substrate degradation, but also for communication and signaling processes, defense against competing organisms, a source of virulence in pathogenic fungi, and regulation of their immediate environment (reviewed in (Girard et al., 2013)).

This thesis explores the secretomes of filamentous fungi in the phylum Ascomycota that have the ability to oxidize manganese (Mn)(II) to Mn(III/IV) oxides. Fungal, or mycogenic, Mn oxides were first documented in the 1960s (Perfil'ev and Gabe, 1961) (when they were thought to be of bacterial origin) and have since been identified in diverse environments across the globe, including swamps (Perfil'ev and Gabe, 1961), the oxic-anoxic interface in temperate lakes (Klaveness, 1977; Gregory et al., 1980; Maki et al., 1987), lake ores (Dubinina, 1984), brackish waters (Neretin et al., 2003), boreal and tundra soils (Timonin et al., 1972), ferromanganese-rich desert rock varnishes (Krumbein and Jens, 1981), building stones (de la Torre and Gomez-

Alarcon, 1994), and even ancient environments such as Precambrian sedimentary formations and Cretaceous-Paleogene cherts (Crerar et al., 1980). Not only are biogenic Mn oxides ubiquitous in the environment, but they are also among the most reactive mineral phases on Earth due to their small particle size, large surface area, and high sorptive and oxidative capacities. As such, they can impact a variety of biogeochemical processes, including degradation of recalcitrant organic compounds such as humic acids (Stone and Morgan, 1984; Sunda and Kieber, 1994) and organic contaminants (Rubert and Pedersen, 2006), adsorption and redox cycling of trace metals (Nelson et al., 1999; Murray and Tebo, 2007), and anaerobic respiration coupled to carbon oxidation (Nealson and Saffarini, 1994).

Of particular interest is the ability of Mn(II)-oxidizing fungi to aid in the remediation of metal-contaminated waters (Santelli et al., 2010; Luan et al., 2012). Three of the fungi investigated in this work (*Alternaria alternata* SRC1lrK2f, *Stagonospora* sp. SRC1lsM3a, and *Pyrenochaeta* sp. DS3sAY3a) were isolated from passive coal mine drainage treatment systems in central Pennsylvania (USA) in which microbial Mn oxide formation is actively used to remove toxic trace metals from contaminated drainage waters via adsorption and settling (Santelli et al., 2010). In fact, although the aim of the original isolation study was to obtain bacterial Mn(II)-oxidizers, approximately 90 percent of the isolates obtained were Ascomycete fungi (Santelli et al., 2010), suggesting their importance in the remediation process. The fourth Mn(II)-oxidizing fungus investigated in this work, *Paraconiothyrium sporulosum* AP3s5-JAC2a, was isolated from a freshwater lake in Massachusetts (USA) that was historically contaminated with high concentrations of metals, including iron and manganese, and is currently undergoing remediation (Santelli et al., 2014). While the bioremediation potential of these fungi is promising, the mechanisms by which these isolates oxidize Mn(II) to Mn oxides have not yet

been characterized and remain poorly understood, limiting our understanding of how to optimize their application in the field.

In addition to their engineering applications, Mn(II)-oxidizing fungi are of great commercial and industrial interest due to their ability to harness the oxidation of Mn(II) in the breakdown of recalcitrant lignocellulosic plant material (Perez et al., 2002; Ruiz-Duenas and Martinez, 2009). In wood degrading fungi in the phylum Basidiomycota, such as the model white-rot fungus *Phanerochaete chrysosporium*, extracellular enzymes including Mn peroxidases and laccases oxidize Mn(II) to form Mn(III) and other reactive intermediates, which non-specifically oxidize the phenolic groups of lignin polymers and aid in the breakdown of cellulose and hemicellulose (Glenn et al., 1986; Perez and Jeffries, 1992; Wariishi et al., 1992; Höfer and Schlosser, 1999; Hofrichter, 2002; Schlosser and Höfer, 2002). Thus, *Mn(II) oxidation is directly linked to carbon oxidation* in these fungi, and these coupled processes are *mediated by the secretome*. As plant cell walls, composed primarily of lignocellulose, constitute the most abundant source of organic carbon on Earth, secretome-based oxidative capacity represents a powerful tool in the bioconversion of this renewable energy reservoir.

Although considerably less is known about the mechanisms by which Ascomycete fungi oxidize Mn(II) than their Basidiomycete counterparts, enzymes in the secretome are thought to play a similarly important role in this extracellular process. Initial demonstration of an enzymatic Mn(II) oxidation mechanism distinct from Basidiomycete Mn peroxidases (de la Torre and Gomez-Alarcon, 1994) has been followed by several studies implicating secreted laccase-like multicopper oxidases (LMCOs) in Mn(II) oxidation by phylogenetically diverse Ascomycetes (Miyata et al., 2004; Miyata et al., 2006b; Miyata et al., 2006a; Thompson et al., 2006). In *Acremonium* sp. strain KR21-2, the LMCO exhibits sequence similarity to bilirubin

oxidase and polyphenol oxidase, although it has not yet been definitively identified (Miyata et al., 2006a). Furthermore, extracellular superoxide (a reactive oxygen species) generated by transmembrane NADPH oxidases has been recently implicated in Mn(II) oxidation by *Stilbella aciculosa* (Hansel et al., 2012). Taken together, these studies shed light on the roles of both secretome-hosted enzymes and low molecular weight oxidants in Ascomycete Mn(II) oxidation. However, while several Mn(II)-oxidizing Ascomycetes have demonstrated the ability to degrade cellulose (Nilsson et al., 1989; Shary et al., 2007), including the four fungi investigated in this thesis (C.M. Santelli, unpublished data), a definitive link between Mn(II) and carbon oxidation in Ascomycetes remains elusive.

The work presented herein builds on these previous studies of secretome-based, Ascomycete Mn(II) oxidation. Chapter 2 demonstrates that extracellular superoxide is responsible for Mn(II) oxidation in two additional fungi, *Stagonospora* sp. and *Pyrenochaeta* sp., during growth on solid substrate, and moreover, suggests a role for secreted organic polymers in Mn(III) complexation and Mn oxide templation. Chapter 3 demonstrates that species-specific secreted enzymes confer Mn(II) oxidative capacity in the cell-free, liquid secretomes of these two fungi and *P. sporulosum*, identifying candidate Mn(II)-oxidizing enzymes that can be targeted for future mechanistic and biogeochemical investigations. Intriguingly, data in this chapter also suggest an enzymatic link between Mn(II) oxidation by Ascomycetes and cellulose degradation by brown-rot Basidiomycetes. This work furthers our understanding of Ascomycete Mn(II) oxidation mechanisms, highlights the diversity of mechanisms among phylogenetically diverse species, and adds to the growing body of knowledge surrounding the oxidative capacity of fungal secretomes.

The substantial advancement of analytical techniques in microbial genomics, transcriptomics, proteomics, and metabolomics over the past several years has facilitated the expansion of secretome investigations beyond targeted enzymatic studies to complete characterization of secretome composition, allowing researchers to delve more deeply into the mechanistic underpinnings of complex microbially-mediated process in the environment. In particular, comparative proteomics has proven to be a valuable tool in investigating the response of fungal secretomes to different carbon sources and teasing apart the diverse and elaborate mechanisms by which these organisms attack recalcitrant plant-based material. Previous studies of the fungal secretome have demonstrated an increase in secretome size and diversity when the organisms are presented with a more complex substrate (Medina et al., 2004; Phalip et al., 2005; Lu et al., 2010; Liu et al., 2013). Furthermore, by incorporating quantitative time-course analyses into secretome characterization studies, researchers have illustrated dynamic shifts in metabolic strategies as the fungi accumulate compounds of interest (Shi et al., 2013), adjust to diminishing resource availability (Nitsche et al., 2012), or alter enzyme regulation patterns as they sequentially degrade a complex substrate (Saykhedkar et al., 2012).

Critical to these large proteomic studies and the resulting insights into fungal carbon degradation mechanisms is the availability of sequenced genomes of the organisms of interest. While our understanding of lignin and cellulose degradation mechanisms by classic white-rot Basidiomycete wood-degraders (Vanden Wymelenberg et al., 2010; Hori et al., 2014) and model Ascomycete fungi in the *Aspergillus* (Lu et al., 2010; Liu et al., 2013) and *Fusarium* (Phalip et al., 2005) genera have benefited from early genome sequencing, sequencing of other filamentous Ascomycetes, particularly those of environmental isolates, lags behind. As such, *the contribution of these abundant yet understudied organisms to recalcitrant carbon turnover in*

terrestrial environments remains poorly understood. The work presented herein helps to address this data gap and includes sequencing of all four Mn(II)-oxidizing, Ascomycete isolates (*A. alternata*, *P. sporulosum*, *Stagonospora* sp., and *Pyrenochaeta* sp.) and deposition in the Joint Genome Institute (JGI) fungal genomics resource MycoCosm (Grigoriev et al., 2014) as part of the 1000 Fungal Genomes Project. Funded by the United States Department of Energy, it is our hope that this genomic and proteomic information will add to the growing body of knowledge on filamentous Ascomycetes and facilitate more complete analyses of fungal ‘omic datasets by researches in bioenergy production, biogeochemistry, microbial ecology, and other diverse fields.

Adding to the comparative lack of secretome characterization studies on environmental isolates, side-by-side comparisons of multiple species, particularly phylogenetically diverse organisms, have thus far been limited (see (Shi et al., 2013) for an example using yeasts and (Vanden Wymelenberg et al., 2010) for Basidiomycete wood-degraders). Results presented in Chapter 3 of this thesis demonstrate that the secretome-hosted enzymes likely responsible for Mn(II) oxidation in our isolates vary by species, and the Mn(II) oxidative capacity of the fungi changes over time. This mechanistic diversity among species and environmental conditions lends further support for extending secretome characterization studies to phylogenetically diverse organisms and comparing dynamic enzyme regulation patterns among species.

The work presented in Chapters 4 and 5 of this thesis fully characterizes the proteomic composition of the secretomes of our four Mn(II)-oxidizing, Ascomycete fungi, including implications for carbon degradation strategies employed by these organisms during batch culture on a complex medium. Chapter 4 highlights the rich functional diversity and oxidative capacity of these fungal secretomes, identifying a suite of enzymes capable of both direct enzymatic

cellulose oxidation and indirect carbon breakdown through the production of reactive intermediates. Additionally, side-by-side comparison of the secretomes reveals a functionally similar suite of extracellular enzymes among the four organisms, despite the presence of many species-specific proteins. Chapter 5 extends secretome characterization to a quantitative time-course analysis, demonstrating that the organisms exhibit striking differences in regulation of carbon-degrading enzymes while utilizing the same substrate under the same growth conditions. These data illustrate species-specific and temporal shifts in carbon utilization strategies among the four phylogenetically diverse fungi. Taken together, these chapters highlight the utility of genome sequencing and comparative proteomics in elucidating secretome-based carbon degradation mechanisms and shed light on the diversity of operative metabolic pathways in these filamentous Ascomycetes.

Thesis Summary. Overall, this work seeks to elucidate the secretome-based mechanisms of both Mn(II) and carbon oxidation by a group of filamentous Ascomycete fungi isolated from metal-contaminated environments. Moreover, this work seeks to explore the potential presence and character of a mechanistic link between Mn(II) and carbon oxidation via common secreted enzymes and reactive metabolite generation pathways.

Specific objectives include the following:

- (i) Understanding the mechanisms of Mn(II) oxidation by three phylogenetically diverse, filamentous Ascomycetes growing under different environmental conditions (i.e., solid and liquid medium);
- (ii) Presenting a first look at the proteomic composition of the secretomes of four filamentous Ascomycetes and evaluating their potential lignocellulose degradation capacity; and

- (iii) Gaining insight into the carbon utilization strategies employed by the organisms and the dynamic shifts in enzyme regulation patterns over time.

This thesis addresses these objectives in the following chapters:

- Chapter 1 Introduction
- Chapter 2 Fungal oxidative dissolution of the Mn(II)-bearing mineral rhodochrosite and the role of metabolites in manganese oxide formation
- Chapter 3 Mechanisms of Mn(II) oxidation by filamentous Ascomycete fungi vary with species and time as a function of secretome composition
- Chapter 4 Comparative analysis of secretome profiles of four Mn(II)-oxidizing Ascomycete fungi
- Chapter 5 Quantitative iTRAQ-based secretome analysis reveals species-specific and temporal shifts in carbon utilization strategies among Mn(II)-oxidizing Ascomycete fungi

References

- Agrawal, G.K., Jwa, N.S., Lebrun, M.H., Job, D., and Rakwal, R. (2010) Plant secretome: unlocking secrets of the secreted proteins. *Proteomics* **10**: 799-827.
- Crerar, D.A., Fisher, A.G., and Plaza, C.L. (1980) *Metallogenium* and biogenic deposition of manganese from Precambrian to recent time. In *Geology and Geochemistry of Manganese Volume III Manganese on the Bottom of Recent Basins*. Vanentsov, I.M., and Grasselly, G. (eds). Verlagsbuchhandlung: Stuttgart, pp. 285-303.
- de la Torre, M.A., and Gomez-Alarcon, G. (1994) Manganese and iron oxidation by fungi isolated from building stone. *Microb Ecol* **27**: 177-188.
- Dubinina, G.A. (1984) Infection of procaryotic and eukaryotic microorganisms with *Metallogenium*. *Curr Microbiol* **11**: 349-356.
- Girard, V., Dieryckx, C., Job, C., and Job, D. (2013) Secretomes: The fungal strike force. *Proteomics* **13**: 597-608.
- Glenn, J.K., Akileswaran, L., and Gold, M.H. (1986) Mn(II) oxidation is the principal function of the extracellular Mn-peroxidase from *Phanerochaete chrysosporium*. *Arch Biochem Biophys* **251**: 688-696.
- Gregory, E., Perry, R.S., and Staley, J.T. (1980) Characterization, distribution, and significance of *Metallogenium* in Lake Washington. *Microb Ecol* **6**: 125-140.
- Grigoriev, I.V., Nikitin, R., Haridas, S., Kuo, A., Ohm, R., Otilar, R. et al. (2014) MycoCosm portal: Gearing up for 1000 fungal genomes. *Nucleic Acids Res* **42**.
- Hansel, C.M., Zeiner, C.A., Santelli, C.M., and Webb, S.M. (2012) Mn(II) oxidation by an ascomycete fungus is linked to superoxide production during asexual reproduction. *PNAS* **109**: 12621-12625.
- Höfer, C., and Schlosser, D. (1999) Novel enzymatic oxidation of Mn²⁺ to Mn³⁺ catalyzed by a fungal laccase. *FEBS Lett* **451**: 186-190.
- Hofrichter, M. (2002) Review: lignin conversion by manganese peroxidase (MnP). *Enzyme Microb Technol* **30**: 454-466.
- Hori, C., Gaskell, J., Igarashi, K., Kersten, P., Mozuch, M., Samejima, M., and Cullen, D. (2014) Temporal alterations in the secretome of the selective lignolytic fungus *Ceriporiopsis subvermispora* during growth on aspen wood reveal this organism's strategy for degrading lignocellulose. *Appl Environ Microbiol* **80**: 2062-2070.

Klavness, D. (1977) Morphology, distribution and significance of manganese-accumulating microorganism *Metallogenium* in lakes. *Hydrobiologia* **56**: 25-33.

Krumbein, W.E., and Jens, K. (1981) Biogenic rock varnishes of the Negev Desert (Israel): An ecological study of iron and manganese transformation by cyanobacteria and fungi. *Oecologia* **50**: 25-38.

Liu, D., Li, J., Zhao, S., Zhang, R., Wang, M., Miao, Y. et al. (2013) Secretome diversity and quantitative analysis of cellulolytic *Aspergillus fumigatus* Z5 in the presence of different carbon sources. *Biotechnol Biofuels* **6**: 149.

Lu, X., Sun, J., Nimtz, M., Wissing, J., Zeng, A.-P., and Rinas, U. (2010) The intra- and extracellular proteome of *Aspergillus niger* growing on defined medium with xylose or maltose as carbon substrate. *Microb Cell Fact* **9**: 23.

Luan, F., Santelli, C.M., Hansel, C.M., and Burgos, W.D. (2012) Defining manganese(II) removal processes in passive coal mine drainage treatment systems through laboratory incubation experiments. *Appl Geochem* **27**: 1567-1578.

Maki, J.S., Tebo, B.M., Palmer, F.E., Nealson, K.H., and Staley, J.T. (1987) The abundance and biological activity of manganese-oxidizing bacteria and *Metallogenium*-like morphotypes in Lake Washington, USA. *FEMS Microbiol Ecol* **45**: 21-29.

Medina, M.L., Kiernan, U.A., and Francisco, W.A. (2004) Proteomic analysis of rutin-induced secreted proteins from *Aspergillus flavus*. *Fungal Genet Biol* **41**: 327-335.

Miyata, N., Tani, Y., Iwahori, K., and Soma, M. (2004) Enzymatic formation of manganese oxides by an *Acremonium*-like hyphomycete fungus, strain KR21-2. *FEMS Microbiol Ecol* **47**: 101-109.

Miyata, N., Tani, Y., Maruo, K., Tsuno, H., Sakata, M., and Iwahori, K. (2006a) Manganese(IV) oxide production by *Acremonium* sp. strain KR21-2 and extracellular Mn(II) oxidase activity. *Appl Environ Microbiol* **72**: 6467-6473.

Miyata, N., Maruo, K., Tani, Y., Tsuno, H., Seyama, H., Soma, M., and Iwahori, K. (2006b) Production of biogenic manganese oxides by anamorphic ascomycete fungi isolated from streambed pebbles. *Geomicrobiol J* **23**: 63-73.

Murray, K.J., and Tebo, B.M. (2007) Cr(III) is indirectly oxidized by the Mn(II)-oxidizing bacterium *Bacillus* sp. strain SG-1. *Environ Sci Technol* **41**: 528-533.

Nealson, K.H., and Saffarini, D. (1994) Iron and manganese in anaerobic respiration - Environmental significance, physiology, and regulation. *Annu Rev Microbiol* **48**: 311-343.

Nelson, Y.M., Lion, L.W., Ghiorse, W.C., and Shuler, M.L. (1999) Production of biogenic Mn oxides by *Leptothrix discophora* SS-1 in a chemically defined growth medium and evaluation of their Pb adsorption characteristics. *Appl Environ Microbiol* **65**: 175-180.

Neretin, L.N., Pohl, C., Jost, G., Leipe, T., and Pollehne, F. (2003) Manganese cycling in the Gotland Deep, Baltic Sea. *Mar Chem* **82**: 125-143.

Nilsson, T., Daniel, G., Kirk, T.K., and Obst, J.R. (1989) Chemistry and microscopy of wood decay by some higher ascomycetes. *Holzforschung* **43**: 11-18.

Nitsche, B.M., Jørgensen, T.R., Akeroyd, M., Meyer, V., and Ram, A.F.J. (2012) The carbon starvation response of *Aspergillus niger* during submerged cultivation: Insights from the transcriptome and secretome. *BMC Genomics* **13**: 380.

Perez, J., and Jeffries, T.W. (1992) Roles of manganese and organic acid chelators in regulating lignin degradation and biosynthesis of peroxidases by *Phanerochaete chrysosporium*. *Appl Environ Microbiol* **58**: 2402-2409.

Perez, J., Munoz-Dorado, J., de la Rubia, T., and Martinez, J. (2002) Biodegradation and biological treatments of cellulose, hemicellulose, and lignin: an overview. *Int Microbiol* **5**: 53-63.

Perfil'ev, B.V., and Gabe, D.R. (1961) *The capillary methods of studying microorganisms [in Russian]*. Moscow: Izdatel'stvo Akademii Nauk SSSR.

Phalip, V., Delalande, F., Carapito, C., Goubet, F., Hatsch, D., Leize-Wagner, E. et al. (2005) Diversity of the exoproteome of *Fusarium graminearum* grown on plant cell wall. *Curr Genet* **48**: 366-379.

Rubert, K.F., and Pedersen, J.A. (2006) Kinetics of oxytetracycline reaction with a hydrous manganese oxide. *Environ Sci Technol* **40**: 7216-7221.

Ruiz-Duenas, F.J., and Martinez, A.T. (2009) Microbial degradation of lignin: how a bulky recalcitrant polymer is efficiently recycled in nature and how we can take advantage of this. *Microb Biotechnol* **2**: 164-177.

Santelli, C.M., Chaput, D.L., and Hansel, C.M. (2014) Microbial communities promoting Mn(II) oxidation in Ashumet Pond, a historically polluted freshwater pond undergoing remediation. *Geomicrobiol J* **31**: 605-616.

Santelli, C.M., Pfister, D.H., Lazarus, D., Sun, L., Burgos, W.D., and Hansel, C.M. (2010) Promotion of Mn(II) oxidation and remediation of coal mine drainage in passive treatment systems by diverse fungal and bacterial communities. *Appl Environ Microbiol* **76**: 4871-4875.

- Saykhedkar, S., Ray, A., Ayoubi-Canaan, P., Hartson, S.D., Prade, R., and Mort, A.J. (2012) A time course analysis of the extracellular proteome of *Aspergillus nidulans* growing on sorghum stover. *Biotechnol Biofuels* **5**: 52.
- Schlosser, D., and Höfer, C. (2002) Laccase-catalyzed oxidation of Mn^{2+} in the presence of natural Mn^{3+} chelators as a novel source of extracellular H_2O_2 production and its impact on manganese peroxidase. *Appl Environ Microbiol* **68**: 3514-3521.
- Shary, S., Ralph, S.A., and Hammel, K.E. (2007) New insights into the lignolytic capability of a wood decay ascomycete. *Appl Environ Microbiol* **73**: 6691-6694.
- Shi, J., Feng, H., Lee, J., and Ning Chen, W. (2013) Comparative proteomics profile of lipid-cumulating oleaginous yeast: An iTRAQ-coupled 2-D LC-MS/MS analysis. *PLoS ONE* **8**: e85532.
- Stone, A.T., and Morgan, J.J. (1984) Reduction and dissolution of manganese(III) and manganese(IV) oxides by organics. 1. Reaction with hydroquinone. *Environ Sci Technol* **18**: 450-456.
- Sunda, W.G., and Kieber, D.J. (1994) Oxidation of humic substances by manganese oxides yields low-molecular-weight organic substrates. *Nature* **367**: 62-64.
- Thompson, I.A., Huber, D.M., and Schulze, D.G. (2006) Evidence of a multicopper oxidase in Mn oxidation by *Gaeumannomyces graminis* var. *tritici*. *Phytopathology* **96**: 130-136.
- Timonin, M.I., Hartgering, T., and Illman, W.I. (1972) Oxidation of manganous salts of manganese by soil fungi. *Can J Microbiol* **18**: 793-799.
- Tjalsma, H., Bolhuis, A., Jongbloed, J.D.H., Bron, S., and Maarten van Dijk, J. (2000) Signal peptide-dependent protein transport in *Bacillus subtilis*, a genome-based survey of the secretome. *Microbiol Mol Biol Rev* **64**: 515-547.
- Vanden Wymelenberg, A., Gaskell, J., Mozuch, M., Sabat, G., Ralph, J., Skyba, O. et al. (2010) Comparative transcriptome and secretome analysis of wood decay fungi *Postia placenta* and *Phanerochaete chrysosporium*. *Appl Environ Microbiol* **76**: 3599-3610.
- Wariishi, H., Valli, K., and Gold, M.H. (1992) Manganese(II) oxidation by manganese peroxidase from the basidiomycete *Phanerochaete chrysosporium* - Kinetic mechanism and role of chelators. *J Biol Chem* **267**: 23688-23695.

CHAPTER 2

Fungal oxidative dissolution of the Mn(II)-bearing mineral rhodochrosite and the role of metabolites in manganese oxide formation

This chapter was published in the journal *Environmental Microbiology*.
(Tang Y.*, Zeiner C.A.*, Santelli C.M, Hansel C.M. Vol. 15, pp. 1063-1077, 2013)

* These authors contributed equally to this work.

Supplemental Material for this chapter is presented in **Appendix 1**.

Abstract

Microbially-mediated oxidation of Mn(II) to Mn(III/IV) oxides influences the cycling of metals and remineralization of carbon. Despite the prevalence of Mn(II)-bearing minerals in nature, little is known regarding the ability of microbes to oxidize mineral-hosted Mn(II). Here, we explored oxidation of the Mn(II)-bearing mineral rhodochrosite (MnCO_3) and characteristics of ensuing Mn oxides by six Mn(II)-oxidizing Ascomycete fungi. All fungal species substantially enhanced rhodochrosite dissolution and surface modification. Mineral-hosted Mn(II) was oxidized resulting in formation of Mn(III/IV) oxides that were all similar to $\delta\text{-MnO}_2$ but varied in morphology and distribution in relation to cellular structures and the MnCO_3 surface. For four fungi, Mn(II) oxidation occurred along hyphae, likely mediated by cell wall associated proteins. For two species, Mn(II) oxidation occurred via reaction with fungal-derived superoxide produced at hyphal tips. This pathway ultimately resulted in structurally unique Mn oxide clusters formed at substantial distances from any cellular structure. Taken together, findings for these two fungi strongly point to a role for fungal-derived organic molecules in Mn(III) complexation and Mn oxide templation. Overall, this study illustrates the importance of fungi in rhodochrosite dissolution, extends the relevance of biogenic superoxide-based Mn(II) oxidation, and highlights the potential role of mycogenic exudates in directing mineral precipitation.

Introduction

Mn(III, IV) oxides are ubiquitous in the environment, including terrestrial and aquatic systems. Due to their small particle size, large surface area, and high sorptive and oxidative capacities, Mn oxides are among the most reactive mineral phases in the environment. They influence a variety of biogeochemical reactions, such as the degradation of organic matter (Stone and Morgan, 1984; Sunda and Kieber, 1994), cycling of metals (Murray and Tebo, 2007; Murray et al., 2007; Lafferty et al., 2010), and anaerobic respiration coupled to carbon oxidation (Nealson and Saffarini, 1994). The majority of natural Mn oxides are thought to be formed either from direct or indirect microbial Mn(II) oxidation (Tebo et al., 2004). A large diversity of Mn(II)-oxidizing bacteria and fungi have been identified in a wide range of ecological niches spanning from desert sediments to surface marine waters (de la Torre and Gomez-Alarcon, 1994; Tebo et al., 2005; Hansel and Francis, 2006; Miyata et al., 2006a; Miyata et al., 2007; Cahyani et al., 2009; Santelli et al., 2010). At present, Mn(II)-oxidizing fungi are limited to the phyla Ascomycota and Basidiomycota, where Basidiomycota (specifically the wood rotting fungi) have received considerably more attention due to their importance in the degradation of lignin. Recently, we have discovered an abundant and diverse group of Mn(II)-oxidizing Ascomycota within Mn-laden treatment systems (Santelli et al., 2010) and a freshwater lake (Santelli et al., 2014).

While Mn(II) oxidation to Mn(III) has been extensively studied for Basidiomycota, the mechanisms and pathways of Mn(II) oxidation by Ascomycota are poorly understood. The primary enzymes implicated in Mn(II) oxidation are manganese peroxidases by Basidiomycete fungi (Glenn et al., 1986; Wariishi et al., 1992) and lacasses or laccase-like metalloproteins in Ascomycetes (Höfer and Schlosser, 1999; Schlosser and Höfer, 2002; Miyata et al., 2004).

Recently, extracellular superoxide (O_2^-) has been identified as the oxidant of Mn(II) to Mn(III) in the common Ascomycete fungus *Stilbella aciculosa* (Hansel et al., 2012). Surprisingly, superoxide mediated Mn(II) oxidation has also recently been discovered for the marine bacterium *Roseobacter* sp. Azwk-3b (Learman et al., 2011a), revealing an unforeseen homology in fungal and bacterial Mn(II) oxidation pathways. In fact, these findings are consistent with thermodynamic modeling of Mn(II) oxidation reactions indicating that while the oxidation of Mn(II) to Mn(III) by oxygen is thermodynamically prohibited, oxidation by superoxide is thermodynamically favorable over all relevant pH ranges (Luther, 2010). In fact, superoxide was found to be a rapid oxidant of Mn(II) in natural seawater and following photoexcitation of humic substances (Nico et al., 2002; Hansard et al., 2011). The production of extracellular reactive oxygen species (ROS), and particularly that of superoxide, is widespread throughout the fungal kingdom (Bedard et al., 2007), where it is employed for various physiological processes, including the regulation of cell differentiation (Takemoto et al., 2007) and apical dominance in hyphal growth (Semighini and Harris, 2008). However, the prevalence of an ROS-mediated Mn(II) oxidation mechanism in fungi is unknown.

Both enzymatic and superoxide-mediated Mn(II) oxidation are one electron transfer reactions leading to the formation of Mn(III) (Glenn et al., 1986; Höfer and Schlosser, 1999; Hansard et al., 2011). The fate of Mn(III) and processes responsible for subsequent formation of Mn oxides are unknown. Mn(III) may be further oxidized or may disproportionate leading to Mn(IV) production and spontaneous precipitation of Mn oxides. Due to the instability of Mn(III) in the absence of stabilizing ligands (Kostka et al., 1995; Klewicki and Morgan, 1998; Luther et al., 1998; Klewicki and Morgan, 1999), either exogenous or endogenous organic molecules may be important in the formation of Mn oxides following microbial Mn(II)

oxidation. In fact, protein and polysaccharide polymers have been identified underlying Mn oxides produced by a *Pedomicrobium*-like bacterium (Ghiorse and Hirsch, 1979) and an unidentified Basidiomycete fungus (Emerson et al., 1989), where they possibly play a mechanistic role in Mn oxide formation. Recent studies have also shown that organic molecules and specifically proteins may serve as mineral nucleation sites to facilitate particle aggregation in the biomineralization of zinc, iron, and selenium (Moreau et al., 2007; Chan et al., 2011; Chen et al., 2011; Lenz et al., 2011). Collectively, the mechanisms responsible for the oxidation of Mn(II) and ultimate formation of Mn oxides by Ascomycete fungi as well as within the environment are poorly understood.

Despite the large variety of natural and synthetic Mn oxides known to exist (over 30), the predominant form of biogenic Mn oxides formed at circumneutral pH is a highly disordered, nanocrystalline, phyllo-manganate phase, similar to hexagonal birnessite (Villalobos et al., 2003; Bargar et al., 2005; Webb et al., 2005). This phase is highly reactive and can undergo abiotic transformation and ripening to form more ordered and crystalline phases such as todorokite, feitknechtite, and triclinic birnessite (Bargar et al., 2005; Feng et al., 2010; Learman et al., 2011b). Within the natural environment, Ascomycete fungi generally grow attached to substrates, particularly minerals, yet most exploration of Mn(II) oxidation by Ascomycete fungi has focused on growth in liquid media or on agar solidified media (Miyata et al., 2006b; Cahyani et al., 2009; Petkov et al., 2009; Saratovsky et al., 2009; Santelli et al., 2011). In fact, Santelli et al. (2011) found that growth conditions (*i.e.*, planktonic versus surface-attached growth) impacted the composition and structure of Mn oxides formed. Considering the widely observed role of fungi in the chemical and mechanical alteration of minerals (Gadd, 1999; Sterflinger, 2000; Gadd, 2007), they are likely important weathering agents of Mn(II)-hosted minerals

(Golden et al., 1992). Yet little is known regarding the ability of fungi to oxidize mineral-hosted Mn(II), the mechanisms of oxidation, and the morphological and structural characteristics of the ensuing Mn oxides.

In this study, we examined the interaction of six Mn(II)-oxidizing fungal species with the mineral rhodochrosite (MnCO_3), a common Mn(II)-bearing mineral found in a wide range of environments including terrestrial soils and marine sediments. By combining chemical assays and a variety of microscopic and spectroscopic techniques, we examined the oxidation of rhodochrosite by six fungal species and the properties of the ensuing Mn oxides. For a subset of fungi, we also examined the mechanisms of Mn(II) oxidation and Mn oxide precipitation. Results from this study provide a better understanding of the mechanisms of rhodochrosite dissolution and alteration, the diverse characteristics of fungal Mn oxides, as well as the biogeochemical cycling of manganese in the environment.

Materials and Methods

Fungal species and growth conditions. We explored a total of six Mn(II)-oxidizing Ascomycetes isolated from two locations. Four species were isolated from passive coal mine drainage treatment systems in Central Pennsylvania that attenuate high concentrations of Mn (Santelli et al., 2010): *Stagonospora* sp. SRC1lsM3a, *Phoma* sp. DS1swM30b, *Pyrenochaeta* sp. DS3sAY3a, and *Pithomyces chartarum* DS1bioJ1b (Santelli et al., 2010). Two species were isolated from Ashumet Pond, MA, a natural freshwater lake: *Phoma* sp. AP3s5J1a and *Pleosporales* sp. AP3s5JAC2b (Santelli et al., 2014). This field site was previously contaminated with a sewage plume from Massachusetts Military Reservation (MMR) containing elevated concentrations of phosphorus and other constituents such as manganese.

MnCO₃ (sample # 96030, Colorado) was obtained from the Harvard University Mineralogical Museum. Fresh flat surfaces (mm in size) were prepared by cleaving large crystals with a razor blade along the {1014} plane and sterilized by autoclaving at 121°C for 15 minutes.

All fungal species were grown in HEPES-buffered (20 mM, pH 7) AY medium composed of 0.25 g/L sodium acetate, 0.15 g/L yeast extract, and 1 mL/L trace element stock (10 mg/L CuSO₄·5H₂O, 44 mg/L ZnSO₄·7H₂O, 20 mg/L CoCl₂·6H₂O, and 13 mg/L Na₂MoO₄·2H₂O) supplemented with MnCl₂ (0-200 μM), CuCl₂ (0-200 μM), ZnCl₂ (0-200 μM), and/or DPI (0-50 μM). Fungal cultures were first initiated in petri dishes containing agar-solidified (2% agar) AY medium without supplements. After growth proceeded radially outward from the inoculation point for approximately 2 weeks, the fungal mycelia were sampled with either a sterile coring device (for rhodochrochite cultures) or a sterile wooden inoculation stick (for plate cultures).

For cultures grown on rhodochrochite, a petri dish containing 3 – 5 mL of liquid AY medium (without any additional sources of Mn(II)) was filled with sterile quartz sand to maintain moisture and provide a solid support for the rhodochrochite crystals. Several crystals were gently placed on the sand. Mycelia-containing agar plugs obtained with the sterile coring device were then placed on the rhodochrochite surfaces. Cultures were incubated for 2-3 weeks at room temperature. Growth of fungal mycelia and production of dark brown Mn oxides were monitored with a light microscope (as described below). The formation of Mn(III, IV) oxides (MnO_x) was confirmed with the LBB method (Krumbein and Altmann, 1973) using a Cary 50 UV-vis spectrophotometer (Varian).

To compare the relative efficiency of Mn oxide production from rhodochrochite among the six fungal species, a separate set of experiments was conducted. For each species, a petri dish

containing 3 mL of AY medium (without Mn(II) or other supplements) and 258 ± 48 mg rhodochrosite was inoculated with a mycelia-containing agar plug. Care was taken to ensure that all agar plugs were of similar size. Triplicates were conducted for each species. After 22 days, production of dark brown Mn oxides was examined for all species. From each petri dish, 0.25 mL of the spent media was syringe filtered (0.2 μ m PTFE membrane), and Mn(II) concentration was analyzed using the formaldoxime method (Goto et al., 1962). The rest of the solution and all reacted crystals were sacrificed and analyzed for Mn(III, IV) oxide concentration using the LBB method.

For plate cultures, new AY agar plates (with or without supplements) were inoculated with wooden inoculation sticks and allowed to grow for 2-3 weeks, at which point ROS detection assays and/or imaging with a stereo microscope were performed (described below). All cultures were incubated at room temperature.

Reactive oxygen species detection. Extracellular ROS were detected using stains that precipitate upon reaction with ROS, thus maintaining spatial distribution of ROS production on agar-solidified media. Cultures grown on AY plates were point inoculated with NBT or DAB for superoxide and hydrogen peroxide detection, respectively. The NBT assay involved addition of 2.5 mM NBT chloride (Sigma Corp., St. Louis, MO) in 5 mM 3-(*N*-morpholino) propanesulfonate-NaOH, pH 7.6, which forms a blue precipitate upon reaction with $O_2^{\cdot-}$. The DAB assay involved addition of 2.5 mM DAB and 5 purpurogallin units/mL of horseradish peroxidase (HRP) in potassium phosphate buffer, pH 6.9, which forms a reddish-brown precipitate upon reaction with H_2O_2 , a dismutation product of the highly reactive superoxide radical. All reagents for the DAB assay were obtained from a HRP chromogen kit (GeneTex, Irvine, CA). For both assays, plates were incubated with the stain for 30 minutes in the dark.

Then, excess reagents were decanted, and the plates were incubated for an additional 2-24 hours until sufficient color had developed. The plates were imaged using a stereo microscope (as described below).

Light and electron microscopy. Light microscopy images of pristine and fungal-reacted rhodochrosite crystals and agar-supported plate cultures were recorded at various time stages using a SZX16 Zoom Stereo Microscope (Olympus America Inc.) fitted with an Olympus DP72 Microscope Digital Camera.

For scanning electron microscopy (SEM), rhodochrosite crystals covered with fungal mycelia and Mn oxides were fixed in 2.5% glutaraldehyde, washed 3 times in 0.2 M phosphate buffer (pH 7.4), and subjected to a series of ethanol dehydration. After the fixation process, desiccated samples were mounted on double-sided carbon tape and sputter-coated with Pt/Pd prior to imaging. SEM was performed at the Harvard University Center for Nanoscale Systems (CNS) using field emission SEMs (FESEM; Zeiss Ultra55 and Supra55) with a high efficiency in-lens secondary electron detector.

For transmission electron microscopy (TEM), dehydrated cultures that were grown in liquid media) were embedded in LR White resin and cured at 60 °C overnight. Hardened resin blocks were sectioned to 70 nm with a Diatome 45° diamond knife using a Leica UCT ultramicrotome (Leica Microsystems). Both un-embedded dehydrated cultures and embedded sections were mounted on 100 mesh copper grids with formvar support film coated with carbon. Unstained sections were imaged with an FEI Tecnai T-12 cryo-TEM. Thin sections were examined using a JEOL 2010 high resolution TEM (HR-TEM) equipped with an Oxford ISIS Energy-dispersive X-ray spectroscopy (EDS) microanalysis system.

Synchrotron-based microscopic and spectroscopic analysis. Rhodochrosite crystals reacted with *Phoma* sp. DS1wsM30b, *Pyrenochaeta* sp. DS3sAY3a, and *Stagonospora* sp. SRC1lsM3a were examined by coupled synchrotron-based micro-X-ray fluorescence (μ -XRF) microscopy and micro-X-ray absorption spectroscopy (μ -XAS) at beamline 2-3 at the Stanford Synchrotron Radiation Lightsource (SSRL) for the location and oxidation state of the associated Mn. Reacted crystals were air dried and embedded in EpoHeat Epoxy (Buehler). Cross sections (~ 100 μm thickness) of the embedded crystals were obtained using a diamond saw, fixed to a high-purity quartz slide using Hillquist Thin Section Epoxy A-B (Hillquist), and polished to ~ 50 μm thickness. Spatially-resolved (micron scale) XRF and XAS were conducted by collecting spectra at select points of interest or rastering a defined region. The beam size on the sample was 2×2 μm . Monochromatic X-rays were selected using a Si(111) $\Phi = 90$ double crystal monochromator. Multiple elements were mapped simultaneously by collecting fluorescence on a multi-channel Si Vortex detector (SII Nano Technology) using an incident monochromator energy of 13200 eV which is above the absorption edge of all the elements of interest. Maps were also collected at several discrete incident energies (6553, 6558, 6562 eV) in continuous raster scanning mode in order to collect the fluorescence at several distinguishing points within the Mn absorption edge. X-ray absorption near edge structure (XANES) spectra were collected at spots of interest to confirm the oxidation state at discrete locations. The line shapes (peak position and peak shape) of the XANES spectra were used to compare the relative proportions of Mn(II), Mn(III), and Mn(IV) in the Mn oxides (Bargar et al., 2005; Webb et al., 2005). Fluorescence maps and XANES spectra were analyzed using the MicroAnalysis Toolkit (Webb, 2006) and SIXPACK (Webb, 2005), respectively.

Bulk X-ray absorption spectroscopy data were also collected on the fungal Mn oxides to identify their speciation and structure. For all six species, mycogenic Mn oxides from reacted rhodochrosite were carefully separated by hand picking with tweezers under a microscope or brief ultrasonication in DI water. The collected Mn oxides were vacuum filtered using 0.2 μm polycarbonate membranes and rinsed with DI water. Multiple crystals were processed to achieve enough mass. The moist filter membranes loaded with Mn oxides were then mounted in a Teflon sample holder covered with Kapton tape for XAS data analysis. Samples were frozen at $-20\text{ }^{\circ}\text{C}$ and thawed prior to analysis. Manganese K-edge XAS spectra were collected at beam line 11-2 (SSRL) and beam line X18B at National Synchrotron Light Source, Brookhaven National Laboratory (NSLS-BNL) with a Si (220) or (111) double crystal monochromator (40% detuning). Energy calibration used a Mn foil (6539 eV). Data were collected in both fluorescence and transmission mode using a 30-element Ge solid-state detector with a Cr filter at beam line 11-2 (SSRL) and a PIPS detector at beam line X18B (NSLS). Analysis of the near edge region of consecutive XAS spectra for each sample showed no photo-induced reduction of Mn oxides under the X-ray beam.

Analysis of the bulk XAS data was performed using the programs SIXPACK (Webb, 2005) and Ifeffit (Ravel and Newville, 2005). The composition and structure of fungal Mn oxides were determined using both the XANES and EXAFS (extended X-ray absorption fine structure) regions. For EXAFS analysis, spectra were k^3 -weighted and analyzed at $3 - 12\text{ \AA}^{-1}$. Principal component analysis (PCA), combined with target transformation and linear combination fitting (LCF), were performed on the EXAFS spectra to establish the number of components representing the entire data set. A spectral reference library of model Mn compounds was used to identify and quantify the structural components. The model compounds

used were previously described (Bargar et al., 2005) and include: δ -MnO₂, hexagonal Na-birnessite, triclinic Ca-birnessite, groutite (α -MnOOH), feitknechtite (β -MnOOH), manganite (γ -MnOOH), hausmannite (Mn₃O₄), synthetic todorokite ((Na,Ca,K)(Mg,Mn)Mn₆O₁₄·5H₂O), pyrolusite (β -MnO₂), synthetic Mn₂O₃, aqueous Mn(III) pyrophosphate, aqueous MnCl₂, and aqueous MnSO₄.

Results and Discussion

Fungal alteration and oxidation of rhodochrosite. Fungal growth on rhodochrosite surfaces resulted in the production of oxidized Mn, as Mn(III) and Mn(IV), and removal of aqueous Mn(II) (Figure 2.1). Figure 2.1A shows the concentrations of Mn(II) and Mn(III/IV) produced after 22 days of reaction between rhodochrosite and each of the six fungal species employed in this study (see Table 2.1 for fungal species name). The relative percentages of the Mn(II) in solution and Mn(III/IV) produced following reaction, as compared to the initial total Mn provided (as MnCO₃), are shown in Figure 2.1B. The control sample (rhodochrosite without fungi) contained ~45 μ M of Mn(II) in solution, accounting for ~7% of the total initial MnCO₃ present, owing to (abiotic) dissolution of rhodochrosite in the AY medium. As evidenced by a lack of reaction with lecuoberbelin blue (LBB), oxidized Mn was not detected in the control sample, consistent with the thermodynamic inhibition of Mn(II) oxidation by molecular oxygen (Luther, 2005) and slow reaction kinetics of mineral-catalyzed Mn(II) oxidation under these conditions (Diem and Stumm, 1984). On the contrary, the growth of all six fungal species caused a significant decrease in dissolved Mn(II) concentrations in the growth medium (below 2 μ M for all species except *Pyrenochaeta* sp. DS3sAY3a), accompanied by high concentrations (110 to 240 μ M) of Mn(III/IV). Since MnCO₃ is the only Mn source in these systems, the

produced Mn(III/IV) must be from the fungal oxidation of Mn(II) originating from the rhodochrosite, either via direct oxidation of mineral-hosted Mn(II) or oxidation of aqueous Mn(II) provided by enhanced dissolution of MnCO₃. Either way, the amount of “released Mn” as dissolved Mn(II) and oxidized Mn as Mn(III/IV) accounts for 9 – 25% of the total initial Mn (as MnCO₃), as compared to ~7% in the control sample, illustrating enhanced mineral dissolution in the presence of all fungal species.

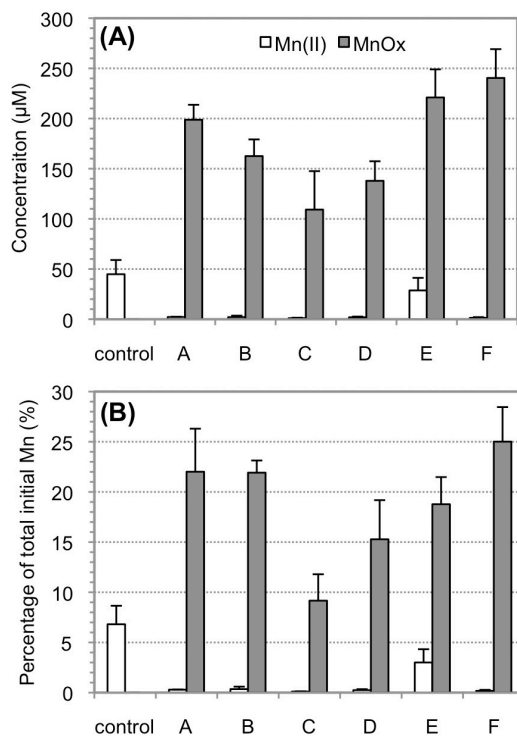


Figure 2.1. (A) Concentration and (B) percentage of Mn(II) and Mn(III, IV) oxides of the total initial Mn added as MnCO₃ at day 22 for rhodochrosite reacted with fungal species A – F (see Table 2.1 for species name).

Table 2.1. Mn(III/IV) oxide location, morphology and structure based on linear combination fitting (LCF) results for six fungal species.

ID	Species name	Mn(III/IV) oxide location and morphology	LCF components and parameters				
			Mn ²⁺ _(aq)	MnCO ₃	δ-MnO ₂	R factor	χ ²
A	<i>Phoma</i> sp. DS1wsM30b	Spherical, discrete precipitates along hyphae	0.06	0.48	0.45	0.06	0.25
B	<i>Pleosporales</i> sp. AP3s5JAC2b	Continuous coating along hyphae	0.14	0.5	0.36	0.18	0.69
C	<i>Pithomyces chartarum</i> DS1bioJ1b	Spherical, discrete precipitates along hyphae and on MnCO ₃ surface	0.09	0.79	0.12	0.12	0.37
D	<i>Phoma</i> sp. AP3s5J1a	Continuous coating along hyphae and on MnCO ₃ surface	0.15	0.31	0.54	0.03	0.14
E	<i>Pyrenochaeta</i> sp. DS3sAY3a	Flower-shaped oxide clusters on MnCO ₃ , sometimes underneath hyphae	0.06	0.46	0.48	0.06	0.28
F	<i>Stagonospora</i> sp. SRC1lsM3a	Flower-shaped oxide clusters on MnCO ₃ , no hyphal association	0.09	0.53	0.37	0.14	0.48

Microscopic interrogation of the fungal-MnCO₃ surface points to enhanced rhodochrosite dissolution via fungal activity, likely of both chemical and physical nature (Figure S2.1). In the control sample (rhodochrosite without fungal inoculation), the surface after reaction with AY medium shows edge steps and isolated dissolution pits, but is otherwise smooth at the micrometer scale (Figure S2.1A). Rhodochrosite crystals reacted with fungi show isolated deep dissolution pits as well as high degrees of surface etching (Figure S2.1B-D). Further, hyphae were frequently observed growing into cracks and dissolution pits, suggesting a possible role for mechanical breakdown of the mineral thus increasing the surface area and reactivity of surface sites (*e.g.*, Figure S2.2). The importance of chemical and mechanical activity by fungi in mineral dissolution and alteration is widely known (Gadd, 2007). For instance, special penetrative structures (appressoria) in fungi possess high internal pressures that are believed responsible for hyphal penetration of plant tissues and rock/mineral surfaces (Howard et al., 1991; Money, 1999; Bonneville et al., 2009). In addition, many fungal species exude large concentrations of organic acids such as oxalic, citric, and acetic acids that are responsible for increased mineral dissolution

or precipitation of secondary mineral phases (Jongmans et al., 1997; Gadd, 1999; Sterflinger, 2000). In fact, high oxalate production by *Aspergillus niger* and *Serpula himantioides* has been shown to induce the dissolution and conversion of both rhodochrosite and Mn oxides to Mn oxalate minerals (Sayer et al., 1997; Wei et al., 2012). Here, we did not observe Mn oxalate formation via microscopic and spectroscopic analysis, likely due to the low Mn(II) levels maintained here as a result of rapid Mn(II) oxidation to Mn(III/IV).

Extensive organic surface coatings are also observed on the fungal-reacted rhodochrosite surfaces, likely contributing to mineral dissolution. For instance, on the rhodochrosite surface reacted with *Pithomyces chartarum* DS1bioJ1b (Figure S2.3A and B) and *Pleosporales* sp. AP3s5JAC2b (Figure S2.3C) a thin homogenous film is present consisting of a fibrous network identified at higher resolution (Figure S2.3B and C). In some cases, the entire mineral surface is coated with an organic-based film, which is sometimes observed peeling away from the surface, likely a consequence of biofilm desiccation during sample preparation and analysis (Figure S2.3A). Based on energy dispersive X-ray (EDX) analysis, the films are not Mn oxides and instead are composed of dominantly carbon, thus likely representing an organic matrix exuded by the fungi during growth. Fungal biofilms, which are composed of a heterogeneous mixture of extracellular polymeric substances (EPS), have been implicated in bioweathering of a variety of man-made and natural structures, including a wide range of rocks and minerals (see (Gorbushina et al., 2007) and references therein). Thus, the organic matrix observed here may exert an additional physical and chemical force on MnCO_3 weathering.

Distribution and speciation of oxidized Mn on rhodochrosite. Synchrotron-based micro-X-ray fluorescence (μ -XRF) of thin sections of rhodochrosite reacted with three fungal species (*Phoma* sp. DS1wsM30b, *Pyrenochaeta* sp. DS3sAY3a, and *Stagonospora* sp.

SRC1lsM3a) illustrated a coating of oxidized Mn, primarily as Mn(IV), on the rhodochrosite surface (Figure 2.2A-C). XRF maps were collected at several incident energies around the Mn K-edge, which revealed a transition from Mn(II) within the mineral to Mn(IV) at the surface. In a section of MnCO₃ reacted with *Stagonospora* sp. SRC1lsM3a, μ -XANES (2 × 2 mm resolution) spectra were collected at a Mn(IV) hot spot and along a transect traversing the bulk MnCO₃ and surface oxide rind confirming the energy-specific m-XRF maps (Figure 2.2C-D). The bulk MnCO₃ spectra is nearly identical to that of the Mn(II) reference compound MnCO₃, with a prominent peak at ~6552 eV and a shoulder at ~6563 eV; the shoulder is a structural feature of the extended XAS spectra and not due to Mn(IV) with the MnCO₃ spectra. Moving outward from the bulk MnCO₃ to the surface rind, the main Mn(II) peak at ~6551 eV decreases in height, while the Mn(IV) peak at ~6563 eV increases, indicating an increased ratio of Mn(IV) to Mn(II) species from the bulk mineral to the oxide rind. The spectrum at the Mn(IV) hot spot (labeled “spot”) exhibits a dominant Mn(IV) peak at ~6563 eV and a small Mn(II) shoulder at ~6552 eV, indicating that the majority of Mn is present as Mn(IV) at this location. The Mn(II) signal is likely a consequence of Mn(II) incorporation within the Mn oxide structure as observed previously for both bacteria (Bargar et al., 2005; Webb et al., 2005) and for fungi grown on agar-solidified media (Santelli et al., 2011). Similar XANES results were also observed for rhodochrosite crystals reacted with *Phoma* sp. DS1wsM30b and *Pyrenochaeta* sp. DS3sAY3a (data not shown).

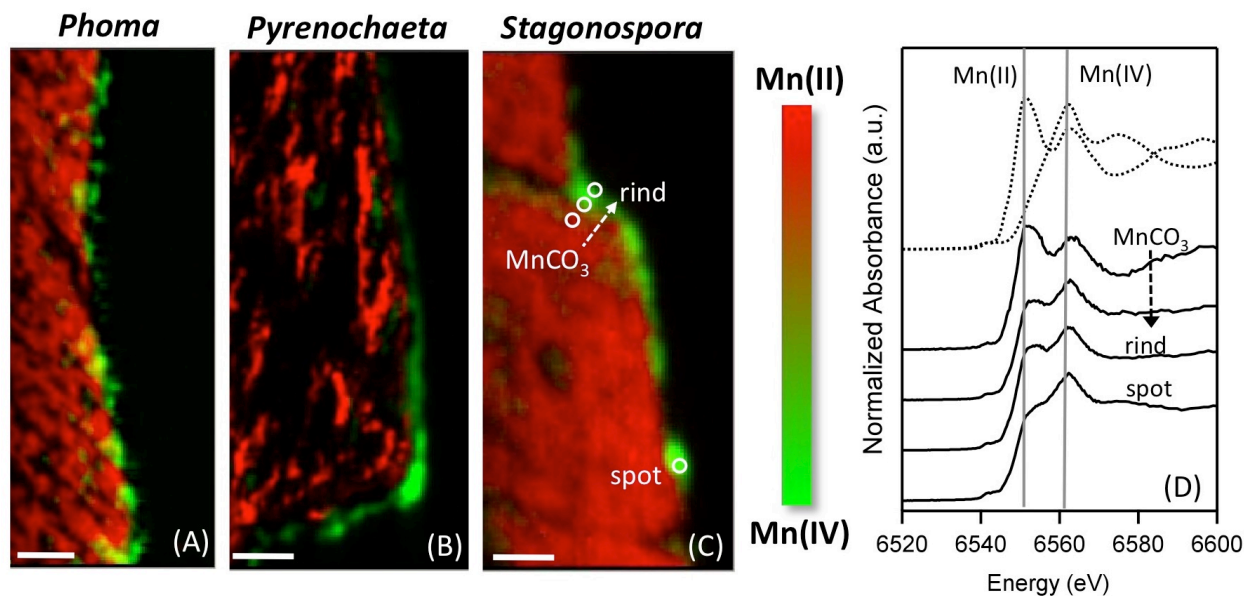


Figure 2.2. Energy-specific synchrotron μ -X-ray fluorescence (μ -XRF) maps showing Mn(II) (red color) and Mn(IV) (green color) distribution in thin sections of rhodochrosite reacted with (A) *Phoma* sp. DS1wsM30b, (B) *Pyrenochaeta* sp. DS3sAY3a, and (C) *Stagonospora* sp. SRC1lsM3a. Scale bar represents 10 mm. (D) μ -XANES spectra taken at the white circled areas in (C) (black lines), including a transect from bulk MnCO₃ to the Mn oxide rind and a Mn oxide hot spot. Also shown are the spectra of Mn(II) and Mn(IV) reference compounds (MnCO₃ and δ -MnO₂, respectively; dotted lines) and their peak positions (gray lines).

The oxidized Mn produced by all the fungal species exists as Mn oxides within the birnessite group. Principle component analysis (PCA) and linear combination fitting (LCF) of the Mn K-edge EXAFS spectra for each can be reconstructed with two dominant mineral components consisting of MnCO₃ and δ -MnO₂ (Figure S2.4 and Table 2.1). δ -MnO₂ is a synthetic phase similar to naturally occurring vernadite, which is a poorly-ordered, nanocrystalline phyllo-manganate with hexagonal symmetry. In many cases the Mn oxide products were firmly attached to the rhodochrosite surface, thus during Mn oxide harvesting for EXAFS analysis residual MnCO₃ particles were collected with the Mn oxide products. Addition of a minor aqueous Mn²⁺ component increased the goodness of fit (Table 2.1). The Mn oxides formed by all 6 fungi grown on rhodochrosite here are similar to the frequently observed biogenic Mn oxides formed by both bacteria (Villalobos et al., 2003; Bargar et al., 2005; Webb

et al., 2005; Learman et al., 2011b) and fungi (Miyata et al., 2006b; Miyata et al., 2006a; Grangeon et al., 2010; Santelli et al., 2011) under a variety of growth and environmental conditions, including the same species grown on agar-solidified media (Santelli et al., 2011).

Distribution of fungal Mn oxides. Although the Mn oxide structures did not vary among the fungal species, the distribution of Mn(III/IV) oxides varied considerably and can be summarized as (1) associated with hyphal surfaces, (2) precipitated on the rhodochrosite surface or (3) a combination of the two (Figure 2.3, Table 2.1). Rhodochrosite crystals in the absence of active fungi are pink and transparent by light microscopy (not shown). Upon reaction with the six fungal species, the crystals are gradually covered with mycelia growing radially outward from the inoculation point and extending into the media-submerged quartz sand. The fungal hyphae are colorless, whereas the precipitated fungal Mn(III/IV) oxides are brown/dark brown in color.

Two of the six species, *Phoma* sp. DS1wsM30b and *Pleosporales* sp. AP3s5JAC2b, accumulated Mn oxides along the length of their hyphae (Figure 2.3A-B, respectively). SEM images show that *Phoma* sp. DS1wsM30b produces spherical shaped Mn oxides whereas the Mn oxides formed by *Pleosporales* sp. AP3s5JAC2b uniformly coat the hyphae, over time encrusting the full length of hyphae (Figure 2.3B).

Pithomyces chartarum DS1bioJ1b and *Phoma* sp. AP3s5J1a also accumulated Mn oxides on the hyphal surface but a substantial amount of Mn oxides were also found on the MnCO₃ surface adjacent to the hyphae (Figure 2.3C-D). *Pithomyces chartarum* DS1bioJ1b produced small clusters of spherical shaped Mn oxides (Figure 2.3C), while *Phoma* sp. AP3s5J1a produced Mn oxides that encrust the hyphae (Figure 2.3D), similar to *Pleosporales* sp. AP3s5JAC2b (Figure 2.3B) but with a denser appearance.

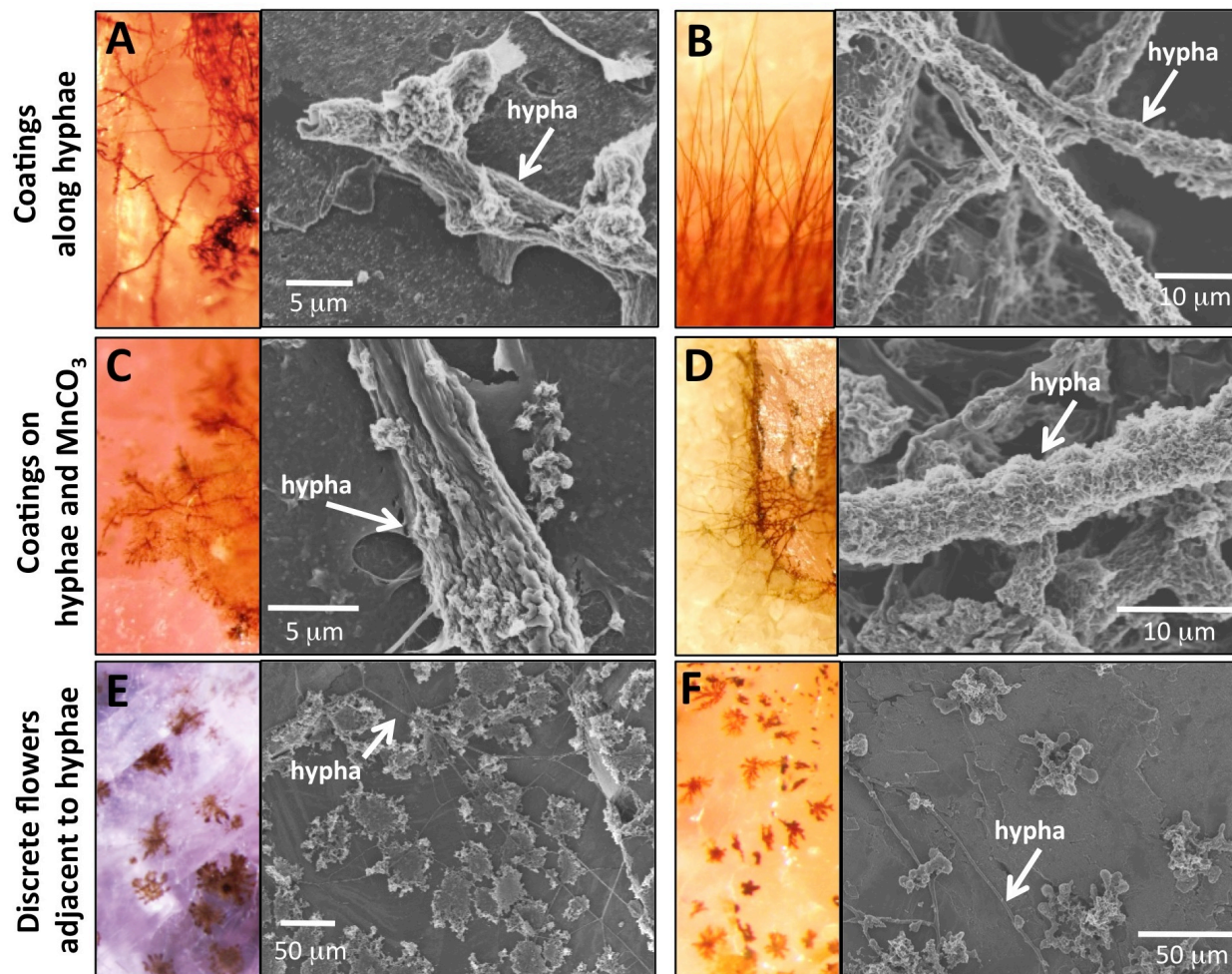


Figure 2.3. Light and electron microscopy images showing the morphology and location of Mn(II) oxides on rhodochrosite reacted with six fungal species (A – F; see Table 2.1 for species name). The brown/black color in light microscope images represents precipitated fungal Mn(III/IV) oxides.

Interestingly, two species (*Pyrenochaeta* sp. DS3sAY3a and *Stagonospora* sp. SRC11sM3a) produced discrete, isolated flower-shaped Mn oxide clusters on MnCO₃ (Figure 2.3E-F) that were typically not associated with any cellular structure. Mn oxides produced by *Pyrenochaeta* sp. DS3sAY3a (Figure 2.3E) always spread laterally (20 to 100 μm in diameter) on the MnCO₃ surface, sometimes underneath hyphae. Oxides produced by *Stagonospora* sp. SRC11sM3a appeared as flower-shaped clusters that are more structured three-dimensionally (Figure 2.3F) than those produced by *Pyrenochaeta* sp. DS3sAY3a. Further, the distance

between the Mn oxides and hyphae at times approached 100 μm – a substantial distance away from any visible cellular structure. Intact, undisturbed hyphae were observed on the MnCO_3 surface, indicating that the lack of association of hyphae and Mn oxides was not an artifact of the preparation procedure.

The striking difference in the morphology and location of Mn oxides formed by different species likely points to different Mn(II) oxidation pathways or precipitation mechanisms, including but not limited to direct enzymatic oxidation, metabolite (*e.g.*, O_2^-) mediated oxidation, and/or organic-mediated complexation and/or precipitation. For example, the production of Mn oxide coatings on hyphal surfaces (*e.g.*, Figure 2.3B) likely involves cell wall associated enzymes (*e.g.*, laccase-like multicopper oxidases as found in *Acremonium strictum* strain KR21-2) (Miyata et al., 2004; Miyata et al., 2006a). On the contrary, the production of extracellular Mn oxide clusters that are not associated with cellular structures (*e.g.*, Figure 2.3E-F) may point to either a metabolite induced oxidation or surface associated oxidation to Mn(III) followed by complexation, transport away from the cell, and ultimate precipitation at a distance. We have previously observed a similar species-based variability in Mn oxide distributions on agar-solidified media, which included Mn oxide formation by *Stagonospora* sp. SRC1lsM3a on envisaged organic polymers adjacent to hyphae (Santelli et al., 2011). A striking finding with this current study and not noticed previously, however, is the presence of completely isolated Mn oxides precipitated on the MnCO_3 surface at substantial distances from cellular structures. We focus the remaining discussion on *Pyrenochaeta* sp. DS3sAY3a and *Stagonospora* sp. SRC1lsM3a to identify a plausible pathway for Mn oxide accumulation in the absence of cellular structures.

Mechanisms of Mn(II) oxidation. The oxidation of Mn(II) by *Pyrenochaeta* sp. DS3sAY3a and *Stagonospora* sp. SRC1sM3a is a cell-associated process and not a result of soluble extracellular proteins or stable metabolites. Cell-free filtrate (*i.e.*, spent media) from both organisms, obtained for cells grown both in AY liquid and on AY media-saturated quartz sand, did not oxidize either aqueous Mn(II) or Mn(II) hosted in rhodochrosite (data not shown). Thus, Mn oxide formation required the presence of actively growing hyphal cells, likely due to either cell-associated enzymes or short-lived reactive metabolites. These results are in contrast to recent findings of superoxide-mediated oxidation of Mn(II) by bacteria where the proteins involved in superoxide production were present and active in cell-free filtrate, suggesting the involvement of soluble enzyme(s) in that case (Learman et al., 2011a).

Incubation of fungal cultures with ROS-specific stains and various amendments to the AY growth medium implicate extracellular superoxide as the oxidant of Mn(II) by *Pyrenochaeta* sp. DS3sAY3a and *Stagonospora* sp. SRC1sM3a (Figure 2.4). Yellow, water-soluble nitroblue tetrazolium (NBT) is reduced by superoxide to form blue, water-insoluble formazan. Since the stain precipitates upon reaction with superoxide, the location of the stain precipitates reveals the site of reaction with the superoxide. Both actively growing organisms stain positively for the production of O_2^- (appearance of a blue color when incubated with NBT; Figure 2.4A and B). Superoxide production is localized primarily at the hyphal tips of the leading growth edge (Figure 2.4C), areas known for high metabolic activity and active cell construction.

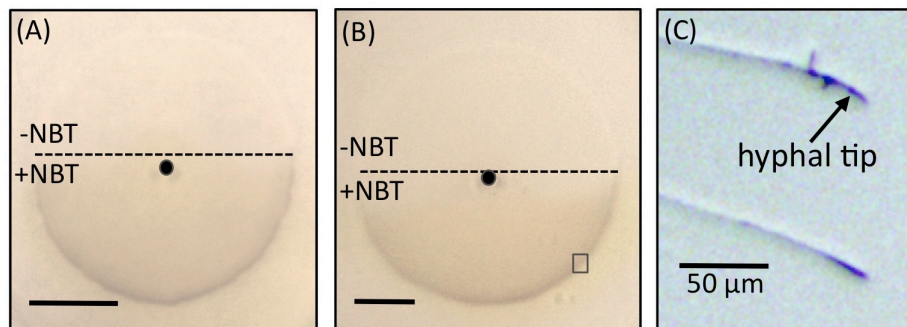


Figure 2.4. Distribution of superoxide for *Pyrenochaeta* sp. DS3sAY3a (A) and *Stagonospora* sp. SRC11sM3a (B and C). Images show circular fungal mycelia on AY agar plates after approximately 2 weeks of growth starting from a center inoculation point (indicated by a black dot). (A, B) Lower portions of mycelia (below dotted lines) were stained with NBT. Blue color indicates the presence of O_2^- . Cells were grown without added Mn(II). Scale bars are 1 cm. (C) Higher magnification image of the leading hyphal edge of *Stagonospora* sp. SRC11sM3a (as indicated in boxed region in (B)) indicating the distribution of superoxide at the hyphal tip. Scale bar = 50 μ m.

Furthermore, Mn(II) oxidation showed a concentration dependent inhibition by Cu(II). At the highest concentration (200 mM), Mn oxide precipitation is strongly inhibited for both *Pyrenochaeta* and *Stagonospora* (Figure 2.5C and G, respectively), whereas the addition of the same concentration of Zn(II) does not appreciably affect Mn oxidation (Figure 2.5D and H). Cu(II) catalyzes the dismutation of O_2^- into O_2 and H_2O_2 (Zafiriou et al., 1998) and is a more effective scavenger of O_2^- than Mn(II), thereby diverting fungal produced extracellular superoxide away from Mn(II) in the media. Zn(II) is used as a control, since this metal imparts a similar level of toxicity to the organisms as Cu(II) but does not interact with O_2^- . Although 200 μ M Cu and Zn each impart a slight reduction in growth rate of the fungal mycelium in both organisms (e.g., compare Figure 2.5C and G with A and E, respectively), the impacts of the two metals are similar and do not confound the implication of O_2^- in Mn(II) oxidation. Taken together with the observations of superoxide formation at hyphal tips, these findings implicate superoxide as the oxidant of Mn(II) by both fungal species. The primary enzymes responsible

for superoxide production in fungi are NADPH oxidases within the NOX family (Aguirre et al., 2005; Scott and Eaton, 2008).

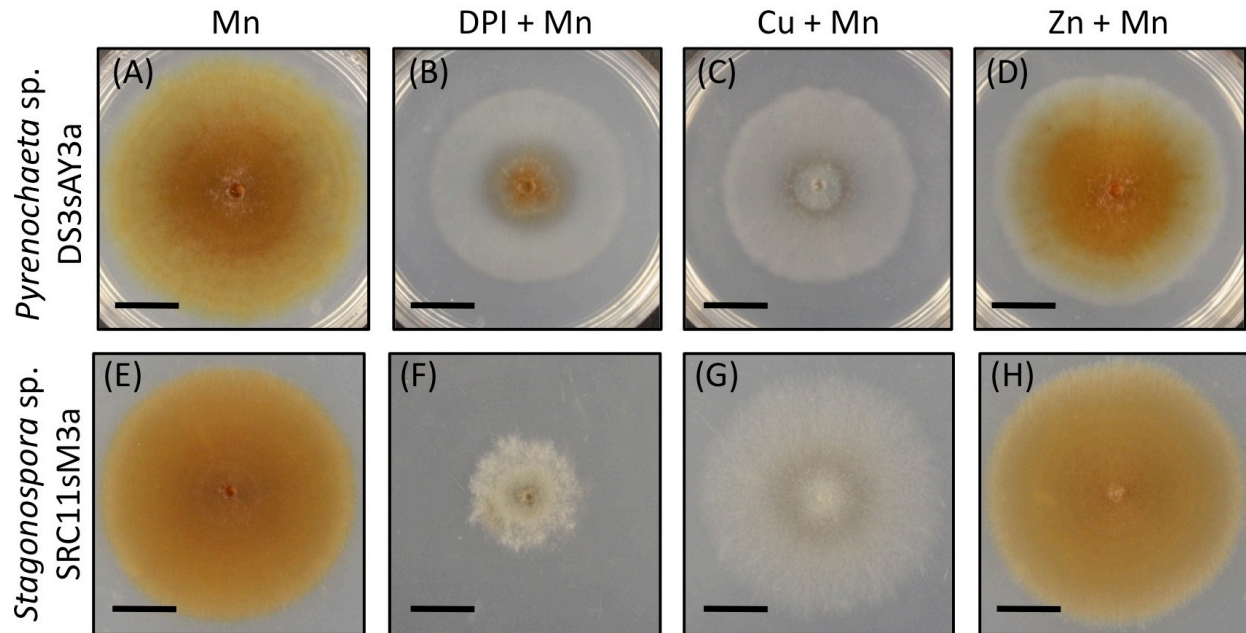


Figure 2.5. Impact of chemical/enzyme inhibitors on Mn oxide formation by *Pyrenochaeta* sp. DS3sAY3a (A to D) and *Stagonospora* sp. SRC11sM3a (E to H). (A,E) AY agar controls amended with 200 μ M Mn(II). Brown color indicates mycogenic Mn oxides. (B,F) Cells grown with 200 μ M Mn(II) and 25 μ M (B) or 10 μ M (F) DPI, an inhibitor of NADPH oxidases. (C,G) Cells grown with 200 μ M Mn(II) and 200 μ M Cu(II), a scavenger of superoxide. (D,H) Cells grown with 200 μ M Mn(II) and 200 μ M Zn(II). Zn(II) imparts a similar level of toxicity as Cu(II) but does not react with superoxide. All scale bars are 1 cm.

Indeed, superoxide production and subsequent Mn(II) oxidation is linked to the activity of NADPH oxidases in both *Pyrenochaeta* sp. DS3sAY3a and *Stagonospora* sp. SRC1sM3a. Mn oxide precipitation is substantially decreased in the presence of 25 μ M (Figure 2.5B) and 10 mM (Figure 2.5F) diphenylene iodonium (DPI) chloride, an inhibitor of oxidoreductases and other NAD(P)H binding enzymes known to produce superoxide in fungi (O'Donnell et al., 1993). This superoxide is involved in host defense, post-translational modification of proteins, apical growth and branching of hyphae, cell signaling, and cell differentiation (Aguirre et al., 2005). Here, in addition to Mn(II) oxidation inhibition, the addition of DPI leads to a decrease in fungal

growth, particularly for *Stagonospora* sp. SRC1sM3a, likely due to disruption of hyphal growth. NOX proteins in fungi are transmembrane proteins that transport electrons from cytosolic NADPH via FAD and two hemes to extracellular molecular oxygen to generate O_2^- . This localization is consistent with the lack of Mn(II) oxidation activity in cell-free extracts, whereby the production of superoxide occurs at the cell surface leading to reaction between superoxide and Mn(II) near the hyphal surface. These results are similar to recent findings that the Ascomycete *Stilbella aciculosa* oxidizes Mn(II) via superoxide production during asexual reproduction (Hansel et al., 2012), suggesting that this ROS-mediated Mn(II) oxidation mechanism may be common among Ascomycetes.

Interestingly, in both *Pyrenochaeta* sp. DS3sAY3a and *Stagonospora* sp. SRC1sM3a, small, spherical Mn oxides (confirmed via addition of LBB) were produced at a distance from fungal hyphae in the presence of high Cu(II) levels (Figure S2.5C and G) and DPI (Figure S2.5B and F). It is unclear at this time the mechanism of Mn(II) oxidation responsible for these structures, but considering they are observed only in the presence of high Cu and DPI, this may be a consequence of a stress response.

Taken together, the primary mechanism of Mn(II) oxidation by *Pyrenochaeta* sp. DS3sAY3a and *Stagonospora* sp. SRC1sM3a is a result of extracellular superoxide production at the hyphal surface (Figures 2.4 and 2.5) due to the activity of transmembrane NADPH oxidases. The oxidation of Mn(II) by superoxide produces Mn(III), which is thermodynamically unstable in aqueous solutions. Yet, the Mn oxides produced by *Pyrenochaeta* sp. DS3sAY3a and *Stagonospora* sp. SRC1sM3a show no association with hyphae and appear as discrete clusters at a substantial distance (10-100 μ m) from cellular structures (Figure 2.3). This suggests that either Mn(III) is being stabilized and transported away from the cell surface or superoxide is

diffusing away from the hyphal tip and reacting with Mn(II) away from the cell. However, the localized precipitation of the NBT stain at hyphal tips suggests that superoxide is not diffusing far from the site of formation (Figure 2.4). Instead, stabilization of Mn(III) could occur via complexation with an organic ligand and/or siderophore allowing for its transport away from the hyphae until the discrete flower-shaped Mn oxides precipitate.

Mn oxides formed following superoxide mediated Mn(II) oxidation. The Mn oxides produced by *Pyrenochaeta* sp. DS3sAY3a and *Stagonospora* sp. SRC1lsM3a are unique in character and illustrate an intriguing ordered morphology (Figure 2.6) suggesting that mineral growth was directed by an unknown organic template. Although the oxides produced by *Pyrenochaeta* sp. DS3sAY3a were more spread out laterally (Figure 2.6A) and those produced by *Stagonospora* sp. SRC1lsM3a were more structured three dimensionally (Figure 2.6D), close examination of both fungal Mn oxides revealed similar densely packed threads of oxides that were tens to hundreds of nanometers in diameter and a few microns in length (Figure 2.6B, C, E, and F). Some aggregated fibers observed for *Stagonospora* sp. SRC1lsM3a had a round feature at the end (Figure 2.6F and Figure 2.7), which to our knowledge is a morphology unique to this organism. The interesting morphology of Mn oxides produced by these two species is similar to previously reported *Metallogenium*-like structures (Klaveness, 1977; Emerson et al., 1989). Such structures have been observed in a variety of modern and ancient aquatic and terrestrial environments (Perfil'ev and Gabe, 1961; Crerar et al., 1980; Gregory et al., 1980; Dubinina, 1984; Neretin et al., 2003). *Metallogenium* was originally described as a genus of bacteria that is capable of oxidizing Mn(II) (Perfil'ev and Gabe, 1961). However, a later study (Emerson et al., 1989) revealed that these filamentous Mn oxides were not templated on any cellular structure

(bacterial or fungal) and were instead precipitated on a matrix of anionic polymers, likely consisting of acidic polysaccharides and/or proteins.

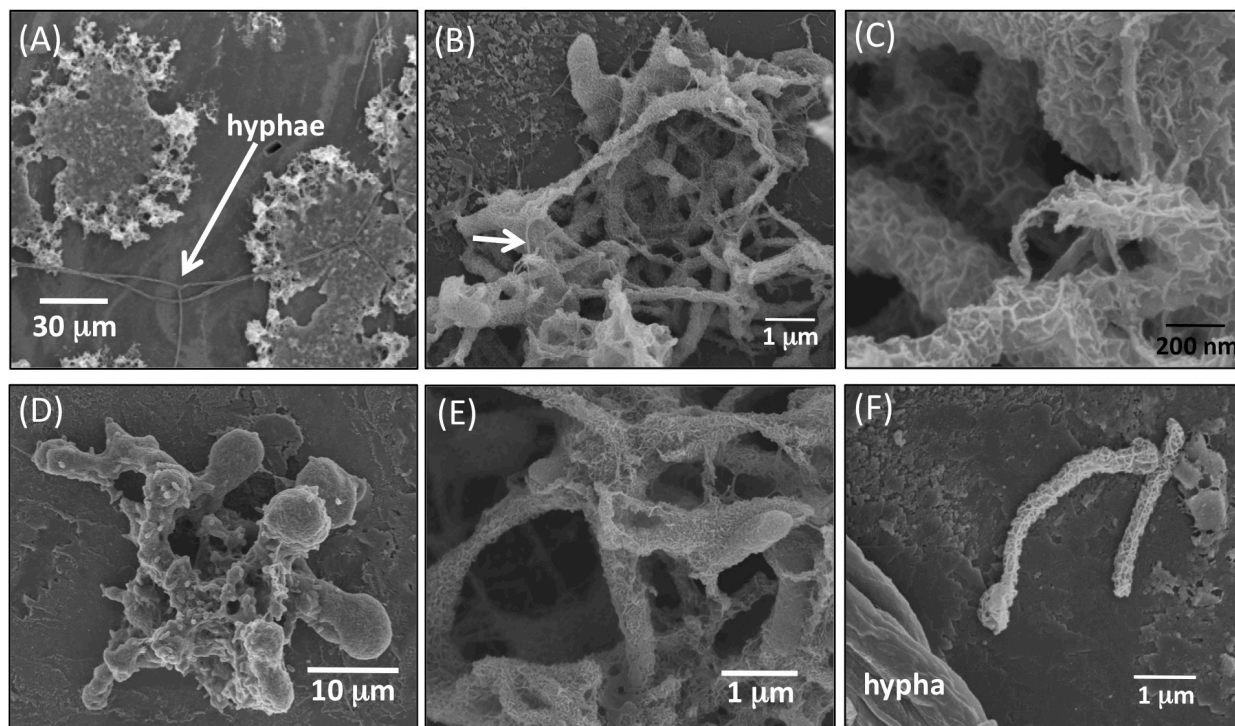


Figure 2.6. SEM images of the Mn oxides formed by (A – C) *Pyrenochaeta* sp. DS3sAY3a and (D – F) *Stagonospora* sp. SRC1lsM3a grown on rhodochrosite. Images illustrate structurally unique Mn oxides with visible unknown filaments (see arrow in B) within the oxides. Hyphae are not in the field of view for images B through E.

Indeed, similar to *Metallogenium*-like structures, high resolution TEM imaging of the Mn oxides did not reveal any observable cellular structures associated with the Mn oxides (Figure 2.7). We have shown previously that the Mn oxides formed by *Stagonospora* sp. on Mn(II)-supplemented agar-solidified medium and in liquid culture appeared as dense masses of Mn oxides composed of filaments not templated on any visible cellular structure (Santelli et al., 2011). Both TEM imaging of whole mounts (Figure 2.7A-C) and high resolution imaging of thin sections (Figure 2.7D) do not reveal any visible cellular structure within the Mn oxides. Instead, the Mn oxides appear highly ordered with radial growth along what appears to be a

directed growth front. In fact, thin unidentified filaments are observed emerging from the Mn oxides precipitated on MnCO_3 (see arrow in Figure 2.6B) that are not Mn oxides and are too thin to be fungal hyphae. These filaments may in fact be involved in the directed growth. Similarly, organic-directed growth has been proposed for Mn and Fe oxide encrustations on the surfaces of budding and sheathed bacteria (Ghiorse, 1984) and bacterial stalks (Chan et al., 2004; Chan et al., 2009). In fact, our preliminary μ -FTIR analysis of Mn oxides reveals the presence of various organic functional groups (*e.g.*, amide I and II groups) (Figure S2.6), hinting at the presence of protein templates. We are actively investigating the mechanisms of Mn(III) transport and Mn oxide formation, including the role of organic templates, by *Pyrenochaeta* sp. DS3sAY3a and *Stagonospora* sp. SRC1lsM3a.

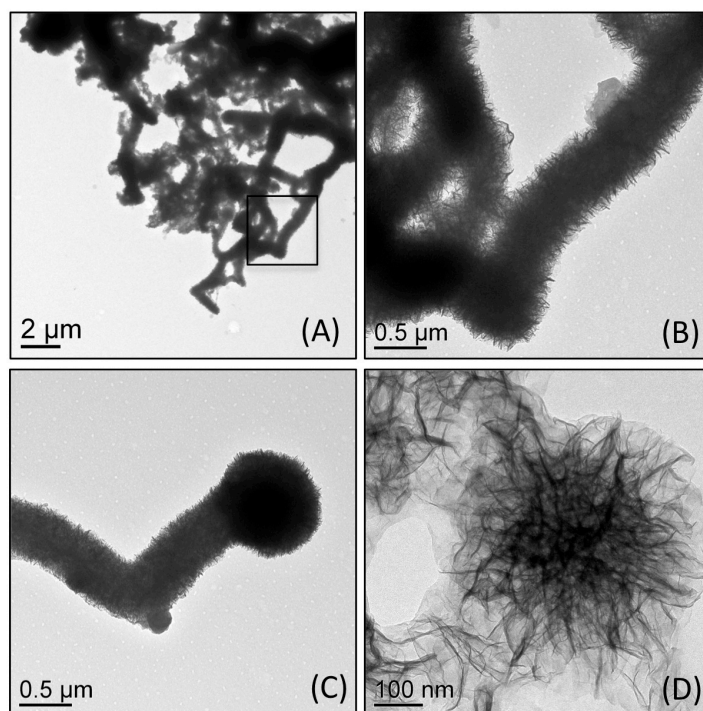


Figure 2.7. TEM images of whole mounts (A – C) and cross-section (D) of Mn oxides produced by *Stagonospora* sp. SRC1lsM3a grown in liquid AY medium. (A) An aggregate of extracellular, thread-like Mn oxides. (B) Magnified view of boxed area in (A). (C) An individual thread-like Mn oxide filament with a ball-like feature at the tip. (D) Cross-section of a ball-like feature (modified from Santelli et al., 2011).

In this study, we show that fungi can be agents of rhodochrosite dissolution and conversion to Mn oxides, minerals of substantial relevance in metal and nutrient availability and transport. Rhodochrosite dissolution was substantially enhanced in the presence of the fungi. In particular, the activity of some fungi released/oxidized up to 25% of the mineral-hosted Mn(II) within 22 days. Fungal activity could therefore be a dominant process for rhodochrosite dissolution within sediments and soils. Despite the similarity in the structures of the Mn oxides produced by 6 fungal species, we show that the morphology of the oxides produced and the location relative to the fungal and mineral surface varies among the species. As suggested previously for agar-supported fungal growth (Santelli et al., 2011), these differences likely point to more than one operative Mn(II) oxidation pathway employed by fungi. The formation of Mn oxides at substantial distances away from the hyphae of *Pyrenochaeta* sp. DS3sAY3a and *Stagonospora* sp. SRC11sM3a are attributed to Mn(II) oxidation by extracellular superoxide at the hyphal surface likely followed by Mn(III)-complexation and ultimately heterogeneous precipitation. Thus, these findings expand the group of organisms that oxidize Mn(II) by producing superoxide (Learman et al., 2011a; Hansel et al., 2012), where here it is likely a result of cell differentiation. The unique morphology of the isolated flower-like Mn oxide clusters and presence of organic functional groups associated with these oxides suggests a role of mycogenic organic polymers in Mn oxide templation. Further investigations are underway to define the role and composition of organic molecules (likely protein) in directed precipitation. These findings highlight the diversity of fungi-Mn oxide relationships and processes responsible for fungal Mn oxide precipitation. Building off this foundation, this research will shed light on environmental Mn oxide formation, including the frequently observed *Metallogenium*-like Mn oxide structures.

Acknowledgements

The authors thank Adiari I. Vázquez-Rodríguez for help with thin section preparation, Christopher Lentini and Emily Estes for help with EXAFS data collection, and Alice Dohnalkova (EMSL) for assistance in TEM collection. The authors also thank Associate Editor Victoria Orphan and the anonymous reviewers for their helpful suggestions. Portions of this research were conducted at the Stanford Synchrotron Radiation Lightsource (SSRL), the National Synchrotron Light Source (NSLS), the Center for Nanoscale Systems (CNS) at Harvard University, and the Environmental Molecular Sciences Lab (EMSL). SSRL is a national user facility operated by Stanford University on behalf of the U.S. Department of Energy, Office of Basic Energy Sciences. The SSRL Structural Molecular Biology Program is supported by the Department of Energy, Office of Biological and Environmental Research, and by the National Institutes of Health, National Center for Research Resources, Biomedical Technology Program. NSLS is supported by the US Department of Energy, Office of Science, Office of Basic Energy Sciences, under Contract No. DE-AC02-98CH10886. CNS is a member of the National Nanotechnology Infrastructure Network (NNIN), which is supported by the National Science Foundation under NSF Award No. ECS-0335765. CNS is part of the Faculty of Arts and Sciences at Harvard University. EMSL is a national scientific user facility sponsored by the Department of Energy's Office of Biological and Environmental Research located at Pacific Northwest National Laboratory. This project was funded by the National Science Foundation, Grant Number EAR-0846715, awarded to C.M.H.

References

- Aguirre, J., Rios-Momberg, M., Hewitt, D., and Hansberg, W. (2005) Reactive oxygen species and development in microbial eukaryotes. *Trends Microb* **13**: 111-118.
- Bargar, J.R., Tebo, B.M., Bergmann, U., Webb, S.M., Glatzel, P., Chiu, V.Q., and Villalobos, M. (2005) Biotic and abiotic products of Mn(II) oxidation by spores of the marine *Bacillus* sp. strain SG-1. *Am Mineral* **90**: 143-154.
- Bedard, K., Lardy, B., and Krause, K.H. (2007) NOX family NADPH oxidases: Not just in mammals. *Biochimie* **89**: 1107-1112.
- Bonneville, S., Smits, M.M., Brown, A., Harrington, J., Leake, J.R., Brydson, R., and Benning, L.G. (2009) Plant-driven fungal weathering: Early stages of mineral alteration at the nanometer scale. *Geology* **37**: 615-618.
- Cahyani, V.R., Murase, J., Ishibashi, E., Asakawa, S., and Kimura, M. (2009) Phylogenetic positions of Mn(2+)-oxidizing bacteria and fungi isolated from Mn nodules in rice field subsoils. *Biology and Fertility of Soils* **45**: 337-346.
- Chan, C.S., Fakra, S.C., Edwards, D.C., Emerson, D., and Banfield, J.F. (2009) Iron oxyhydroxide mineralization on microbial extracellular polysaccharides. *Geochimica Et Cosmochimica Acta* **73**: 3807-3818.
- Chan, C.S., Fakra, S.C., Emerson, D., Fleming, E.J., and Edwards, K.J. (2011) Lithotrophic iron-oxidizing bacteria produce organic stalks to control mineral growth: implications for biosignature formation. *ISME J* **5**: 717-727.
- Chan, C.S., De Stasio, G., Welch, S.A., Girasole, M., Frazer, B.H., Nesterova, M.V. et al. (2004) Microbial polysaccharides template assembly of nanocrystal fibers. *Science* **303**: 1656-1658.
- Chen, G.Q., Zou, Z.J., Zeng, G.M., Yan, M., Fan, J.Q., Chen, A.W. et al. (2011) Coarsening of extracellularly biosynthesized cadmium crystal particles induced by thioacetamide in solution. *Chemosphere* **83**: 1201-1207.
- Crerar, D.A., Fisher, A.G., and Plaza, C.L. (1980) *Metallogenium* and biogenic deposition of manganese from Precambrian to recent time. In *Geology and Geochemistry of Manganese Volume III Manganese on the Bottom of Recent Basins*. Vanentsov, I.M., and Grasselly, G. (eds). Verlagsbuchhandlung: Stuttgart, pp. 285-303.
- de la Torre, M.A., and Gomez-Alarcon, G. (1994) Manganese and iron oxidation by fungi isolated from building stone. *Microb Ecol* **27**: 177-188.

- Diem, D., and Stumm, W. (1984) Is dissolved Mn^{2+} being oxidized by O_2 in absence of Mn-bacteria or surface catalysts. *Geochimica et Cosmochimica Acta* **48**: 1571-1573.
- Dubinina, G.A. (1984) Infection of procaryotic and eukaryotic microorganisms with *Metallogenium*. *Current Microbiology* **11**: 349-356.
- Emerson, D., Garen, R.E., and Ghiorse, W.C. (1989) Formation of *Metallogenium*-like structures by a manganese-oxidizing fungus. *Arch Microbiol* **151**: 223-231.
- Feng, X.H., Zhu, M.Q., Ginder-Vogel, M., Ni, C.Y., Parikh, S.J., and Sparks, D.L. (2010) Formation of nano-crystalline todorokite from biogenic Mn oxides. *Geochimica et Cosmochimica Acta* **74**: 3232-3245.
- Gadd, G.M. (1999) Fungal production of citric and oxalic acid: Importance in metal speciation, physiology and biogeochemical processes. *Advances in Microbial Physiology, Vol 41* **41**: 47-92.
- Gadd, G.M. (2007) Geomycology: biogeochemical transformations of rocks, minerals, metals and radionuclides by fungi, bioweathering and bioremediation. *Mycological Research* **111**: 3-49.
- Ghiorse, W.C. (1984) Biology of iron- and manganese-depositing bacteria. *Annual Review of Microbiology* **38**: 515-550.
- Ghiorse, W.C., and Hirsch, P. (1979) Ultrastructural-study of iron and manganese deposition associated with extracellular polymers of *Pedomicrobium*-like budding bacteria. *Arch Microbiol* **123**: 213-226.
- Glenn, J.K., Akileswaran, L., and Gold, M.H. (1986) Mn(II) oxidation is the principal function of the extracellular Mn-peroxidase from *Phanerochaete chrysosporium*. *Arch Biochem Biophys* **251**: 688-696.
- Golden, D., Zuberer, D., and Dixon, J. (1992) Manganese oxides produced by fungal oxidation of manganese from siderite and rhodochrosite. In *Biomineralization processes of iron and manganese: Modern and ancient environments (Catena Supplement)*. Skinner, H.C.W., and Fitzpatrick, R.W. (eds). Germany: Cremlingen-Destedt, pp. 161-168.
- Gorbushina, A.A., Kort, R., Schulte, A., Lazarus, D., Schnetger, B., Brumsack, H.J. et al. (2007) Life in Darwin's dust: intercontinental transport and survival of microbes in the nineteenth century. *Environmental Microbiology* **9**: 2911-2922.
- Goto, K., Komatsu, T., and Furukawa, T. (1962) Rapid colorimetric determination of manganese in waters containing iron - A modification of formaldoxime method. *Analytica Chimica Acta* **27**: 331-334.

- Grangeon, S., Lanson, B., Miyata, N., Tani, Y., and Manceau, A. (2010) Structure of nanocrystalline phyllomanganates produced by freshwater fungi. *American Mineralogist* **95**: 1608-1616.
- Gregory, E., Perry, R.S., and Staley, J.T. (1980) Characterization, distribution, and significance of *Metallogenium* in Lake Washington. *Microb Ecol* **6**: 125-140.
- Hansard, S.P., Easter, H.D., and Voelker, B.M. (2011) Rapid reaction of nanomolar Mn(II) with superoxide radical in seawater and simulated freshwater. *Environ Sci Technol* **45**: 2811-2817.
- Hansel, C.M., and Francis, C.A. (2006) Coupled photochemical and enzymatic Mn(II) oxidation pathways of a planktonic *Roseobacter*-like bacterium. *Appl Environ Microbiol* **72**: 3543-3549.
- Hansel, C.M., Zeiner, C.A., Santelli, C.M., and Webb, S.M. (2012) Mn(II) oxidation by an ascomycete fungus is linked to superoxide production during asexual reproduction. *PNAS* **109**: 12621-12625.
- Höfer, C., and Schlosser, D. (1999) Novel enzymatic oxidation of Mn²⁺ to Mn³⁺ catalyzed by a fungal laccase. *FEBS Lett* **451**: 186-190.
- Howard, R.J., Ferrari, M.A., Roach, D.H., and Money, N.P. (1991) Penetration of hard substrates by a fungus employing enormous turgor pressures. *Proceedings of the National Academy of Sciences of the United States of America* **88**: 11281-11284.
- Jongmans, A.G., vanBreemen, N., Lundstrom, U., vanHees, P.A.W., Finlay, R.D., Srinivasan, M. et al. (1997) Rock-eating fungi. *Nature* **389**: 682-683.
- Klaveness, D. (1977) Morphology, distribution and significance of manganese-accumulating microorganism *Metallogenium* in lakes. *Hydrobiologia* **56**: 25-33.
- Klewicki, J.K., and Morgan, J.J. (1998) Kinetic behavior of Mn(III) complexes of pyrophosphate, EDTA, and citrate. *Environmental Science & Technology* **32**: 2916-2922.
- Klewicki, J.K., and Morgan, J.J. (1999) Dissolution of beta-MnOOH particles by ligands: Pyrophosphate, ethylenediaminetetraacetate, and citrate. *Geochimica Et Cosmochimica Acta* **63**: 3017-3024.
- Kostka, J.E., Luther, G.W., and Nealson, K.H. (1995) Chemical and biological reduction of Mn(III)-pyrophosphate complexes - potential importance of dissolved Mn(III) as an environmental oxidant. *Geochim Cosmochim Acta* **59**: 885-894.

- Krumbein, W.E., and Altmann, H.J. (1973) A new method for detection and enumeration of manganese oxidizing and reducing microorganisms. *Helgolander Wissenschaftliche Meeresuntersuchungen* **25**: 347-356.
- Lafferty, B.J., Ginder-Vogel, M., and Sparks, D.L. (2010) Arsenite oxidation by a poorly crystalline manganese oxide. 1. Stirred-flow experiments. *Environ Sci Technol* **44**: 8460-8466.
- Learman, D.R., Voelker, B.M., Vazquez-Rodriguez, A.I., and Hansel, C.M. (2011a) Formation of manganese oxides by bacterially generated superoxide. *Nature Geoscience* **4**: 95-98.
- Learman, D.R., Wankel, S.D., Webb, S.M., Martinez, N., Madden, A.S., and Hansel, C.M. (2011b) Coupled biotic-abiotic Mn(II) oxidation pathway mediates the formation and structural evolution of biogenic Mn oxides. *Geochimica et Cosmochimica Acta* **75**: 6048-6063.
- Lenz, M., Kolvenbach, B., Gygax, B., Moes, S., and Corvini, P.F.X. (2011) Shedding light on selenium biomineralization: Proteins associated with bionanominerals. *Appl Environ Microbiol* **77**: 4676-4680.
- Luther, G.W. (2005) Manganese(II) oxidation and Mn(IV) reduction in the environment - Two one-electron transfer steps versus a single two-electron step. *Geomicrobiol J* **22**: 195-203.
- Luther, G.W. (2010) The role of one- and two-electron transfer reactions in forming thermodynamically unstable intermediates as barriers in multi-electron redox reactions. *Aquatic Geochem* **16**: 395-420.
- Luther, G.W., Ruppel, D.T., and Burkhard, C. (1998) Reactivity of dissolved Mn(III) complexes and Mn(IV) species with reductants: Mn redox chemistry without a dissolution step. In *ACS Symposium Series, vol 715 Mineral-Water Interfacial Reactions: Kinetics and Mechanisms*. Sparks, D.L., and Grundl, T.J. (eds). Washington, D. C.: American Chemical Society, pp. 265-280.
- Miyata, N., Tani, Y., Iwahori, K., and Soma, M. (2004) Enzymatic formation of manganese oxides by an *Acremonium*-like hyphomycete fungus, strain KR21-2. *FEMS Microbiol Ecol* **47**: 101-109.
- Miyata, N., Tani, Y., Sakata, M., and Iwahori, K. (2007) Microbial manganese oxide formation and interaction with toxic metal ions. *Journal of Bioscience and Bioengineering* **104**: 1-8.
- Miyata, N., Tani, Y., Maruo, K., Tsuno, H., Sakata, M., and Iwahori, K. (2006a) Manganese(IV) oxide production by *Acremonium* sp. strain KR21-2 and extracellular Mn(II) oxidase activity. *Appl Environ Microbiol* **72**: 6467-6473.

- Miyata, N., Maruo, K., Tani, Y., Tsuno, H., Seyama, H., Soma, M., and Iwahori, K. (2006b) Production of biogenic manganese oxides by anamorphic ascomycete fungi isolated from streambed pebbles. *Geomicrobiology Journal* **23**: 63-73.
- Money, N.P. (1999) Biophysics - Fungus punches its way in. *Nature* **401**: 332-333.
- Moreau, J.W., Weber, P.K., Martin, M.C., Gilbert, B., Hutcheon, I.D., and Banfield, J.F. (2007) Extracellular proteins limit the dispersal of biogenic nanoparticles. *Science* **316**: 1600-1603.
- Murray, K.J., and Tebo, B.M. (2007) Cr(III) is indirectly oxidized by the Mn(II)-oxidizing bacterium *Bacillus* sp. strain SG-1. *Environ Sci Technol* **41**: 528-533.
- Murray, K.J., Webb, S.M., Bargar, J.R., and Tebo, B.M. (2007) Indirect oxidation of Co(III) in the presence of the marine Mn(II)-oxidizing bacterium *Bacillus* sp. strain SG-1. *Appl Environ Microbiol* **73**: 6905-6909.
- Nealson, K.H., and Saffarini, D. (1994) Iron and manganese in anaerobic respiration - Environmental significance, physiology, and regulation. *Annual Review of Microbiology* **48**: 311-343.
- Neretin, L.N., Pohl, C., Jost, G., Leipe, T., and Pollehne, F. (2003) Manganese cycling in the Gotland Deep, Baltic Sea. *Marine Chemistry* **82**: 125-143.
- Nico, P.S., Anastasio, C., and Zamoski, R.J. (2002) Rapid photo-oxidation of Mn(II) mediated by humic substances. *Geochim Cosmochim Acta* **66**: 4047-4056.
- O'Donnell, V.B., Tew, D.G., Jones, T.G.E., and England, P.J. (1993) Studies on the inhibitory mechanism of iodonium compounds with special reference to neutrophil NADPH oxidase. *Biochem J* **290**: 41-49.
- Perfil'ev, B.V., and Gabe, D.R. (1961) *The capillary methods of studying microorganisms [in Russian]*. Moscow: Izdatel'stvo Akademii Nauk SSSR.
- Petkov, V., Ren, Y., Saratovsky, I., Pasten, P., Gurr, S.J., Hayward, M.A. et al. (2009) Atomic-scale structure of biogenic materials by total X-ray diffraction: A study of bacterial and fungal MnO_x. *ACS Nano* **3**: 441-445.
- Ravel, B., and Newville, M. (2005) ATHENA, ARTEMIS, HEPHAESTUS: data analysis for X-ray absorption spectroscopy using IFEFFIT. *Journal of Synchrotron Radiation* **12**: 537-541.
- Santelli, C.M., Chaput, D.L., and Hansel, C.M. (2014) Microbial communities promoting Mn(II) oxidation in Ashumet Pond, a historically polluted freshwater pond undergoing remediation. *Geomicrobiol J* **31**: 605-616.

Santelli, C.M., Webb, S.M., Dohnalkova, A.C., and Hansel, C.M. (2011) Diversity of Mn oxides produced by Mn(II)-oxidizing fungi. *Geochimica et Cosmochimica Acta* **75**: 2762-2776.

Santelli, C.M., Pfister, D.H., Lazarus, D., Sun, L., Burgos, W.D., and Hansel, C.M. (2010) Promotion of Mn(II) oxidation and remediation of coal mine drainage in passive treatment systems by diverse fungal and bacterial communities. *Appl Environ Microbiol* **76**: 4871-4875.

Saratovsky, I., Gurr, S.J., and Hayward, M.A. (2009) The structure of manganese oxide formed by the fungus *Acremonium* sp. strain KR21-2. *Geochim Cosmochim Acta* **73**: 3291-3300.

Sayer, J.A., Kierans, M., and Gadd, G.M. (1997) Solubilisation of some naturally occurring metal-bearing minerals, limescale, and lead phosphate by *Aspergillus niger*. *FEMS Microbiol Lett* **154**: 29-35.

Schlosser, D., and Höfer, C. (2002) Laccase-catalyzed oxidation of Mn²⁺ in the presence of natural Mn³⁺ chelators as a novel source of extracellular H₂O₂ production and its impact on manganese peroxidase. *Appl Environ Microbiol* **68**: 3514-3521.

Scott, B., and Eaton, C.J. (2008) Role of reactive oxygen species in fungal cellular differentiations. *Curr Op Microb* **11**: 488-493.

Semighini, C.P., and Harris, S.D. (2008) Regulation of apical dominance in *Aspergillus nidulans* hyphae by reactive oxygen species. *Genetics* **179**: 1919-1932.

Sterflinger, K. (2000) Fungi as geologic agents. *Geomicrobiology Journal* **17**: 97-124.

Stone, A.T., and Morgan, J.J. (1984) Reduction and dissolution of manganese(III) and manganese(IV) oxides by organics. 1. Reaction with hydroquinone. *Environmental Science & Technology* **18**: 450-456.

Sunda, W.G., and Kieber, D.J. (1994) Oxidation of humic substances by manganese oxides yields low-molecular-weight organic substrates. *Nature* **367**: 62-64.

Takemoto, D., Tanaka, A., and Scott, B. (2007) NADPH oxidases in fungi: Diverse roles of reactive oxygen species in fungal cellular differentiation. *Fungal Genet Biol* **44**: 1065-1076.

Tebo, B.M., Johnson, H.A., McCarthy, J.K., and Templeton, A.S. (2005) Geomicrobiology of manganese(II) oxidation. *Trends in Microbiology* **13**: 421-428.

Tebo, B.M., Bargar, J.R., Clement, B.G., Dick, G.J., Murray, K.J., Parker, D. et al. (2004) Biogenic manganese oxides: Properties and mechanisms of formation. *Annual Review of Earth and Planetary Sciences* **32**: 287-328.

Villalobos, M., Toner, B., Bargar, J.R., and Sposito, G. (2003) Characterization of the manganese oxide produced by *Pseudomonas putida* strain MnB1. *Geochim Cosmochim Acta* **67**: 2649-2662.

Wariishi, H., Valli, K., and Gold, M.H. (1992) Manganese(II) oxidation by manganese peroxidase from the basidiomycete *Phanerochaete chrysosporium* - Kinetic mechanism and role of chelators. *J Biol Chem* **267**: 23688-23695.

Webb, S.M. (2005) SIXpack: a graphical user interface for XAS analysis using IFEFFIT. *Physica Scripta* **T115**: 1011-1014.

Webb, S.M. (2006) SMAK: Sam's Microprobe Analysis Kit, v.0.25. In: Stanford Synchrotron Radiation Laboratory.

Webb, S.M., Tebo, B.M., and Bargar, J.R. (2005) Structural characterization of biogenic Mn oxides produced in seawater by the marine *Bacillus* sp. strain SG-1. *American Mineralogist* **90**: 1342-1357.

Wei, Z., Hillier, S., and Gadd, G.M. (2012) Biotransformation of manganese oxides by fungi: solubilization and production of manganese oxalate biominerals. *Environmental Microbiology* **14**: 1744-1752.

Zafiriou, O.C., Voelker, B.M., and Sedlak, D.L. (1998) Chemistry of the superoxide radical O_2^- in seawater: Reactions with inorganic copper complexes. *J Phys Chem A* **102**: 5693-5700.

CHAPTER 3

Mechanisms of manganese(II) oxidation by filamentous ascomycete fungi vary with species and time as a function of secretome composition

This chapter was submitted to the journal *Applied and Environmental Microbiology*.
(Zeiner C.A., Purvine S.O., Zink E., Wu S., Paša-Tolić L.,
Chaput D.L., Santelli C.M., Hansel C.M.)

Supplemental Material for this chapter is presented in **Appendix 2**.

Abstract

Manganese (Mn) oxides are among the strongest oxidants and sorbents in the environment, and Mn(II) oxidation to Mn(III/IV) (hydr)oxides includes both abiotic and microbially-mediated processes. While white-rot Basidiomycete fungi oxidize Mn(II) using laccases and manganese peroxidases in association with lignocellulose degradation, the mechanisms by which filamentous Ascomycete fungi oxidize Mn(II) and a physiological role for Mn(II) oxidation in these organisms remain poorly understood. Here we use a combination of chemical and in-gel assays, bulk mass spectrometry, and iTRAQ proteomics to demonstrate secretome-based Mn(II) oxidation in three phylogenetically diverse Ascomycetes that is mechanistically distinct from hyphal-associated Mn(II) oxidation on solid substrates. We show that Mn(II) oxidative capacity of these fungi is dictated by species-specific secreted enzymes and varies with secretome age, and we observe direct, enzymatic Mn(II) oxidation in native PAGE gels in the absence of added reductants. Specifically, we identify the probable drivers of Mn(II) oxidation as bilirubin oxidase in *Stagonospora* sp. SRC11sM3a, family S41 serine peptidases in *Pyrenochaeta* sp. DS3sAY3a, and GMC oxidoreductase and bilirubin oxidase in *Paraconiothyrium sporulosum* AP3s5-JAC2a. Furthermore, we reveal a mechanistic link between Mn(II) oxidation in Ascomycetes and cellulose degradation in Basidiomycetes that likely involves reactive intermediates such as hydroxyl radical. The diversity of the Mn(II)-oxidizing

enzymes identified in this study is remarkable and suggests that the ability of fungal secretomes to oxidize Mn(II) may be more widespread than previously thought.

Introduction

Manganese (Mn) (III/IV) (hydr)oxide minerals are ubiquitous in the environment, including terrestrial and aquatic systems. Due to their small particle size, large surface area, and high sorptive and oxidative capacities, Mn oxides are among the most reactive mineral phases in the environment. Mn oxides can impact a variety of biogeochemical processes, including degradation of recalcitrant organic compounds such as humic acids (Stone and Morgan, 1984; Sunda and Kieber, 1994) and organic contaminants (Rubert and Pedersen, 2006), adsorption and redox cycling of trace metals (Nelson et al., 1999; Murray and Tebo, 2007), and anaerobic respiration coupled to carbon oxidation (Nealson and Saffarini, 1994). Furthermore, Mn(II) oxidation has been implicated in remediation of metal-contaminated waters (Santelli et al., 2010; Luan et al., 2012) and degradation of lignocellulose (Glenn et al., 1986; Höfer and Schlosser, 1999), a key carbon reservoir for renewable energy production.

Abiotic oxidation of Mn(II) by molecular oxygen is thermodynamically prohibited at circumneutral pH, owing to an energetic barrier in the first electron transfer step from Mn(II) to Mn(III) (Luther, 2010). Complexation of Mn(II) to destabilizing ligands, mineral surfaces, and/or enzyme active sites removes this energetic barrier, allowing for rapid O₂-induced Mn(II) oxidation to Mn(III) and further oxidation of Mn(III) to Mn(IV) to ultimately precipitate Mn oxides (Bargar et al., 2005; Duckworth and Sposito, 2005; Madden and Hochella Jr., 2005; Learman et al., 2011b). Furthermore, the reactive oxygen species (ROS) superoxide (O₂⁻) rapidly oxidizes Mn(II) to Mn(III) under a wide range of conditions (Nico et al., 2002; Hansard

et al., 2011; Learman et al., 2013). Within the environment, precipitation of Mn(III/IV) oxide minerals is mediated to a great extent by either direct or indirect microbiological activity. A large and diverse group of Mn(II)-oxidizing bacteria and fungi have been identified to date. Although the molecular mechanisms by which they catalyze this reaction are being elucidated for some organisms, the physiological basis remains enigmatic.

Bacterial Mn(II) oxidation has been studied extensively in model organisms such as *Bacillus* sp. strain SG-1, *Pseudomonas putida* strains GB-1 and MnB1, and *Leptothrix discophora* strains SS-1 and SP-6. These organisms enzymatically oxidize Mn(II) using multicopper oxidases (MCOs) localized in an extracellular, exopolymeric matrix (reviewed in (Tebo et al., 2004), (Butterfield et al., 2013)) or via a two-component regulatory protein (Geszvain and Tebo, 2010). Other studies have implicated extracellular animal heme peroxidases (AHP) as Mn(II)-oxidizing enzymes in three alphaproteobacteria (Anderson et al., 2009; Andeer et al., In press). For one of these organisms, *Roseobacter* sp. Azwk-3b, it has been shown that AHP produces the ROS superoxide that directly oxidizes Mn(II) to Mn(III) (Learman et al., 2011a; Andeer et al., In press).

Investigations of fungal Mn(II) oxidation have traditionally focused on model white-rot Basidiomycetes such as *Phanerochaete chrysosporium* due to their ability to effectively degrade lignocellulose from plant material. In these organisms, Mn(II) oxidation is directly linked to lignocellulose degradation and is catalyzed by extracellular enzymes including laccases (Höfer and Schlosser, 1999), Mn peroxidases (Glenn et al., 1986; Wariishi et al., 1992; Hofrichter, 2002), or a cooperative combination of the two (Schlosser and Höfer, 2002). These mechanisms are intimately linked to the cycling of ROS, as laccases can indirectly produce ROS as by-products of Mn(II) or other substrate oxidation (Schlosser and Höfer, 2002), and Mn peroxidases

require H₂O₂ as an electron acceptor (Wariishi et al., 1992). Both enzymes oxidize Mn(II) to Mn(III) complexes, which are either reduced back to Mn(II) coupled to lignocellulose oxidation, or abiotically disproportionate to form Mn(III/IV) oxides (Perez and Jeffries, 1992).

Significantly less is known about the mechanisms by which Mn(II) is oxidized by filamentous Ascomycete fungi, a ubiquitous yet understudied group of predominantly soil-dwelling organisms. Recent work, however, has begun to elucidate these processes and distinguish them from those catalyzed by Basidiomycetes. Initial demonstration of an enzymatic Mn(II) oxidation mechanism distinct from Basidiomycete Mn peroxidases (de la Torre and Gomez-Alarcon, 1994) has been followed by several studies implicating secreted laccase-like MCOs (LMCOs). Mn(II) oxidation by LMCOs has been observed in several phylogenetically diverse Ascomycetes, demonstrating oxidation of traditional laccase substrates and inhibition by copper chelators (Miyata et al., 2004; Miyata et al., 2006b; Miyata et al., 2006a), and even suggesting a link between enzymatic Mn(II) oxidation and plant pathogenicity (Thompson et al., 2006). For *Acremonium* sp. strain KR21-2, the LMCO exhibits similarity to bilirubin oxidase and polyphenol oxidase, although it has not yet been definitively identified (Miyata et al., 2006a). Interestingly, Ascomycete laccases and LMCOs (e.g., bilirubin oxidase, ascorbate oxidase) are phylogenetically distinct from each other and from Basidiomycete laccases (Hoegger et al., 2006), suggesting that different mechanisms may exist for each class of secreted enzyme. Additionally, the physiological role of Ascomycete Mn(II) oxidation remains poorly understood. Unlike for Basidiomycetes, Mn(II) oxidation by Ascomycetes has not been linked to lignocellulose degradation or acquisition of other carbon or nutrient sources, although several Mn(II)-oxidizing Ascomycetes have demonstrated cellulose oxidation capacity (Nilsson et al., 1989; Shary et al., 2007).

Previous work by our laboratory has demonstrated the involvement of both hyphal-associated reactive metabolites and secreted organic polymers in Mn(II) oxidation by filamentous Ascomycetes. Superoxide produced by transmembrane NADPH oxidases has been shown as the oxidant of Mn(II) to Mn(III) in three genera (*Stilbella*, *Stagonospora*, and *Pyrenochaeta*) during growth on agar-solidified medium (Hansel et al., 2012; Tang et al., 2013), demonstrating an interesting homology to the O₂⁻-mediated mechanism in the bacterium *R. Azwk-3b* (Learman et al., 2011a). Additionally, Mn(III/IV) oxide precipitation at distances away from the hyphae combined with observations of thin, carbonaceous filaments intimately associated with the mycogenic Mn oxides suggest a role for secreted proteins as a Mn(III) chelator and/or mineral nucleation template (Tang et al., 2013). The ability of proteins secreted by these organisms to directly oxidize Mn(II), however, remains unknown, as does the role, if any, of ROS in an extracellular enzymatic Mn(II) oxidation mechanism.

In this study, we expand our exploration of the mechanisms of Mn(II) oxidation by filamentous Ascomycetes, focusing on secreted Mn(II)-oxidizing factors in the cell-free secretome of three phylogenetically diverse fungi: *Stagonospora* sp. SRC11sM3a, *Pyrenochaeta* sp. DS3sAY3a, and *Paraconiothyrium sporulosum* AP3s5-JAC2a. By combining chemical assays, gel electrophoresis, bulk mass spectrometry, and iTRAQ proteomics, we demonstrated secretome-based Mn(II) oxidative capacity in each fungus that is mechanistically unique to each species and changes over time. We also identified the primary secreted enzymes likely responsible for extracellular Mn(II) oxidation in each organism. This work highlights the diversity of Mn(II) oxidation mechanisms among Ascomycete fungi, identifies several candidate enzymes not previously implicated in Mn(II) oxidation in fungi or bacteria, and reveals a mechanistic link between fungal Mn(II) and cellulose oxidation. Results of this study provide a

better understanding of the oxidative capacity of fungal secretomes, the mechanisms of Mn oxide formation by microorganisms, and the biogeochemical cycling of Mn in the environment.

Materials and Methods

Fungal species and culture medium. We investigated three Mn(II)-oxidizing Ascomycete fungi isolated from two locations. Two species were isolated from passive coal mine drainage treatment systems in central Pennsylvania that attenuate high concentrations of Mn (Santelli et al., 2010): *Stagonospora* sp. SRC11sM3a and *Pyrenochaeta* sp. DS3sAY3a. The third species was isolated from Ashumet Pond, Massachusetts, a natural freshwater lake (Santelli et al., 2014): *Paraconiothyrium sporulosum* AP3s5-JAC2a. This field site was historically polluted with elevated concentrations of phosphate and metals, including Fe and Mn, and is currently undergoing remediation.

All fungal species were grown in HEPES-buffered (20 mM, pH 7) AY medium containing 0.25 g L⁻¹ sodium acetate, 0.15 g L⁻¹ yeast extract, and 1 mL L⁻¹ trace element stock (10 mg L⁻¹ CuSO₄•5H₂O, 44 mg L⁻¹ ZnSO₄•7H₂O, 20 mg L⁻¹ CoCl₂•6H₂O, and 13 mg L⁻¹ Na₂MoO₄•2H₂O) supplemented with MnCl₂ (0-200 μM). All chemicals were reagent grade or higher. Fungal cultures were maintained on petri dishes containing agar-solidified (2% agar) AY medium with 200 μM Mn(II) (hereafter AY + Mn).

Culture conditions and secretome harvesting. Homogenized inocula were used for all culture experiments. Inocula were prepared by aseptically removing the entire contents of a 90 mm petri dish (including fungal mycelia and associated agar) that had incubated at room temperature (20°C) until the mycelia had reached the edge of the agar. The contents were then placed in an autoclaved kitchen blender (Oster model BVLB07) with 100 mL of AY + Mn

medium and homogenized on high speed for 2 minutes. On the same day that the homogenized inocula were prepared, 100 μ L of the inoculum was used to inoculate 100 mL liquid cultures in AY + Mn medium.

For characterization of secretome samples over time, liquid cultures of each of the 3 fungi were incubated at room temperature and ambient light, without agitation, for 7, 14, or 21 days. For each fungus, individual 100 mL cultures were combined into 500 mL samples. Samples were prepared in quadruplicate to account for the inherent unpredictability of fungal cultures. Upon harvesting, bulk biomass was removed with a sterile wooden stick and discarded, and the spent medium was filtered through a 0.45 μ m polyethersulfone membrane (VWR) to remove remaining cells and Mn oxides. Samples were then concentrated using a centrifugal filter with a 10 kDa, low protein adhesion membrane (EMD Millipore). Centrifugation proceeded at $2200 \times g$ on a Sorvall RT 6000B centrifuge with H1000B swing-bucket rotor until all liquid had passed through the membrane. The resulting secretome samples were rinsed with 20 mM HEPES, pH 7 and stored at -80°C until analysis.

Protein and Mn oxide quantification. Protein in secretome samples was quantified using a PierceTM BCA protein assay kit (Thermo Fisher Scientific) as conducted previously (Smith et al., 1985). The quantity of protein recovered from 500 mL secretome samples generally ranged between 250 and 1000 μ g, depending on species and secretome age.

The amount of Mn(III/IV) oxides generated by the secretome samples was quantified with a colorimetric method using the Leucoberbelin blue (LBB) reagent (Krumbein and Altmann, 1973). LBB produces a deep blue color in the presence of Mn in any oxidation state higher than Mn(II). Samples were incubated with LBB in the dark for 15 minutes, followed by measurement of their spectrophotometric adsorption at 620 nm on a SpectraMax[®] i3 microplate

reader (FAS Center for Systems Biology, Harvard). Standard curves were prepared with LBB and KMnO_4 .

Protein electrophoresis and in-gel Mn(II) oxidation assay. Secretome samples from all 3 fungi and 3 time points were separated using standard native PAGE on pre-cast AnyKdTM tris-glycine gels (BioRad) with approximately 10 μg protein loaded per lane. Protein samples were not boiled or denatured to retain Mn(II)-oxidizing activity. Duplicate gels were prepared for all samples: one gel was stained with BioSafe Coomassie G250 (BioRad) for 1 hour to visualize all secreted proteins, and the other gel was incubated with 400 μM Mn(II) for 2 hours followed by staining with LBB to visualize Mn(II)-oxidizing bands. All gels were rinsed with ultrapure water. LBB-stained Mn(II)-oxidizing bands were excised in a laminar flow hood, in addition to control bands from lanes run with sample buffer only. Bands were stored at -80°C until analysis via LC/MS/MS.

Protein identification by LC/MS/MS. Peptide sequencing of all secretome samples (excised Mn(II)-oxidizing gel bands and whole secretome samples for 3 fungi and 3 time points) was performed at the Environmental Molecular Sciences Laboratory, part of Pacific Northwest National Laboratory. Four and two biological replicates of gel band samples and whole secretome samples were analyzed, respectively.

(a) Preparation of gel band samples. A preliminary comparison of proteins identified in LBB-stained bands and those identified in corresponding Coomassie-stained bands revealed that the presence of LBB did not interfere with LC/MS/MS analysis (data not shown). Therefore, all gel bands selected for protein analysis were taken from LBB-stained gels to ensure accuracy in identifying Mn(II)-oxidizing bands.

The in-gel digestion procedure was similar to previously described (Shevchenko et al., 2007). Briefly, the excised gel bands were cut into small pieces and were destained with 100 mM ammonium bicarbonate/acetonitrile (1:1, vol/vol) for 30 minutes before drying in acetonitrile. The gel slices were then saturated with a 1.5 μ M solution of trypsin in 50 mM ammonium bicarbonate, pH 8.0 at 4°C for 1 hour, then incubated for 1 hour at 58°C with 1000 rpm shaking. The reaction was quenched with 50% formic acid in water, and the peptides were extracted with a 1:2 (vol/vol) 5% formic acid/acetonitrile solution (incubated at 37°C for 15 minutes followed by centrifugation). The extraction was repeated and the combined supernatants were concentrated in a vacuum concentrator to 100 μ L. After ultracentrifugation at 100k rpm the resulting supernatant was further concentrated to 30 μ L and transferred to an autosampler compatible vial for LC/MS/MS analysis.

(b) Preparation of whole secretome samples for iTRAQ proteomics. Whole secretome samples were prepared for mass spectrometry using a trypsin digestion (Callister et al., 2008). In summary, the preteins were denatured with urea (8 M) and reduced with 5 mM dithiothreitol (DTT, Sigma–Aldrich) for 30 min at 60°C. The samples were then diluted 10-fold with 100 mM ammonium bicarbonate with 1 mM CaCl₂ and then digested for 3 h at 37°C using porcine sequencing-grade trypsin (Promega) at a substrate/enzyme mass ratio of 50:1. The digestion was quenched by adding 10% trifluoroacetic acid to a final concentration of 0.1% before desalting with a C-18 solid phase extraction column (Supelco, St. Louis, MO), performed using a Gilson GX-274 Liquid Handler. The resulting peptide solution was concentrated to 50 μ L in a vacuum concentrator, and a BCA assay was performed to estimate the protein concentration, as above. To enable quantitation, the samples were isobarically labeled with Isobaric Tags for Relative and Absolute Quantitation (iTRAQ) 8-plex Reagent using the

manufacturer's instructions (ABSciex, PN#4352135). Moreover, a universal reference sample created by pooling all the iTRAQ-labeled samples was used to enable normalization between the samples. The labeled samples were desalted with a C-18 solid phase extraction column (Supelco) and then fractionated with a reverse-phase C18 column and pooled using concatenation (Wang et al., 2011). The resulting fractions were diluted to 0.07 ug/uL and were then analyzed using LC/MS/MS.

(c) LC/MS/MS for gel band samples. The peptide solution was processed on a custom built LC system using two Agilent 1200 nanoflow pumps and one Agilent 1200 cap pump (Agilent Technologies) with various Valco valves (Valco Instruments Co.), and utilizing a PAL autosampler (Leap Technologies) that were fully automated with custom software to allow parallel processing of two columns. The reversed-phase columns (40 cm x 360 μm o.d. x 75 μm i.d fused silica (Polymicro Technologies Inc.)) were packed in-house with 3 μm Jupiter C18 (Phenomenex). A 1 cm sol-gel frit was used for media retention and a 4-cm length, 5 μm Jupiter C18 trapping column with a frit on both ends were also utilized (Maiolica et al., 2005). The mobile phases were 0.1% formic acid in water (A) and 0.1% formic acid in acetonitrile (B) and were processed at 300 nL min^{-1} . Peptides (5 μL) were initially trapped and washed on the columns at 3- $\mu\text{L min}^{-1}$ for 20 minutes prior to eluting with the following gradient profile (min:%B): 0:5, 2:8, 20:12, 75:35, 97:60, 100:85. Data acquisition began 10 minutes after the start of the gradient and ended 10 minutes after the gradient end to account for column dead volume and allow the best gradient overlap with the two column system.

Data were acquired using a Velos Orbitrap mass spectrometer (Thermo Scientific) with a custom-made electrospray ionization (ESI) interface, using custom made, chemically-etched fused silica electrospray emitters (150 μm o.d. x 20 μm i.d. fused silica) (Kelly et al., 2006). The

heated capillary temperature was set to 200°C with a spray voltage of 2.2 kV. Data were acquired for a total of 100 minutes with a 10 minute delay from the start of the gradient. Orbitrap spectra (AGC 1x10⁴) were collected from 400-2000 m/z at a resolution of 60k followed by data dependant CID MS/MS (collision energy 35%, AGC 1x10⁶) of the six most abundant ions, excluding single charge states. A dynamic exclusion time of 30 sec was used to discriminate against previously analyzed ions using a 0.55 to 1.55 Da mass window.

(d) LC/MS/MS for whole secretome samples via iTRAQ proteomics. The iTRAQ labeled fractions were processed on a Waters nano-Acquity dual pumping UPLC system with a custom on-line trapping system for a 5 μ L injection processed at 3 μ L min⁻¹. The trapped sample was then reverse eluted onto the analytical column at a 300 nL min⁻¹ flow rate. Both the trapping column (150 μ m i.d. x 4 cm long) and analytical column (75 μ m i.d. x 70 cm long) were packed in-house using Jupiter C18 media (Phenomenex) particles (5 μ m for the trapping column and 3 μ m for the analytical column) into 360 μ m o.d. fused silica (Polymicro Technologies Inc.) with 1 cm sol-gel frits for media retention (Maiolica et al., 2005). The gradient began with mobile phase A (0.1% formic acid in water) and switched to mobile phase B (0.1% formic acid in acetonitrile) with the following gradient profile (min, %B): 0, 1; 2, 8; 20, 12; 75, 30; 97, 45; 100, 95; 110, 95; 115, 1; 150, 1.

Data was acquired using a LTQ Orbitrap Velos mass spectrometer (Thermo Scientific) with a custom made nano-electrospray ionization interface utilizing custom made, chemically-etched fused silica electrospray emitters (150 μ m o.d. x 20 μ m i.d) (Kelly et al., 2006). The heated capillary temperature was set to 350°C with a spray voltage of 2.2 kV. Data was acquired for a total of 100 min after a 15 min delay from sample injection. FT-MS spectra were acquired

from 300-1800 m/z at a resolution of 30k and while the top 10 FT-HCD-MS/MS spectra were acquired in data dependent mode at a resolution of 7.5k using a normalized collision energy of 45.

(e) Bioinformatics. MS/MS spectra were converted to ASCII text using the DeconMSn tool (Mayampurath et al., 2008) which helps account for incorrect monoisotope assignments. Spectra were then searched with MSGFPlus (Kim and Pevzner, 2014) using a protein FASTA containing newly sequenced genomes of the 3 fungal species (see details below) and amended with common contaminants (e.g., trypsin and human keratin sequences). All peptide candidate sequences were statically modified with the iTRAQ 8-plex reporter ion conjugate mass (+304.205353 Da on Lysine residues and peptide N-terminus), dynamically modified for oxidized methionine, with a parent mass tolerance of +/- 20ppm. Other settings include partially tryptic cleavages, +/-1 Da parent corrections (to further account for incorrect monoisotope assignments), MS level data centroiding, and decoy search mode enabled. The MASIC software tool (Monroe et al., 2008) was used to extract the iTRAQ 8-plex reporter ion abundances from the MS/MS spectra with +/- 10ppm mass tolerance.

An in-house analysis pipeline was used to combine the peptide identifications with their related iTRAQ 8-plex reporter ion abundances. Briefly, the pipeline imports the peptide identification results, filters the peptide results to 1% FDR (using MSGFPlus' reported Q-value ≤ 0.01 , which is derived using the standard decoy approach (Elias and Gygi, 2010)), sums reporter ion intensities per peptide across multiple strong cation exchange fractions within a given sample, and outputs the peptide sequence with associated reporter ion intensities for each fractionated sample. Proteins associated with each peptide were reported separately. For this dataset, the occurrence of peptide sequences occurring in more than one protein were rare, but in those cases where redundancy did occur all proteins associated with a peptide were identified.

For biological interpretation of the data, only the first protein reference associated with a peptide was used, and the function of this protein was manually checked against other protein matches to ensure that all protein functions for a particular peptide were similar.

Peptide-level relative abundance data were normalized by mean central tendency normalization using the Inferno implementation of the Dante analysis tool (Polpitiya et al., 2008). Since the relative abundances of peptides in pooled samples were similar in all pools, pools were not used for normalization. The limit of quantitation (LOQ) for peptide relative abundance was defined as 2 standard deviations below the average log₂ transformed relative abundance of all peptides across all samples; this LOQ roughly corresponds to the lower 95% confidence interval. To determine which abundance data were below the LOQ, the log₂ transformed relative abundances of each peptide were averaged (including zeros for samples in which the peptide was not detected) between the two biological replicates for each fungus and time point. Averages below the LOQ were removed from the dataset. Relative abundance data for averaged pairs was then anti-logged, and, for each protein, summed for all peptides that mapped to that protein. Relative abundance data were then re-normalized using mean central tendency normalization to correct for any variability introduced during processing. Finally, data were log₂ transformed for biological interpretation using MultiExperiment Viewer, version 4.9 (TM4).

Two methods were used to match identified peptides (exhibiting relative abundance data above the LOQ) with associated proteins. For gel band data, peptides from each of the 3 fungi were searched against 3 frame stop-to-stop translations of their respective genomes, which were still in contig form at the time this work was performed. For whole secretome data, peptides from all 3 fungi were searched as a combined dataset against a combined FASTA file with all 3

fungal genomes, as described above. Individual peptides were first searched against the *P. sporulosum* genome, then *Pyrenochaeta* sp., and finally *Stagonospora* sp. When a peptide detected in one fungus was mapped to a protein in the genome of another fungus, the predicted function of the corresponding protein in the genome of original fungus was manually checked to ensure it agreed with the function of the assigned protein.

Functional information was obtained by searching a combined database of NCBI and UniProt fungal protein sequences for proteins identified in this study using BLAST. For proteins for which the highest-scoring (lowest E-value) match was hypothetical or uncharacterized, the highest-scoring non-hypothetical match was reported. Proteins with no matches (hypothetical or otherwise) having an E-value below 10^{-10} were reported as hypothetical. Only proteins with at least 2 peptide observations per protein were considered in biological interpretations. Functional information obtained via BLAST analysis was manually checked against automatically assigned annotations in the newly-sequenced genomes. All proteins were then functionally categorized according to the Carbohydrate-Active Enzymes (CAZy) Database (www.cazy.org) and MEROPS Peptidase Database (<http://merops.sanger.ac.uk/>) classification systems, using UniProt family and domain designations to aid in categorization.

The genome sequences and annotations for the 3 fungi in this study are available at the Joint Genome Institute (JGI) fungal genomics resource MycoCosm (Grigoriev et al., 2014) at <http://genome.jgi-psf.org/programs/fungi/index.jsf>.

Results

Mn(II) oxidative capacity of the fungal secretome. Patterns of Mn oxide formation in the cell-free secretome were species-specific and varied over time (Figure 3.1). Secretome

samples from *Stagonospora* sp. exhibited high Mn(II) oxidative capacity early in growth but decreased in capacity over time, while those from *Pyrenochaeta* sp. exhibited Mn(II) oxidative capacity only after 21 days. The *P. sporulosum* secretome was characterized by consistently high Mn(II) oxidative capacity across the entire 3-week study.

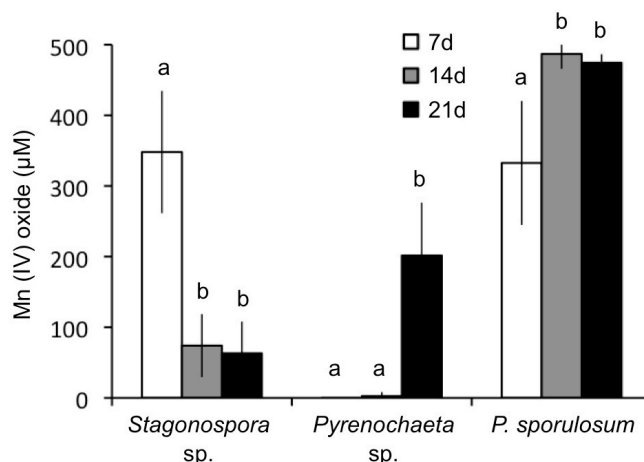


Figure 3.1. Mn(II) oxidation by cell-free fungal secretomes. All experiments conducted with 500 μM Mn(II) and 200 $\mu\text{g mL}^{-1}$ fungal protein. Samples were incubated with Mn(II) for 1 hour prior to Mn oxide quantification. Within each organism, letters indicate significant differences by a Tukey-Kramer test with $P < 0.05$. All error bars represent ± 1 standard deviation over 4 biological replicates.

These temporal changes in Mn(II) oxidative capacity were visually evident in the liquid cultures of *Pyrenochaeta* sp. and *P. sporulosum* prior to biomass removal and secretome harvest (Figure S3.1). For these cultures, extracellular, dark brown Mn oxides were visible in the growth medium above the biomass, and to a lesser extent associated with the biomass itself (for *P. sporulosum* only), at time points for which substantial Mn(II) oxidative capacity was measured. In *Stagonospora* sp. cultures, although particulate Mn oxides were visible at all time points and visually increased in density over time (Figure S3.1), this pattern did not correspond with measured Mn(II) oxidative capacity and likely reflects changes in the Mn oxide structure and/or morphology during ripening (aging). For all 3 fungi, < 10 kDa filtrate remaining after secretome

harvest did not exhibit any Mn(II) oxidative capacity measurable with LBB (data not shown). Mn(II) oxidative capacity in the >10 kDa secretome was nearly or completely abolished by boiling or by adding 1 mg mL⁻¹ proteinase K (fungal, Sigma) for all 3 fungi (Figure S3.2). Interestingly, the secretomes from all 3 fungi exhibited Mn(II) oxidative capacity whether or not they were grown in the presence of Mn(II) (data not shown).

Proteins involved in Mn(II) oxidation. While each fungal secretome was rich in protein (as evidenced by Coomassie staining; Figure S3.3) and exhibited a species-specific migration pattern in native PAGE gels, each secretome displayed only one primary Mn(II)-oxidizing band (Figure 3.2). Within each fungus, Mn(II)-oxidizing bands migrated to a consistent position in the gels over all time points for which Mn(II) oxidative capacity was measured (Figure S3.3). LC/MS/MS analysis of excised gel bands revealed a variety of redox-active secreted proteins, many of which have not been previously implicated in Mn(II) oxidation by either fungi or bacteria. Proteins likely involved in Mn(II) oxidation were identified by examining whole secretome relative abundance patterns of proteins identified in gel bands, and comparing these patterns to temporal patterns of Mn(II) oxidation in the samples. Results for each fungus are discussed individually below.

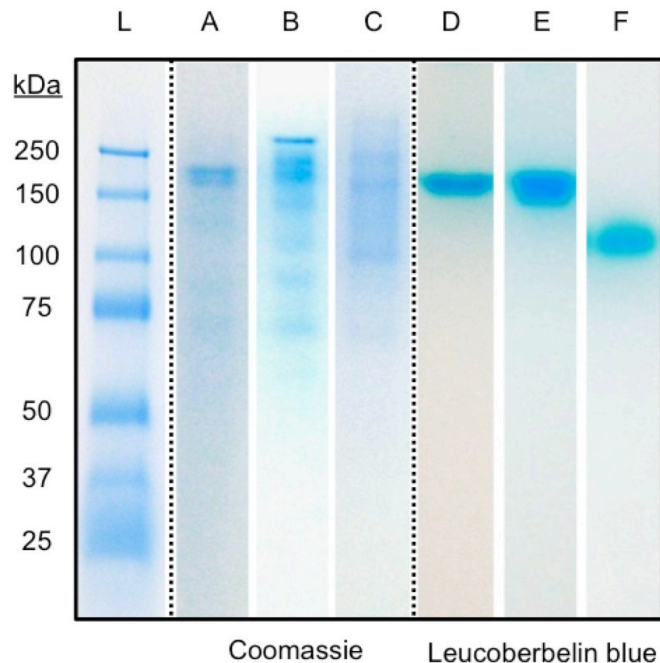


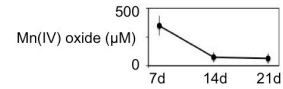
Figure 3.2. Native PAGE of selected secretome samples from *Stagonospora* sp. (A, D), *Pyrenochaeta* sp. (B, E), and *P. sporulosum* (C, F). Left (L): Pre-stained blue molecular mass markers with sizes in kDa to left of image. Center panel: Secretome samples after staining with Coomassie G-250 for 1 hour. Right panel: Replicate gel of the same secretome samples after incubation with 400 μ M Mn(II) for 2 hours followed by staining with Leucoberbelin blue, which turns blue in the presence of Mn(III/IV) oxides. Images shown are representative of 4 biological replicates of each of 3 time points.

(a) *Stagonospora* sp. Redox-active proteins identified in Mn(II)-oxidizing gel bands (bold in Figure 3.3) include multicopper oxidases (MCOs) (e.g., tyrosinase and bilirubin oxidase), a radical copper oxidase (glyoxal oxidase), glucose-methanol-choline (GMC) oxidoreductases, and unspecified FAD-binding proteins, among others. Additionally, an Xaa-Pro aminopeptidase was identified in the 14d and 21d bands; this metalloprotease binds 2 Mn ions per subunit (UniProt). Secretome samples from which gel band data were generated exhibited Mn(II) oxidative capacity in all 3 time points (Figure S3.3A). The only redox-active or Mn-binding proteins present in gel bands from all 3 time points were tyrosinase (JGI protein ID 211028) and glyoxal oxidase (protein 323207).

Figure 3.3. Proteins detected in Mn(II)-oxidizing gel bands (via LC/MS/MS) and their associated relative abundance in whole secretome samples (via iTRAQ proteomics) from *Stagonospora* sp. Proteins are displayed in descending order of number of gel band peptide observations for the time point during which maximum Mn(II) oxidative capacity was measured (7d; inset). EC numbers were derived from JGI genome annotations (regular text) or assigned manually (italics). Redox-active proteins are shown in bold. • Redox-active proteins that are detected in all Mn(II)-oxidizing gel bands (here, all 3 time points). * Proteins that exhibit relative abundance patterns over time that correlate with Mn(II) oxidation pattern (inset). Scale bar indicates relative abundance (\log_2 transformed).

Figure 3.3 (Continued)

Stagonospora sp.



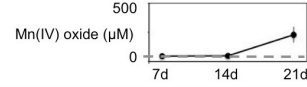
Protein ID	EC Number	Best BLAST Hit	Protein Family	Putative Function	Gel Band Peptides			Whole Secretome Relative Abundance			Whole Secretome Peptides	
					7d	14d	21d	7d	14d	21d		
211028	1.14.18.1	C5GH85_AJEDR	CAZy AA1_3	Tyrosinase	32	61	81	●				39
119700	1.3.3.5	W3WQC6_9PEZI	CAZy AA1_3	Bilirubin oxidase	22	27	--	*				13
323207	1.1.3.-	E4ZTP3_LEPMJ	CAZy AA5_1	Glyoxal oxidase	10	38	42	●				30
295700	Unknown	E5A293_LEPMJ	CAZy Unknown	Chitin-binding protein	10	7	11					10
284632	2.4.1.-	M2QUS6_COCSN	CAZy GH72	Beta-1,3-glucanosyltransglycosylase	9	7	--					18
287383	3.1.1.74	W6Y4A3_COCCA	CAZy CE5	Cutinase	7	6	2					13
292969	Unknown	G2WXK1_VERDV	N/A	Cell wall protein PhiA	6	6	5					9
277810	3.1.1.1	B2W8L6_PYRTR	N/A	Acetylcholinesterase	5	2	--					28
197954	Unknown	C6H786_AJECH	N/A	BYS1 domain-containing protein	3	3	4					3
243316	5.3.1.9	Q0U3Q6_PHANO	N/A	Glucose-6-phosphate isomerase	--	19	16					32
278452	3.3.1.1	Q0UM97_PHANO	N/A	Adenosylhomocysteinase	--	14	133					27
330396	1.15.1.1	Q0UEY3_PHANO	N/A	Superoxide dismutase	--	10	--					2
305412	3.2.1.58	B2WE48_PYRTR	CAZy GH55/PL	Exo-beta-1,3-glucanase, pectin lyase	--	10	103					13
339955	2.4.1.-	B2W8K5_PYRTR	CAZy GH72	Beta-1,3-glucanosyltransglycosylase	--	7	--					9
307091	2.6.1.19	E5A984_LEPMJ	N/A	4-aminobutyrate aminotransferase	--	7	38					6
216085	3.3.2.6	LKHA4_PHANO	N/A	Leukotriene A-4 hydrolase homolog	--	5	16					11
292538	3.5.2.6	L2G4M6_COLGN	N/A	Beta-lactamase domain protein	--	4	--					4
261684	Unknown	K2SHI2_MACPH	CAZy AA3	GMC oxidoreductase	--	4	24					33
231262	2.6.1.44	B2W0Z7_PYRTR	N/A	Purine catabolism protein	--	4	4					4
304339	4.1.3.1	Q0URI8_PHANO	N/A	Isocitrate lyase	--	3	--					3
291332	Unknown	B2WMF9_PYRTR	N/A	FAD-binding protein	--	3	16					25
285016	3.1.27.1	B2W8V0_PYRTR	N/A	Ribonuclease M	--	3	3					5
333545	3.4.13.9	AMPP3_PHANO	MEROPS M24	Xaa-Pro aminopeptidase	--	3	2					12
285757	N/A	Q6Q890_LEPMC	Hypothetical	Hypothetical	--	2	--					15
80159	N/A	E5AF70_LEPMJ	Hypothetical	Hypothetical, secreted	--	2	--					3
222292	Unknown	E5A859_LEPMJ	CAZy Unknown	Chitin-binding protein	--	2	--					9
335319	N/A	B6HA41_PENCW	Hypothetical	Hypothetical	--	2	3					2
260460	3.4.14.4	B2VQV5_PYRTR	MEROPS M49	Dipeptidyl peptidase III	--	2	3					23
265794	3.2.1.-	Q76G11_9HYPO	CAZy GH5	Beta-1,3-mannanase	--	2	2					9
113154	3.2.1.58	W6ZDB1_COCSN	CAZy GH17	Glucan 1,3-beta-glucosidase	--	2	2					12
78588	3.4.21.-	E4ZK33_LEPMJ	MEROPS S8/S53	Subtilisin-like serine protease	--	2	2					6
256827	2.3.1.9	B2VZ30_PYRTR	N/A	Acetyl-CoA acetyltransferase	--	--	25					3
30123	3.4.17.21	E4ZNY0_LEPMJ	MEROPS M28	N-acetylated-alpha-linked acidic dipeptidase	--	--	23					4
251441	Unknown	T0L7L0_COLGC	N/A	FAD-binding protein	--	--	22					30
373589	3.2.1.20	R0KFU4_SETT2	CAZy GH31	Alpha-glucosidase	--	--	18					4
88030	Unknown	E4ZJ62_LEPMJ	N/A	Necrosis-and ethylene-inducing protein	--	--	17					6
266710	Unknown	R1EAR3_BOTPV	MEROPS S41	Peptidase	--	--	16					20
312635	3.4.24.11	K2RGA5_MACPH	MEROPS M13	Nepriylsin	--	--	14					42
260169	1.4.3.6	Q0TYR0_PHANO	N/A	Amine oxidase, Cu containing	--	--	10					10
80736	3.2.1.39	M2RHU4_COCSN	CAZy GH81	Endo-beta-1,3-glucanase	--	--	9					3
312944	3.2.1.14	M2SSU6_COCSN	CAZy GH18	Chitinase	--	--	8					5
343359	1.2.1.16	B2WAB8_PYRTR	N/A	Succinate-semialdehyde dehydrogenase	--	--	8					15
217423	3.2.1.1	Q0U4B3_PHANO	CAZy GH13	Alpha-amylase	--	--	7					7
289958	3.1.1.1	M3BS21_SPHMS	N/A	Alpha/beta hydrolase	--	--	7					10
296929	1.15.1.1	Q0UPE0_PHANO	N/A	Superoxide dismutase, Fe/Mn	--	--	7					2
372088	Unknown	R8BU37_TOGMI	MEROPS M6	Metalloprotease	--	--	5					5
82112	N/A	R1GSH0_BOTPV	Hypothetical	Hypothetical	--	--	4					10
355904	3.2.1.113	R0KB56_SETT2	CAZy GH47	Mannosyl-oligosaccharide 1,2-alpha-mannosidase	--	--	3					3
356098	3.2.1.73	B2WMZ3_PYRTR	CAZy GH16	Extracellular cell wall glucanase	--	--	2					21
134696	3.2.1.39	M2TC31_COCSN	CAZy GH64	Beta-1,3-glucanase	--	--	2					5
288759	3.1.1.45	K1WWH1_MARBU	N/A	Dienelactone hydrolase	--	--	2					5
291458	3.4.11.-	B2WGG4_PYRTR	MEROPS M28	Leupeptin-inactivating enzyme 1	--	--	2					7
Proteins detected in gel bands but not in whole secretome samples:												
276876	Unknown	R1GKF0_BOTPV	N/A	Transcription factor protein C6	4	--	4					--
No match	N/A	M7TV87_BOTF1	Hypothetical	Hypothetical	--	2	--					--
297700	Unknown	B2WIW3_PYRTR	N/A	Amino acid/polyamine transporter I	--	--	3					--
292194	Unknown	B2W3J1_PYRTR	CAZy CBM	Starch-binding protein	--	--	2					--



Surprisingly, the relative abundance patterns of these proteins over time in whole secretomes (i.e., high in 14d and 21 samples) did not correspond with patterns of Mn(II) oxidation (i.e., low in 14d and 21d samples) (Figure 3.3, inset). Instead, bilirubin oxidase (protein 119700) exhibited a relative abundance pattern that corresponds with Mn(II) oxidation patterns (i.e., higher in 7d samples, lower in 14d and 21d samples). While this enzyme was present in 7d and 14d gel band samples, it was not identified in 21d gel bands. Notably, gel bands from 21d secretome samples produced a visible but weak reaction to the in-gel Mn(II) oxidation assay (Figure S3.3A). Therefore, this bilirubin oxidase correlates well with both whole secretome (Figure 3.3) and in-gel (Figure S3.3) Mn(II) oxidation patterns and is likely the primary enzyme responsible for Mn(II) oxidation in this organism. Other redox-active enzymes identified in the gel bands, including tyrosinase and glyoxal oxidase, may supplement Mn(II) oxidative capacity.

(b) *Pyrenochaeta* sp. Compared to *Stagonospora* sp., a much smaller suite of redox-active proteins was identified in gel bands from *Pyrenochaeta* sp. These proteins were primarily FAD-binding proteins, including GMC oxidoreductases and bifunctional solanapyrone synthase (bold in Figure 3.4). The protein with the highest number of peptide observations in all time points was tripeptidyl peptidase (protein 584947), a serine-type peptidase with potential metallopeptidase activity (Lin et al., 2011). Secretome samples from which gel band data were generated exhibited Mn(II) oxidative capacity in the 14d and 21d samples only (Figure S3.3B). Two redox-active enzymes were identified in both of these Mn(II)-oxidizing samples: bifunctional solanapyrone synthase (protein 524095) and an unspecified FAD-binding protein (protein 640056).

Pyrenochaeta sp.



Protein ID	EC Number	Best BLAST Hit	Protein Family	Putative Function	Gel Band Peptides		Whole Secretome Relative Abundance			Whole Secretome Peptides
					14d	21d	7d	14d	21d	
584947	3.4.14.9	E5AA57_LEPMJ	MEROPS S53	Tripeptidyl peptidase	34	20				61
226676	3.2.1.39	M2RHU4_COCSN	CAZy GH81	Endo-beta-1,3-glucanase	--	16				3
678105	Unknown	W6Z446_COCEMI	CAZy AA3	GMC oxidoreductase	--	11				32
495802	Unknown	R1EAR3_BOTPV	MEROPS S41	Peptidase	5	10	*			27
520005	3.2.1.58	R0IQE4_SETT2	CAZy GH17	Glucan 1,3-beta-glucosidase	13	9				30
591166	N/A	F9XJA7_MYCGM	Hypothetical	Hypothetical	4	5				12
524095	1.1.3.42/5.5.1.20	SOL5_ALTSO	N/A	Bifunctional solanapyrone synthase	5	4	•			16
640056	Unknown	M7T199_EUTLA	N/A	FAD-binding protein	8	3	•			27
602398	Unknown	R8BU37_TOGMI	MEROPS M6	Metalloprotease	2	3				34
587762	Unknown	K2SHI2_MACPH	CAZy AA3	GMC oxidoreductase	--	2				10
594303	N/A	W6ZVD2_COCEMI	CAZy CBM18	Carbohydrate-binding module	3	2				69
166454	Unknown	E5A071_LEPMJ	MEROPS S41	Peptidase	2	2	*			27
585702	Unknown	S0EAR2_GIBF5	N/A	Beta-transducin	16	--				34
506627	Unknown	E5ACIO_LEPMJ	N/A	Endonuclease/exonuclease/phosphatase	6	--				10
587321	3.3.1.1	E4ZLQ8_LEPMJ	N/A	Adenosylhomocysteinase	5	--				14
586913	1.4.3.6	E5AAU1_LEPMJ	N/A	Amine oxidase	3	--				32
510927	Unknown	E4ZNU8_LEPMJ	N/A	Endonuclease/exonuclease/phosphatase	2	--				25
252677	3.4.21.4	E5A5U3_LEPMJ	MEROPS S1	Trypsin-like protease 1	2	--				8
585899	N/A	SEC24_SCHPO	Hypothetical	Hypothetical	2	--				5
681286	Unknown	M7SD75_EUTLA	N/A	FAD-binding protein	2	--				10
Proteins detected in gel bands but not in whole secretome samples:										
No match	N/A	A0A067TP34_9AGAR	Hypothetical	Hypothetical	--	6				--
No match	N/A	[No match]	Hypothetical	Hypothetical	1	--				--



Figure 3.4. Proteins detected in Mn(II)-oxidizing gel bands (via LC/MS/MS) and their associated relative abundance in whole secretome samples (via iTRAQ proteomics) from *Pyrenochaeta* sp. Proteins are displayed in descending order of number of gel band peptide observations for the time point during which maximum Mn(II) oxidative capacity was measured (21d; inset). EC numbers were derived from JGI genome annotations (regular text) or assigned manually (italics). Redox-active proteins are shown in bold. • Redox-active proteins that are detected in all Mn(II)-oxidizing gel bands (here, 14d and 21d). * Proteins that are detected in all Mn(II)-oxidizing gel bands and exhibit relative abundance patterns over time that correlate with Mn(II) oxidation pattern (inset). Scale bar indicates relative abundance (log₂ transformed).

Like in *Stagonospora* sp., the relative abundance patterns of the redox-active proteins identified in all gel band samples exhibiting Mn(II) oxidative capacity did not correspond to patterns of Mn(II) oxidation in whole secretome samples. Instead, two MEROPS family S41 (serine-type) peptidases (proteins 495802 and 166454) exhibited relative abundance patterns that follow Mn(II) oxidation patterns (i.e., lower in 7d and 14d samples, and higher in 21d samples) in whole secretomes (Figure 3.4, inset). Both of these enzymes were identified in both the 14d and 21d gel band samples, and, as such, agree with both in-gel and whole secretome Mn(II)

oxidation patterns. It is likely that these S41 peptidases are the primary drivers of Mn(II) oxidation in this organism, potentially supplemented by redox-active enzymes (e.g., bifunctional solanapyrone synthase and FAD-binding proteins) and even the highly abundant tripeptidyl peptidase.

(c) *P. sporulosum*. Redox-active enzymes identified in gel bands from *P. sporulosum* include GMC oxidoreductases and other FAD-binding proteins, multicopper oxidases (e.g., bilirubin oxidase, ascorbate oxidase, and an unspecified MCO), and 2-methylcitrate dehydratase (which binds a 4Fe/4S cluster; UniProt), among others (Figure 3.5). Secretome samples from which gel band data were generated exhibited substantial Mn(II) oxidative capacity in all 3 time points (Figures 3.1 and S3.3C). Two redox-active enzymes were identified in all 3 samples: GMC oxidoreductase (protein 1152844) and bilirubin oxidase (protein 1129270). GMC oxidoreductase was identified with the highest number of peptide observations in all 3 time points.

In this organism, relative abundance patterns of these redox-active enzymes identified in all 3 gel band samples corresponded well to Mn(II) oxidation patterns in whole secretomes (Figure 3.5, inset). Both enzymes exhibited moderate relative abundance in 7d samples and high relative abundance in 14d and 21d samples. Additionally, a hypothetical protein (protein 1166911) that was identified in all 3 gel band samples exhibited similar patterns of relative abundance and Mn(II) oxidation. Performing a BLAST analysis on the amino acid sequence of this protein did not yield any functional information, and additional investigation would be needed to elucidate any role in Mn(II) oxidation in this organism. Because of its low peptide observation counts compared to the two redox-active enzymes discussed above, it is likely that any role in Mn(II) oxidation is supplementary at best. Therefore, it is likely that GMC

oxidoreductase and bilirubin oxidase are the primary enzymes responsible for Mn(II) oxidative capacity in *P. sporulosum*.

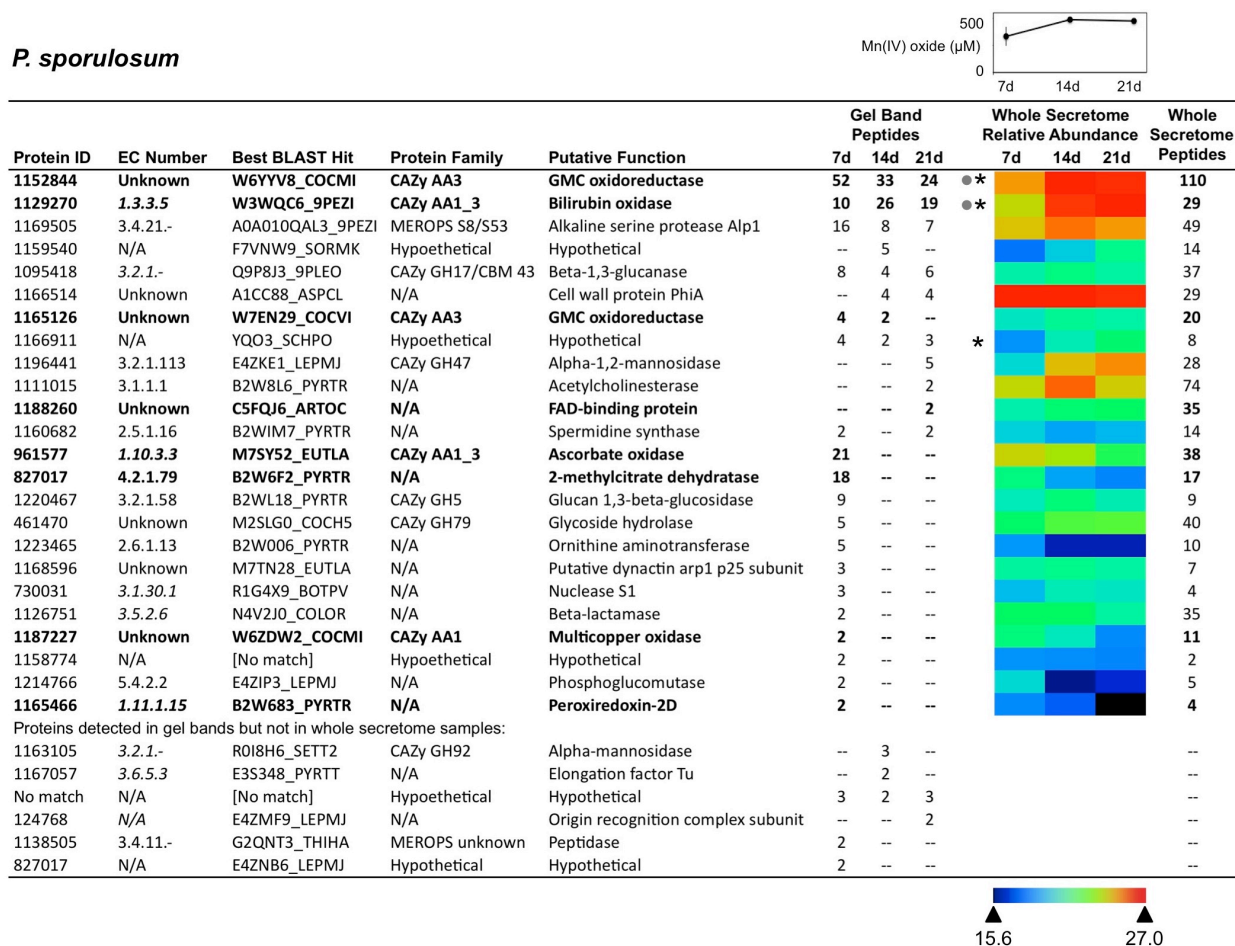


Figure 3.5. Proteins detected in Mn(II)-oxidizing gel bands (via LC/MS/MS) and their associated relative abundance in whole secretome samples (via iTRAQ proteomics) from *P. sporulosum*. Proteins are displayed in descending order of number of gel band peptide observations for the time point during which maximum Mn(II) oxidative capacity was measured (14d; inset). EC numbers were derived from JGI genome annotations (regular text) or assigned manually (italics). Redox-active proteins are shown in bold. • Redox-active proteins that are detected in all Mn(II)-oxidizing gel bands (here, all 3 time points). * Proteins that are detected in all Mn(II)-oxidizing gel bands and exhibit relative abundance patterns over time that correlate with Mn(II) oxidation pattern (inset). Scale bar indicates relative abundance (log₂ transformed).

The total number of proteins identified in each gel band for each of the 3 fungi over the 3 time points ranged from 10 to 45 (Figures 3.3-3.5). Non-redox-active proteins primarily included those involved in extracellular digestion (e.g., carbohydrate-degrading enzymes and

peptidases), transferases (e.g., adenosylhomocysteinase), and intracellular proteins that were likely released via cell lysis during culture growth or sample processing.

Discussion

Mn(II) oxidative capacity of the fungal secretome. Here we demonstrate extracellular Mn(II) oxidative capacity in the cell-free secretomes of three phylogenetically diverse, filamentous Ascomycete fungi (Figure 3.1) that is mediated by secreted proteins (Figure S3.2, Figures 3.3-3.5). Interestingly, cell-free oxidative capacity in liquid culture represents a distinct Mn(II) oxidation mechanism from the hyphal-associated, superoxide-mediated mechanism we have previously observed for two of these organisms (*Stagonospora* sp. and *Pyrenochaeta* sp.) (Tang et al., 2013) and a third fungus, *Stilbella aciculosa* (Hansel et al., 2012), during growth on agar-solidified medium. While transmembrane NADPH oxidases (and therefore vegetative cells) are required for O_2^- production and Mn(II) oxidation at the cell surface, here we show Mn(II) oxidation in the absence of cells and these membrane-associated enzymes.

The utilization of two (or potentially more) distinct Mn(II) oxidation mechanisms is likely dictated by environmental conditions. On a solid substrate, O_2^- is actively exuded by hyphae as they grow and branch to acquire new, geographically remote substrate (Gessler et al., 2007; Semighini and Harris, 2008). In contrast, cells in liquid medium are surrounded by substrate at all times, presumably reducing the need for hyphal extension and perhaps extracellular O_2^- production. While cells in liquid culture still exude O_2^- for hyphal growth and a variety of other physiological reasons (Gessler et al., 2007), and while a hyphal-associated, O_2^- mediated mechanism may indeed contribute to Mn(II) oxidation in liquid culture, clearly a distinct enzymatic mechanism is present in the cell-free, liquid secretome.

When the fungi were grown on solid substrate in a previous study (Tang et al., 2013), Mn(II) oxidation was inhibited by diphenylene iodonium (DPI), which prevents reduction of the FAD domain in NADPH oxidases and other flavoproteins (Ellis et al., 1988; O'Donnell et al., 1993; Williams and Griendling, 2007) and thereby inhibits superoxide-mediated Mn(II) oxidation. Because the primary Mn(II)-oxidizing enzymes in the *Stagonospora* sp. and *Pyrenochaeta* sp. secretomes are not flavoproteins (as shown in this study), the previously observed DPI-mediated inhibition on agar plates suggests little, if any, contribution of these secretome-based Mn(II)-oxidizing enzymes to Mn(II) oxidation on solid medium. While it is possible that the fungi, when growing on agar, could secrete Mn(II)-oxidizing flavoproteins (other than O₂⁻-generating NADPH oxidases) that would be inhibited by DPI and that were not identified in the liquid secretomes in this study, this would represent yet another distinct Mn(II) oxidation mechanism. Thus, the hyphal-associated O₂⁻ mechanism reported previously and the secretome-associated mechanisms reported here indeed represent two distinct Mn(II) oxidation pathways that are likely dependent on growth conditions. It is tempting to speculate that the functional redundancy offered by two distinct Mn(II) oxidation mechanisms may be indicative of a physiological benefit of Mn oxide formation, but such a benefit remains unknown.

While Mn(II) oxidative capacity in the extracellular secretome is a common characteristic of diverse Mn(II)-oxidizing fungi and bacteria (Learman et al., 2011a), to our knowledge this is the first report of significant (P<0.05) variability in secretome-based Mn(II) oxidative capacity over time. Furthermore, we show the species-specific nature of this variability, both in terms of temporal patterns of oxidative capacity and dependence on particular secreted enzymes. Temporal variability may be explained by age-dependent dynamics of enzyme secretion, such as an apparent 1-2 week lag in *Pyrenochaeta* sp. or constitutive expression in *P. sporulosum*

(Figure 3.1). These patterns are supported by visual observations of Mn oxide formation in the spent medium above the fungal biomass in liquid culture (Figure S3.1). However, it is interesting that a steady increase in Mn oxide formation in *Stagonospora* sp. cultures (as observed visually in the flasks; Figure S3.1) is accompanied by a significant drop in Mn(II) oxidative capacity of the secretome (Figure 3.1). This may indicate that initial enzymatic Mn(II) oxidation early in growth is followed by a non-enzymatic mechanism, such as abiotic mineral surface-catalyzed oxide formation, as the culture ages.

Proteins involved in Mn(II) oxidation. Like the temporal patterns of Mn(II) oxidative capacity, the primary enzymes responsible for Mn(II) oxidation in each of the three fungal secretomes are species-specific. Interestingly, while the quantitative Mn(II) oxidative capacity of the fungi varies with time (Figure 3.1), the primary Mn(II)-oxidizing enzymes observed in the Mn(II)-oxidizing bands do not (Figure S3.3, Figures 3.3-3.5). Thus, the enzymatic mechanism in each organism is consistent over the 3-week period investigated in this study, suggesting that the temporal variability must stem from changes in enzyme production and/or secretion. Our investigation of these filamentous Ascomycetes identifies a suite of enzymes not previously implicated in Mn(II) oxidation, expanding the complement of potential fungal Mn(II)-oxidizing enzymes beyond laccases and Mn peroxidases (in Basidiomycetes) and LMCOs (in Ascomycetes).

Our findings point to bilirubin oxidase as the primary enzyme oxidizing Mn(II) in *Stagonospora* sp. Bilirubin oxidase is a LMCO that is classified in the CAZy AA1 (MCO) family along with traditional laccases (Levasseur et al., 2013), a group of enzymes known to oxidize Mn(II) to Mn(III) in white-rot Basidiomycetes (Höfer and Schlosser, 1999) and generate ROS (Schlosser and Höfer, 2002). The active site of bilirubin oxidase is structurally similar to

fungal laccases in that it contains a mononuclear type I Cu center that interacts with the substrate and a trinuclear type II/III Cu cluster that reduces the electron acceptor (Tanaka and Murao, 1981; Solomon et al., 1996). Numerous bilirubin oxidases have been isolated from fungi (Hiromi et al., 1992; Masuda-Nishimura et al., 1999) and bacteria (Sakasegawa et al., 2006; Durand et al., 2012), including Mn(II)-oxidizing organisms. Notably, extracellular Mn(II)-oxidizing enzymes from both the fungus *Acremonium* sp. strain KR21-2 and the bacterium *L. discophora* strain SS-1 have exhibited sequence similarity to bilirubin oxidase (Corstjens et al., 1997; Miyata et al., 2006a). While direct Mn(II) oxidation by bilirubin oxidase has not been established, these similarities suggest a role for this enzyme in Mn(II) oxidation across multiple domains of life. The structural similarity of bilirubin oxidase with Mn(II)-oxidizing laccases lends further support for its potential Mn(II) oxidative capacity. Here, we identified bilirubin oxidase in all *Stagonospora* sp. gel bands that exhibited strong Mn(II) oxidative capacity (Figures 3.3 and S3.3A) and observed relative abundance patterns of this enzyme in whole secretome samples that correspond to Mn(II) oxidation patterns. Taken together, our data and that of other researchers strongly suggest that fungal bilirubin oxidase can oxidize Mn(II).

For *Pyrenochaeta* sp., our data suggest that two family S41 peptidases are the primary enzymes involved in Mn(II) oxidation. To our knowledge, this is the first report of a peptidase, and family S41 peptidases in particular, being identified as potential Mn(II)-oxidizing enzymes. The MEROPS S41 family of serine-type peptidases is classified in the SK clan of peptidases and consists of two structurally distinct members: a C-terminal processing peptidase and a tricon core protein (Page and Di Cera, 2008). While these proteins have been reasonably well studied in bacteria, archaea, and plants, little is known about their function in fungi. Thus far, S41 peptidases have been identified in several fungal phyla (e.g., Basidiomycota, Ascomycota, and

Chytridiomycota) and are thought to play a role in pathogenicity or programmed cell death (Rosenblum et al., 2008; Iketani et al., 2013; Liang et al., 2013). In plant chloroplasts, the S41 C-terminal processing peptidase cleaves the precursor of the D1 protein of photosystem II, which then ligates the tetranuclear manganese cluster (Anbudurai et al., 1994; Taguchi et al., 1995). To our knowledge, no other interactions of S41 peptidases with transition metals have been identified. It is unknown if these peptidases have a redox-active cofactor, and furthermore, if they can oxidize Mn(II). While additional investigation of these enzymes is needed to verify Mn(II) oxidative capacity, our data strongly suggest the involvement of S41 peptidases in Mn(II) oxidation in *Pyrenochaeta* sp.

Interestingly, a link between other peptidases and Mn has been previously reported. In particular, a fungal tripeptidyl peptidase (TPP) isolated from the zygomycete *Rhizopus oligosporus* appears to interact with transition metals, exhibiting stimulation by Mn(II) and Co(II) and inhibition by Cu(II), and may be both a metallo- and serine-type protease (Lin et al., 2011). Here, we observe a high abundance of TPP in the *Pyrenochaeta* sp. secretome and Mn(II)-oxidizing gel bands; yet, we ruled out its primary involvement in Mn(II) oxidation as whole secretome abundance and Mn(II) oxidation patterns are not consistent. While this enzyme has been studied extensively in mammals and bacteria, it has not been well characterized in fungi, and only a handful of fungal TPPs have been identified to date (Reichard et al., 2006; Lin et al., 2011).

Our observation that the Mn(II) oxidative capacity of the *Pyrenochaeta* sp. secretome is inhibited by o-phenanthroline (Figure S3.4) is consistent with a metalloenzyme as the Mn(II)-oxidizing factor. Although TPP may be a metalloenzyme, much remains unknown about this protease, including the nature of a potential metal-containing active site, the molecular basis for

the demonstrated interactions with transition metals, and any redox capacity. If TPP supplements Mn(II) oxidative capacity in this organism, it would lend support for this protein as a metalloprotease and raise the question as to whether the family S41 peptidases identified in this study may similarly exhibit both serine- and metallopeptidase activity.

A pair of enzymes, GMC oxidoreductase and bilirubin oxidase, are likely responsible for Mn(II) oxidation by *P. sporulosum*. To our knowledge, this is the first report of a GMC oxidoreductase being identified as a potential Mn(II)-oxidizing enzyme in fungi or bacteria, and additional investigation is needed to pinpoint its identity and function within the GMC superfamily. GMC oxidoreductases comprise a large and diverse superfamily of redox-active, H₂O₂-generating enzymes, many of which are represented in the CAZy AA3 family (Levasseur et al., 2013). They contain a highly-conserved FAD-binding domain (Zamocky et al., 2004), generally stripping two electrons from a broad range of substrates and reducing molecular oxygen. Their interactions with transition metals have not been well characterized.

Based on UniProt molecular function designations and NCBI BLAST results, the GMC oxidoreductase identified in *P. sporulosum* (protein 1152844) may be a choline dehydrogenase (CHD) (EC 1.1.99.1). This enzyme catalyzes the four-electron oxidation of choline (a quaternary ammonium salt often grouped with the B vitamins) to betaine aldehyde. Due to difficulties in purifying this enzyme, it is poorly characterized across all domains of life, particularly in fungi (recently reviewed in (Salvi and Gadda, 2013)). Unlike other GMC oxidoreductases, the redox cofactor in CHD has not been definitively identified and may consist of FAD, pyrroloquinoline quinone (PQQ) (Ameyama et al., 1985; Gadda and McAllister-Wilkins, 2003), an iron/sulfur cluster, or a combination of these (Huang and Lin, 2003).

The gel band and whole secretome data for *P. sporulosum* also suggest bilirubin oxidase as an Mn(II)-oxidizing enzyme in this organism (Figure 3.5). Thus, bilirubin oxidase is a strong candidate for Mn(II) oxidizing activity in two of the Ascomycetes investigated in this study, *Stagonospora* sp. and *P. sporulosum*, in addition to its similarity to the Mn(II)-oxidizing factors in *Acremonium* sp. and *L. discophora* as discussed above. The role of MCOs in microbial Mn(II) oxidation has been well established in both fungi (i.e., laccases and LMCOs) (Höfer and Schlosser, 1999) and bacteria (Tebo et al., 2004), but here we expand the suite of organisms in which MCO-mediated Mn(II) oxidation has been identified and enhance our understanding of the specific MCOs (e.g., bilirubin oxidase) that catalyze this reaction.

Other abundant and/or redox-active enzymes were identified in the gel bands and may contribute to the Mn(II) oxidative capacity of the organisms in this study as well. For instance, tyrosinase, glyoxal oxidase, GMC oxidoreductase, and other FAD-binding proteins were identified with non-negligible peptide observation counts in the *Stagonospora* sp. gel bands (Figure 3.3). Further, redox-active enzymes, including bifunctional solanapyrone synthase and an unspecified FAD-binding protein, were identified in the *Pyrenochaeta* sp. gel bands and whole secretome samples (Figure 3.4) and may contribute to the peptidase-driven Mn(II) oxidative capacity of this organism. However, the lack of a clear correlation between the oxidative capacity of the secretome and the abundance/presence of these enzymes in the gel bands and whole secretome samples suggest only a minor contribution, if any, to overall oxidative capacity. Additional characterization of these enzymes would be needed to elucidate any involvement in Mn(II) oxidation.

Mechanisms of secretome-based Mn(II) oxidation. While the mechanism(s) by which the enzymes identified in this study mediate Mn(II) oxidation remain unknown, our data and that

of other researchers suggest that both direct enzymatic Mn(II) oxidation and indirect Mn(II) oxidation via production of reactive intermediates are possible. Indeed, our observations of Mn oxide formation in native PAGE gels indicate that direct enzymatic Mn(II) oxidation is occurring in all 3 fungi. Thus, our data suggest that bilirubin oxidase (in *Stagonospora* sp. and *P. sporulosum*), family S41 peptidases (in *Pyrenochaeta* sp.), and GMC oxidoreductase (in *P. sporulosum*) can directly utilize Mn(II) as a substrate for oxidation. Mn oxides readily formed in the repeatedly rinsed, organic-poor gel environment without the addition of any reagent other than Mn(II) to the active, immobilized enzymes. In contrast, previous investigation of the indirect, superoxide-mediated Mn(II) oxidation mechanism in the bacterium *Roseobacter* sp. Azwk-3b revealed the requirement of an added reductant (e.g., NADH) for O₂⁻ production (Andeer et al., In press). Furthermore, it has recently been shown that the putative MCO responsible for Mn(II) oxidation in *Bacillus* sp. strain SG-1 can directly, enzymatically catalyze both Mn(II) and Mn(III) oxidation (Butterfield et al., 2013), further suggesting that the MCOs identified in this study (e.g., bilirubin oxidase) may have similar, direct Mn(II) oxidative capability.

Direct enzymatic Mn(II) oxidation in the laboratory gel environment may not be representative of processes occurring in the complex environment of the secretome, however. Here, other mechanisms could be operative in addition to, or instead of, a direct enzymatic mechanism. Specifically, organics and other reductants are likely available for ROS production, and therefore, the enzymes identified in this study may indirectly mediate Mn(II) oxidation via production of reactive intermediates. For example, laccases secreted by the Basidiomycete *Stropharia rugosoannulata* can generate organic radicals, such as CO₂⁻, through oxidation of reduced organic carbon compounds in the secretome (Schlosser and Höfer, 2002). This

organic radical can then react with O₂ to produce the superoxide radical, a reactive intermediate which can oxidize Mn(II). If a secretome-associated, ROS-mediated mechanism is present, it is unlikely that superoxide contributes substantially to this process since the Mn(II) oxidative capacity of *Stagonospora* sp. and *Pyrenochaeta* sp. secretomes was unaffected by the addition of superoxide dismutase (P>0.05) (Figure S3.5). Although the Mn(II) oxidative capacity was slightly increased with SOD for *P. sporulosum* (P<0.05), any involvement of superoxide should have resulted in decreased Mn(II) oxidation with SOD. Thus, a secretome-based, ROS-directed Mn(II) oxidation mechanism in *Stagonospora* sp. or *Pyrenochaeta* sp. would represent a distinct process from the hyphal-associated, superoxide-mediated mechanism we have previously observed on solidified growth medium (Hansel et al., 2012; Tang et al., 2013). It is likely that OH radical, as opposed to superoxide, would be the oxidant of Mn(II) in such a mechanism. The one-electron oxidation of Mn(II) by OH radical is thermodynamically favorable above pH 1 (Luther, 2010) and could proceed as follows:



Several of the primary Mn(II)-oxidizing enzymes we identified in *Stagonospora* sp. and *P. sporulosum* may have the ability to produce OH radical. For instance, bilirubin oxidase and other MCOs with structural similarity to laccases could contribute to Fe(III) reduction and OH radical formation via Fenton chemistry as described previously for a fungal laccase (Guillén et al., 2000). GMC oxidoreductases are considered to be key producers of the extracellular H₂O₂ needed by lignolytic peroxidases in white-rot Basidiomycetes. As such, these enzymes can also contribute to OH radical production via Fenton chemistry in the presence of ferrous iron (reviewed in (Dashtban et al., 2010)). Cellobiose dehydrogenase, a well-studied member of the GMC oxidoreductase superfamily, can additionally generate OH radical via reduction of

hydroquinones to Fe(III)-reducing semiquinone radicals (Henriksson et al., 2000; Dashtban et al., 2010; Hatakka and Hammel, 2010).

Similarly, enzymes that may supplement Mn(II) oxidation in these Ascomycetes may indirectly oxidize Mn(II) via OH radical production in the secretome. Both tyrosinase and glyoxal oxidase directly generate H₂O₂ (Kersten and Kirk, 1987; Ramsden and Riley, 2014), and tyrosinase is involved in quinone redox cycling and potentially Fe(III) reduction (del Mar Garcia-Molina et al., 2014). As such, these enzymes could contribute to Fenton-mediated OH radical generation as described above.

Although direct Mn(II) oxidation by tyrosinase or glyoxal oxidase has not been established, both enzymes have been shown to interact with transition metals. Tyrosine oxidation by cephalopod and mammalian tyrosinase is stimulated by Fe(II) (and indeed, tyrosinase can directly catalyze Fe(II) oxidation (Boyer et al., 1986)), but this reaction is inhibited by Mn(II) and Cu(II) (Palumbo et al., 1985; Palumbo et al., 1990). Enzyme inhibition by Mn(II) was also preliminarily extended to mushroom tyrosinase (Palumbo et al., 1985). In contrast, Cu(II) was shown to stimulate the activity of tyrosinase isolated from fungal sources (Inamdar et al., 2014; Zou et al., 2014). Glyoxal oxidase has been shown to reduce Mn(III) to Mn(II) (Whittaker et al., 1996), but it is unknown whether the activated enzyme can then oxidize Mn(II) back to Mn(III) coupled to the reduction of another electron acceptor, such as O₂.

The mechanism(s) by which family S41 peptidases (potentially supplemented by TPP) may facilitate Mn(II) oxidation in the *Pyrenochaeta* sp. secretome is unknown. The enzymes may directly oxidize Mn(II) (as observed in the gels), facilitate as-yet-unknown ROS or quinone redox cycling, or employ another mechanism entirely.

While it is clear that enzymes identified in all 3 fungi can directly oxidize Mn(II) as a substrate in the gel environment, the extent to which ROS-mediated and/or direct enzymatic Mn(II) oxidation occur in the secretome remains poorly understood. Isolation and purification of the candidate Mn(II)-oxidizing enzymes will be required to confirm that these enzymes can act directly on Mn(II), and future culturing studies are needed to determine the role, if any, of ROS or other reactive metabolites in secretome-based Mn(II) oxidation.

Mechanistic link between Mn(II) and cellulose oxidation. Several of the candidate Mn(II)-oxidizing enzymes identified in this study, specifically GMC oxidoreductase in *P. sporulosum* and tyrosinase and glyoxal oxidase in *Stagonospora* sp., have also been implicated in cellulose oxidation by the brown-rot Basidiomycete, *Postia placenta* (Martinez et al., 2009). This fungus lacks traditional cellulases and Basidiomycete peroxidases (e.g., LiP, MnP) but was shown to efficiently degrade cellulose through secretion of a diverse suite of enzymes, including radical copper oxidases, GMC oxidoreductases (methanol and glucose oxidases), LMCOs (polyphenol oxidase and tyrosinase), quinone reductases, and iron reductases. The enzyme-mediated production of low molecular weight oxidants, specifically OH radical generated via Fenton chemistry, was suggested as the primary cellulose degradation mechanism.

Like the cellulose-degrading enzymes in *P. placenta*, the candidate Mn(II)-oxidizing enzymes identified in this study also contribute to quinone redox cycling and Fe(III) reduction (tyrosinase and some GMC oxidoreductases) and H₂O₂ generation (glyoxal oxidase and GMC oxidoreductases), and thus could facilitate Mn(II) oxidation via OH radical production as described above. The identification of the same oxidative enzymes in carbon oxidation by a brown-rot Basidiomycete and Mn(II) oxidation by filamentous Ascomycetes establishes an interesting mechanistic link between these two oxidative processes in fungal secretomes. While

the Ascomycetes in this study have the ability to degrade cellulose (C.M. Santelli, unpublished data), the mechanism(s) responsible for this process and their relationship, if any, to the candidate Mn(II)-oxidizing enzymes identified in this study remain unknown.

Conclusions. Here we have demonstrated species-specific, age-dependent, and enzyme-directed Mn(II) oxidative capacity in the secretomes of three filamentous Ascomycete fungi. We have identified enzymatic Mn(II) oxidation mechanisms in the liquid secretome that are distinct from the hyphal-associated, superoxide-mediated mechanism previously observed on solid substrate. The proteomic composition of Mn(II)-oxidizing gel bands from each of the fungi was diverse and unique, resulting in different Mn(II) oxidation mechanisms in each organism. While the secretomes of these fungi contain a complex suite of oxidative enzymes, we have identified candidate Mn(II)-oxidizing enzymes in each organism that can be targeted for additional investigation. We observed direct enzymatic Mn(II) oxidation in native PAGE gels in all 3 fungi, but mechanisms in the secretome may be more complex and involve reactive intermediates. Additionally, each fungus exhibited temporal patterns of Mn(II) oxidative capacity that are uniquely dependent on changing secretome composition over time.

The diversity and versatility of the candidate Mn(II)-oxidizing enzymes identified in the 3 Ascomycetes is remarkable and suggests that the ability of fungal secretomes to oxidize Mn(II) may be more widespread than previously thought and may extend to phylogenetically diverse fungi that secrete these oxidative enzymes. Isolation, purification, and biogeochemical investigation of the enzymes identified herein will further elucidate fungal Mn(II) oxidation mechanisms, aid in identifying a physiological role for Mn(II) oxidation in Ascomycetes, and expand our knowledge of the oxidative capacity of fungal secretomes.

Acknowledgements

This work was supported by the National Science Foundation, grant numbers EAR-1249489 and CBET-1336496, both awarded to C.M.H, and by a JGI-EMSL Collaborative Science Initiative grant (proposal number 48100) awarded to C.M.H. and C.M.S. Personal support for C.A.Z was also provided by Harvard University and by a Ford Foundation Predoctoral Fellowship administered by the National Academies.

Part of this research was performed at the Environmental Molecular Sciences Laboratory, a national scientific user facility sponsored by the U.S. DOE's Office of Biological and Environmental Research and located at the Pacific Northwest National Laboratory. Part of this research was performed at the Bauer Core Facility of the FAS Center for Systems Biology at Harvard University. A portion of the bioinformatics analysis was performed at Harvard's FAS Research Computing facility.

We thank Joshua Aldrich (EMSL) and Michele Clamp (Harvard) for bioinformatic analyses at various stages of this project, and Therese R. Clauss (EMSL) for expertise in LC/MS/MS instrumentation throughout this project.

The authors disclaim endorsement of any products mentioned in this paper.

References

- Ameyama, M., Shinagawa, E., Matsushita, K., Takimoto, K., Nakashima, K., and Adachi, O. (1985) Mammalian choline dehydrogenase is a quinoprotein. *Agric Biol Chem* **49**: 3623-3626.
- Anbudurai, P.R., Mor, T.S., Ohad, I., Shestakov, S.V., and Pakrasi, H.B. (1994) The *ctpA* gene encodes the C-terminal processing protease for the D1 protein of the photosystem II reaction center complex. *PNAS* **91**: 8082-8086.
- Andeer, P.F., Learman, D.R., McIlvin, M., Dunn, J.A., and Hansel, C.M. (In press). Extracellular heme peroxidases mediate Mn(II) oxidation in a marine *Roseobacter* bacterium via superoxide production [WWW document].
- Anderson, C.R., Johnson, H.A., Caputo, N., Davis, R.E., Torpey, J.W., and Tebo, B.M. (2009) Mn(II) oxidation is catalyzed by heme peroxidases in *Aurantimonas manganoxydans* strain SI85-9A1 and *Erythrobacter* sp. strain SD-21. *Appl Environ Microbiol* **75**: 4130-4138.
- Bargar, J.R., Tebo, B.M., Bergmann, U., Webb, S.M., Glatzel, P., Chiu, V.Q., and Villalobos, M. (2005) Biotic and abiotic products of Mn(II) oxidation by spores of the marine *Bacillus* sp. strain SG-1. *Am Mineral* **90**: 143-154.
- Boyer, R.F., Mascotti, P.D., and Schori, B.E. (1986) Ferroxidase activity of mushroom tyrosinase. *Phytochemistry* **25**: 1281-1283.
- Butterfield, C.N., Soldatova, A.V., Lee, S.-W., Spiro, T.G., and Tebo, B.M. (2013) Mn(II,III) oxidation and MnO₂ mineralization by an expressed bacterial multicopper oxidase. *PNAS* **110**: 11731-11735.
- Callister, S.J., McCue, L.A., Turse, J.E., Monroe, M.E., Auberry, K.J., Smith, R.D. et al. (2008). Comparative bacterial proteomics: analysis of the core genome concept [WWW document].
- Corstjens, P.L.A.M., de Vrind, J.P.M., Goosen, T., and de Vrind-de Jong, E.W. (1997) Identification and molecular analysis of the *Leptothrix discophora* SS-1 *mofA* gene, a gene putatively encoding a manganese-oxidizing protein with copper domains. *Geomicrobiol J* **14**: 91-108.
- Dashtban, M., Schraft, H., Syed, T.A., and Qin, W. (2010) Fungal biodegradation and enzymatic modification of lignin. *Int J Biochem Mol Biol* **1**: 36-50.
- de la Torre, M.A., and Gomez-Alarcon, G. (1994) Manganese and iron oxidation by fungi isolated from building stone. *Microb Ecol* **27**: 177-188.

del Mar Garcia-Molina, M., Muñoz-Muñoz, J.L., Berna, J., García-Ruiz, P.A., Rodríguez-Lopez, J.N., and Garcia-Canovas, F. (2014) Catalysis and inactivation of tyrosinase in its action on hydroxyhydroquinone. *Int U Biochem Mol Biol* **66**: 122-127.

Duckworth, O.W., and Sposito, G. (2005) Siderophore-manganese(III) interactions. I. Air-oxidation of manganese(II) promoted by desferrioxamine B. *Environ Sci Technol* **39**: 6037-6044.

Durand, F., Kjaergaard, C.H., Suraniti, E., Gounel, S., Hadt, R.G., Solomon, E.I., and Mano, N. (2012) Bilirubin oxidase from *Bacillus pumilus*: a promising enzyme for the elaboration of efficient cathodes in biofuel cells. *Biosens Bioelectron* **35**: 140-146.

Elias, J.E., and Gygi, S.P. (2010) Methods Mol Biol. *Target-decoy search strategy for mass spectrometry-based proteomics* **604**: 55-71.

Ellis, J.A., Mayer, S.J., and Jones, O.T.G. (1988) The effect of the NADPH oxidase inhibitor diphenylene iodonium on aerobic and anaerobic microbicidal activities of human neutrophils. *Biochem J* **251**: 887-891.

Gadda, G., and McAllister-Wilkins, E.E. (2003) Cloning, expression, and purification of choline dehydrogenase from the moderate halophile *Halomonas elongata*. *Appl Environ Microbiol* **69**: 2126-2132.

Gessler, N.N., Aver'yanov, A.A., and Belozerskaya, T.A. (2007) Reactive oxygen species in regulation of fungal development. *Biochemistry-Moscow* **72**: 1091-1109.

Geszvain, K., and Tebo, B.M. (2010) Identification of a two-component regulatory pathway essential for Mn(II) oxidation in *Pseudomonas putida* GB-1. *Appl Environ Microbiol* **76**: 1224-1231.

Glenn, J.K., Akileswaran, L., and Gold, M.H. (1986) Mn(II) oxidation is the principal function of the extracellular Mn-peroxidase from *Phanerochaete chrysosporium*. *Arch Biochem Biophys* **251**: 688-696.

Grigoriev, I.V., Nikitin, R., Haridas, S., Kuo, A., Ohm, R., Otilar, R. et al. (2014) MycoCosm portal: Gearing up for 1000 fungal genomes. *Nucleic Acids Res* **42**.

Guillén, F., Gómez-Toribio, V., Martínez, M.J., and Martínez, A.T. (2000) Production of hydroxyl radical by the synergistic action of fungal laccase and aryl alcohol oxidase. *Arch Biochem Biophys* **383**: 142-147.

Hansard, S.P., Easter, H.D., and Voelker, B.M. (2011) Rapid reaction of nanomolar Mn(II) with superoxide radical in seawater and simulated freshwater. *Environ Sci Technol* **45**: 2811-2817.

- Hansel, C.M., Zeiner, C.A., Santelli, C.M., and Webb, S.M. (2012) Mn(II) oxidation by an ascomycete fungus is linked to superoxide production during asexual reproduction. *PNAS* **109**: 12621-12625.
- Hatakka, A., and Hammel, K.E. (2010) Fungal biodegradation of lignocellulose. In *The Mycota X: Industrial Applications*. Hofrichter, M. (ed). Berlin: Springer-Verlag, pp. 319-340.
- Henriksson, G., Johansson, G., and Pettersson, G. (2000) A critical review of cellobiose dehydrogenases. *J Biotechnol* **78**: 93-113.
- Hiromi, K., Yamaguchi, S., Sugiura, Y., Iwamoto, H., and Hirose, J. (1992) Bilirubin oxidase from *Trachyderma tsunodae* K-2593, a multicopper enzyme. *Biosci Biotech Biochem* **56**: 1349-1350.
- Hoegger, P.J., Kilaru, S., James, T.Y., Thacker, J.R., and Kües, U. (2006) Phylogenetic comparison and classification of laccase and related multicopper oxidase protein sequences. *FEBS J* **273**: 2308-2326.
- Höfer, C., and Schlosser, D. (1999) Novel enzymatic oxidation of Mn²⁺ to Mn³⁺ catalyzed by a fungal laccase. *FEBS Lett* **451**: 186-190.
- Hofrichter, M. (2002) Review: lignin conversion by manganese peroxidase (MnP). *Enzyme Microb Technol* **30**: 454-466.
- Huang, S., and Lin, Q. (2003) Functional expression and processing of rat choline dehydrogenase precursor. *Biochem Biophys Res Commun* **309**: 344-350.
- Iketani, A., Nakamura, M., Suzuki, Y., Awai, K., and Shioi, Y. (2013) A novel serine protease with caspase- and legumain-like activities from edible basidiomycete *Flammulina velutipes*. *Fungal Biol* **117**: 173-181.
- Inamdar, S., Joshi, S., Bapat, V., and Jadhav, J. (2014) Purification and characterization of RNA allied extracellular tyrosinase from *Aspergillus* species. *Appl Biochem Biotechnol* **172**: 1183-1193.
- Kelly, R.T., Page, J.S., Luo, Q., Moore, R.J., Orton, D.J., Tang, K., and Smith, R.D. (2006) Chemically etched open tubular and monolithic emitters for nanoelectrospray ionization mass spectrometry. *Anal Chem* **78**: 7796-7801.
- Kersten, P.J., and Kirk, T.K. (1987) Involvement of a new enzyme, glyoxal oxidase, in extracellular H₂O₂ production by *Phanerochaete chrysosporium*. *J Bacteriol* **169**: 2195-2201.

Kim, S., and Pevzner, P.A. (2014) MS-GF+ makes progress towards a universal database search tool for proteomics. *Nat Commun* **5**: 5277.

Krumbein, W.E., and Altmann, H.J. (1973) A new method for the detection and enumeration of manganese oxidizing and reducing microorganisms. *Helgolander wiss Meeresunters* **25**: 347-356.

Learman, D.R., Voelker, B.M., Vázquez-Rodríguez, A.I., and Hansel, C.M. (2011a) Formation of manganese oxides by bacterially generated superoxide. *Nat Geosci* **4**: 95-98.

Learman, D.R., Voelker, B.M., Madden, A.S., and Hansel, C.M. (2013) Constraints on superoxide mediated formation of manganese oxides. *Front Microbiol* **4**: Article 262.

Learman, D.R., Wankel, S.D., Webb, S.M., Martinez, N., Madden, A.S., and Hansel, C.M. (2011b) Coupled biotic-abiotic Mn(II) oxidation pathway mediates the formation and structural evolution of biogenic Mn oxides. *Geochim Cosmochim Acta* **75**: 6048-6063.

Levasseur, A., Drula, E., Lombard, V., Coutinho, P.M., and Henrissat, B. (2013). Expansion of the enzymatic repertoire of the CAZy database to intergrate auxiliary redox enzymes [WWW document].

Liang, L., Wu, H., Liu, Z., Shen, R., Gao, H., Yang, J.Y., and Zhang, K. (2013) Proteomic and transcriptional analyses of *Arthrobotrys oligospora* cell wall related proteins reveal complexity of fungal virulence against nematodes. *Appl Microbiol Biotechnol* **97**.

Lin, J.-S., Lee, S.-K., Y., C., Lin, W.-D., and Kao, C.-H. (2011) Purification and characterization of a novel extracellular tripeptidyl peptidase from *Rhizopus oligosporus*. *J Agric Food Chem* **59**: 11330-11337.

Luan, F., Santelli, C.M., Hansel, C.M., and Burgos, W.D. (2012) Defining manganese(II) removal processes in passive coal mine drainage treatment systems through laboratory incubation experiments. *Appl Geochem* **27**: 1567-1578.

Luther, G.W. (2010) The role of one- and two-electron transfer reactions in forming thermodynamically unstable intermediates as barriers in multi-electron redox reactions. *Aquatic Geochem* **16**: 395-420.

Madden, A.S., and Hochella Jr., M.F. (2005) A test of geochemical reactivity as a function of mineral size: Manganese oxidation promoted by hematite nanoparticles. *Geochim Cosmochim Acta* **69**: 389-398.

Maiolica, A., Borsotti, D., and Rappsilber, J. (2005) Self-made frits for nanoscale columns in proteomics. *Proteomics* **5**: 3847-3850.

- Martinez, D., Challacombe, J., Morgenstern, I., Hibbett, D., Schmoll, M., Kubicek, C.P. et al. (2009) Genome, transcriptome, and secretome analysis of wood decay fungus *Postia placenta* supports unique mechanisms of lignocellulose conversion. *PNAS* **106**: 1954-1959.
- Masuda-Nishimura, I., Ichikawa, K., Hatamoto, O., Abe, K., and Koyama, Y. (1999) cDNA cloning of bilirubin oxidase from *Pleurotus ostreatus* strain *Shinshu* and its expression in *Aspergillus sojae*: an efficient screening of transformants, using the laccase activity of bilirubin oxidase. *J Gen Appl Microbiol* **45**: 93-97.
- Mayampurath, A.M., Jaitly, N., Purvine, S.O., Monroe, M.E., Auberry, K.J., Adkins, J.N., and Smith, R.D. (2008) DeconMSn: a software tool for accurate parent ion monoisotopic mass determination for tandem mass spectra. *Bioinformatics* **24**: 1021-1023.
- Miyata, N., Tani, Y., Iwahori, K., and Soma, M. (2004) Enzymatic formation of manganese oxides by an *Acremonium*-like hyphomycete fungus, strain KR21-2. *FEMS Microbiol Ecol* **47**: 101-109.
- Miyata, N., Tani, Y., Maruo, K., Tsuno, H., Sakata, M., and Iwahori, K. (2006a) Manganese(IV) oxide production by *Acremonium* sp. strain KR21-2 and extracellular Mn(II) oxidase activity. *Appl Environ Microbiol* **72**: 6467-6473.
- Miyata, N., Maruo, K., Tani, Y., Tsuno, H., Seyama, H., Soma, M., and Iwahori, K. (2006b) Production of biogenic manganese oxides by anamorphic ascomycete fungi isolated from streambed pebbles. *Geomicrobiol J* **23**: 63-73.
- Monroe, M.E., Shaw, J.L., Daly, D.S., Adkins, J.N., and Smith, R.D. (2008) MASIC: a software program for fast quantitation and flexible visualization of chromatographic profiles from detected LC-MS(/MS) features. *Comput Biol Chem* **32**: 215-217.
- Murray, K.J., and Tebo, B.M. (2007) Cr(III) is indirectly oxidized by the Mn(II)-oxidizing bacterium *Bacillus* sp. strain SG-1. *Environ Sci Technol* **41**: 528-533.
- Nealson, K.H., and Saffarini, D. (1994) Iron and manganese in anaerobic respiration - Environmental significance, physiology, and regulation. *Annu Rev Microbiol* **48**: 311-343.
- Nelson, Y.M., Lion, L.W., Ghiorse, W.C., and Shuler, M.L. (1999) Production of biogenic Mn oxides by *Leptothrix discophora* SS-1 in a chemically defined growth medium and evaluation of their Pb adsorption characteristics. *Appl Environ Microbiol* **65**: 175-180.
- Nico, P.S., Anastasio, C., and Zamoski, R.J. (2002) Rapid photo-oxidation of Mn(II) mediated by humic substances. *Geochim Cosmochim Acta* **66**: 4047-4056.

Nilsson, T., Daniel, G., Kirk, T.K., and Obst, J.R. (1989) Chemistry and microscopy of wood decay by some higher ascomycetes. *Holzforschung* **43**: 11-18.

O'Donnell, V.B., Tew, D.G., Jones, O.T.G., and England, P.J. (1993) Studies on the inhibitory mechanism of iodonium compounds with special reference to neutrophil NADPH oxidase. *Biochem J* **290**: 41-49.

Page, M.J., and Di Cera, E. (2008) Serine peptidases: Classification, structure and function. *Cell Mol Life Sci* **65**: 1220-1236.

Palumbo, A., Misuraca, G., D'Ischia, M., and Prota, G. (1985) Effect of metal ions on the kinetics of tyrosine oxidation catalysed by tyrosinase. *Biochem J* **228**: 647-651.

Palumbo, A., D'Ischia, M., Misuraca, G., Carratu, L., and Prota, G. (1990) Activation of mammalian tyrosinase by ferrous ions. *Biochim Biophys Acta* **1033**: 256-260.

Perez, J., and Jeffries, T.W. (1992) Roles of manganese and organic acid chelators in regulating lignin degradation and biosynthesis of peroxidases by *Phanerochaete chrysosporium*. *Appl Environ Microbiol* **58**: 2402-2409.

Polpitiya, A.D., Qian, W.-J., Jaitly, N., Petyuk, V.A., Adkins, J.N., Camp, D.G. et al. (2008) DANTE: a statistical tool for quantitative analysis of -omics data. *Bioinformatics* **24**: 1556-1558.

Ramsden, C.A., and Riley, P.A. (2014) Tyrosinase: The four oxidation states of the active site and their relevance to enzymatic activation, oxidation, and inactivation. *Bioorg Med Chem* **22**: 2388-2395.

Reichard, U., Léchenne, B., Asif, A.R., Streit, F., Grouzmann, E., Jousson, O., and Monod, M. (2006) Sedolisins, a new class of secreted proteins from *Aspergillus fumigatus* with endoprotease or tripeptidyl peptidase activity at acidic pHs. *Appl Environ Microbiol* **72**: 1739-1748.

Rosenblum, E.B., Stajich, J.E., Maddox, N., and Eisen, M.B. (2008) Global gene expression profiles for life stages of the deadly amphibian pathogen *Batrachochytrium dendrobatidis*. *PNAS* **105**: 17034-17039.

Rubert, K.F., and Pedersen, J.A. (2006) Kinetics of oxytetracycline reaction with a hydrous manganese oxide. *Environ Sci Technol* **40**: 7216-7221.

Sakasegawa, S., Ishikawa, H., Imamura, S., Sakuraba, H., Goda, S., and Ohshima, T. (2006) Bilirubin oxidase activity of *Bacillus subtilis* CotA. *Appl Environ Microbiol* **72**: 972-975.

Salvi, F., and Gadda, G. (2013) Human choline dehydrogenase: Medical promises and biochemical challenges. *Arch Biochem Biophys* **537**: 243-252.

Santelli, C.M., Chaput, D.L., and Hansel, C.M. (2014) Microbial communities promoting Mn(II) oxidation in Ashumet Pond, a historically polluted freshwater pond undergoing remediation. *Geomicrobiol J* **31**: 605-616.

Santelli, C.M., Pfister, D.H., Lazarus, D., Sun, L., Burgos, W.D., and Hansel, C.M. (2010) Promotion of Mn(II) oxidation and remediation of coal mine drainage in passive treatment systems by diverse fungal and bacterial communities. *Appl Environ Microbiol* **76**: 4871-4875.

Schlosser, D., and Höfer, C. (2002) Laccase-catalyzed oxidation of Mn²⁺ in the presence of natural Mn³⁺ chelators as a novel source of extracellular H₂O₂ production and its impact on manganese peroxidase. *Appl Environ Microbiol* **68**: 3514-3521.

Semighini, C.P., and Harris, S.D. (2008) Regulation of apical dominance in *Aspergillus nidulans* hyphae by reactive oxygen species. *Genetics* **179**: 1919-1932.

Shary, S., Ralph, S.A., and Hammel, K.E. (2007) New insights into the lignolytic capability of a wood decay ascomycete. *Appl Environ Microbiol* **73**: 6691-6694.

Shevchenko, A., Tomas, H., Havli, J., Olsen, J.V., and Mann, M. (2007) In-gel digestion for mass spectrometric characterization of proteins and proteomes. *Nat Prot* **1**: 2856-2860.

Smith, P.K., Krohn, R.I., Hermanson, G.T., Mallia, A.K., Gartner, F.H., Provenzano, M.D. et al. (1985) Measurement of protein using bicinchoninic acid. *Anal Biochem* **150**: 76-85.

Solomon, E.I., Sundaram, U.M., and Machonkin, T.E. (1996) Multicopper oxidases and oxygenases. *Chem Rev* **96**: 2563-2605.

Stone, A.T., and Morgan, J.J. (1984) Reduction and dissolution of manganese(III) and manganese(IV) oxides by organics. 1. Reaction with hydroquinone. *Environ Sci Technol* **18**: 450-456.

Sunda, W.G., and Kieber, D.J. (1994) Oxidation of humic substances by manganese oxides yields low-molecular-weight organic substrates. *Nature* **367**: 62-64.

Taguchi, F., Yamamoto, Y., and Satoh, K. (1995) Recognition of the structure around the site of cleavage by the carboxyl-terminal processing protease for D1 precursor protein of the photosystem II reaction center. *J Biol Chem* **270**.

Tanaka, N., and Murao, S. (1981) A new enzyme bilirubin oxidase produced by *Myrothecium verrucaria* MT-1. *Agric Biol Chem* **45**: 2383-2384.

Tang, Y., Zeiner, C.A., Santelli, C.M., and Hansel, C.M. (2013) Fungal oxidative dissolution of the Mn(II)-bearing mineral rhodochrosite and the role of metabolites in manganese oxide formation. *Environ Microbiol* **15**: 1063-1077.

Tebo, B.M., Bargar, J.R., Clement, B.G., Dick, G.J., Murray, K.J., Parker, D. et al. (2004) Biogenic manganese oxides: properties and mechanisms of formation. *Annu Rev Earth Planet Sci* **32**.

Thompson, I.A., Huber, D.M., and Schulze, D.G. (2006) Evidence of a multicopper oxidase in Mn oxidation by *Gaeumannomyces graminis var. tritici*. *Phytopathology* **96**: 130-136.

Wang, Y., Yang, F., Gritsenko, M.A., Wang, Y., Clauss, T., Liu, T. et al. (2011) Reversed-phase chromatography with multiple fraction concatenation strategy for proteome profiling of human MCF10A cells. *Proteomics* **10**: 2019-2026.

Wariishi, H., Valli, K., and Gold, M.H. (1992) Manganese(II) oxidation by manganese peroxidase from the basidiomycete *Phanerochaete chrysosporium* - Kinetic mechanism and role of chelators. *J Biol Chem* **267**: 23688-23695.

Whittaker, M.M., Kersten, P.J., Nakamura, N., Sanders-Loehr, J., Schweizer, E.S., and Whittaker, J.W. (1996) Glyoxal oxidase from *Phanerochaete chrysosporium* is a new radical-copper oxidase. *J Biol Chem* **271**: 681-687.

Williams, H.C., and Griendling, K.K. (2007) NADPH oxidase inhibitors: New anti hypertensive agents? *J Cardiovasc Pharmacol* **50**: 9-16.

Zamocky, M., Hallberg, M., Ludwig, R., Divne, C., and Haltrich, D. (2004) Ancestral gene fusion in cellobiose dehydrogenases reflects a specific evolution of GMC oxidoreductases in fungi. *Gene* **338**: 1-14.

Zou, Y., Hu, W., Jiang, A., and Ma, K. (2014) Partial purification and characterization of a novel extracellular tyrosinase from *Auricularia auricula*. *Appl Biochem Biotechnol* **172**: 1460-1469.

CHAPTER 4

Comparative analysis of secretome profiles of four manganese(II)-oxidizing ascomycete fungi

This chapter is currently in preparation for journal submittal.
(Zeiner C.A., Purvine S.O., Zink E., Wu S., Paša-Tolić L.,
Chaput D.L., Santelli C.M., Hansel C.M.)

Supplemental Material for this chapter is presented in **Appendix 3**.

Abstract

Fungal secretomes contain a wide range of hydrolytic enzymes, including cellulases, hemicellulases, pectinases, and lignin-degrading accessory enzymes, that synergistically drive litter decomposition in the environment. While secretome studies of model organisms such as *Phanerochaete chrysosporium* and *Aspergillus* species have greatly expanded our knowledge of these oxidative enzymes, few have extended secretome characterization to environmental isolates or conducted side-by-side comparisons of phylogenetically diverse species. Here we use a combination of iTRAQ proteomics and customized bioinformatic analyses to characterize and compare the proteomic composition of the secretomes of four Mn(II)-oxidizing Ascomycetes growing on a complex medium. We demonstrate that the organisms produce a rich yet functionally similar suite of extracellular oxidative enzymes, with species-specific differences in secretome composition arising from unique amino acid sequences rather than overall protein function. Furthermore, we identify not only a wide range of carbohydrate-active enzymes that can directly oxidize recalcitrant carbon, but also an impressive suite of redox-active auxiliary activities that suggests a role for Fenton-based hydroxyl radical formation in indirect, non-specific lignocellulose attack. Our findings highlight the diverse oxidative capacity of these environmental isolates and enhance our understanding of the role of filamentous Ascomycetes in carbon turnover in the environment.

Introduction

Fungal secretomes are reservoirs of a diverse suite of oxidative enzymes and reactive metabolites that are specialized to breakdown recalcitrant plant and animal material in the environment. In particular, fungi secrete a wide range of hydrolytic enzymes, including cellulases, hemicellulases, pectinases, and lignin-degrading accessory enzymes that generate reactive oxygen species (ROS), which synergistically drive litter decomposition in natural systems and can be harnessed for industrial applications (Perez et al., 2002; Ruiz-Duenas and Martinez, 2009; Dashtban et al., 2010; Hatakka and Hammel, 2010). As such, fungal secretomes are critical drivers of global carbon cycling and climate dynamics, as well as an essential mediator in renewable energy production.

The continued advancement of analytical techniques in microbial genomics, transcriptomics, proteomics, and metabolomics has allowed researchers to delve more deeply into the mechanistic underpinnings of complex microbially-mediated processes in the environment, generating a considerable amount of data and facilitating new insights into microbial metabolism. In particular, comparative proteomics has proven to be a valuable tool in investigating the response of fungal secretomes to different growth conditions and environmental stimuli, including substrate composition (Medina et al., 2004; Lu et al., 2010; Vanden Wymelenberg et al., 2010; Liu et al., 2013), growth phase (Saykhedkar et al., 2012), lifestyle (Liang et al., 2013), starvation (Nitsche et al., 2012), and response of a fungal pathogen to its host (Phalip et al., 2005) or vice versa (Muñoz-Gómez et al., 2014). These comprehensive secretome characterization studies have included both Basidiomycetes and Ascomycetes, primarily focusing on elucidating the mechanisms of demonstrated lignin degradation capacity of white-rot Basidiomycetes (Vanden Wymelenberg et al., 2010; Rohr et al., 2013; Hori et al.,

2014) and optimizing the production of cellulose-degrading enzymes in model Ascomycete fungi in the *Aspergillus* (Nitsche et al., 2012; Saykhedkar et al., 2012) and *Fusarium* (Phalip et al., 2005) genera. While our knowledge surrounding the oxidative enzymes secreted by these organisms is expanding rapidly, few studies have extended secretome characterization efforts beyond model organisms to environmental isolates, and as such, the mechanisms underlying their contribution to recalcitrant carbon degradation in terrestrial systems remain poorly understood.

We have recently isolated over a dozen strains of manganese (Mn)(II)-oxidizing, filamentous Ascomycetes from passive coal mine drainage treatment systems (Santelli et al., 2010) and a historically metal-contaminated freshwater lake (Santelli et al., 2014). These organisms have demonstrated cellulose-degradation capacity (C. M. Santelli, unpublished data), although the mechanisms by which they catalyze this process remain unknown. Indeed, the primary carbon source supporting these organisms at the coal mine drainage treatment site is waste plant material (e.g., corn cobs). Furthermore, while it is unclear whether these organisms' ability to oxidize Mn(II) is linked to their ability to breakdown cellulose, Mn(II) oxidation has been directly linked to lignocellulose degradation in white-rot Basidiomycetes, in which it is dictated by extracellular enzymes and reactive oxygen species in the secretome (Glenn et al., 1986; Wariishi et al., 1992; Höfer and Schlosser, 1999; Schlosser and Höfer, 2002).

Recent work by our laboratory has demonstrated that Mn(II) oxidation in three of our isolates is similarly driven by secretome composition (Tang et al., 2013; Zeiner et al., In review) and, moreover, that some of the enzymes implicated in Mn(II) oxidation in these Ascomycetes (e.g., GMC oxidoreductases, radical copper oxidases) have also demonstrated cellulose degradation capacity in Basidiomycete wood-degraders (Zeiner et al., In review). Interestingly,

the extracellular enzymes responsible for Mn(II) oxidation in our isolates varied by species, and the organisms' Mn(II) oxidative capacity changed over time (Zeiner et al., In review). The mechanistic diversity among species and environmental conditions lends support for extending secretome characterization studies to a wide variety of phylogenetically diverse organisms. In addition, few studies have directly compared the secretome composition of multiple organisms side-by-side (see (Shi et al., 2013) for an example using yeasts and (Vanden Wymelenberg et al., 2010) for wood decay Basidiomycetes), a valuable tool in investigating this species-specific diversity in extracellular oxidative processes and identifying new enzymatic targets for industrial applications.

In this study, we begin to address these knowledge gaps by fully characterizing the proteomic composition of the secretomes of four phylogenetically diverse, Mn(II)-oxidizing, Ascomycete fungi: *Alternaria alternata* SRC11rK2f, *Stagonospora* sp. SRC11sM3a, *Pyrenochaeta* sp. DS3sAY3a, and *Paraconiothyrium sporulosum* AP3s5-JAC2a. Using iTRAQ proteomics and customized bioinformatic analyses, we directly compared the composition and functional diversity of the secretomes among organisms, demonstrating that the fungi produce a rich yet functionally similar suite of extracellular enzymes, despite the presence of many species-specific proteins. Furthermore, we identified numerous lignocellulose-degrading enzymes in each of the 4 fungi that may be used as targets for future mechanistic investigations of the cellulose-degrading capacity of these organisms. This work highlights the rich functional diversity and oxidative capacity of these fungal secretomes, demonstrates the utility of iTRAQ proteomics in interspecies comparisons, and enhances our understanding of the role of filamentous Ascomycetes in plant material turnover in the environment.

Materials and Methods

Fungal species and culture medium. We investigated four filamentous Ascomycete fungi isolated from two locations. Three species were isolated from passive coal mine drainage treatment systems in central Pennsylvania that attenuate high concentrations of Mn (Santelli et al., 2010): *Alternaria alternata* SRC1lrK2f, *Stagonospora* sp. SRC1lsM3a, and *Pyrenochaeta* sp. DS3sAY3a. The fourth species was isolated from Ashumet Pond, Massachusetts, a natural freshwater lake (Santelli et al., 2014): *Paraconiothyrium sporulosum* AP3s5-JAC2a. This field site was historically polluted with elevated concentrations of phosphate and metals, including Fe and Mn, and is currently undergoing remediation. Three of the fungi (*Stagonospora* sp., *Pyrenochaeta* sp., and *P. sporulosum*) are Mn(II) oxidizers; *A. alternata* lost its ability to oxidize Mn(II) during laboratory culture.

All fungal species were grown in HEPES-buffered (20 mM, pH 7) AY medium containing 0.25 g L⁻¹ sodium acetate, 0.15 g L⁻¹ yeast extract, and 1 mL L⁻¹ trace element stock (10 mg L⁻¹ CuSO₄•5H₂O, 44 mg L⁻¹ ZnSO₄•7H₂O, 20 mg L⁻¹ CoCl₂•6H₂O, and 13 mg L⁻¹ Na₂MoO₄•2H₂O) supplemented with MnCl₂ (0-200 μM). All chemicals were reagent grade or higher. Fungal cultures were maintained on petri dishes containing agar-solidified (2% agar) AY medium with 200 μM Mn(II) (hereafter AY + Mn).

Culture conditions and secretome harvesting. Homogenized inocula were used for all culture experiments. Inocula were prepared by aseptically removing the entire contents of a 90 mm petri dish (including fungal mycelia and associated agar) that had incubated at room temperature (20°C) until the mycelia had reached the edge of the agar. The contents were then placed in an autoclaved kitchen blender (Oster model BVLB07) with 100 mL of AY + Mn medium and homogenized on high speed for 2 minutes. On the same day that the homogenized

inocula were prepared, 100 μ L of the inoculum was used to inoculate 100 mL liquid cultures in AY + Mn medium.

For characterization of secretome samples, liquid cultures of each of the 4 fungi were incubated at room temperature and ambient light, without agitation, for 7, 14, or 21 days. For each fungus and each time point, individual 100 mL cultures were combined into 500 mL samples. All samples were prepared in duplicate. Upon harvesting, bulk biomass was removed with a sterile wooden stick and discarded, and the spent medium was filtered through a 0.45 μ m polyethersulfone membrane (VWR) to remove remaining cells and Mn oxides. Samples were then concentrated using a centrifugal filter with a 10 kDa, low protein adhesion membrane (EMD Millipore). Centrifugation proceeded at $2200 \times g$ on a Sorvall RT 6000B centrifuge with H1000B swing-bucket rotor until all liquid had passed through the membrane. The resulting secretome samples were rinsed with 20 mM HEPES, pH 7 and stored at -80°C until analysis.

Protein quantification. Protein in secretome samples was quantified using a PierceTM BCA protein assay kit (Thermo Fisher Scientific) as conducted previously (Smith et al., 1985). The quantity of protein recovered from 500 mL secretome samples generally ranged between 200 and 1000 μ g, depending on species and secretome age.

Protein identification by iTRAQ proteomics. Peptide sequencing of all secretome samples was performed at the Environmental Molecular Sciences Laboratory, part of Pacific Northwest National Laboratory.

(a) Sample preparation. Secretome samples were prepared for mass spectrometry using a trypsin digestion (Callister et al., 2008). In summary, the proteins were denatured with urea (8 M) and reduced with 5 mM dithiothreitol (DTT, Sigma–Aldrich) for 30 min at 60°C . The samples were then diluted 10-fold with 100 mM ammonium bicarbonate with 1 mM CaCl_2 and

then digested for 3 h at 37°C using porcine sequencing-grade trypsin (Promega) at a substrate/enzyme mass ratio of 50:1. The digestion was quenched by adding 10% trifluoroacetic acid to a final concentration of 0.1% before desalting with a C-18 solid phase extraction column (Supelco), performed using a Gilson GX-274 Liquid Handler. The resulting peptide solution was concentrated to 50 mL in a vacuum concentrator, and a BCA assay was performed to estimate the protein concentration, as above. To enable quantitation, the samples were isobarically labeled with Isobaric Tags for Relative and Absolute Quantitation (iTRAQ) 8-plex Reagent using the manufacturer's instructions (ABSciex, PN#4352135). Moreover, a universal reference sample created by pooling all the iTRAQ-labeled samples was used to enable normalization between the samples. The labeled sample were desalted with a C-18 solid phase extraction column (Supelco) and then fractionated with a reverse-phase C18 column and pooled using concatenation (Wang et al., 2011). The resulting fractions were diluted to 0.07 ug/uL and were then analyzed using LC/MS/MS.

(b) LC/MS/MS analysis. The iTRAQ labeled fractions were processed on a Waters nano-Acquity dual pumping UPLC system with a custom on-line trapping system for a 5 μL injection processed at 3 $\mu\text{L min}^{-1}$. The trapped sample was then reverse eluted onto the analytical column at a 300 nL min^{-1} flow rate. Both the trapping column (150 $\mu\text{m i.d.} \times 4 \text{ cm}$ long) and analytical column (75 $\mu\text{m i.d.} \times 70 \text{ cm}$ long) were packed in-house using Jupiter C18 media (Phenomenex) particles (5 μm for the trapping column and 3 μm for the analytical column) into 360 $\mu\text{m o.d.}$ fused silica (Polymicro Technologies Inc.) with 1 cm sol-gel frits for media retention (Maiolica et al., 2005). The gradient began with mobile phase A (0.1% formic acid in water) and switched to mobile phase B (0.1% formic acid in acetonitrile) with the

following gradient profile (min, %B): 0, 1; 2, 8; 20, 12; 75, 30; 97, 45; 100, 95; 110, 95; 115, 1; 150, 1.

Data were acquired using a LTQ Orbitrap Velos mass spectrometer (Thermo Scientific) with a custom made nano-electrospray ionization interface utilizing custom made, chemically-etched fused silica electrospray emitters (150 μm o.d. x 20 μm i.d) (Kelly et al., 2006). The heated capillary temperature was set to 350°C with a spray voltage of 2.2 kV. Data were acquired for a total of 100 min after a 15 min delay from sample injection. FT-MS spectra were acquired from 300-1800 m/z at a resolution of 30k and while the top 10 FT-HCD-MS/MS spectra were acquired in data dependent mode at a resolution of 7.5k using a normalized collision energy of 45.

(c) Bioinformatics. MS/MS spectra were converted to ASCII text using the DeconMSn tool (Mayampurath et al., 2008) which helps account for incorrect monoisotope assignments. Spectra from all 4 fungi were then searched as a combined dataset with MSGFPlus (Kim and Pevzner, 2014) using a custom protein FASTA containing genomes of all 4 fungal species. At the time this work was performed, the fungal genomes had been newly sequenced by the Joint Genome Institute (JGI) and were still in contig form. The FASTA was amended with common contaminants (e.g., trypsin and human keratin sequences). Within the combined FASTA, individual peptides were first searched against the *A. alternata* genome, followed by *P. sporulosum*, *Pyrenochaeta* sp., and finally *Stagonospora* sp.

All peptide candidate amino acid sequences were statically modified with the iTRAQ 8-plex reporter ion conjugate mass (+304.205353 Da on Lysine residues and peptide N-terminus), dynamically modified for oxidized methionine, with a parent mass tolerance of +/- 20ppm. Other settings include partially tryptic cleavages, +/-1 Da parent corrections (to further account for

incorrect monoisotope assignments), MS level data centroiding, and decoy search mode enabled. The MASIC software tool (Monroe et al., 2008) was used to extract the iTRAQ 8-plex reporter ion abundances from the MS/MS spectra with +/- 10ppm mass tolerance.

An in-house analysis pipeline was used to combine the peptide identifications with their related iTRAQ 8-plex reporter ion abundances. Briefly, the pipeline imports the peptide identification results, filters the peptide results to 1% FDR (using MSGFPlus' reported Q-value \leq 0.01, which is derived using the standard decoy approach (Elias and Gygi, 2010)), sums reporter ion intensities per peptide across multiple strong cation exchange fractions within a given sample, and outputs the peptide sequence with associated reporter ion intensities for each fractionated sample. Proteins associated with each peptide were reported separately. For this dataset, the occurrence of peptide sequences occurring in more than one protein were rare, but in those cases where redundancy did occur all proteins associated with a peptide were identified. For biological interpretation of the data, only the first protein reference associated with a peptide was used, and the function of this protein was manually checked against other protein matches to ensure that all protein functions for a particular peptide were similar.

Peptide-level relative abundance data were normalized by mean central tendency normalization using the Inferno implementation of the Dante analysis tool (Polpitiya et al., 2008). Since the relative abundances of peptides in pooled samples were similar in all pools, pools were not used for normalization. The limit of quantitation (LOQ) for peptide relative abundance was defined as 2 standard deviations below the average log 2 transformed relative abundance of all peptides across all samples; this LOQ roughly corresponds to the lower 95% confidence interval. To determine which abundance data were below the LOQ, the log 2 transformed relative abundances of each peptide were averaged (including zeros for samples in

which the peptide was not detected) between the two biological replicates for each fungus and time point. Averages below the LOQ were removed from the dataset. Relative abundance data for averaged pairs was then anti-logged, and, for each protein, summed for all peptides that mapped to that protein. Relative abundance data were then re-normalized using mean central tendency normalization to correct for any variability introduced during processing. Finally, data were log 2 transformed for biological interpretation.

Functional information was obtained by searching a combined database of NCBI and UniProt fungal protein sequences for proteins identified in this study using BLAST and a custom script. For proteins for which the highest-scoring (lowest E-value) match was hypothetical or uncharacterized, the highest-scoring non-hypothetical match was reported. Proteins with no matches (hypothetical or otherwise) having an E-value below 10^{-9} (for proteins with 1 identified peptide) or 10^{-6} (for proteins with 2+ identified peptides) were reported as hypothetical. Functional information obtained via BLAST analysis was manually checked against automatically assigned annotations in the newly-sequenced genomes. To facilitate this, proteins identified in this study were mapped to JGI protein IDs, which were then used to retrieve and check genome annotations. As automatically-assigned annotations often contain errors (Krijger et al., 2014), emphasis was placed on functional information from the BLAST analysis, as has been done by others (Vanden Wymelenberg et al., 2010). All proteins were then functionally categorized according to the Carbohydrate-Active Enzymes (CAZy) Database (www.cazy.org) (Lombard et al., 2014) and MEROPS Peptidase Database (<http://merops.sanger.ac.uk/>) (Rawlings et al., 2014) classification systems, using UniProt family and domain designations to aid in categorization.

The genome sequences and annotations for the 4 fungi in this study are available at the Joint Genome Institute (JGI) fungal genomics resource MycoCosm (Grigoriev et al., 2014) at <http://genome.jgi-psf.org/programs/fungi/index.jsf>.

Separate chapters. Overall secretome composition, functional diversity, and interspecies comparisons are presented in this chapter, exclusive of protein relative abundance data and changes in secretome composition over time. A quantitative time-course analysis is presented in Chapter 5.

Results

Full datasets. A complete list of the proteins identified in each of the four fungal secretomes, including predicted functions and CAZy and MEROPS classifications (for carbohydrate-active enzymes and peptidases, respectively), is presented in Table S4.1 (submitted electronically).

Number of proteins identified in the secretome. Over 1,300 proteins were identified in the secretome of each of the 4 fungi, ranging from 1,369 identified proteins in the *Pyrenochaeta* sp. secretome to 1,618 identified proteins in the *Stagonospora* sp. secretome (Figure 4.1). Within CAZy and MEROPS classifications, between 511 (in the *Pyrenochaeta* sp. secretome) and 569 (in the *Stagonospora* sp. secretome) extracellular enzymes were identified.

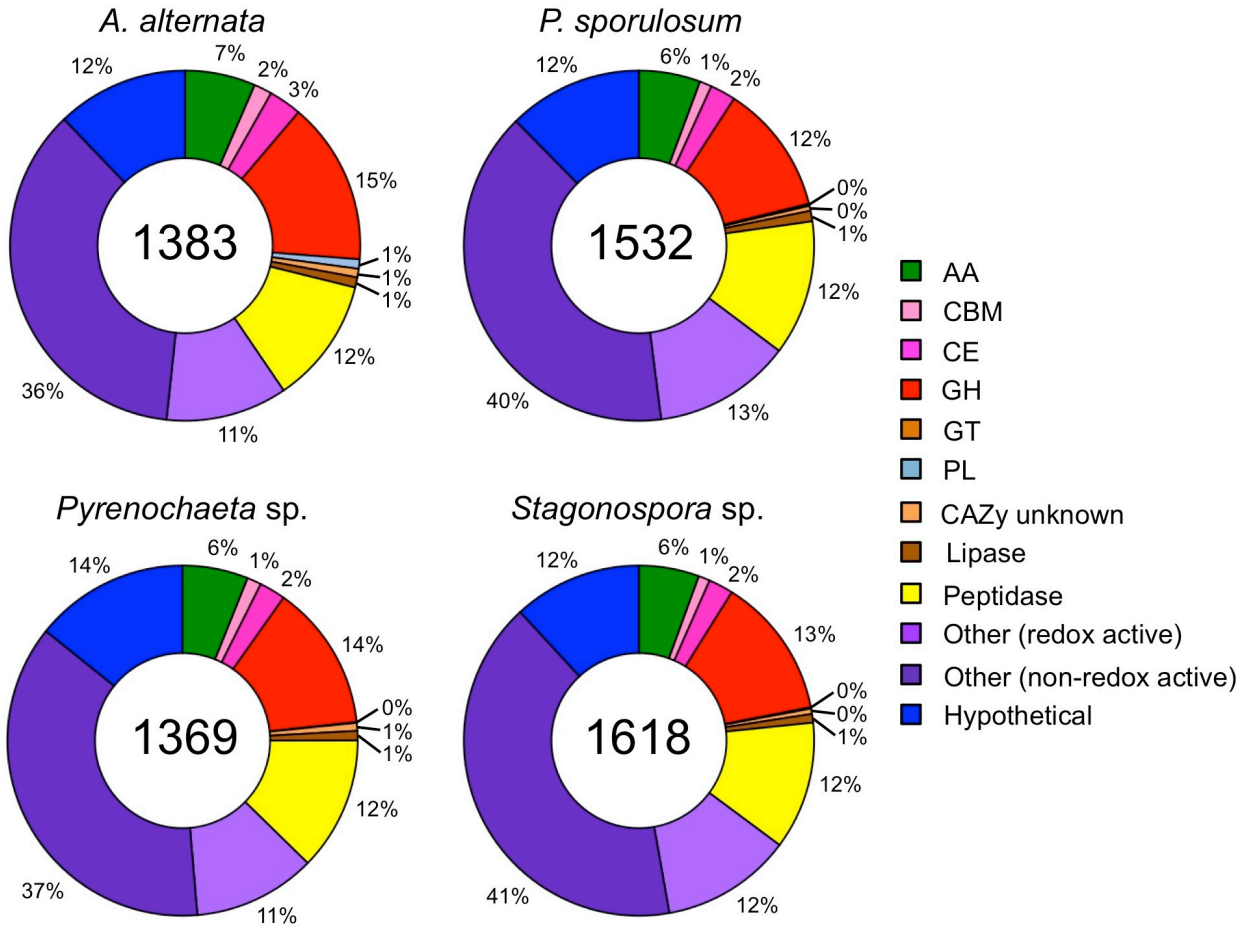


Figure 4.1. Distribution of proteins identified via iTRAQ proteomics in secretomes of 4 Ascomycete fungi grown on AY+Mn medium. For each fungus, proteins are shown if they were identified in any time point. Total number of proteins identified for each fungus, inclusive of all time points, is indicated in center of circles. Abbreviations from CAZy database: AA = auxiliary activities; CBM = carbohydrate-binding module; CE = carbohydrate esterase; GH = glycoside hydrolase; GT = glucosyltransferase; PL = polysaccharide lyase.

Secretome diversity across broad functional groups. Categorizing the proteins in each secretome based on broad functional groups according to the CAZy and MEROPS databases reveals a striking similarity in secretome functional diversity among the four organisms (Figure 4.1). The total proportion of CAZymes identified in the secretomes ranged from 22% in *P. sporulosum* to 28% in *A. alternata* and consisted predominantly of glycoside hydrolases (GHs; 12-15%) and redox-active auxiliary activities (AAs; 6-7%) in all four fungi. Peptidases

comprised 12% of identified proteins in each of the fungal secretomes, while lipases comprised only 1%. Identified proteins that are not considered by the CAZy or MERPOS databases were categorized as “other” and constituted a large portion of the secretome for each fungus, ranging from 47% in *A. alternata* to 53% in both *P. sporulosum* and *Stagonospora sp.* Approximately one-third of “other” identified proteins were redox-active and included dehydrogenases, oxidases, reductases, and FAD-binding proteins, among others. Non-redox active “other” proteins varied widely in predicted function and included many proteins likely of intracellular origin. Hypothetical proteins, for which no function could be predicted based on genome annotations and a BLAST analysis against sequenced fungal genomes in NCBI and UniProt, comprised 12-14% of the fungal secretomes.

Lignocellulose degrading enzymes (i.e., CAZymes) were identified in high numbers and with rich diversity in all four fungi (Table 4.1), representing all major CAZy classes. The quantity and diversity of CAZymes was highest among GHs, with over 40 families represented and approximately 200 proteins identified in this class in each fungus. Redox-active AAs and carbohydrate esterases (CEs) were also well represented. In all CAZy classes except glucosyltransferases (GTs; which were poorly represented in all four organisms), the secretome of *A. alternata* exhibited the greatest number of identified CAZymes and the richest family diversity.

Table 4.1. Summary of identified CAZymes in secretomes of four Ascomycete fungi.

Species	CAZyme Class											
	Glycoside hydrolases (GH)		Glycosyltransferases (GT)		Carbohydrate binding modules (CBM)		Carbohydrate esterases (CE)		Polysaccharide lyases (PL)		Auxiliary activities (AA)	
	Families	Proteins	Families	Proteins	Families	Proteins	Families	Proteins	Families	Proteins	Families	Proteins
<i>A. alternata</i>	46	219	0	0	8	23	6	42	4	12	6	90
<i>P. sporulosum</i>	43	193	1	1	6	17	5	36	2	2	6	87
<i>Pyrenochaeta sp.</i>	41	196	0	0	7	18	6	33	1	1	5	83
<i>Stagonospora sp.</i>	42	219	0	0	6	17	5	37	1	2	6	90

Secretome diversity among protein families. Interestingly, when secretome functional diversity is examined at a deeper level, focusing on individual protein families within CAZy classes, the marked similarity across these phylogenetically diverse fungi persists (Figure 4.2). Furthermore, the rich diversity of identified CAZymes in each organism is more clearly illustrated. Within the GH class (Figure 4.2A), the most frequently identified protein families included GH1 (cellulose-degrading β -glucosidases), GH5 (a diverse family of cellulases and hemicellulases), GH13 (a large family dominated by starch-degrading α -amylase), GH16-17 (diverse cellulases and hemicellulases), GH18 (chitinase), GH55/PL (exo- β -1,3-glucanase), and GH72/GT (β -1,3-glucanosyltransglycosylase). The most well-represented class of GHs was GH5 with 19-24 proteins identified in each organism. Other CAZy families (Figure 4.2D) that were well-represented in the secretomes included CBM18 (carbohydrate-binding modules with demonstrated chitin-binding function), CE1 (mainly carboxylesterases and acetyl xylan esterases), CE4 (polysaccharide deacetylases), CE5 (cutinase), and CAZymes whose family designations were unknown.

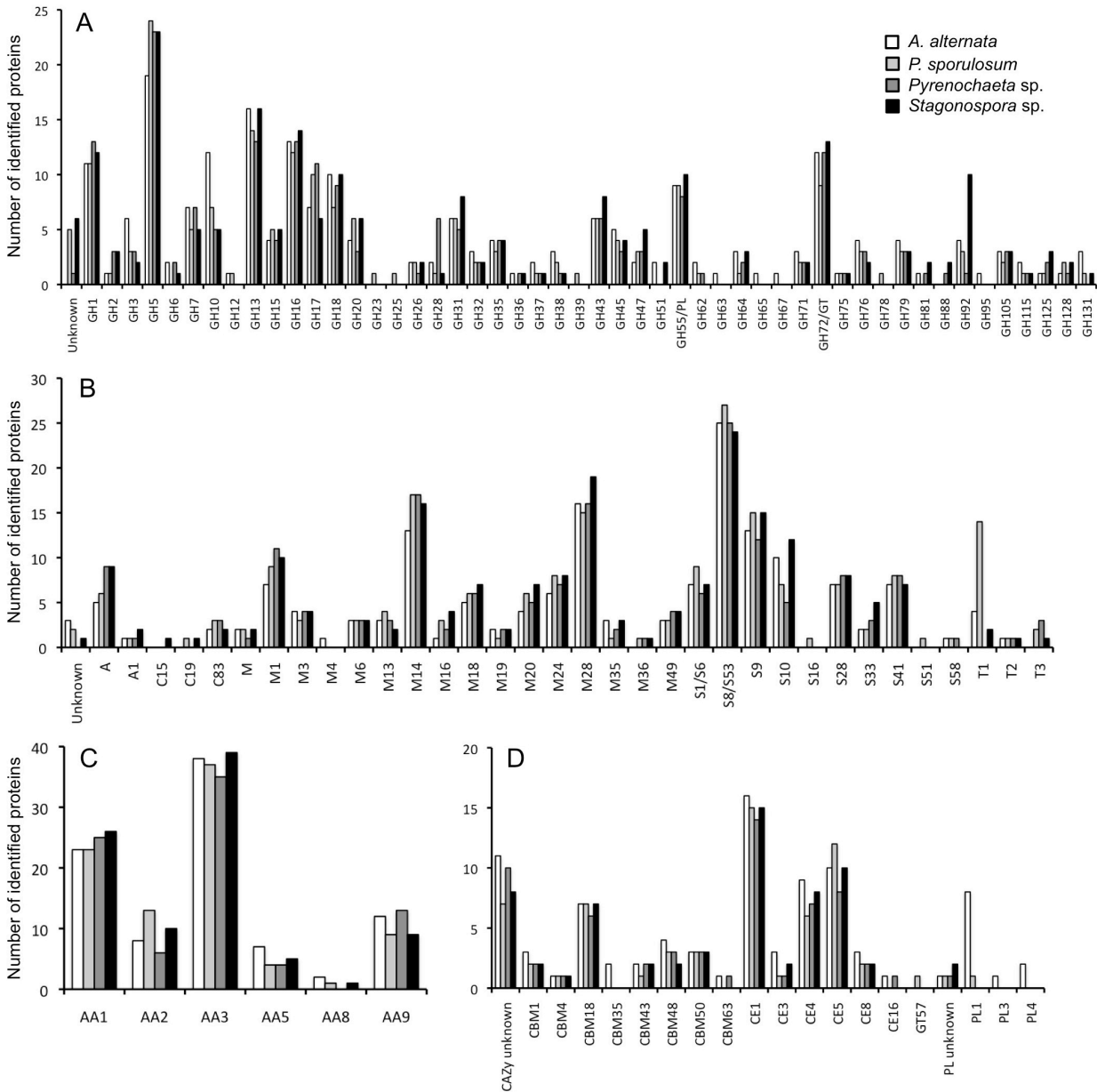


Figure 4.2. Distribution of proteins identified via iTRAQ proteomics in fungal secretomes among protein families according to the CAZy and MEROPS databases. (A) CAZy glycoside hydrolase families. (B) MEROPS peptidase families. (C) CAZy auxiliary activity families. (D) Other CAZyme families. For each fungus, proteins are counted if they were identified in any time point. Abbreviations as in Figure 4.1.

Among redox-active AAs (Figure 4.2C), the AA3 family (GMC oxidoreductases, predominantly with FAD cofactors) contained the highest number of identified proteins (approximately 35) in each fungus, and included choline dehydrogenases, cellobiose

dehydrogenases, and alcohol oxidases. Notably, numerous cellobiohydrolases and cellobiose dehydrogenases were identified in all 4 organisms. The AA1 family (multicopper oxidases) was also well represented, with approximately 25 proteins per fungus; identified proteins in this family included ascorbate oxidase, bilirubin oxidase, coproporphyrinogen III oxidase, tyrosinase, and two proteins that mapped to traditional fungal laccases. Neither of the laccases were identified in the *Pyrenochaeta* sp. secretome, although this organism produced numerous other multicopper oxidases for which specific enzyme names were unavailable. The AA2 (class II peroxidase) family was only moderately represented in these Ascomycete secretomes and was comprised primarily of catalases. Lignin-degrading peroxidases typically found in Basidiomycetes were rare, with one ligninase and one heme peroxidase identified; at least one of these enzymes was identified in each of the 4 fungi. The AA5 (radical copper oxidase) family was even less well represented, consisting of one glyoxal oxidase, five galactose oxidases, and several unspecified radical copper oxidases; enzymes of each type were identified in all 4 fungi. Three iron reductases, two of which with noted cellulose-binding capacity, in the AA8 family were identified, although none appeared in the *Pyrenochaeta* sp. secretome. Finally, numerous lytic polysaccharide monooxygenases in the AA9 family (formerly GH61) were identified in all 4 fungi.

Like the CAZy protein families, the functional diversity among MEROPS peptidase families was high in each organism and remained similar across the four fungi (Figure 4.2B). Peptidase families that were well populated in the secretomes included metallo- (M) and serine-type (S) peptidases such as M1 (aminopeptidase), M14 (carboxypeptidases), M28 (aminopeptidases and carboxypeptidases), S8/S53 (subtilisin/kexin/sedolisin, tripeptidyl peptidase I, and oryzin), S9 (dipeptidyl peptidase IV/V), and S10 (carboxypeptidases). While

metallo- and serine-type peptidases were the most frequently observed in the secretomes, other identified peptidase classes included aspartic (A), cysteine (C), and threonine (T); no glutamic-type (G) or mixed (P) peptidases were identified.

Despite the striking similarity among the four organisms, a few exceptions were identified in which protein families were dominated by proteins from a single fungus. Approximately twice as many proteins were identified in the GH3 (cellulase and hemicellulase) and GH10 (endo-1,4- β -xylanase) families in the *A. alternata* secretome than in any of the other three fungi, and several GH families (GH 63, 65, 67, and 95) were identified only in *A. alternata*. Additionally, polysaccharide lyases (PLs), other than GH55/PL family proteins, were almost exclusively identified in the *A. alternata* secretome and consisted predominantly of PL1 family proteins (pectate lyases). Like that of *A. alternata*, the *P. sporulosum* secretome included several GH families identified exclusively in this organism's secretome (GH23, 25, 39, and 78). The *Pyrenochaeta* sp. secretome exhibited more than twice as many identified proteins in the GH28 (pectinase) family than that of any other organism, while the GH92 (α -mannosidase) family was dominated by *Stagonospora* sp. proteins. Finally, more than three times as many proteins were identified in the MEROPS T1 family (proteasome peptidases involved in intracellular protein turnover) in the *P. sporulosum* secretome than in that of any other fungus.

Although “other” proteins were too numerous and varied to summarize concisely in distinct families, enzymes potentially involved in lignocellulose degradation were indeed observed. Particularly noteworthy were proteins potentially contributing to quinone redox cycling, including copper-containing amine oxidases with quinone-binding capability, which were identified in all 4 fungi.

Proteins unique to each fungus. Notwithstanding the pronounced similarities in proteomic composition of the secretome among the four fungi, we identified comparable levels of unique and shared amino acid sequences among the organisms (Figure 4.3). A total of 569 identified proteins were shared among all four organisms, comprising 35% (in *Stagonospora* sp.) to 42% (in *A. alternata*) of the total number of identified proteins in each fungus. Similarly, the number of proteins uniquely identified in each organism ranged from 25% (in *Pyrenochaeta* sp.; 381 proteins) to 42% (in *P. sporulosum*; 578 proteins) of the total for each fungus. The secretomes of *Pyrenochaeta* sp. and *Stagonospora* sp. exhibited the highest degree of similarity, with 836 shared sequences, while lower levels of shared sequences were observed between these two fungi and either *A. alternata* or *P. sporulosum*. Among pairs of fungi, the *P. sporulosum* and *Pyrenochaeta* sp. secretomes displayed the lowest level of similarity with 740 shared sequences. These observations correlate well with the previously-established phylogeny of the organisms (Santelli et al., 2014).

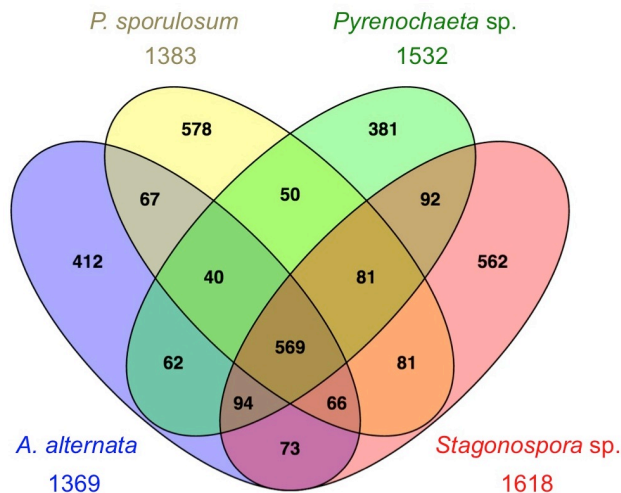


Figure 4.3. Venn diagram showing number of unique and shared proteins identified by iTRAQ proteomics in secretomes of 4 Ascomycete fungi. For each fungus, proteins were counted if they were identified in any time point. Total number of proteins identified for each fungus, inclusive of all time points, is indicated outside of diagram. Diagram generated with Venny 2.0 (Oliveros, J.C. (2007-2015) Venny. An interactive tool for comparing lists with Venn's diagrams. <http://bioinfogp.cnb.csic.es/tools/venny/index.html>).

Examination of unique and shared protein sequences among individual GH families yields further insight into the degree of interspecies similarity among the four fungal secretomes. While most GH families contained proteins that were identified in more than one fungus, the extent to which unique versions of these enzymes were identified in individual fungi varied among the families (Table 4.2). For instance, while GH20 and GH35 families comprised primarily (>80%) shared proteins, GH3 and GH92 families contained predominantly species-specific sequences (with only 20% of proteins shared by more than one fungus). Moreover, it is noteworthy that no GH families containing more than 3 identified proteins were represented exclusively by shared sequences; thus, species-specific versions of functionally similar enzymes were an inherent characteristic of these fungal secretomes. The example shown here for GH families was chosen for its rich diversity, but the patterns identified herein were representative of other CAZy and MEROPS protein families (data not shown).

GH Family	Percent shared	Total	Shared		Unique to one fungus			
			4 fungi	2-3 fungi	<i>A. alt.</i>	<i>P. spor.</i>	<i>Pyreno.</i>	<i>Stago.</i>
GH26	100%	2	1	1	0	0	0	0
GH62	100%	2	0	2	0	0	0	0
GH64	100%	3	1	2	0	0	0	0
GH75	100%	1	1	0	0	0	0	0
GH20	86%	7	1	5	0	1	0	0
GH35	83%	6	2	3	1	0	0	0
GH1	82%	17	5	9	0	0	2	1
GH47	80%	5	1	3	0	0	0	1
GH7	78%	9	3	4	0	0	2	0
GH79	75%	4	3	0	1	0	0	0
GH15	67%	6	3	1	0	1	0	1
GH38	67%	3	1	1	1	0	0	0
GH71	67%	3	1	1	1	0	0	0
GH72/GT	67%	18	5	7	1	1	1	3
GH17	64%	14	5	4	1	2	2	0
GH55/PL	64%	14	7	2	1	2	0	2
GH18	63%	16	2	8	2	1	1	2
GH105	60%	5	0	3	1	0	0	1
GH2	57%	7	0	4	1	0	1	1
GH5	55%	42	7	16	2	6	6	5
GH43	53%	17	0	9	2	3	1	2
GH36	50%	2	0	1	0	0	0	1
GH37	50%	2	1	0	1	0	0	0
GH81	50%	4	0	2	0	0	1	1
GH88	50%	2	0	1	0	0	0	1
GH115	50%	2	1	0	1	0	0	0
GH125	50%	6	1	2	0	0	1	2
GH13	48%	27	8	5	6	3	2	3
GH16	44%	25	3	8	4	3	3	4
GH32	40%	5	1	1	1	1	0	1
GH10	38%	16	2	4	6	2	1	1
GH31	38%	16	1	5	1	4	2	3
GH45	38%	8	2	1	2	2	0	1
GH6	33%	3	0	1	1	0	1	0
GH28	33%	9	0	3	1	0	4	1
GH128	33%	3	1	0	0	1	0	1
Unknown	33%	9	0	3	0	3	0	3
GH76	27%	11	1	2	3	2	2	1
GH3	20%	10	1	1	5	1	1	1
GH92	20%	15	0	3	2	2	0	8
GH12	0%	2	0	0	1	1	0	0
GH23	0%	1	0	0	0	1	0	0
GH25	0%	1	0	0	0	1	0	0
GH39	0%	1	0	0	0	1	0	0
GH51	0%	4	0	0	2	0	0	2
GH63	0%	1	0	0	1	0	0	0
GH65	0%	1	0	0	1	0	0	0
GH67	0%	1	0	0	1	0	0	0
GH78	0%	1	0	0	0	1	0	0
GH95	0%	1	0	0	1	0	0	0
GH131	0%	5	0	0	3	1	0	1
Total	--	395	72	128	59	47	34	55

Table 4.2. Number of shared and unique identified proteins in glycoside hydrolase families among the four fungal secretomes. *A. alt.* = *A. alternata*; *P. spor.* = *P. sporulosum*; *Pyreno.* = *Pyrenochaeta* sp.; *Stago.* = *Stagonospora* sp. Percent shared = total number of proteins shared between 2-4 fungi divided by total number of proteins identified.

Proteins unique to each fungus spanned the full range of broad CAZy and MEROPS functional groups that were identified in the full secretomes (Figure 4.4A). However, the proportion of CAZymes was considerably lower among unique proteins (ranging from 15% in *Stagonospora* sp. to 18% in *Pyrenochaeta* sp.) than in the whole secretomes, except in *A. alternata* where CAZymes comprised 30% of unique sequences. This difference was primarily attributed to the large number of unique GHs (59 proteins) identified in the *A. alternata* secretome and correlates with observations of unique GH families in this organism (Figure 4.2A), as discussed above. Few unique peptidases (4-6% of the total number of identified proteins) were identified in the secretomes of each fungus, while the majority of unique sequences consisted of “other” (44-61%) and hypothetical (18-28%) proteins. The “other” proteins exhibited a large range of functional diversity and included many intracellular proteins that may have been released via lysis during growth or sample processing. A complete list of proteins uniquely identified in each fungus is presented in Tables S4.2-S4.5 (submitted electronically).

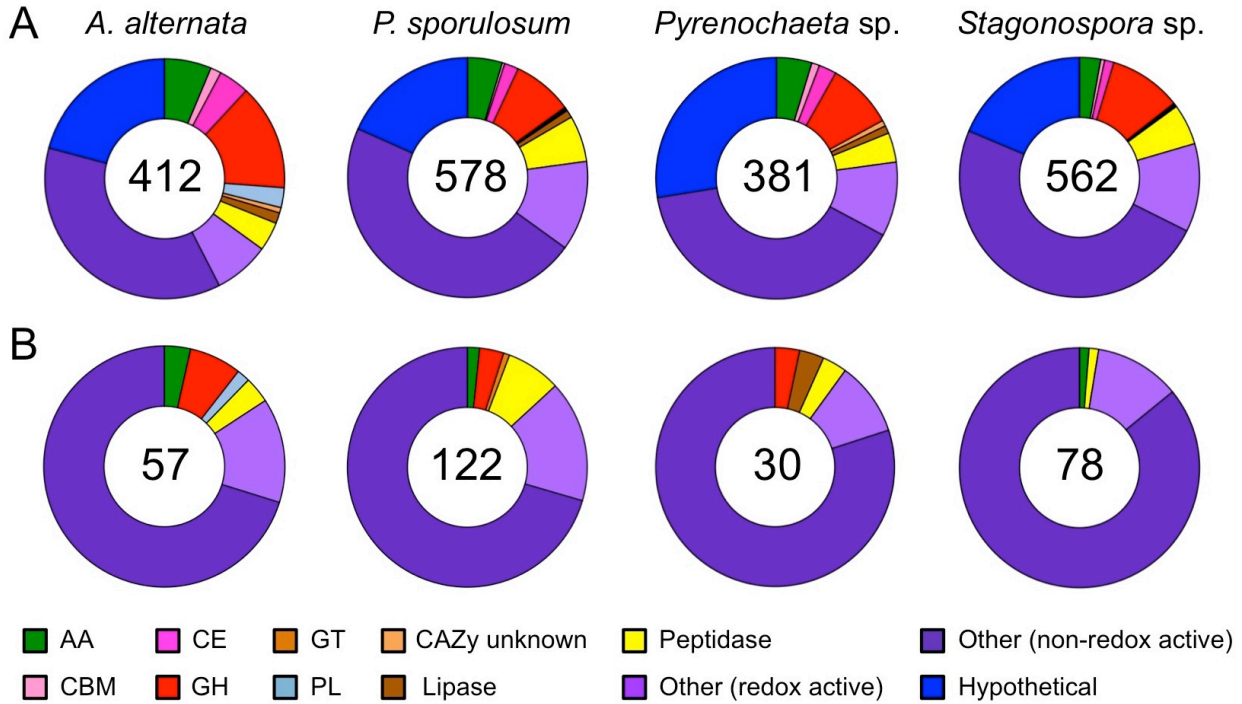


Figure 4.4. Distribution of proteins (A) unique to each fungus based on amino acid sequence (as determined by JGI protein ID) and (B) unique to each fungus based on predicted function (evaluated manually). Proteins identified via iTRAQ proteomics. For each fungus, proteins are included if they were identified in any time point. Total number of unique proteins identified for each fungus, inclusive of all time points, is indicated in center of circles. Abbreviations as in Figure 4.1.

Manually examining the predicted function of the identified proteins unique to each fungus revealed that only a small subset (ranging from 30 proteins in *Pyrenochaeta* to 122 proteins in *P. sporulosum*) of unique protein sequences were truly functionally unique to each organism (Figure 4.4B), thereby reinforcing the levels of interspecies similarity in secretome functional diversity as discussed above. The proportion of functionally unique CAZymes was very low (ranging from 12% in *A. alternata* to only 1% in *Stagonospora* sp.), while the vast majority of functionally unique enzymes identified in the secretomes were “other” proteins. (Hypothetical proteins were excluded from this analysis since their function is unknown.) In agreement with earlier observations, the secretome *A. alternata* exhibited the highest number of

functionally unique identified CAZymes (7 proteins), including 4 GHs (1 each in GH63, GH65, GH67, and GH95 families) and 2 AAs (a vanadium chloroperoxidase in the AA2 family and a cellulose binding protein in the AA9 family). The *P. sporulosum* secretome contained the largest number of functionally unique peptidases (9 proteins, 6 of which were MEROPS T1 proteasome peptidases), while only two non-“other” functionally unique proteins were identified in the *Stagonospora* sp. secretome (a peroxidase in the AA2 family and a MEROPS C15 peptidase). Functionally unique proteins identified in the *Pyrenochaeta* sp. secretome included a pectin-degrading rhamnogalacturonase in the GH28 family, an aspartic peptidase (candidapepsin), an unspecified lipase, and numerous “other” proteins. Notably, several “other” proteins potentially involved in quinone redox cycling were functionally unique to the *P. sporulosum* secretome, including a hydroxyquinol 1,2-dioxygenase, two quinone oxidoreductases, and a quinate permease.

Discussion

Secretome size. The secretomes we characterize in this study are quite large compared to published estimates and other experimental reports. In a computational study of the impact of phylogeny and fungal lifestyle on secretome size, Krijger et al. (2014) predicted a mean of approximately 900 proteins for Pezizomycotina, with higher estimates (up to approximately 1,600 proteins) for plant pathogens within this Ascomycota sub-phylum. Additionally, they estimated a secretome size of between approximately 600 and 1,500 proteins in fungi with genome sizes between 30 and 40 Mb. With secretome sizes of approximately 1,300-1,600 proteins (Figure 4.1) and genome sizes of 33 to 39 Mb (JGI Mycocosm), the plant pathogenic Ascomycetes we studied sit at the high end of both estimates. As it has been reported that

secretome sizes predicted by gene sequences may substantially underestimate the total number of secreted proteins (Antelmann et al., 2001), the large secretomes characterized in this study may indeed be representative of fungi with similar taxonomy and lifestyle. A conservative estimate excluding “other” and hypothetical proteins, whose functions are unknown and/or potentially intracellular, still places these fungi within or near both estimates, albeit at the low end.

Comprehensive secretome studies of other filamentous fungi have generally reported less than 350 proteins identified in the secretomes of filamentous Ascomycetes (Lu et al., 2010; Nitsche et al., 2012; Saykhedkar et al., 2012) and Basidiomycetes (Vanden Wymelenberg et al., 2010; Hori et al., 2014) based on protein harvests and LC/MS/MS analysis, including iTRAQ proteomic studies (Adav et al., 2010; Liu et al., 2013; Muñoz-Gómez et al., 2014), although these numbers are increasing over time concomitant with technological advancements.

Nonetheless, here we report substantially larger secretomes, even when “other” and hypothetical proteins are excluded. As we used standard sample preparation and protein digestion techniques, the large secretome sizes may be associated with the plant pathogenic lifestyle of these fungi, the identification of many proteins likely of intracellular origin in the secretomes, the efficacy with which iTRAQ proteomics can identify low-abundance proteins, or a combination of these.

Regardless, the large secretomes identified herein shed new light on the rich functional diversity of extracellular proteins of these organisms.

Functional diversity of the secretome. The striking similarity in functional diversity of the secretomes among the four phylogenetically diverse Ascomycetes in this study, in addition to the differences that arise between our results and those of other researchers, can likely be attributed to substrate and growth conditions. It is well established that the suite of extracellular enzymes secreted by fungi is highly dependent on substrate composition, and that functional

diversity increases when the organisms are presented with more complex and recalcitrant material (reviewed in (Girard et al., 2013); demonstrated in an early secretome study by Phalip et al. (2005)). Here, we cultured four fungi under identical growth conditions using the same, easily digestible substrate, with acetate and yeast extract (roughly 70% protein and 15% carbohydrates) (Acumedia, 2011) as carbon sources, resulting in similar proportions of identified GHs and peptidases in the secretome (Figure 4.1). In contrast, Liu et al. (2013) observed substantially more cellulases and hemicellulases than peptidases secreted by *Aspergillus fumigatus* Z5 (in the same sub-phylum as the fungi in this study) growing on cellulosic substrates, with few identified oxidoreductases, and a marked increase in oxidoreductases when the carbon source was switched to glucose. Similarly, Hori et al. (2014) reported a large ratio of GHs to peptidases secreted by the white-rot Basidiomycete *Ceriporiopsis subvermispora* during growth on aspen wood, with roughly equal proportions of peptidases and redox-active AAs. Notwithstanding the phylogenetic differences between these organisms and the Mn(II)-oxidizing fungi in this study, these data suggest that the proportion of GHs would similarly increase when growing these fungi on plant-derived substrates, as more cellulases and hemicellulases would likely be required to utilize this more recalcitrant carbon source. Thus, the functional diversity of the secretomes of these fungi may be even greater than our data demonstrate. It is probable that the relative proportion of AAs identified in fungal secretomes is dependent on both substrate and phylogeny, as the larger proportion of AAs reported by Hori et al. was primarily driven by an abundance of peroxidases in the AA2 family, characteristic of Basidiomycete lignin degraders (Dashtban et al., 2010; Hatakka and Hammel, 2010).

(a) Carbohydrate-degrading enzymes. The wide variety of extracellular hydrolytic enzymes identified in the secretomes of these Ascomycetes is remarkable, particularly in light of

their relatively simple, non-cellulosic substrate. Between 40 and 46 families of glycoside hydrolases and up to 219 individual proteins in this class were identified in each organism (Table 4.1). For comparison, other studies that classified secretome data in a similar manner reported 11 (Nitsche et al., 2012), 20 (Phalip et al., 2005), or 39 (Saykhedkar et al., 2012) GH families identified in other filamentous Ascomycete secretomes and 31 (Hori et al., 2014) and 35 (Rohr et al., 2013) GH families identified in those of white-rot Basidiomycetes; all of these studies except Nitsche et al. (2012) (11 GH families) represented growth on plant-based substrate. Notably, a genome-based estimate of 42 GH families in the predicted secretome of *Stagonospora nodorum* (Krijger et al., 2014) correlates well with our laboratory-based identification of 42 GH families in *Stagonospora sp.* SRC11sM3a.

The diverse range and large quantities of carbohydrate-degrading enzymes identified in the secretomes of these Ascomycetes suggests that their carbon oxidative capacity is robust. The secretomes contained identified proteins spanning a large range of cellulases (e.g., glucanases, glucosidases, galactosidases), hemicellulases (e.g., xylanases, mannanases), and starch-degrading enzymes (α -amylase), rather than being dominated by a single type of hydrolytic enzyme (Figure 4.2A). These data suggest a synergistic approach to carbon degradation among diverse extracellular enzymes in these organisms. The profiles of identified GHs and other CAZymes presented in this study, particularly frequently observed families such as GH1, 5, 16, and 17, may be used as a baseline for future investigations of the mechanisms underlying the cellulose degrading capacity of these organisms.

(b) Auxiliary activities and potential Fenton-based lignocellulose oxidation. The profiles of redox-active AAs identified in the secretomes of these Mn(II)-oxidizing fungi (Figure 4.2C) suggest that the cellulose degradation capacity of these organisms may involve both direct

carbohydrate breakdown via glycoside hydrolases as well as indirect carbon oxidation via Fenton-based hydroxyl radical formation. The combination of H₂O₂-generating enzymes (e.g., GMC oxidoreductases (Levasseur et al., 2013) and radical copper oxidases (Whittaker et al., 1996; Kersten and Cullen, 2014)), enzymes involved in hydroquinone redox cycling (e.g., cellobiose dehydrogenase and (Henriksson et al., 2000) tyrosinase (del Mar Garcia-Molina et al., 2014)), and Fe(III) reductases could supply the necessary reagents for Fenton chemistry in the presence of ferrous iron. While it has been demonstrated that the production of high levels of oxalate can form Fe(III)-oxalate chelates that are poorly reduced by hydroquinones (Jensen et al., 2001), future metabolomic characterization of the secretomes of these organisms would be necessary to evaluate the potential inhibitory effect of secreted oxalate on any Fenton-based carbon degradation mechanisms in these fungi.

Although the lignin-degrading capacity of these organisms has not been evaluated and remains unknown, a non-specific, Fenton-based carbon oxidation mechanism could potentially attack phenolic as well as cellulosic substrates. This possibility is particularly intriguing in *P. sporulosum*, where we observed several enzymes involved in quinone redox cycling that were not present in the other 3 fungi, including hydroxyquinone 1,2-dioxygenase which is thought to play a role in aromatic metabolism of lignin in *Phanerochaete chrysosporium* (Rieble et al., 1994). The secretomes of these Ascomycetes lacked traditional lignin-degrading enzymes such as manganese and versatile peroxidases and had a substantially smaller proportion of AA2 enzymes than in published Basidiomycete secretomes (Hori et al., 2014) and transcriptomes (Rohr et al., 2013). However, the diversity and high number of other identified AAs, including two laccases, which can degrade diverse phenolic compounds directly as a substrate (reviewed in (Baldrian, 2006)) and indirectly through Mn(II) oxidation and ROS production (Höfer and

Schlosser, 1999; Schlosser and Höfer, 2002), is promising and warrants further investigation into the lignocellulolytic degradation potential of these organisms.

(c) Peptidases. While we identified a wide variety of peptidases in the secretomes of these Ascomycetes (Figure 4.2B), the relative functional diversity of these organisms compared to other filamentous fungi is difficult to assess since few secretome studies have published family-level peptidase classifications.

The most frequently identified peptidases in this study, S8/S53 family peptidases, represent a large and diverse group of serine-type proteases whose biological function does not appear to be well characterized in fungi. Family S8 proteins (subtilisins) have been identified in nearly all domains of life and are thought to be of ancient origin (Siezen and Leunissen, 1997), and family S53 proteins (serine carboxypeptidases known as sedolisins) are known for one member, CLN2, involved in a human neurodegenerative disorder (Sleat et al., 1997; Wlodawer et al., 2003). Our identification of numerous family M14 zinc carboxypeptidases agrees well with observations by Krijger et al. (2014) that this domain is expanded in a variety of plant pathogenic Pezizomycotina; these peptidases typically degrade extracellular matrix proteins and are thought to play a role in cell defense against attack by a plant host. Overall, the diverse complement of peptidases identified in these Ascomycetes suggests that many structurally diverse proteins can be degraded by these organisms. In this study, these peptidases may have contributed to consumption of the proteinaceous yeast extract substrate during growth and aided in fungal cell wall remodeling and nutrient recycling as the cultures aged and substrate likely became scarce (Nitsche et al., 2012).

(d) Hypothetical proteins and proteins with limited functional information. The role of hypothetical proteins in the fungal secretome remains ambiguous due to either the lack of

functional information assigned to these proteins or the lack of a protein match with an acceptable E value in the NCBI and UniProt databases. Hypothetical proteins comprise a non-negligible proportion (up to 14%) of identified proteins in the secretome and include up to 200 individual proteins (Figure 4.1). As such, at least some of these proteins likely play important roles in extracellular carbon transformations.

Another challenge in working with large proteomic datasets, particularly for environmental isolates of fungal species for which relatively little proteomic information is available for closely-related organisms, is the incompleteness of functional information in existing fungal databases, even for non-hypothetical proteins. For instance, many of the proteins we identified in this study were mapped to proteins for which only family-level annotations were available (e.g, “glycoside hydrolase family 5” or “M18 metallopeptidase”), rather than a specific enzyme name, thus limiting our understanding of which enzymes are present and which reactions they may be catalyzing in the secretome. As research on fungal genomics and proteomics is rapidly increasing, we look forward to delving more deeply into datasets such as these as more information becomes available.

Species-specific secretome characteristics. The Mn(II)-oxidizing Ascomycetes in this study produce a rich yet functionally similar suite of extracellular enzymes under the evaluated growth conditions, with species-specific differences arising from unique amino acid sequences rather than overall protein function. While our data indicate that up to 42% of the identified proteins in the secretomes represent species-specific sequences (Figure 4.3) that span the full range of CAZy and MEROPS functional groups (Figure 4.4A), very few of these proteins confer unique functionality to the fungi (Figure 4.4B). Moreover, functionally unique enzymes were overwhelmingly “other” proteins, many of which were likely of intracellular origin;

identification of functionally unique proteins in this category may indicate incomplete release of these enzymes into the secretomes via lysis. Targeting intracellular proteins in a future study would further elucidate the degree of species-specific functional capacity. Overall, the identification of few functionally unique, extracellular, carbon-degrading enzymes suggests that these hydrolytic enzymes are well represented among all four fungi and that the organisms possess a similar carbon-degrading capacity under the evaluated growth conditions.

Of the few exceptions to this interspecies functional similarity that we identified at the protein family level (Figure 4.2), many may be dampened by functional redundancy within the secretomes. For example, while the GH63 family (α -glucosidases and α -mannosidases) was identified exclusively in the *A. alternata* secretome, α -glucosidases in the GH31 family were identified in all four organisms, as were proteins in families GH38, GH47, GH76, and GH92, all of which contain α -mannosidases. Notably, the predominance of GH92 family α -mannosidases in the *Stagonorpora* sp. secretome is similarly offset by the presence of these functionally related families. The acid trehalase in the GH65 family and the α -glucuronidase in the GH67 family, both identified only in the *A. alternata* secretome, may share functionality with trehalases in the GH37 family and proteins in the GH115 family, respectively, both of which were identified in all four fungi. The GH23 and GH25 families, uniquely identified in the *P. sporulosum* secretome, are described as lysozymes, peptidoglycan lyases, and chitinases in the CAZy database; these families share similar functionality with GH18 family proteins, which were identified in the secretomes of all four organisms. Thus, even proteins identified as functionally unique based on GH family appear to be complemented by similar enzymes in other families, underscoring the levels of interspecies functional similarity among organisms. Future

unambiguous identification of all identified proteins by enzyme name as opposed to family, as discussed above, would aid in clarifying these interspecies comparisons.

Exceptions to these observations of functional redundancy include an *o*-mannosyltransferase in the GH39 family, an α -rhamnosidase in the GH78 family, and MEROPS T1 proteasome peptidases, all exclusively identified in the *P. sporulosum* secretome.

Our finding that the four fungi in this study produce species-specific versions of functionally similar enzymes (Figure 4.2, Table 4.2) likely stems from the phylogenetic ancestry of the organisms. It has been previously demonstrated that phylogeny strongly influences fungal secretome composition, in addition to lifestyle adaptation (e.g., saprotroph vs. plant pathogen) and environmental conditions (Krijger et al., 2014). Here we demonstrate that the level of interspecies sequence similarity among secreted proteins correlates well with the phylogenetic relationships among the organisms, with *Pyrenochaeta* sp. and *Stagonospora* sp. (members of the same order) exhibiting the greatest overlap. Additionally, it is interesting to note that different protein families exhibit varying levels of shared sequences among the organisms, suggesting that the individual structural features by which enzymes are categorized (for glycoside hydrolases, for example) may also exhibit unique phylogenetic histories. A more detailed investigation of each protein family would be required to elucidate these relationships.

As *A. alternata* is the most phylogenetically distant organism in this study and the only fungus in which Mn(II) oxidative capacity was lost after its original isolation from the field, it is intriguing that this organism exhibited the greatest diversity among CAZyme classes (Table 4.1) and the largest proportion of CAZymes in its secretome (Figure 4.1). Although little unique functionality was identified under the growth conditions we utilized here, we recommend that

this organism be used as a starting point in future investigations of the mechanisms underlying the cellulose-degrading capacity of these fungi.

Conclusions. Here we have presented a first look at the proteomic composition of the secretomes of four Mn(II)-oxidizing, filamentous Ascomycete fungi. We have identified a rich yet functionally similar suite of extracellular oxidative enzymes among the organisms growing on a complex medium, with species-specific differences in secretome composition arising from unique amino acid sequences rather than overall protein function. Furthermore, the identification of a diverse range of cellulases and hemicellulases, in combination with redox-active auxiliary activities that support ROS production and quinone redox cycling, suggests that the cellulose-degrading capacity of these organisms may involve both direct enzymatic carbohydrate breakdown as well as indirect carbon oxidation via Fenton-based hydroxyl radical formation. We look forward to future investigations of these organisms on lignocellulosic substrate and to continuing to enhance our understanding of the role of filamentous Ascomycetes in carbon turnover in the environment.

Acknowledgements

This work was supported by the National Science Foundation, grant numbers EAR-1249489 and CBET-1336496, both awarded to C.M.H, and by a JGI-EMSL Collaborative Science Initiative grant (proposal number 48100) awarded to C.M.H. and C.M.S. Personal support for C.A.Z was also provided by Harvard University and by a Ford Foundation Predoctoral Fellowship administered by the National Academies.

Part of this research was performed at the Environmental Molecular Sciences Laboratory, a national scientific user facility sponsored by the U.S. DOE's Office of Biological and

Environmental Research and located at the Pacific Northwest National Laboratory. Part of this research was performed at the Bauer Core Facility of the FAS Center for Systems Biology at Harvard University. A portion of the bioinformatics analysis was performed at Harvard's FAS Research Computing facility.

We thank Joshua Aldrich (EMSL) and Michele Clamp (Harvard) for bioinformatic analyses at various stages of this project, and Therese R. Clauss (EMSL) for expertise in LC/MS/MS instrumentation throughout this project.

The authors disclaim endorsement of any products mentioned in this paper.

References

- Acumedia (2011). Yeast extract (7184) product information sheet, revision 3. URL http://www.neogen.com/Acumedia/pdf/ProdInfo/7184_PI.pdf
- Adav, S.S., Li, A.A., Manavalan, A., Punt, P., and Kwan Sze, S. (2010) Quantitative iTRAQ secretome analysis of *Aspergillus niger* reveals novel hydrolytic enzymes. *J Proteome Res* **9**: 3932-3940.
- Antelmann, H., Tjalsma, H., Voigt, B., Olhmeier, S., Bron, S., van Dijl, J.M., and Hecker, M. (2001) A proteomic view on genome-based signal peptide predictions. *Genome Res* **11**: 1484-1502.
- Baldrian, P. (2006) Fungal laccases - occurrence and properties. *FEMS Microbiol Rev* **30**: 215-242.
- Callister, S.J., McCue, L.A., Turse, J.E., Monroe, M.E., Auberry, K.J., Smith, R.D. et al. (2008). Comparative bacterial proteomics: analysis of the core genome concept [WWW document].
- Dashtban, M., Schraft, H., Syed, T.A., and Qin, W. (2010) Fungal biodegradation and enzymatic modification of lignin. *Int J Biochem Mol Biol* **1**: 36-50.
- del Mar Garcia-Molina, M., Muñoz-Muñoz, J.L., Berna, J., García-Ruiz, P.A., Rodriguez-Lopez, J.N., and Garcia-Canovas, F. (2014) Catalysis and inactivation of tyrosinase in its action on hydroxyhydroquinone. *Int U Biochem Mol Biol* **66**: 122-127.
- Elias, J.E., and Gygi, S.P. (2010) Methods Mol Biol. *Target-decoy search strategy for mass spectrometry-based proteomics* **604**: 55-71.
- Girard, V., Dieryckx, C., Job, C., and Job, D. (2013) Secretomes: The fungal strike force. *Proteomics* **13**: 597-608.
- Glenn, J.K., Akileswaran, L., and Gold, M.H. (1986) Mn(II) oxidation is the principal function of the extracellular Mn-peroxidase from *Phanerochaete chrysosporium*. *Arch Biochem Biophys* **251**: 688-696.
- Grigoriev, I.V., Nikitin, R., Haridas, S., Kuo, A., Ohm, R., Otilar, R. et al. (2014) MycoCosm portal: Gearing up for 1000 fungal genomes. *Nucleic Acids Res* **42**.
- Hatakka, A., and Hammel, K.E. (2010) Fungal biodegradation of lignocellulose. In *The Mycota X: Industrial Applications*. Hofrichter, M. (ed). Berlin: Springer-Verlag, pp. 319-340.

- Henriksson, G., Johansson, G., and Pettersson, G. (2000) A critical review of cellobiose dehydrogenases. *J Biotechnol* **78**: 93-113.
- Höfer, C., and Schlosser, D. (1999) Novel enzymatic oxidation of Mn^{2+} to Mn^{3+} catalyzed by a fungal laccase. *FEBS Lett* **451**: 186-190.
- Hori, C., Gaskell, J., Igarashi, K., Kersten, P., Mozuch, M., Samejima, M., and Cullen, D. (2014) Temporal alterations in the secretome of the selective lignolytic fungus *Ceriporiopsis subvermispora* during growth on aspen wood reveal this organism's strategy for degrading lignocellulose. *Appl Environ Microbiol* **80**: 2062-2070.
- Jensen, K.A., Jr., Houtman, C.J., Ryan, Z.C., and Hammel, K.E. (2001) Pathways for extracellular Fenton chemistry in the brown rot basidiomycete *Gloeophyllum trabeum*. *Appl Environ Microbiol* **67**: 2705-2711.
- Kelly, R.T., Page, J.S., Luo, Q., Moore, R.J., Orton, D.J., Tang, K., and Smith, R.D. (2006) Chemically etched open tubular and monolithic emitters for nanoelectrospray ionization mass spectrometry. *Anal Chem* **78**: 7796-7801.
- Kersten, P.J., and Cullen, D. (2014) Copper radical oxidases and related extracellular oxidoreductases of wood-decay Agaricomycetes. *Fungal Genet Biol* **72**: 124-130.
- Kim, S., and Pevzner, P.A. (2014) MS-GF+ makes progress towards a universal database search tool for proteomics. *Nat Commun* **5**: 5277.
- Krijger, J.-J., Thon, M.R., Deising, H.B., and Wiersel, S.G.R. (2014) Compositions of fungal secretomes indicate a greater impact of phylogenetic history than lifestyle adaptation. *BMC Genomics* **15**: 722.
- Levasseur, A., Drula, E., Lombard, V., Coutinho, P.M., and Henrissat, B. (2013). Expansion of the enzymatic repertoire of the CAZy database to intergrate auxiliary redox enzymes [WWW document].
- Liang, L., Wu, H., Liu, Z., Shen, R., Gao, H., Yang, J.Y., and Zhang, K. (2013) Proteomic and transcriptional analyses of *Arthrobotrys oligospora* cell wall related proteins reveal complexity of fungal virulence against nematodes. *Appl Microbiol Biotechnol* **97**.
- Liu, D., Li, J., Zhao, S., Zhang, R., Wang, M., Miao, Y. et al. (2013) Secretome diversity and quantitative analysis of cellulolytic *Aspergillus fumigatus* Z5 in the presence of different carbon sources. *Biotechnol Biofuels* **6**: 149.
- Lombard, V., Golaconda, R.H., Drula, E., Coutinho, P.M., and Henrissat, B. (2014) The Carbohydrate-active enzymes database (CAZy) in 2013. *Nucleic Acids Res* **42**: D490-D495.

Lu, X., Sun, J., Nimtz, M., Wissing, J., Zeng, A.-P., and Rinas, U. (2010) The intra- and extracellular proteome of *Aspergillus niger* growing on defined medium with xylose or maltose as carbon substrate. *Microb Cell Fact* **9**: 23.

Maiolica, A., Borsotti, D., and Rappsilber, J. (2005) Self-made frits for nanoscale columns in proteomics. *Proteomics* **5**: 3847-3850.

Mayampurath, A.M., Jaitly, N., Purvine, S.O., Monroe, M.E., Auberry, K.J., Adkins, J.N., and Smith, R.D. (2008) DeconMSn: a software tool for accurate parent ion monoisotopic mass determination for tandem mass spectra. *Bioinformatics* **24**: 1021-1023.

Medina, M.L., Kiernan, U.A., and Francisco, W.A. (2004) Proteomic analysis of rutin-induced secreted proteins from *Aspergillus flavus*. *Fungal Genet Biol* **41**: 327-335.

Monroe, M.E., Shaw, J.L., Daly, D.S., Adkins, J.N., and Smith, R.D. (2008) MASIC: a software program for fast quantitation and flexible visualization of chromatographic profiles from detected LC-MS(/MS) features. *Comput Biol Chem* **32**: 215-217.

Muñoz-Gómez, A., Corredor, M., Benítez-Páez, A., and Peláez, C. (2014) Development of quantitative proteomics using iTRAQ based on the immunological response of *Galleria mellonella* larvae challenged with *Fusarium oxysporum* microconidia. *PLoS ONE* **9**.

Nitsche, B.M., Jørgensen, T.R., Akeroyd, M., Meyer, V., and Ram, A.F.J. (2012) The carbon starvation response of *Aspergillus niger* during submerged cultivation: Insights from the transcriptome and secretome. *BMC Genomics* **13**: 380.

Perez, J., Munoz-Dorado, J., de la Rubia, T., and Martinez, J. (2002) Biodegradation and biological treatments of cellulose, hemicellulose, and lignin: an overview. *Int Microbiol* **5**: 53-63.

Phalip, V., Delalande, F., Carapito, C., Goubet, F., Hatsch, D., Leize-Wagner, E. et al. (2005) Diversity of the exoproteome of *Fusarium graminearum* grown on plant cell wall. *Curr Genet* **48**: 366-379.

Polpitiya, A.D., Qian, W.-J., Jaitly, N., Petyuk, V.A., Adkins, J.N., Camp, D.G. et al. (2008) DAnTE: a statistical tool for quantitative analysis of -omics data. *Bioinformatics* **24**: 1556-1558.

Rawlings, N.D., Waller, M., Barrett, A.J., and Bateman, A. (2014) MEROPS: the database of proteolytic enzymes, their substrates and inhibitors. *Nucleic Acids Res* **42**: D503-D509.

Rieble, S., Joshi, D., and Gold, M.H. (1994) Purification and characterization of a 1,2,4-trihydroxybenzene 1,2-dioxygenase from the basidiomycete *Phanerochaete chrysosporium*. *J Bacteriol* **176**: 4838-4844.

Rohr, C., Levin, L.N., Mentaberry, A.N., and Wirth, S.A. (2013) A first insight into *Pycnoporus sanguineus* BAFC 2126 transcriptome. *PLoS ONE* **8**: e81033.

Ruiz-Duenas, F.J., and Martinez, A.T. (2009) Microbial degradation of lignin: how a bulky recalcitrant polymer is efficiently recycled in nature and how we can take advantage of this. *Microb Biotechnol* **2**: 164-177.

Santelli, C.M., Chaput, D.L., and Hansel, C.M. (2014) Microbial communities promoting Mn(II) oxidation in Ashmet Pond, a historically polluted freshwater pond undergoing remediation. *Geomicrobiol J* **31**: 605-616.

Santelli, C.M., Pfister, D.H., Lazarus, D., Sun, L., Burgos, W.D., and Hansel, C.M. (2010) Promotion of Mn(II) oxidation and remediation of coal mine drainage in passive treatment systems by diverse fungal and bacterial communities. *Appl Environ Microbiol* **76**: 4871-4875.

Saykhedkar, S., Ray, A., Ayoubi-Canaan, P., Hartson, S.D., Prade, R., and Mort, A.J. (2012) A time course analysis of the extracellular proteome of *Aspergillus nidulans* growing on sorghum stover. *Biotechnol Biofuels* **5**: 52.

Schlosser, D., and Höfer, C. (2002) Laccase-catalyzed oxidation of Mn²⁺ in the presence of natural Mn³⁺ chelators as a novel source of extracellular H₂O₂ production and its impact on manganese peroxidase. *Appl Environ Microbiol* **68**: 3514-3521.

Shi, J., Feng, H., Lee, J., and Ning Chen, W. (2013) Comparative proteomics profile of lipid-cumulating oleaginous yeast: An iTRAQ-coupled 2-D LC-MS/MS analysis. *PLoS ONE* **8**: e85532.

Siezen, R.J., and Leunissen, J.A.M. (1997) Subtilisases: The superfamily of subtilisin-like serine proteases. *Protein Sci* **6**: 501-523.

Sleat, D.E., Donnelley, R.J., Lackland, H., Liu, C.G., Sohar, I., Pullarkat, R.K., and Lobel, P. (1997) Association of mutations in a lysosomal protein with classical late-infantile neuronal ceroid lipofuscinosis. *Science* **277**: 1802-1805.

Smith, P.K., Krohn, R.I., Hermanson, G.T., Mallia, A.K., Gartner, F.H., Provenzano, M.D. et al. (1985) Measurement of protein using bicinchoninic acid. *Anal Biochem* **150**: 76-85.

Tang, Y., Zeiner, C.A., Santelli, C.M., and Hansel, C.M. (2013) Fungal oxidative dissolution of the Mn(II)-bearing mineral rhodochrosite and the role of metabolites in manganese oxide formation. *Environ Microbiol* **15**: 1063-1077.

Vanden Wymelenberg, A., Gaskell, J., Mozuch, M., Sabat, G., Ralph, J., Skyba, O. et al. (2010) Comparative transcriptome and secretome analysis of wood decay fungi *Postia placenta* and *Phanerochaete chrysosporium*. *Appl Environ Microbiol* **76**: 3599-3610.

Wang, Y., Yang, F., Gritsenko, M.A., Wang, Y., Clauss, T., Liu, T. et al. (2011) Reversed-phase chromatography with multiple fraction concatenation strategy for proteome profiling of human MCF10A cells. *Proteomics* **10**: 2019-2026.

Wariishi, H., Valli, K., and Gold, M.H. (1992) Manganese(II) oxidation by manganese peroxidase from the basidiomycete *Phanerochaete chrysosporium* - Kinetic mechanism and role of chelators. *J Biol Chem* **267**: 23688-23695.

Whittaker, M.M., Kersten, P.J., Nakamura, N., Sanders-Loehr, J., Schweizer, E.S., and Whittaker, J.W. (1996) Glyoxal oxidase from *Phanerochaete chrysosporium* is a new radical-copper oxidase. *J Biol Chem* **271**: 681-687.

Wlodawer, A., Li, M., Gustchina, A., Oyama, H., Dunn, B.M., and Oda, K. (2003) Structural and enzymatic properties of the sedolisin family of serine-carboxyl peptidases. *Acta Biochim Pol* **50**: 81-102.

Zeiner, C.A., Purvine, S.O., Zink, E., Wu, S., Paša-Tolić, L., Chaput, D.L. et al. (In review) Mechanisms of manganese(II) oxidation by filamentous Ascomycete fungi vary with species and time as a function of secretome composition.

CHAPTER 5

Quantitative iTRAQ-based secretome analysis reveals species-specific and temporal shifts in carbon utilization strategies among manganese(II)-oxidizing ascomycete fungi

This chapter is currently in preparation for journal submittal.
(Zeiner C.A., Purvine S.O., Zink E., Wu S., Paša-Tolić L.,
Chaput D.L., Santelli C.M., Hansel C.M.)

Supplemental Material for this chapter is presented in **Appendix 4**.

Abstract

Fungi generate a wide range of extracellular oxidative enzymes and reactive intermediates, collectively known as the secretome, that synergistically drive litter decomposition in the environment. While secretome studies of model organisms have greatly expanded our knowledge of these hydrolytic enzymes, few have extended secretome characterization to environmental isolates or directly compared temporal patterns of enzyme utilization among phylogenetically diverse species. Here we use a combination of iTRAQ proteomics and custom bioinformatic analyses to compare the proteomic composition of the secretomes of four Mn(II)-oxidizing Ascomycete fungi over a three-week time course. We demonstrate that although the fungi produce a similar suite of extracellular enzymes, they exhibit striking differences in the regulation of these enzymes among species and over time, revealing species-specific and temporal shifts in carbon utilization strategies as they degrade the same substrate. Specifically, our findings suggest that *Paraconiothyrium sporulosum* AP3s5-JAC2a and *Alternaria alternata* SRC11rK2f employ sequential enzyme secretion patterns concomitant with decreasing resource availability, *Stagonospora* sp. SRC11sM3a preferentially degrades proteinaceous substrate before switching to carbohydrates, and *Pyrenochaeta* sp. DS3sAY3a utilizes primarily peptidases to aggressively attack carbon sources in a concentrated burst. This work highlights the diversity of operative metabolic strategies among cellulose-degrading

Ascomycetes and enhances our understanding of their role in carbon turnover in the environment.

Introduction

Fungal secretomes are reservoirs of a diverse suite of oxidative enzymes and reactive metabolites that facilitate the role of filamentous fungi as primary decomposers of recalcitrant plant material in the environment. Specifically, fungi secrete an arsenal of diverse hydrolytic enzymes, including cellulases, hemicellulases, pectinases, and lignin-degrading accessory enzymes that generate reactive intermediates, which synergistically drive litter decomposition in natural systems and can be harnessed for industrial applications (Perez et al., 2002; Ruiz-Duenas and Martinez, 2009; Dashtban et al., 2010; Hatakka and Hammel, 2010). As such, fungal secretomes play a critical role in global carbon cycling and climate dynamics and serve as an essential mediator in renewable energy production.

The ongoing development of analytical techniques in microbial ‘omics has allowed researchers to delve more deeply into the mechanistic underpinnings of complex microbially-mediated processes in the environment, generating large, highly informative datasets that shed new light on the intricacies of microbial metabolism. In particular, comparative proteomics has proven to be a valuable tool in investigating the response of fungal secretomes to different growth conditions and environmental stimuli and evaluating these responses over time. By identifying enzymatic targets for future biochemical investigation and describing the dynamic regulatory profile of these secreted enzymes, researchers can begin to tease apart the diverse and elaborate mechanisms by which these organisms attack recalcitrant material, screen diverse

organisms for hyper-production of enzymes of interest, and optimize the growth conditions and timing to yield a productive secretome harvest for industrial or commercial use.

Proteomic studies of the fungal secretome have already yielded interesting and informative results. By directly comparing the secretome composition of model organisms growing on different carbon sources, researchers have demonstrated that the suite of extracellular enzymes secreted by fungi is highly dependent on substrate composition, and that secretome size and functional diversity increase when the organisms are presented with more complex and recalcitrant material (Medina et al., 2004; Phalip et al., 2005; Lu et al., 2010; Girard et al., 2013; Liu et al., 2013). Taking these comparative analyses a step further, quantitative time-course investigations have illustrated dynamic shifts in metabolic strategies as the organisms accumulate compounds of interest (Shi et al., 2013), adjust to diminishing resource availability (Nitsche et al., 2012), or alter enzyme regulation patterns as they sequentially degrade a recalcitrant substrate (Saykhedkar et al., 2012). In particular, these studies have provided valuable insights into lignocellulose degradation mechanisms by wood-rot Basidiomycetes, such as the secretion of species-specific suites of enzymes that are either diverse and synergistically acting or much more narrow in focus (Vanden Wymelenberg et al., 2010), and predictable patterns of sequential enzyme secretion that transition from specific to non-specific oxidative mechanisms over time as the remaining substrate becomes more difficult to degrade (Hori et al., 2014). As more data emerge, patterns common to diverse organisms are elucidated, such as the combination of glucanases, cellobiose dehydrogenase, and lytic polysaccharide monooxygenases that work together to accelerate lignocellulose degradation after the breakdown of more easily accessible compounds (Langston et al., 2011; Saykhedkar et al., 2012; Hori et al., 2014).

While our knowledge surrounding the oxidative enzymes secreted by filamentous fungi is expanding rapidly, few studies have extended secretome characterization efforts beyond model organisms (such as Ascomycetes in the *Aspergillus* (Lu et al., 2010; Liu et al., 2013) and *Fusarium* (Phalip et al., 2005) genera and white-rot Basidiomycetes (Vanden Wymelenberg et al., 2010; Rohr et al., 2013)) to environmental isolates. As such, the mechanisms underlying their contribution to recalcitrant carbon degradation in terrestrial systems remain poorly understood. Furthermore, due to the inherent complexity in mapping proteins across multiple genomes, particularly those of phylogenetically diverse organisms, side-by-side comparisons of multiple species have thus far been limited (see (Shi et al., 2013) for an example using yeasts). However, preliminary work on interspecies comparisons has resulted in valuable mechanistic insights (Vanden Wymelenberg et al., 2010) and warrants additional study and extension of this work to diverse isolates.

We have recently isolated over a dozen strains of manganese (Mn)(II)-oxidizing, filamentous Ascomycetes from passive coal mine drainage treatment systems (Santelli et al., 2010) and a historically contaminated freshwater lake (Santelli et al., 2014). These organisms have demonstrated cellulose-degrading capacity (C.M. Santelli, unpublished data), yet the mechanisms underlying this process remain unknown. Recent work by our laboratory has demonstrated that Mn(II) oxidation in three of these isolates is driven by extracellular enzymes in the secretome (Tang et al., 2013; Zeiner et al., In review), and furthermore, that some of enzymes implicated in Mn(II) oxidation (e.g., GMC oxidoreductases, radical copper oxidases) are utilized by Basidiomycete wood degraders to breakdown cellulose (Martinez et al., 2009; Zeiner et al., In review). This link between Mn(II) and carbon oxidation bolsters well-established mechanisms by which white-rot Basidiomycetes such as *Phanerochaete*

chyrsosporium employ Mn(II) oxidation and the subsequent production of reactive intermediates to attack lignocellulose (Glenn et al., 1986; Wariishi et al., 1992; Höfer and Schlosser, 1999; Schlosser and Höfer, 2002). Interestingly, the extracellular enzymes responsible for Mn(II) oxidation in our environmental isolates varied by species, and the Mn(II) oxidative capacity of the organisms changed over time (Zeiner et al., In review). This mechanistic diversity among species and environmental conditions lends further support for extending secretome characterization studies to phylogenetically diverse organisms and comparing dynamic enzyme regulation patterns among species.

In this study, we conducted a quantitative, comparative analysis over a three-week time period of the proteomic composition of the secretomes of four Mn(II)-oxidizing, filamentous Ascomycete fungi: *Alternaria alternata* SRC1lrK2f, *Paraconiothyrium sporulosum* AP3s5-JAC2a, *Pyrenochaeta* sp. DS3sAY3a, and *Stagonospora* sp. SRC1lsM3a. Utilizing iTRAQ (isobaric tags for relative and absolute quantification) proteomics, custom bioinformatic analyses, and newly-sequenced genomes of our isolates, we demonstrate that the organisms produce a similar suite of extracellular enzymes but exhibit striking differences in regulation of these enzymes among species and over time. Our findings reveal species-specific and temporal shifts in carbon utilization strategies among these phylogenetically diverse organisms as they degrade the same substrate. This work highlights the utility of iTRAQ proteomics in evaluating interspecies comparisons, demonstrates the diversity of operative metabolic strategies among cellulose-degrading Ascomycetes, and enhances our understanding of the role of these fungi in recalcitrant carbon turnover in the environment.

Materials and Methods

The materials and methods for this work are the same as those presented in Chapter 4.

Separate chapters. This chapter presents a quantitative time-course analysis of proteins identified in the four fungal secretomes, with implications for carbon utilization strategies. Overall secretome composition, functional diversity, and interspecies comparisons, exclusive of temporal changes, are presented in Chapter 4.

Results

Full datasets. A complete list of the proteins identified in each of the four fungi and each of the three time points, including predicted functions, CAZy and MEROPS classifications (for carbohydrate-active enzymes and peptidases, respectively), and relative abundance data for each protein, is presented in Table S5.1.

Secretome functional diversity over time. Categorizing the proteins in each fungal secretome based on broad functional groups according to the CAZy and MEROPS databases reveals that secretome functional diversity was highly similar among all four organisms, and this similarity persisted throughout the 3-week time period of this study (Figure 5.1). Additionally, the number of proteins identified in the secretomes changed little over time, ranging from only 1% (12 proteins) in *A. alternata* to 6% (87 proteins) in *Stagonospora* sp.

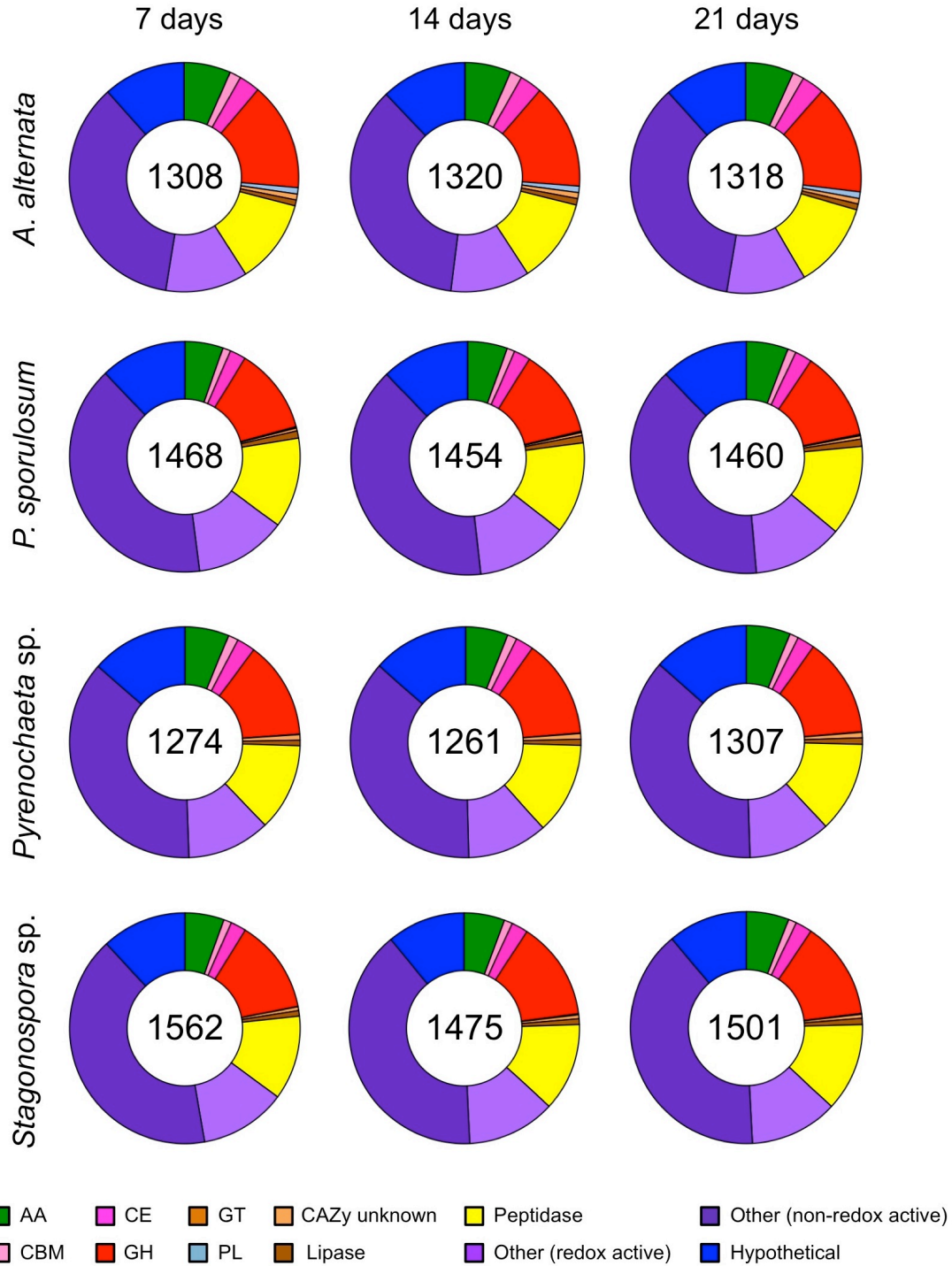


Figure 5.1. Distribution of proteins identified via iTRAQ proteomics in secretomes of 4 Ascomycete fungi after 7 days, 14 days, and 21 days of growth. Total number of proteins identified for each fungus, at each time point, is indicated in center of circles. Abbreviations from CAZy database: AA = auxiliary activities; CBM = carbohydrate-binding module; CE = carbohydrate esterase; GH = glycoside hydrolase; GT = glucosyltransferase; PL = polysaccharide lyase.

Species-specific and temporal patterns of protein regulation. Despite the marked similarities in overall secretome composition, we observed striking differences among the fungi with respect to the relative abundance of extracellular enzymes and temporal patterns of enzyme regulation. To facilitate these interspecies comparisons, we identified the proteins with the most significantly changing relative abundance in each of the two time point transitions evaluated in this study: 7d-14d and 14d-21d. The significance cutoff was defined as a \log_2 relative abundance ratio (e.g., (\log_2 relative abundance of a protein at 14d) – (\log_2 relative abundance of the same protein at 7d)) greater than the 97.5th percentile of \log_2 relative abundance ratios for all proteins in a particular time point transition (for proteins that significantly increased in abundance) or less than the 2.5th percentile (for proteins that significantly decreased in abundance). Percentiles were used because the distributions of \log_2 abundance ratios were negatively skewed, with more proteins increasing in relative abundance over time than decreasing. The results are summarized in Figure 5.2 and Tables 5.1-5.4, and the full list of significantly changing proteins, including fold changes, is presented in Tables S5.2-S5.5.

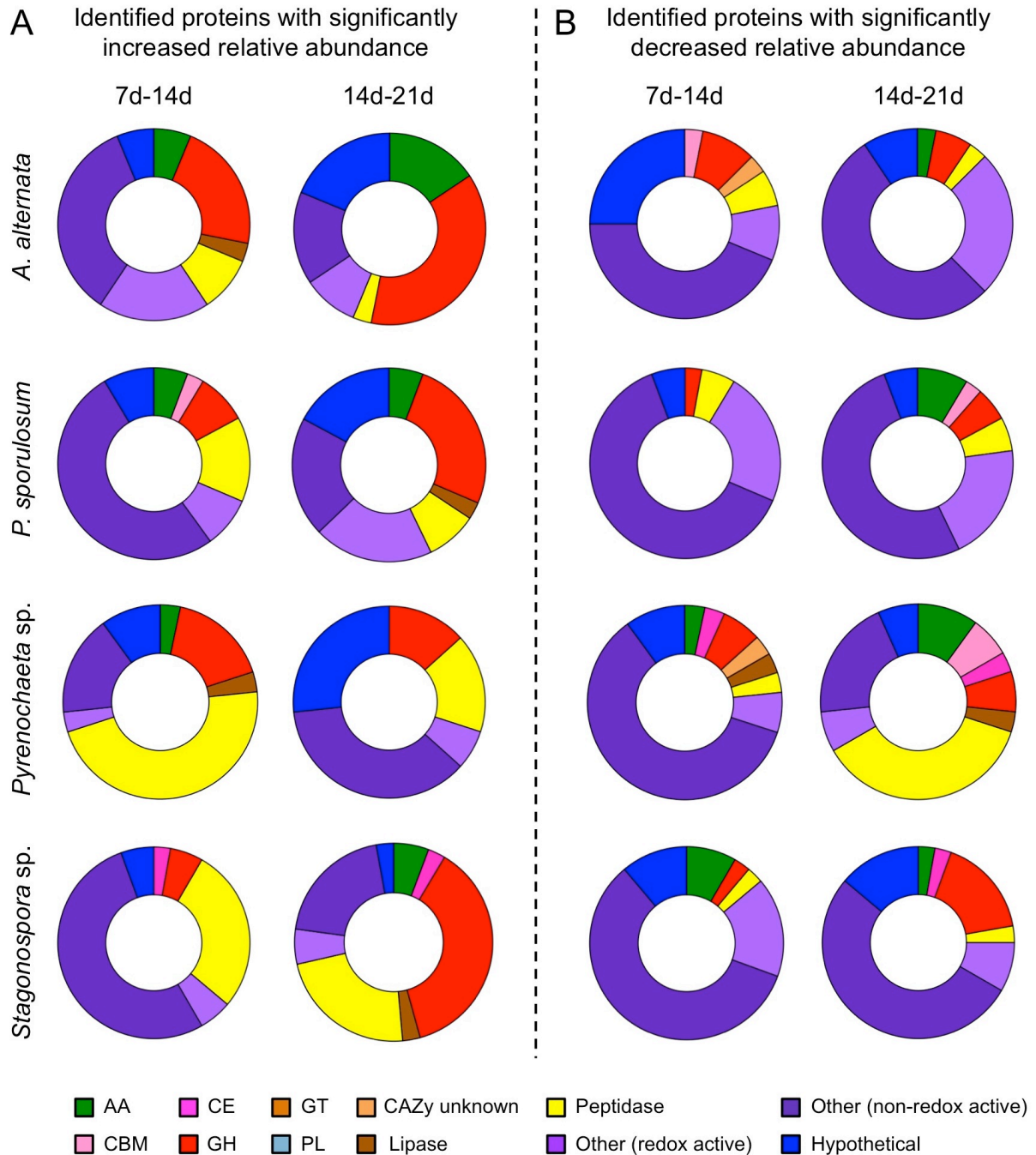


Figure 5.2. Distribution of identified proteins in fungal secretomes that exhibited (A) significantly increasing or (B) significantly decreasing relative abundance with increasing secretome age. Refer to text for explanation of significance cutoffs. Plots include 32, 35, 30, and 36 proteins (corresponding to the top or bottom 2.5th percentile) for *A. alternata*, *P. sporulosum*, *Pyrenochaeta sp.*, and *Stagonospora sp.*, respectively. Only proteins that were identified in all 3 time points were evaluated. Abbreviations as in Figure 5.1.

Table 5.1. Identified proteins with significantly changing relative abundance over time in the *A. alternata* secretome. Only proteins classified in the CAZy or MEROPS databases are shown, in addition to the protein with the highest and lowest fold change for each time point transition (in bold). Proteins that were significantly regulated in more than one time point transition are indicated with an asterisk. Refer to the text for an explanation of significance cutoffs and to Table S5.2 for the full list of significantly changing proteins for this organism.

Genome in which protein was identified	JGI Protein ID	Peptides	CAZyme	Protein Family	Putative Function from Best BLAST Hit	Fold Change
<i>Significantly increased relative abundance 7d-14d</i>						
<i>A. alternata</i>	687369	3	No	N/A	Dihydrodipicolinate synthase	84
<i>Stagonospora</i> sp.	282318	5	No	MEROPS S10	Carboxypeptidase S1	54
<i>A. alternata</i>	231779	4	Yes	CAZy GH92	Glycoside hydrolase	40
<i>A. alternata</i>	991870	11	Yes	CAZy GH7	Endoglucanase 1	32
<i>A. alternata</i>	930263	31	No	MEROPS S53	Tripeptidyl peptidase	25
<i>A. alternata</i>	944615	78	Yes	CAZy AA3	Choline dehydrogenase	21
<i>A. alternata</i>	950076	17	Yes	CAZy GH7	Exoglucanase	19
<i>A. alternata</i>	1061421	4	No	Lipase	Lysophospholipase 3	11
<i>A. alternata</i>	231779	3	Yes	CAZy GH92	Glycoside hydrolase	11
<i>A. alternata</i>	450050	2	Yes	CAZy GH3	Glycoside hydrolase	11
<i>A. alternata</i>	931907	18	Yes	CAZy GH7	* Glycoside hydrolase	10
<i>A. alternata</i>	1025869	17	Yes	CAZy GH10	Glycoside hydrolase	9.0
<i>Pyrenochaeta</i> sp.	324247	1	No	MEROPS S10	Carboxypeptidase S1	8.9
<i>A. alternata</i>	936871	5	Yes	CAZy AA3_3	* Alcohol dehydrogenase 1	7.8
<i>Significantly increased relative abundance 14d-21d</i>						
<i>A. alternata</i>	930096	6	No	Hypothetical	Hypothetical	13
<i>A. alternata</i>	1023909	5	Yes	CAZy GH64	Beta-1,3-glucanase	7.9
<i>A. alternata</i>	966271	5	Yes	CAZy GH31	Alpha-glucosidase	7.8
<i>Pyrenochaeta</i> sp.	421551	4	Yes	CAZy GH6	Cellobiohydrolase II	7.5
<i>A. alternata</i>	991874	1	Yes	CAZy AA9/GH61	Lytic polysaccharide monooxygenase	5.4
<i>A. alternata</i>	2778	7	Yes	CAZy GH18	Glycoside hydrolase	4.0
<i>A. alternata</i>	1023931	3	No	MEROPS S8/S53	Subtilase-type proteinase psp3	3.6
<i>A. alternata</i>	935643	4	Yes	CAZy AA1_3	Tyrosinase	3.6
<i>A. alternata</i>	1019743	2	Yes	CAZy AA9/GH61	Endoglucanase II	3.5
<i>A. alternata</i>	931907	18	Yes	CAZy GH7	* Glycoside hydrolase	3.4
<i>A. alternata</i>	1004357	1	Yes	CAZy GH16	Mixed-linked glucanase	3.4
<i>A. alternata</i>	966271	11	Yes	CAZy GH31	Glycoside hydrolase	3.4
<i>A. alternata</i>	947017	2	Yes	CAZy GH5	Glycoside hydrolase	3.3
<i>A. alternata</i>	1006243	11	Yes	CAZy GH55/PL	Exo-beta-1,3-glucanase, pectin lyase	3.3
<i>A. alternata</i>	1020140	5	Yes	CAZy GH5	Glucan 1,3-beta-glucosidase	3.2
<i>A. alternata</i>	577093	20	Yes	CAZy GH17	GPI-anchored cell wall beta-1,3-endoglucanase	2.9
<i>Pyrenochaeta</i> sp.	590430	3	Yes	CAZy GH10	Endo-beta-1,4-xylanase	2.8
<i>A. alternata</i>	1088641	2	Yes	CAZy AA8	Cellulose binding iron reductase	2.7
<i>A. alternata</i>	545007	3	Yes	CAZy GH5	Endoglucanase	2.7
<i>Significantly decreased relative abundance 7d-14d</i>						
<i>A. alternata</i>	1017397	1	No	MEROPS S33	Proline iminopeptidase	-6.2
<i>A. alternata</i>	382987	7	No	MEROPS M	Matrix metallopeptidase	-6.3
<i>A. alternata</i>	1015915	51	Yes	CAZy CBM18	Carbohydrate binding module	-6.3
<i>P. sporulosum</i>	1080353	35	Yes	CAZy GH16	Glycoside hydrolase	-7.0
<i>P. sporulosum</i>	1131561	5	Yes	CAZy GH15	1,4-alpha-D-glucan glucohydrolase	-7.8
<i>A. alternata</i>	271061	1	Yes	CAZy GH16	Cell wall glucanase Utr2	-10
<i>A. alternata</i>	1028714	12	Yes	CAZy Unknown	Carbohydrate binding protein	-19
<i>A. alternata</i>	1066229	3	No	N/A	Signaling protein, tat pathway	-35
<i>Significantly decreased relative abundance 14d-21d</i>						
<i>A. alternata</i>	1034873	1	Yes	CAZy GH76	Mannan endo-1,6-alpha-mannosidase	-2.7
<i>A. alternata</i>	948433	8	No	MEROPS S53	Tripeptidyl peptidase 1	-2.7
<i>A. alternata</i>	991821	3	Yes	CAZy GH51	Glycoside hydrolase	-3.1
<i>A. alternata</i>	936871	5	Yes	CAZy AA3_3	* Alcohol dehydrogenase 1	-4.7
<i>A. alternata</i>	[No match]	1	No	N/A	Amidase	-11

Table 5.2. Identified proteins with significantly changing relative abundance over time in the *P. sporulosum* secretome. Only proteins classified in the CAZy or MEROPS databases are shown, in addition to the protein with the highest and lowest fold change for each time point transition (in bold). Proteins that were significantly regulated in more than one time point transition are indicated with an asterisk. Refer to the text for an explanation of significance cutoffs and to Table S5.3 for the full list of significantly changing proteins for this organism.

Genome in which protein was identified	JGI Protein ID	Peptides	CAZyme	Protein Family	Putative Function from Best BLAST Hit	Fold Change
<i>Significantly increased relative abundance 7d-14d</i>						
<i>P. sporulosum</i>	1163282	6	Yes	CAZy CBM50	Carbohydrate binding module	40
<i>P. sporulosum</i>	629931	9	Yes	CAZy AA1_3	Tyrosinase	37
<i>P. sporulosum</i>	1152669	5	No	MEROPS S9	* Dipeptidyl peptidase V	30
<i>A. alternata</i>	1020140	5	Yes	CAZy GH5	Glucan beta-1,3-glucosidase	20
<i>P. sporulosum</i>	1196441	28	Yes	CAZy GH47	Mannosyl-oligosaccharide alpha-1,2-mannosidase	19
<i>Stagonospora</i> sp.	282318	5	No	MEROPS S10	Carboxypeptidase S1	14
<i>P. sporulosum</i>	1129270	16	Yes	CAZy AA1	Multicopper oxidase	11
<i>A. alternata</i>	948401	9	No	MEROPS S53	Tripeptidyl peptidase 1	9.5
<i>A. alternata</i>	994290	16	Yes	CAZy GH79	Glycoside hydrolase	8.1
<i>P. sporulosum</i>	99094	6	No	MEROPS S8/S53	Subtilisin-like serine protease	7.4
<i>P. sporulosum</i>	1219704	1	No	MEROPS A	Acid protease, aspartic	7.2
<i>Significantly increased relative abundance 14d-21d</i>						
<i>P. sporulosum</i>	1203498	12	Yes	CAZy GH55/PL	Exo-beta-1,3-glucanase, pectin lyase	15
<i>P. sporulosum</i>	939345	17	Yes	CAZy GH64	Beta-1,3-glucanase	12
<i>P. sporulosum</i>	1203498	5	Yes	CAZy GH55/PL	Exo-beta-1,3-glucanase, pectin lyase	9.2
<i>Pyrenochaeta</i> sp.	540437	15	Yes	CAZy GH55/PL	Exo-beta-1,3-glucanase, pectin lyase	7.9
<i>P. sporulosum</i>	98920	37	No	MEROPS S8/S53	Oryzin	5.8
<i>A. alternata</i>	270636	2	No	Lipase	Lipase 3	5.3
<i>P. sporulosum</i>	1112441	9	Yes	CAZy GH18	Chitinase	4.8
<i>P. sporulosum</i>	1151139	5	No	MEROPS M14A	Carboxypeptidase A	4.7
<i>A. alternata</i>	481604	20	No	MEROPS A1	Vacuolar protease A, pepsin	4.5
<i>P. sporulosum</i>	1118684	4	Yes	CAZy GH31	Glycoside hydrolase	4.5
<i>P. sporulosum</i>	1155558	11	Yes	CAZy GH7	Cellobiohydrolase II	4.3
<i>Pyrenochaeta</i> sp.	508852	10	Yes	CAZy GH35	Beta-galactosidase	4.2
<i>P. sporulosum</i>	1121628	3	Yes	CAZy AA3_1	Cellobiose dehydrogenase	3.8
<i>P. sporulosum</i>	402071	1	Yes	CAZy AA9/GH61	Glycoside hydrolase	3.6
<i>P. sporulosum</i>	1160612	11	Yes	CAZy GH75	Chitosanase	3.5
<i>Significantly decreased relative abundance 7d-14d</i>						
<i>P. sporulosum</i>	1263409	3	No	MEROPS T1	Proteasome subunit, beta type	-11
<i>A. alternata</i>	1025053	8	No	MEROPS M16	Mitochondrial-processing peptidase	-16
<i>P. sporulosum</i>	1097616	11	Yes	CAZy GH72	Beta-1,3-glucanosyltransglycosylase	-22
<i>P. sporulosum</i>	1078544	1	No	N/A	Malate dehydrogenase	-380
<i>Significantly decreased relative abundance 14d-21d</i>						
<i>P. sporulosum</i>	1123932	1	No	MEROPS S16	Lon protease homolog, mitochondrial	-4.1
<i>P. sporulosum</i>	1076891	5	Yes	CAZy GH5	Glucan beta-1,3-glucosidase	-4.2
<i>P. sporulosum</i>	1087598	5	Yes	CAZy AA3	Choline dehydrogenase	-4.3
<i>P. sporulosum</i>	1118226	1	Yes	CAZy AA2	Cytochrome c peroxidase	-4.4
<i>P. sporulosum</i>	1107380	9	Yes	CAZy CBM48	Carbohydrate binding module	-4.7
<i>P. sporulosum</i>	1137665	6	Yes	CAZy GH72	Beta-1,3-glucanosyltransglycosylase	-5.0
<i>P. sporulosum</i>	1187227	11	Yes	CAZy AA1	Multicopper oxidase	-5.4
<i>P. sporulosum</i>	1152669	5	No	MEROPS S9	* Dipeptidyl peptidase V	-7.9
<i>P. sporulosum</i>	1195333	2	No	N/A	Nicotinamidase pyrazinamidase	-11

Table 5.3. Identified proteins with significantly changing relative abundance over time in the *Pyrenochaeta* sp. secretome. Only proteins classified in the CAZy or MEROPS databases are shown, in addition to the protein with the highest and lowest fold change for each time point transition (in bold). Proteins that were significantly regulated in more than one time point transition are indicated with an asterisk. Refer to the text for an explanation of significance cutoffs and to Table S5.4 for the full list of significantly changing proteins for this organism.

Genome in which protein was identified	JGI Protein ID	Peptides	CAZyme	Protein Family	Putative Function from Best BLAST Hit	Fold Change
<i>Significantly increased relative abundance 7d-14d</i>						
Pyrenochaeta sp.	140344	1	No	N/A	Disulfide isomerase A4	100
<i>Pyrenochaeta</i> sp.	504857	23	No	MEROPS M14	* Zinc carboxypeptidase	55
<i>Pyrenochaeta</i> sp.	45016	8	No	MEROPS M14A	* Carboxypeptidase B	40
<i>Pyrenochaeta</i> sp.	45016	4	No	MEROPS M14A	* Carboxypeptidase A1	38
<i>A. alternata</i>	1020796	24	No	MEROPS M28	* Leupeptin-inactivating enzyme 1	33
<i>Pyrenochaeta</i> sp.	584546	16	No	MEROPS M28	* Zn-dependent exopeptidase	25
<i>A. alternata</i>	509520	10	No	MEROPS S1A	Trypsin-like protease 1	22
<i>Pyrenochaeta</i> sp.	684312	1	Yes	CAZy AA3	* GMC oxidoreductase	20
<i>P. sporulosum</i>	1160162	4	Yes	CAZy GH105	Glycoside hydrolase	19
<i>Pyrenochaeta</i> sp.	582836	6	No	MEROPS M28	Leucyl aminopeptidase	19
<i>A. alternata</i>	981151	8	Yes	CAZy GH16	Glycoside hydrolase	18
<i>Pyrenochaeta</i> sp.	585649	13	No	MEROPS S8/S53	Subtilisin-like serine protease	16
<i>Pyrenochaeta</i> sp.	45016	12	No	MEROPS M14A	* Carboxypeptidase A1	14
<i>Pyrenochaeta</i> sp.	594106	3	Yes	CAZy GH5	Glycoside hydrolase	0
<i>Pyrenochaeta</i> sp.	272217	16	No	MEROPS M28	Leupeptin-inactivating enzyme 1	14
<i>Pyrenochaeta</i> sp.	582534	19	No	MEROPS S28	* Serine peptidase	13
<i>Pyrenochaeta</i> sp.	345941	3	Yes	CAZy GH47	Mannosyl-oligosaccharide alpha-1,2-mannosidase	12
<i>Stagonospora</i> sp.	113154	12	Yes	CAZy GH17	Glycoside hydrolase	11
<i>Pyrenochaeta</i> sp.	249590	8	No	MEROPS A	* Aspartic protease PEP1	10
<i>A. alternata</i>	951324	19	No	MEROPS M6	* Metalloprotease	10
<i>Pyrenochaeta</i> sp.	602398	34	No	MEROPS M6	* Metalloprotease	8.7
<i>Pyrenochaeta</i> sp.	514689	9	No	Lipase	* GDSL lipase/acylhydrolase	8.3
<i>Significantly increased relative abundance 14d-21d</i>						
Pyrenochaeta sp.	630201	2	No	N/A	FAD-binding protein	76
<i>Pyrenochaeta</i> sp.	344293	3	No	MEROPS M14	Carboxypeptidase A4	42
<i>Pyrenochaeta</i> sp.	501916	16	No	MEROPS S8/S53	Oryzin	29
<i>Pyrenochaeta</i> sp.	515365	15	Yes	CAZy GH13/CBM20	Starch binding protein	21
<i>P. sporulosum</i>	1221200	30	Yes	CAZy GH13	Alpha-amylase	16
<i>A. alternata</i>	1033470	11	Yes	CAZy GH13	Alpha-amylase	15
<i>Stagonospora</i> sp.	372088	5	No	MEROPS M6	Metalloprotease	14
<i>Pyrenochaeta</i> sp.	540104	6	No	MEROPS M28	N-acetylated-alpha-linked acidic dipeptidase 2	13
<i>A. alternata</i>	279631	3	Yes	GH13/CBM20	Starch binding protein	13
<i>P. sporulosum</i>	1148422	6	No	MEROPS M28	N-acetylated-alpha-linked acidic dipeptidase 2	12
<i>Significantly decreased relative abundance 7d-14d</i>						
<i>A. alternata</i>	1028714	12	Yes	CAZy Unknown	Carbohydrate binding protein	-7.2
<i>Stagonospora</i> sp.	337651	5	No	MEROPS M14A	Carboxypeptidase A1	-7.3
<i>Pyrenochaeta</i> sp.	496913	1	Yes	CAZy CE5	Carbohydrate esterase	-8.4
<i>Pyrenochaeta</i> sp.	592909	1	No	Lipase	Lipase ATG15-1	-8.6
<i>A. alternata</i>	991870	9	Yes	CAZy GH7	Glycoside hydrolase	-9.2
<i>P. sporulosum</i>	1099049	6	Yes	CAZy AA1	Multicopper oxidase	-9.7
<i>Pyrenochaeta</i> sp.	583188	6	Yes	CAZy GH128	Beta-1,3-glucanase	-29
Pyrenochaeta sp.	88989	3	No	N/A	Allergen Asp F 7	-67
<i>Significantly decreased relative abundance 14d-21d</i>						
<i>Pyrenochaeta</i> sp.	249590	8	No	MEROPS A	* Aspartic protease PEP1	-12
<i>A. alternata</i>	1006345	4	No	MEROPS A	Aspartic protease PEP1	-13
<i>Pyrenochaeta</i> sp.	602398	34	No	MEROPS M6	* Metalloprotease	-14
<i>Pyrenochaeta</i> sp.	639090	22	Yes	CAZy CBM18	Carbohydrate binding module	-14
<i>A. alternata</i>	975702	2	Yes	CAZy GH28	Polygalacturonase	-15
<i>Pyrenochaeta</i> sp.	517035	14	Yes	CAZy AA3	GMC oxidoreductase	-15
<i>A. alternata</i>	951324	19	No	MEROPS M6	* Metalloprotease	-15
<i>Pyrenochaeta</i> sp.	498713	5	Yes	CAZy CE1	Carboxylesterase	-15
<i>A. alternata</i>	1020796	24	No	MEROPS M28	* Leupeptin-inactivating enzyme 1	-16
<i>Pyrenochaeta</i> sp.	509392	20	Yes	CAZy AA3_3	FAD/FMN-containing isoamyl alcohol oxidase	-17
<i>Pyrenochaeta</i> sp.	684312	1	Yes	CAZy AA3	* GMC oxidoreductase	-17
<i>Pyrenochaeta</i> sp.	45016	4	No	MEROPS M14A	* Carboxypeptidase A1	-17
<i>A. alternata</i>	1015915	51	Yes	CAZy CBM18	Carbohydrate binding module	-17
<i>Pyrenochaeta</i> sp.	347058	3	Yes	CAZy GH28	Endopolygalacturonase	-22
<i>Pyrenochaeta</i> sp.	45016	12	No	MEROPS M14A	* Carboxypeptidase A1	-23
<i>Pyrenochaeta</i> sp.	582534	19	No	MEROPS S28	* Serine peptidase	-34
<i>Pyrenochaeta</i> sp.	584546	16	No	MEROPS M28	* Zn-dependent exopeptidase	-38
<i>Pyrenochaeta</i> sp.	514689	9	No	Lipase	* GDSL lipase/acylhydrolase	-42
<i>Pyrenochaeta</i> sp.	45016	8	No	MEROPS M14A	* Carboxypeptidase B	-64
Pyrenochaeta sp.	504857	23	No	MEROPS M14	* Zinc carboxypeptidase	-130

Table 5.4. Identified proteins with significantly changing relative abundance over time in the *Stagonospora* sp. secretome. Only proteins classified in the CAZy or MEROPS databases are shown, in addition to the protein with the highest and lowest fold change for each time point transition (in bold). Proteins that were significantly regulated in more than one time point transition are indicated with an asterisk. Refer to the text for an explanation of significance cutoffs and to Table S5.5 for the full list of significantly changing proteins for this organism.

Genome in which protein was identified	JGI Protein ID	Peptides	CAZyme	Protein Family	Putative Function from Best BLAST Hit	Fold Change
<i>Significantly increased relative abundance 7d-14d</i>						
A. alternata	1011227	35	No	N/A	Spermidine synthase	74
<i>Stagonospora</i> sp.	348212	5	Yes	CAZy GH13/GH27	Alpha-galactosidase	24
<i>Stagonospora</i> sp.	219853	5	No	MEROPS S1A	Trypsin-like protease 1	22
<i>A. alternata</i>	1016988	12	No	MEROPS M1	Leukotriene A-4 hydrolase	13
<i>P. sporulosum</i>	1167742	11	No	MEROPS M1	Leukotriene A-4 hydrolase	11
<i>A. alternata</i>	981151	8	Yes	CAZy GH16	Glycoside hydrolase	10
<i>Stagonospora</i> sp.	288541	10	No	MEROPS M19	Dipeptidase	9.3
<i>Stagonospora</i> sp.	282318	5	No	MEROPS S10	Carboxypeptidase S1	9.3
<i>A. alternata</i>	504433	11	No	MEROPS S1A	Trypsin	8.2
<i>Pyrenochaeta</i> sp.	514351	8	No	MEROPS M24	Xaa-Pro aminopeptidase. Mn-binding	7.4
<i>A. alternata</i>	927993	26	No	MEROPS M3A	Thimet oligopeptidase	7.1
<i>Stagonospora</i> sp.	333691	15	No	MEROPS S9	Dipeptidyl peptidase V	6.7
<i>Stagonospora</i> sp.	373691	1	No	MEROPS S10	Carboxypeptidase S1	6.1
<i>A. alternata</i>	950584	1	Yes	CAZy CE5	Cutinase 1	6.0
<i>Significantly increased relative abundance 14d-21d</i>						
Stagonospora sp.	134696	5	Yes	CAZy GH64	Beta-1,3-glucanase	40
<i>Stagonospora</i> sp.	305412	13	Yes	CAZy GH55/PL	Exo-beta-1,3-glucanase, pectin lyase	24
<i>Pyrenochaeta</i> sp.	540437	15	Yes	CAZy GH55/PL	Exo-beta-1,3-glucanase, pectin lyase	9.4
<i>A. alternata</i>	974855	2	No	Lipase	Cellulose binding family II protein	9.4
<i>Pyrenochaeta</i> sp.	678105	32	Yes	CAZy AA3	GMC oxidoreductase	8.3
<i>Stagonospora</i> sp.	283450	1	Yes	CAZy GH5	Endo-beta-1,4-glucanase	7.0
<i>Stagonospora</i> sp.	80736	3	Yes	CAZy GH81	Endo-beta-1,3-glucanase	7.0
<i>Stagonospora</i> sp.	217423	7	Yes	CAZy GH13	Alpha-amylase	6.5
<i>Stagonospora</i> sp.	87487	1	Yes	CAZy GH5	Glucan 1,3-beta-glucosidase	6.0
<i>Stagonospora</i> sp.	323587	1	Yes	CAZy GH32	Glycoside hydrolase	5.9
<i>Stagonospora</i> sp.	271508	8	Yes	CAZy GH15	1,4-alpha-D-glucan glucohydrolase	5.7
<i>A. alternata</i>	577093	20	Yes	CAZy GH17	* GPI-anchored cell wall beta-1,3-endoglucanase	5.6
<i>Stagonospora</i> sp.	333607	2	Yes	CAZy AA9/GH61	Cel1 protein	5.3
<i>P. sporulosum</i>	1162829	1	No	MEROPS S9B	Dipeptidyl-aminopeptidase B	5.3
<i>Stagonospora</i> sp.	320525	4	No	MEROPS S1/S6	Chymotrypsin hap	5.2
<i>A. alternata</i>	119004	8	No	MEROPS S9B	Seprase	5.1
<i>Stagonospora</i> sp.	16908	2	No	MEROPS S10	Carboxypeptidase cpds	4.7
<i>Stagonospora</i> sp.	100958	3	Yes	CAZy AA9/GH61	Glycoside hydrolase	4.7
<i>Stagonospora</i> sp.	275629	5	No	MEROPS M28	Leupeptin-inactivating enzyme 1	4.6
<i>P. sporulosum</i>	1203498	5	Yes	CAZy GH55/PL	Exo-beta-1,3-glucanase, pectin lyase	4.3
<i>Pyrenochaeta</i> sp.	591934	8	No	MEROPS A	Aspartyl proteinase	4.2
<i>Stagonospora</i> sp.	323852	3	Yes	CAZy GH125	Exo-alpha-1,6-mannosidase	4.2
<i>Stagonospora</i> sp.	290606	4	No	MEROPS M18	Aspartyl aminopeptidase	4.2
<i>A. alternata</i>	946519	7	Yes	CAZy GH35	Glycoside hydrolase	4.1
<i>Stagonospora</i> sp.	272022	2	Yes	CAZy CE1	Para-nitrobenzyl esterase (carboxylesterase type B)	4.0
<i>Stagonospora</i> sp.	243823	9	No	MEROPS S9B	Dipeptidyl peptidase IV	4.0
<i>Significantly decreased relative abundance 7d-14d</i>						
<i>A. alternata</i>	1039208	1	Yes	CAZy AA2	Chloroperoxidase	-7.8
<i>Stagonospora</i> sp.	215894	4	Yes	CAZy AA3_3	Alcohol dehydrogenase 1	-8.6
<i>A. alternata</i>	577093	20	Yes	CAZy GH17	* GPI-anchored cell wall beta-1,3-endoglucanase	-11
<i>P. sporulosum</i>	1099049	6	Yes	CAZy AA1	Multicopper oxidase	-22
A. alternata	1025053	8	No	MEROPS M16	Mitochondrial-processing peptidase	-23
<i>Significantly decreased relative abundance 14d-21d</i>						
<i>Pyrenochaeta</i> sp.	592296	23	Yes	CAZy GH72	Beta-1,3-glucanosyltransglycosylase	-2.8
<i>A. alternata</i>	936302	21	Yes	CAZy GH7	Exoglucanase 1	-3.0
<i>Stagonospora</i> sp.	113951	3	Yes	CAZy CE3	Carbohydrate esterase	-3.1
<i>P. sporulosum</i>	1137665	6	Yes	CAZy GH72	Beta-1,3-glucanosyltransglycosylase	-3.1
<i>Stagonospora</i> sp.	224061	2	No	MEROPS M20	Beta-Ala-His dipeptidase	-3.3
<i>P. sporulosum</i>	1129270	16	Yes	CAZy AA1	Multicopper oxidase	-3.6
<i>Stagonospora</i> sp.	210051	8	Yes	CAZy GH128	Beta-1,3-glucanase	-3.8
<i>Stagonospora</i> sp.	339955	9	Yes	CAZy GH72	Beta-1,3-glucanosyltransglycosylase	-4.0
<i>A. alternata</i>	950076	17	Yes	CAZy GH7	Exoglucanase	-4.5
Stagonospora sp.	326816	4	No	N/A	Pyruvate decarboxylase	-21

(a) Proteins with significantly increasing relative abundance over time. *A. alternata* appeared to rely heavily on glycoside hydrolases (GHs) to degrade its substrate, sequentially increasing its production of these enzymes over time (Figure 5.2A, Table 5.1). The most highly regulated proteins in this class from 7d-14d were associated with the GH7 (cellulose-degrading β -1,4-glucanase) and GH92 (α -mannosidase) families, exhibiting up to 40-fold increases in relative abundance. From 14d to 21d, GH31 (cellulase and hemicellulase) and GH64 (β -1,3-glucanase) proteins were the most strongly regulated with fold changes of nearly 8, in addition to a diverse suite of other GHs with both cellulase and hemicellulase-degrading capacity. Redox-active auxiliary activities (AAs), particularly those of the AA3 family, were also highly regulated by *A. alternata*, including a 21-fold increase in the relative abundance of choline dehydrogenase and a nearly 8-fold increase in an alcohol dehydrogenase during the 7d-14d transition. Like patterns of GHs, the diversity of highly regulated AAs increased later in culture. Notably, proteins significantly increasing in abundance over the second time point transition included several involved in quinone redox cycling and Fenton-based hydroxyl radical production, such as tyrosinase (AA1) (del Mar Garcia-Molina et al., 2014), and a cellulose-binding iron reductase (AA8), in addition to two monooxygenases in the AA9 family. Few peptidases were identified with significantly increasing relative abundance in this organism. Overall, the enzymes exhibiting the highest increases during the 7d-14d and 14d-21d transitions were non-CAZymes: dihydrodipicolinate synthase (involved in lysine biosynthesis in bacteria and some fungi) (Vauterin et al., 1999) and a hypothetical protein, respectively.

The *P. sporulosum* secretome exhibited significant increases in nearly all functional groups over time, although this organism most strongly regulated GHs later in culture, similar to *A. alternata* (Figure 5.2A, Table 5.2). The range of highly regulated GHs was diverse, but

GH55/PL proteins (exo- β -1,3-glucanases with pectin lyase activity) were the most frequently identified enzymes in the 14d-21d transition and exhibited the highest fold changes (8-15 fold). Also like *A. alternata*, a β -1,3-glucanase in the GH64 family and a chitinase in the GH18 family exhibited strong increases in relative abundance later in culture. AAs were also highly regulated by *P. sporulosum*, shifting from AA1 family proteins (an unspecified multicopper oxidase and tyrosinase) early in culture to hydroquinone-reducing cellobiose dehydrogenase (AA3) and a lytic polysaccharide monoxygenase (AA9) as the secretome aged. A quinone-binding amine oxidase was also identified with increased relative abundance during the 14d-21d transition. Highly regulated peptidases in this organism consisted exclusively of serine-type peptidases during the 7d-14d transition, with more diversity introduced as the secretome aged.

The *Pyrenochaeta* sp. secretome exhibited the most unique pattern of enzyme regulation under the evaluated growth conditions (Figure 5.2A, Table 5.3), containing 14 peptidases whose relative abundance significantly increased from 7d to 14d. These peptidases were comprised primarily of family M14 carboxypeptidases (with up to 55-fold relative abundance increases) and family M28 amino- and carboxypeptidases (with up to 33-fold increases), supplemented by M6 family metalloendopeptidases and several other proteases. Family M14, M28, and M6 peptidases continued to significantly increase in relative abundance from 14d to 21d as well, although many fewer peptidases were highly regulated during the later time point transition. Notwithstanding the prevalence of peptidases with high fold change increases, some GHs were also highly regulated by this organism, including a diverse range of cellulases and hemicellulases early in culture but switching to starch-degrading α -amylases in the GH13 family as the secretome aged. While neither redox-active AAs nor quinone-related enzymes exhibited significance abundance increases in the *Pyrenochaeta* sp. secretome, we observed three peptidyl-

prolyl cis-trans isomerases (protein folding chaperones) that increased in abundance early in culture, with fold changes up to 12. Overall, the enzyme exhibiting the highest increase during the 7d-14d transition was disulfide isomerase (another protein folding enzyme) with a dramatic 100-fold increase; an unspecified FAD-binding protein was the most highly regulated during the 14d-21d transition.

Patterns of enzyme regulation in the *Stagonospora* sp. secretome were characterized by an increase in production of peptidases early in culture, followed by a shift to increasing the abundance of GHs as the secretome aged (Figure 5.2A, Table 5.4). Highly regulated peptidases during the 7d-14d transition exhibited substantial diversity but included two family S1A trypsin-like peptidases (with fold changes up to 22) and two family M1 leukotriene A-4 hydrolases; proteases with increasing abundance later in culture demonstrated a similar level of diversity but featured three family S9B peptidases and a maximum fold change of 5.3. While few GHs with significantly increased abundance were identified in the 7d-14d transition, a total of 13 GHs were highly regulated during the 14d-21d transition and were dominated by a GH64 family β -1,3-glucanase (with a 40-fold increase; the highest during this time period) and three GH55/PL family exo- β -1,3-glucanases (with up to 24-fold increases). This GH55/GH64 profile later in culture was similar to those observed in both *A. alternata* and *P. sporulosum*. Only a few AAs or quinone redox cycling proteins were highly regulated by *Stagonospora* sp., including a quinone-binding amine oxidase early in culture and two moonoxygenases in the AA9 family later in culture. Highly regulated “other” proteins featured three spermidine synthases during the 7d-14 transition, including one with the highest fold change (74-fold) during this time period; this enzyme is generally associated with mycelial growth, cell differentiation, and asexual reproduction in fungi (Calvo et al., 2002; Valdés-Santiago and Ruiz-Herrera, 2013).

(b) Proteins with significantly decreasing relative abundance over time. In all four fungi, few CAZy or MEROPS enzymes exhibited large decreases in relative abundance as the cultures aged (Figure 5.2B). One notable exception is the large suite of M14, M28, and M6 family peptidases that decreased significantly in relative abundance during the 14d-21d transition in the *Pyrenochaeta* sp. secretome (Table 5.3). As nearly all of these proteins had significantly increased during the earlier time point transition, the data indicate a large peak in relative abundance of these specific peptidases at 14d and illustrate a defining characteristic of this organisms' secretome. While we observed few instances of strongly decreased production of GHs, both the *P. sporulosum* (Table 5.2) and *Stagonospora* sp. (Table 5.4) secretomes exhibited significant decreases in β -1,3-glucanosyltransglycosylase (GH72), an enzyme responsible for the elongation of β -1,3-glucan chains during cell wall synthesis (Mouyna et al., 1998). Additionally, the *Pyrenochaeta* sp. secretome was characterized by decreased GH28 family proteins (pectin-degrading polygalacturonases) (Table 5.3).

The overwhelming majority of proteins with significantly decreasing relative abundance over time were “other” proteins that are not included in the CAZy or MEROPS classification systems (Figure 5.2B). Specifically, these proteins were mostly of intracellular origin and predominantly associated with cell growth and energy generation processes. Commonly observed enzymes included those related to the tricarboxylic acid and glyoxalate cycles (e.g., isocitrate lyase in *A. alternata* and *Stagonospora* sp., citrate synthase in *P. sporulosum*, malate dehydrogenase in *P. sporulosum* and *Stagonospora* sp., and nucleoside diphosphate kinase in *Pyrenochaeta* sp.), glycolysis and gluconeogenesis (glyceraldehyde 3-phosphate dehydrogenase in *A. alternata*, enolase and phosphoenolpyruvate carboxykinase in *A. alternata* and *P. sporulosum*, phosphoglucomutase in *P. splorulosum*, pyruvate carboxylase and decarboxylase in *P.*

sporulosum and *Stagonospora* sp.), protein synthesis (transcription regulators and translation initiation factors in *A. alternata* and *Pyrenochaeta* sp., translation elongation factors and ribosomal proteins in *Stagonospora* sp., several peptidyl-prolyl cis-trans isomerase protein folding chaperones in *Pyrenochatea* sp.), and cell division (ANTH domain containing proteins, which participate in actin filament organization in the cell wall, in *P. sporulosum* and *Stagonospora* sp., and a cell division cycle protein in *P. sporulosum*). Other proteins exhibiting significantly decreased relative abundance were related to stress response; heat shock proteins were identified in all four fungi, most frequently during the 7d-14d transition. Refer to Tables S5.2-S5.5 for a complete list of these enzymes, including fold changes, for each of the four organisms.

Comparative analysis of proteins common to all four fungi. An evaluation of proteins produced by all four organisms, beyond simply those that exhibited significant changes in relative abundance over time, further illustrates the species-specific enzyme utilization patterns in these fungi. Specifically, despite having a similar repertoire of extracellular hydrolytic enzymes at their disposal (Figure 5.1), the organisms utilized these proteins to different extents and at different times to degrade the same substrate under the same environmental conditions (Figure 5.3).

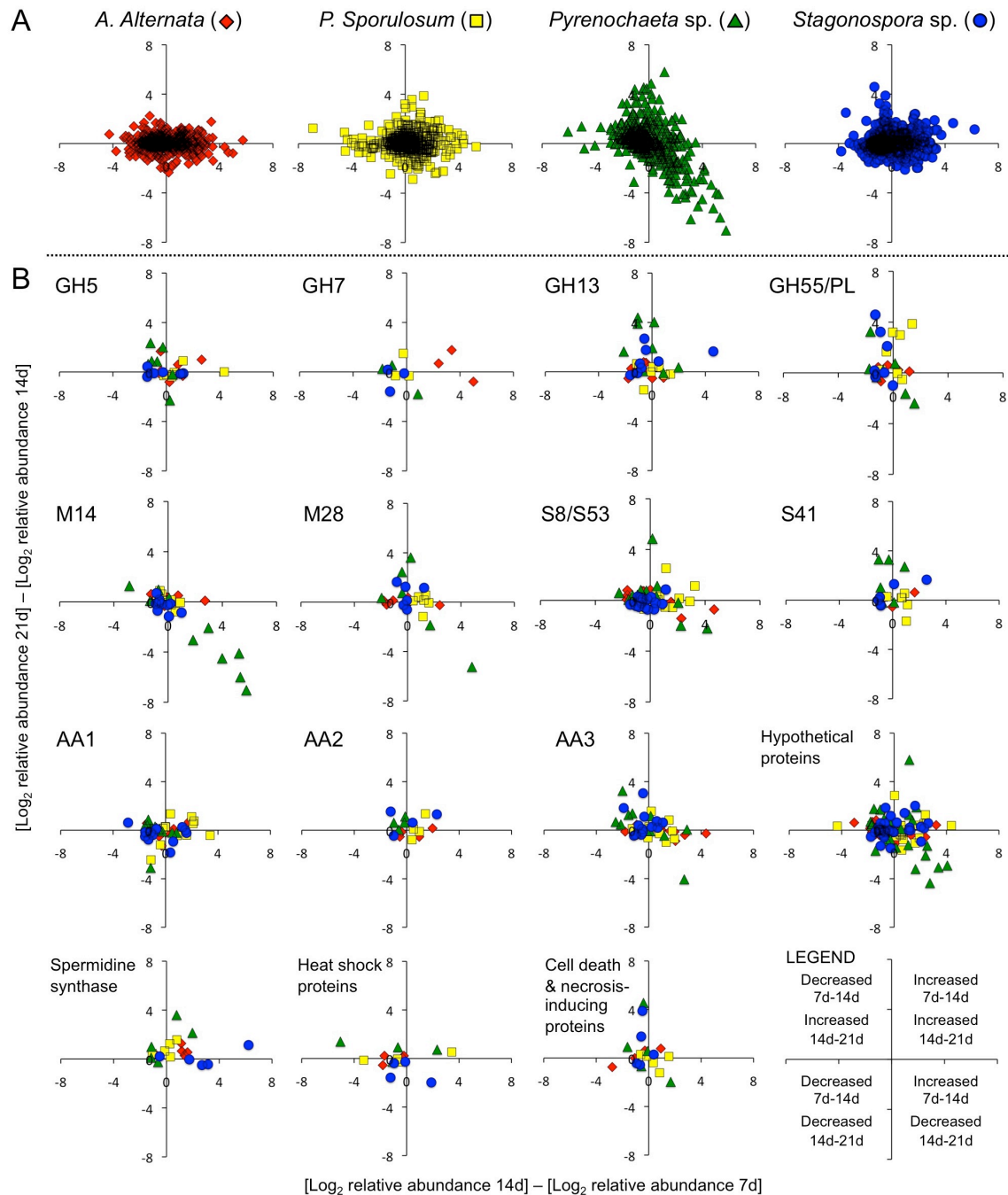


Figure 5.3. Temporal changes in relative abundance of identified proteins common to all four fungal secretomes. (A) All identified proteins; each fungus plotted individually. (B) All 4 fungi plotted together; marker shapes and colors as in (A). 1st row: Selected glycoside hydrolases. 2nd row: Selected peptidases. 3rd row: Selected redox-active and ROS-generating oxidoreductases, and hypothetical proteins. 4th row: Other selected proteins and legend. Legend: Top left quadrant of each plot represents identified proteins whose relative abundance decreased from the 7d sample to the 14d sample, and then increased from the 14d sample to the 21d sample. Other quadrants as noted in legend. Only proteins that were identified in all 3 time points in all 4 fungi are shown. Abbreviations as in Figure 5.1.

Overall patterns of enzyme utilization for proteins common to all four fungi reveal that the *Pyrenochaeta* sp. secretome was characterized by an excursion at 14d that was unique to the fungi we evaluated, consisting of a peak in enzyme production that had dissipated by 21d (Figure 5.3A). The other three organisms regulated enzyme production primarily during the 7d-14d transition, with fewer changes observed during the 14d-21d transition. For example, the cluster of proteins identified in the *A. alternata* secretome is centered mainly around the x-axis in Figure 5.3A, with little variation along the y-axis.

Case studies of individual protein families further highlighted species-specific enzyme utilization patterns (Figure 5.3B). For instance, family GH5 and GH7 proteins are similar in function, here comprising mainly β -1,3-glucosidases and β -glucanases, respectively, and represented frequently observed cellulase families in the fungal secretomes under these growth conditions. Although all four organisms produced proteins of each type, GH5 proteins were favored by *P. sporulosum* during the 7d-14d transition, while GH7 proteins were produced in high quantities by *A. alternata* during the same time frame. Neither *Pyrenochaeta* sp. nor *Stagonospora* sp. highly regulated these specific proteins common to all four fungi, despite being presented with the same substrate, although species-specific versions of GH5 proteins exhibited significant increases in both organisms (Tables 5.3-5.4). In contrast, starch-degrading GH13 family proteins, mainly α -amylases, were utilized to a great extent by *Pyrenochaeta* sp. and *Stagonospora* sp. during the 14d-21d transition, while the abundance of these enzymes in the other two fungi varied little over time. As discussed earlier, exo- β -1,3-glucanases in the GH55 family increased in abundance in nearly all fungi during the 14d-21d transition; β -1,3-glucanases are thought to be involved in fungal autolysis in aging, carbon-limited cultures (McNeil et al., 1998; Nitsche et al., 2012).

Pyrenochaeta sp. exhibited a unique pattern of peptidase production, and the large increases in abundance of M14 and M28 family peptidases during the 7d-14d transition, as discussed above, is observed in the context of all four fungi in Figure 5.3B. While all four organisms produced these proteins, the peak at 14d in the *Pyrenochaeta* sp. secretome appeared to be the defining characteristic in this organism's unique enzyme utilization patterns (Figure 5.3A). Numerous S8/S53 serine-type peptidases were observed in all four fungi, and while three organisms increased their production during the 7d-14d transition, *Stagonospora* sp. did not. Regulation of family S41 peptidases was primarily observed in the *Pyrenochaeta* sp. secretome during the 14d-21d transition; these proteins have been previously implicated in the Mn(II) oxidative capacity of this organism late in culture (Zeiner et al., In review).

Patterns of auxiliary activity utilization were also species-specific and revealed temporal shifts in redox-active enzyme production among the organisms. Specifically, we observed that among multicopper oxidases (AA1 family proteins) produced by all four fungi, these proteins generally increased in abundance in the *P. sporulosum* secretome during the 7d-14d transition while simultaneously decreasing in abundance in the *Stagonospora* sp. secretome. Furthermore, the relative abundance of GMC oxidoreductases (AA3) common to all four organisms increased in the *A. alternata* and *P. sporulosum* secretomes early in culture and in the *Pyrenochaeta* sp. and *Stagonospora* sp. secretomes later in culture.

As noted earlier, "other" proteins were also highly regulated by the fungi and can provide insight into the metabolic state of the organisms at the different sampling points over time. For example, spermidine synthase, an enzyme associated with hyphal growth and cell differentiation, greatly increased in abundance in the *Stagonospora* sp. secretome during the 7d-14d transition, while we observed a delay in the increase of this enzyme in the *Pyrenochaeta* sp. secretome

(Figure 5.3B). As a potential indicator of relief from environmental stressors, a decrease in the abundance of heat shock proteins was observed early in culture for *A. alternata* but later in culture for *Stagonospora* sp. Interestingly, while *Pyrenochaeta* sp. and *Stagonospora* sp. increased the production of cell death-related proteins in the final sampling point, similar increases were not observed in the secretomes of the other two organisms.

The importance of hypothetical proteins in the secretomes of these fungi should not be overlooked. These proteins with unknown or poorly defined function were frequently observed in the secretomes, and since many of them represented proteins that were more strongly regulated than enzymes with known function (Figure 5.3B), they likely played important roles in substrate degradation. We look forward to shedding light on the functions of these proteins as more fungal genomic and proteomic information becomes available.

While this comparative analysis of proteins common to all four fungi is not fully representative of the complete suite of enzymes identified in each of the four organisms, these direct comparisons illustrate the variety with which these phylogenetically diverse fungi utilized the same enzymes to degrade the same substrate under the same growth conditions.

Discussion

Protein abundance, rather than presence, is key to secretome function. Despite the striking similarity in secretome functional diversity among the four phylogenetically diverse Ascomycetes throughout the 3-week time period evaluated in this study (Figure 5.1), species-specific and temporal patterns of enzyme utilization suggest that protein abundance, rather than simply protein presence, dictates secretome functional capacity in these fungi. In a study of the secretome of *Aspergillus nidilans* over the course of 14 days, Saykhedkar et al. (2012) observed

that although most of the identified proteins had been secreted after 24 hours, changes in the relative abundance of these enzymes over time conferred extracellular carbon degradative capacity that varied with diminishing resource availability. Here we demonstrate a similar pattern in which both the size and diversity of the secretome remained fairly constant as the secretome aged, even as substrate in these batch cultures presumably decreased over time, necessitating changes in metabolic strategies (as discussed below). As decreases in secretome size and increases in carbohydrate-active protein diversity have been observed in other fungal systems as the cultures aged (Shi et al., 2013; Hori et al., 2014), it is likely that these patterns are dependent upon numerous factors, including species, substrate type and concentration, and growth conditions.

Species-specific and temporal shifts in carbon utilization strategies. Our findings demonstrate that each of the four fungi exhibits a species-specific pattern of enzyme regulation over time, revealing key differences in the organisms' carbon utilization strategies as they degrade the same substrate under the same growth conditions. Specifically, our data suggest that *P. sporulosum* and *A. alternata* exhibit sequential enzyme secretion patterns as the available substrate becomes more difficult to degrade, *Stagonospora* sp. preferentially attacks proteinaceous substrate before switching to carbohydrates, and *Pyrenochaeta* sp. utilizes primarily peptidases to aggressively attack carbon sources in a concentrated burst. Moreover, it is noteworthy that the secretomes of these organisms contained a wide variety of enzymes implicated in lignocellulose degradation (i.e., CAZymes) despite the lack of plant-derived substrate in their growth medium, supporting our previous observations that these fungi possess cellulose-degrading capacity (unpublished data) and providing insight into the mechanisms by which this capacity is achieved.

The secretome of *P. sporulosum* reveals a metabolic response to decreasing substrate quality over time. We observed proteins increasing in abundance early in culture that specifically target carbohydrates (e.g., GH5 β -glucosidases, GH47 α -mannosidases, and GH79 β -glucuronidases), representing both cellulose and hemicellulose degradation capacity. Later, this suite of enzymes shifts to more non-specific oxidative enzymes including cellobiose dehydrogenase (AA3) and monooxygenases in the AA9 family (formerly GH61), which are known to act synergistically in oxidizing carbon compounds via the production of reactive intermediates (Harris et al., 2010; Quinlan et al., 2011). This shift occurs at the same time as an increase in abundance of a quinone-binding amine oxidase, which could contribute to reduction of hydroquinones and Fenton-based hydroxyl radical production by cellobiose dehydrogenase (Henriksson et al., 2000; Hatakka and Hammel, 2010) to aid in non-specific oxidation of a more recalcitrant carbon source, namely fungal biomass. Indeed, highly regulated GHs shift toward β -1,3-glucanases in the GH55 and GH64 families and chitinases in the GH18 and GH75 families later in culture; both types of enzymes are involved in fungal cell wall remodeling and biomass recycling as autophagy commences (Nitsche et al., 2012). Increases in these enzymes were concomitant with decreases in abundance of cell division and energy generation enzymes, suggesting decreased biomass production as food becomes scarce and more difficult to degrade.

Interestingly, a similar pattern of sequential enzyme secretion (progressing from GH5/GH7 cellulases/hemicellulases to cellobiose dehydrogenase and AA9 monooxygenases) has been described recently for the white-rot Basidiomycete *Ceriporiopsis subvermispora* growing on aspen wood (Hori et al., 2014). This represents an intriguing homology between fungi of different phyla challenged with different carbon sources and may be indicative of a generic, widespread strategy for carbon degradation in the environment. Although the Ascomycetes in

this study were not provided with plant-derived substrate, a shift from degrading the labile yeast extract and acetate growth medium to utilizing fungal biomass as a carbon source may be analogous to the transition from breaking down cellulose and hemicellulose to attacking recalcitrant phenolics (e.g., lignin) in plant material. The ability of these Ascomycetes to degrade lignin remains unknown, but their demonstrated cellulose degrading capacity and similarities in enzyme production patterns to wood-rot fungi warrant further investigation into the oxidative capacity of these organisms.

Temporal patterns of enzyme utilization in *A. alternata* are similar to those observed in *P. sporulosum*, demonstrating a transition from specific to non-specific oxidative mechanisms as labile substrate becomes scarce. Glycoside hydrolases with increasing relative abundance shift from cellulases in the GH7 family and hemicellulases (α -mannosidases and endo-xylanases) in the GH92 and GH10 families early in culture to autophagy-related β -1,3-glucanases in the GH55 and GH64 families and potential chitin-degrading enzymes in the GH18 family later in culture, suggesting biomass recycling. Likewise, we observed a similar increase in non-specific oxidative enzymes such as tyrosinase during the 14d-21d transition, which, in combination with iron reductase, could aid in quinone-mediated hydroxyl radical generation (del Mar Garcia-Molina et al., 2014). While we observed AA9 monooxygenases in high abundance later in culture, we did not identify a concomitant increase in cellobiose dehydrogenase as we did in *P. sporulosum*. Shifts from specific to non-specific oxidative enzymes coincide with a transition from increasing the abundance of proteins involved in growth (i.e., lysine biosynthesis) early in culture to decreasing the abundance of proteins involved in energy generation (i.e., glycolysis and the glyoxalate cycle) later in culture. Unlike *P. sporulosum*, however, we observed a greater emphasis (a 1.5x larger fold change) on AA9 monooxygenases and a lesser emphasis (fold

changes of approximately one-half those in *P. sporulosum*) on β -1,3-glucanases later in culture, highlighting the persistence of species-specific enzyme utilization patterns despite similar overall carbon degradation strategies.

While the secretome of *Stagonospora* sp. shared some characteristic enzyme utilization patterns with those of *P. sporulosum* and *A. alternata*, its overall carbon degradation strategy was notably distinct, defined by a two-tiered approach to substrate breakdown. Like the other two organisms, enzymes likely involved in non-specific oxidative mechanisms increased in abundance later in culture, including two AA9 monooxygenases and an unspecified GMC oxidoreductase in the AA3 family (the same family in which cellobiose dehydrogenase is classified). Additionally, the abundance of β -1,3-glucanases in the GH55 and GH64 families increased substantially as the secretome aged. Taken together, these data once again suggest that fungal biomass recycling may have occurred once more labile carbon sources had been exhausted. Despite these similarities, however, *Stagonospora* sp. was unique in preferentially attacking proteinaceous material early in culture and transitioning to carbohydrates later in culture, utilizing a functionally diverse suite of peptidases and glycoside hydrolases, respectively, to degrade each substrate type. It would be interesting to evaluate whether this two-tiered approach extends to plant-derived substrates containing a greater percentage of recalcitrant carbohydrates and less easily digestible proteinaceous material (e.g., yeast extract).

The most distinct of the fungi in this study, *Pyrenochaeta* sp. heavily utilized peptidases in its secretome, producing them in an aggressive, concentrated burst after 14 days of growth. Many of the same family M14, M28 and M6 metallopeptidases that significantly increased in abundance by day 14 had substantially decreased by day 21, suggesting a highly focused protein degradation strategy. We also observed several H₂O₂-generating AA3 family proteins that

roughly followed patterns of peptidase utilization, suggesting a synergistic approach in which both specific and non-specific oxidative mechanisms are employed simultaneously to degrade proteinaceous substrate. Interestingly, another unique characteristic of this organism's secretome was a transition from a diverse suite of GHs early in culture to a focus on starch-degrading enzymes in the GH13 family later, after the burst of peptidases had dissipated. This differs from the other three fungi in that autolysis-related glucanases and chitinases were not among the most highly regulated GHs later in culture; however, GH55 and GH18 family proteins are included in the list of significantly increasing proteins during the 14d-21d transition when we expand our significance cutoff to the 95th percentile instead of the 97.5th (data not shown). While the importance of peptidases in this organism's arsenal of hydrolytic enzymes is clear, as evidenced by this study and our previous observations that family S41 peptidases are likely responsible for the Mn(II) oxidative capacity of this fungus (Zeiner et al., In review), the mechanistic significance of these enzymes remains enigmatic. Furthermore, as with *Stagonospora* sp., it would be interesting to determine whether the predominance of peptidases in the *Pyrenochaeta* sp. secretome extends to growth on more recalcitrant, lignocellulosic substrate.

It remains unclear whether the burst of metallopeptidases observed in the *Pyrenochaeta* sp. secretome was targeted at proteinaceous substrate in the original growth medium, proteinaceous fungal biomass after depletion of the initial substrate, or was indicative of a more complex metabolic response or signaling mechanism. Rapid proteolysis has been observed in submerged batch cultures prior to the onset of cellular degradation in response to carbon starvation (Rober et al., 1986; Dosoretz et al., 1990; McNeil et al., 1998) and is similarly thought to be involved in nutrient (i.e., nitrogen) recycling as autophagy commences (Nitsche et al., 2012). Specifically, metallopeptidases have been implicated in both the early and late stages of

autolysis, maintaining cryptic growth after biomass recycling had been exhausted (Pusztahelyi et al., 1997) and signaling the “point of no return” in which biomass growth ceased (McIntyre et al., 2000) and the degradation of nucleic acids commenced (Klionsky et al., 1990; Gordon and Lilly, 1995). While a handful of fungal cell wall remodeling proteins (GH55, GH18) were observed with increasing relative abundance following the peptidase peak in the *Pyrenochaeta* sp. secretome, future culturing and proteomic studies would be necessary to unambiguously link these peptidases with biomass recycling. Fungal peptidases have also been implicated in the activation of cellulases (specifically, endo- β -1,4-glucanases) (Eriksson and Pettersson, 1982, 1988) and the inactivation of ligninases (Dosoretz et al., 1990). Although no highly regulated ligninases were observed in the *Pyrenochaeta* sp. secretome, unspecified GH5 and GH16 family proteins (potential endo- β -1,4-glucanases) were identified with increasing abundance at the same time as the peak in peptidase secretion. The fact that numerous hypothetical proteins were identified with similar regulation patterns as the metallopeptidases (Figure 5.3, Table S5.4) provides an additional challenge interpreting the role of these seemingly important enzymes in this organism.

In addition to the species-specific patterns of enzyme utilization, we identified several feruloyl esterases in each of the four fungi, including one with significantly increased relative abundance during the 7d-14d transition in the *A. alternata* secretome. Several other fungal secretome studies have noted the importance of this enzyme in removing aromatic compounds (i.e., ferulic acid) from plant cell walls (Adav et al., 2010; Lu et al., 2010; Saykhedkar et al., 2012). Here we observed secretion of feruloyl esterase by these Ascomycetes even in the absence of plant-derived substrate; secretion may be more pronounced in the presence of cellulosic material.

Proteins common to all four fungi highlight secretome functional redundancy. The comparative analysis of proteins produced by all four organisms (Figure 5.3) not only underscores the species-specific enzyme utilization patterns among the fungi, but it also emphasizes our previous findings that the secretomes are characterized by species-specific versions of functionally similar enzymes (Zeiner et al., In preparation). For instance, while *P. sporulosum* produced a common version of a GH5 family protein in high abundance early in culture (Figure 5.3B), enzymes in this family that exhibited significant increases in abundance in the *Pyrenochaeta* sp. and *Stagonospora* sp. secretomes were only identified in three and one fungus, respectively, and therefore do not appear in Figure 5.3B. This apparent species-specific preference for particular versions of functionally similar enzymes is intriguing and hints at the inherent complexity of fungal proteomic responses to substrate types and environmental conditions.

Conclusions. Here we have presented a quantitative, comparative analysis of the proteomic composition of the secretomes of four Mn(II)-oxidizing, filamentous Ascomycete fungi over a three-week time period. We demonstrate that the organisms produce a similar suite of extracellular enzymes but exhibit striking differences in regulation of these enzymes among species and over time. These findings suggest that the fungi employ different carbon utilization strategies to degrade the same substrate under the same growth conditions and that relative abundance of particular enzymes, rather than simply presence of these proteins, confers species-specific secretome functional capacity. Although additional biochemical investigation is needed to elucidate and confirm the mechanisms we have identified, this iTRAQ-based comparative proteomic study provides a first look at metabolic processes that may be operative in these

organisms, how they differ among diverse species, and how they may impact carbon turnover during growth on plant-derived substrate in the environment.

Acknowledgements

This work was supported by the National Science Foundation, grant numbers EAR-1249489 and CBET-1336496, both awarded to C.M.H, and by a JGI-EMSL Collaborative Science Initiative grant (proposal number 48100) awarded to C.M.H. and C.M.S. Personal support for C.A.Z was also provided by Harvard University and by a Ford Foundation Predoctoral Fellowship administered by the National Academies.

Part of this research was performed at the Environmental Molecular Sciences Laboratory, a national scientific user facility sponsored by the U.S. DOE's Office of Biological and Environmental Research and located at the Pacific Northwest National Laboratory. Part of this research was performed at the Bauer Core Facility of the FAS Center for Systems Biology at Harvard University. A portion of the bioinformatics analysis was performed at Harvard's FAS Research Computing facility.

We thank Joshua Aldrich (EMSL) and Michele Clamp (Harvard) for bioinformatic analyses at various stages of this project, and Therese R. Clauss (EMSL) for expertise in LC/MS/MS instrumentation throughout this project.

The authors disclaim endorsement of any products mentioned in this paper.

References

- Adav, S.S., Li, A.A., Manavalan, A., Punt, P., and Kwan Sze, S. (2010) Quantitative iTRAQ secretome analysis of *Aspergillus niger* reveals novel hydrolytic enzymes. *J Proteome Res* **9**: 3932-3940.
- Calvo, A.M., Wilson, R.A., Woo Bok, J., and Keller, N.P. (2002) Relationship between secondary metabolism and fungal development. *Microb Mol Biol Rev* **66**: 447-459.
- Dashtban, M., Schraft, H., Syed, T.A., and Qin, W. (2010) Fungal biodegradation and enzymatic modification of lignin. *Int J Biochem Mol Biol* **1**: 36-50.
- del Mar Garcia-Molina, M., Muñoz-Muñoz, J.L., Berna, J., García-Ruiz, P.A., Rodriguez-Lopez, J.N., and Garcia-Canovas, F. (2014) Catalysis and inactivation of tyrosinase in its action on hydroxyhydroquinone. *Int U Biochem Mol Biol* **66**: 122-127.
- Dosoretz, C.D., Chen, H.-C., and Grethlein, H.E. (1990) Effect of environmental conditions on extracellular protease activity in lignolytic cultures of *Phanerochaete chrysosporium*. *Appl Environ Microbiol* **56**: 395-400.
- Eriksson, K.-E., and Pettersson, B. (1982) Purification and partial characterization of two acidic proteases from the white-rot fungus *Sporotrichum pulverulentum*. *Eur J Biochem* **124**: 635-642.
- Eriksson, K.-E., and Pettersson, B. (1988) Acid proteases from *Sporotrichum pulverulentum*. *Methods Enzymol* **160**: 500-508.
- Girard, V., Dieryckx, C., Job, C., and Job, D. (2013) Secretomes: The fungal strike force. *Proteomics* **13**: 597-608.
- Glenn, J.K., Akileswaran, L., and Gold, M.H. (1986) Mn(II) oxidation is the principal function of the extracellular Mn-peroxidase from *Phanerochaete chrysosporium*. *Arch Biochem Biophys* **251**: 688-696.
- Gordon, L.J., and Lilly, W.W. (1995) Quantitative analysis of *Shizophyllum commune* metalloprotease ScPrB activity in SDS-gel-limitation induced autolysis. *Curr Microbiol* **30**: 337-343.
- Harris, P.V., Welner, D., McFarland, K.C., Re, E., Navarro Poulsen, J.-C., Brown, K. et al. (2010) Stimulation of lignocellulosic biomass hydrolysis by proteins of glycoside hydrolase family 61: Structure and function of a large, enigmatic family. *Biochem* **49**: 3305-3316.
- Hatakka, A., and Hammel, K.E. (2010) Fungal biodegradation of lignocellulose. In *The Mycota X: Industrial Applications*. Hofrichter, M. (ed). Berlin: Springer-Verlag, pp. 319-340.

- Henriksson, G., Johansson, G., and Pettersson, G. (2000) A critical review of cellobiose dehydrogenases. *J Biotechnol* **78**: 93-113.
- Höfer, C., and Schlosser, D. (1999) Novel enzymatic oxidation of Mn²⁺ to Mn³⁺ catalyzed by a fungal laccase. *FEBS Lett* **451**: 186-190.
- Hori, C., Gaskell, J., Igarashi, K., Kersten, P., Mozuch, M., Samejima, M., and Cullen, D. (2014) Temporal alterations in the secretome of the selective lignolytic fungus *Ceriporiopsis subvermispora* during growth on aspen wood reveal this organism's strategy for degrading lignocellulose. *Appl Environ Microbiol* **80**: 2062-2070.
- Klionsky, D.J., Herman, P.K., and Emr, S.D. (1990) The fungal vacuole: composition, function, and biogenesis. *Microbiol Rev* **9**: 266-292.
- Langston, J.A., Shaghasi, T., Abbate, E., Xu, F., Vlasenko, E., and Sweeney, M.D. (2011) Oxidoreductive cellulose depolymerization by the enzymes cellobiose dehydrogenase and glycoside hydrolase 61. *Appl Environ Microbiol* **77**: 7007-7015.
- Liu, D., Li, J., Zhao, S., Zhang, R., Wang, M., Miao, Y. et al. (2013) Secretome diversity and quantitative analysis of cellulolytic *Aspergillus fumigatus* Z5 in the presence of different carbon sources. *Biotechnol Biofuels* **6**: 149.
- Lu, X., Sun, J., Nimtz, M., Wissing, J., Zeng, A.-P., and Rinas, U. (2010) The intra- and extracellular proteome of *Aspergillus niger* growing on defined medium with xylose or maltose as carbon substrate. *Microb Cell Fact* **9**: 23.
- Martinez, D., Challacombe, J., Morgenstern, I., Hibbett, D., Schmoll, M., Kubicek, C.P. et al. (2009) Genome, transcriptome, and secretome analysis of wood decay fungus *Postia placenta* supports unique mechanisms of lignocellulose conversion. *PNAS* **106**: 1954-1959.
- McIntyre, M., Berry, D.R., and McNeil, B. (2000) Role of proteases in autolysis of *Penicillium chrysogenum* chemostat cultures in response to nutrient depletion. *Appl Microbiol Biotechnol* **53**: 235-242.
- McNeil, B., Berry, D.R., Harvey, L.M., Grant, A., and White, S. (1998) Measurement of autolysis in submerged batch cultures of *Penicillium chrysogenum*. *Biotechnol Bioeng* **57**: 297-305.
- Medina, M.L., Kiernan, U.A., and Francisco, W.A. (2004) Proteomic analysis of rutin-induced secreted proteins from *Aspergillus flavus*. *Fungal Genet Biol* **41**: 327-335.

- Mouyna, I., Hartland, R.P., Fontaine, T., Diaquin, M., Simenel, C., Delepierre, M. et al. (1998) A 1,3-beta-glucanosyltransferase isolated from the cell wall of *Aspergillus fumigatus* is a homologue of the yeast Bgl2p. *Microbiology* **144**: 3171-3180.
- Nitsche, B.M., Jørgensen, T.R., Akeroyd, M., Meyer, V., and Ram, A.F.J. (2012) The carbon starvation response of *Aspergillus niger* during submerged cultivation: Insights from the transcriptome and secretome. *BMC Genomics* **13**: 380.
- Perez, J., Munoz-Dorado, J., de la Rubia, T., and Martinez, J. (2002) Biodegradation and biological treatments of cellulose, hemicellulose, and lignin: an overview. *Int Microbiol* **5**: 53-63.
- Phalip, V., Delalande, F., Carapito, C., Goubet, F., Hatsch, D., Leize-Wagner, E. et al. (2005) Diversity of the exoproteome of *Fusarium graminearum* grown on plant cell wall. *Curr Genet* **48**: 366-379.
- Pusztahelyi, T., Pócsi, I., and Szentirmai, A. (1997) Ageing of *Penicillium chrysogenum* cultures under carbon starvation: II protease and *N*-acetyl- β -D-hexosaminidase production. *Biotechnol Appl Biochem* **25**: 87-93.
- Quinlan, R.J., Sweeney, M.D., Lo Leggio, L., Otten, H., Poulsen, J.-C.N., Johansen, K.S. et al. (2011) Insights into the oxidative degradation of cellulose by a copper metalloenzyme that exploits biomass components. *Proc Natl Acad Sci* **108**: 15079-15084.
- Rober, B., Riemay, K.H., and Hilpert, A. (1986) Growth and autolysis of the ascomycete *Hypomyces ochraceus*. Metabolism of U-¹⁴C-L-leucine 2-¹⁴C-DL-threonine and U-¹⁴C-L-aspartic acid. *J Basic Microbiol* **26**: 475-482.
- Rohr, C., Levin, L.N., Mentaberry, A.N., and Wirth, S.A. (2013) A first insight into *Pycnoporus sanguineus* BAFC 2126 transcriptome. *PLoS ONE* **8**: e81033.
- Ruiz-Duenas, F.J., and Martinez, A.T. (2009) Microbial degradation of lignin: how a bulky recalcitrant polymer is efficiently recycled in nature and how we can take advantage of this. *Microb Biotechnol* **2**: 164-177.
- Santelli, C.M., Chaput, D.L., and Hansel, C.M. (2014) Microbial communities promoting Mn(II) oxidation in Ashumet Pond, a historically polluted freshwater pond undergoing remediation. *Geomicrobiol J* **31**: 605-616.
- Santelli, C.M., Pfister, D.H., Lazarus, D., Sun, L., Burgos, W.D., and Hansel, C.M. (2010) Promotion of Mn(II) oxidation and remediation of coal mine drainage in passive treatment systems by diverse fungal and bacterial communities. *Appl Environ Microbiol* **76**: 4871-4875.

Saykhedkar, S., Ray, A., Ayoubi-Canaan, P., Hartson, S.D., Prade, R., and Mort, A.J. (2012) A time course analysis of the extracellular proteome of *Aspergillus nidulans* growing on sorghum stover. *Biotechnol Biofuels* **5**: 52.

Schlosser, D., and Höfer, C. (2002) Laccase-catalyzed oxidation of Mn^{2+} in the presence of natural Mn^{3+} chelators as a novel source of extracellular H_2O_2 production and its impact on manganese peroxidase. *Appl Environ Microbiol* **68**: 3514-3521.

Shi, J., Feng, H., Lee, J., and Ning Chen, W. (2013) Comparative proteomics profile of lipid-cumululating oleaginous yeast: An iTRAQ-coupled 2-D LC-MS/MS analysis. *PLoS ONE* **8**: e85532.

Tang, Y., Zeiner, C.A., Santelli, C.M., and Hansel, C.M. (2013) Fungal oxidative dissolution of the Mn(II)-bearing mineral rhodochrosite and the role of metabolites in manganese oxide formation. *Environ Microbiol* **15**: 1063-1077.

Valdés-Santiago, L., and Ruiz-Herrera, J. (2013). Stress and polyamine metabolism in fungi [WWW document].

Vanden Wymelenberg, A., Gaskell, J., Mozuch, M., Sabat, G., Ralph, J., Skyba, O. et al. (2010) Comparative transcriptome and secretome analysis of wood decay fungi *Postia placenta* and *Phanerochaete chrysosporium*. *Appl Environ Microbiol* **76**: 3599-3610.

Vauterin, M., Frankard, V., and Jacobs, M. (1999) The *Arabidopsis thaliana dhds* gene encoding dihydrodipicolinate synthase, key enzyme of lysine biosynthesis, is expressed in a cell-specific manner. *Plant Mol Biol* **39**: 695-708.

Wariishi, H., Valli, K., and Gold, M.H. (1992) Manganese(II) oxidation by manganese peroxidase from the basidiomycete *Phanerochaete chrysosporium* - Kinetic mechanism and role of chelators. *J Biol Chem* **267**: 23688-23695.

Zeiner, C.A., Purvine, S.O., Zink, E., Wu, S., Paša-Tolić, L., Chaput, D.L. et al. (In preparation) Comparative analysis of secretome profiles of four manganese(II)-oxidizing Ascomycete fungi.

Zeiner, C.A., Purvine, S.O., Zink, E., Wu, S., Paša-Tolić, L., Chaput, D.L. et al. (In review) Mechanisms of manganese(II) oxidation by filamentous Ascomycete fungi vary with species and time as a function of secretome composition.

APPENDIX 1

Supplemental Material for Chapter 2

Fungal oxidative dissolution of the Mn(II)-bearing mineral rhodochrosite and the role of metabolites in manganese oxide formation

This material was published in the journal *Environmental Microbiology*.
(Tang Y.*, Zeiner C.A.*, Santelli C.M, Hansel C.M. Vol. 15, pp. 1063-1077, 2013)

* These authors contributed equally to this work.

Supplementary Figures

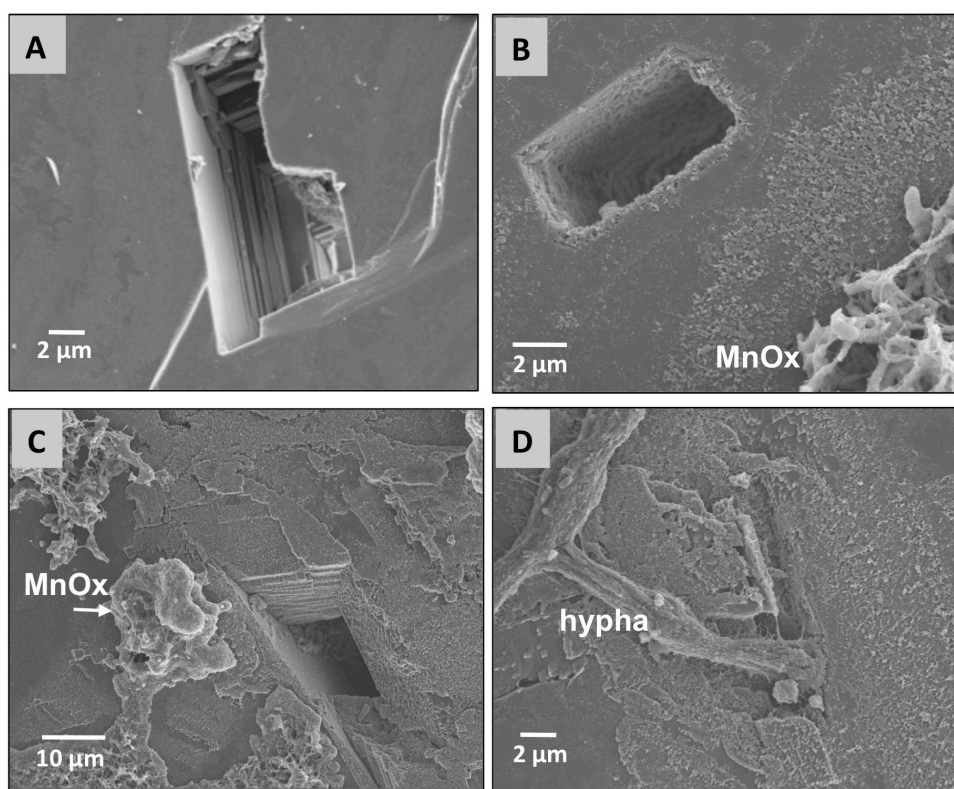


Figure S2.1. SEM images showing the surface features of rhodochrosite crystals after reaction with (A) no fungi (control sample), (B) *Pyrenochaeta* sp. DS3sAY3a, and (C-D) *Stagonospora* sp. SRC11sM3a. In contrast to the control sample, in the presence of fungi, extensive surface etching of the MnCO_3 surface is evident both within dissolution pits and on basal surfaces.

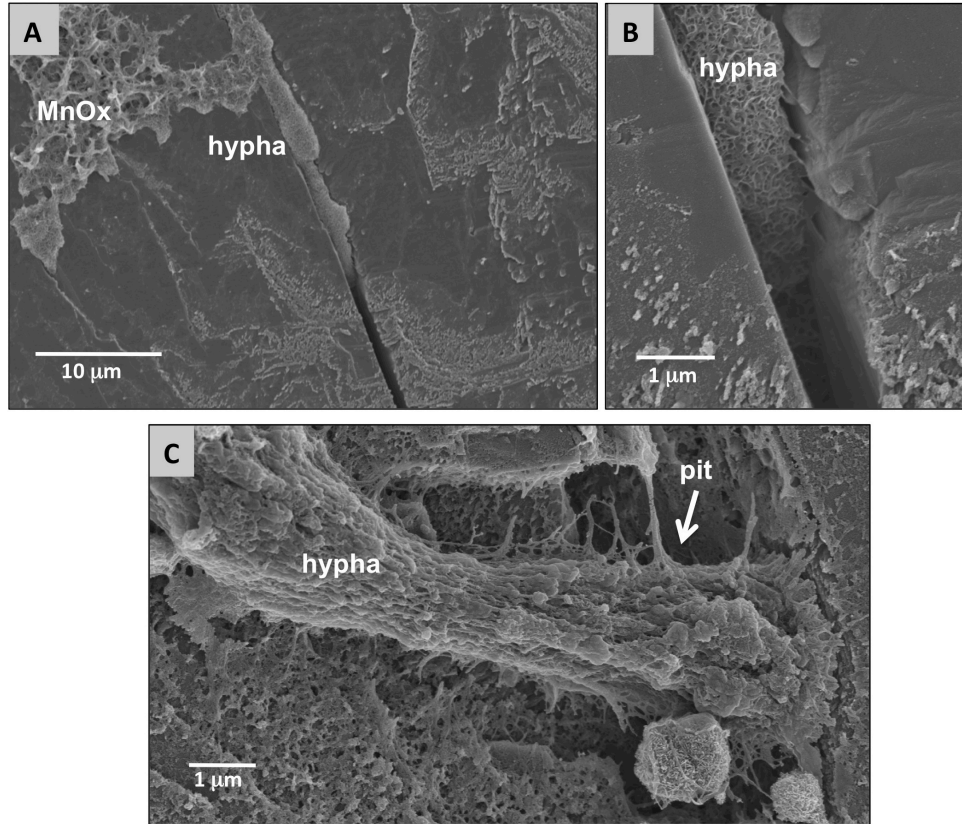


Figure S2.2. SEM images showing *Stagonospora* sp. SRC11sM3a hyphae growing into cracks (A-B) and dissolution pits (C) on the surface of rhodochrosite crystals.

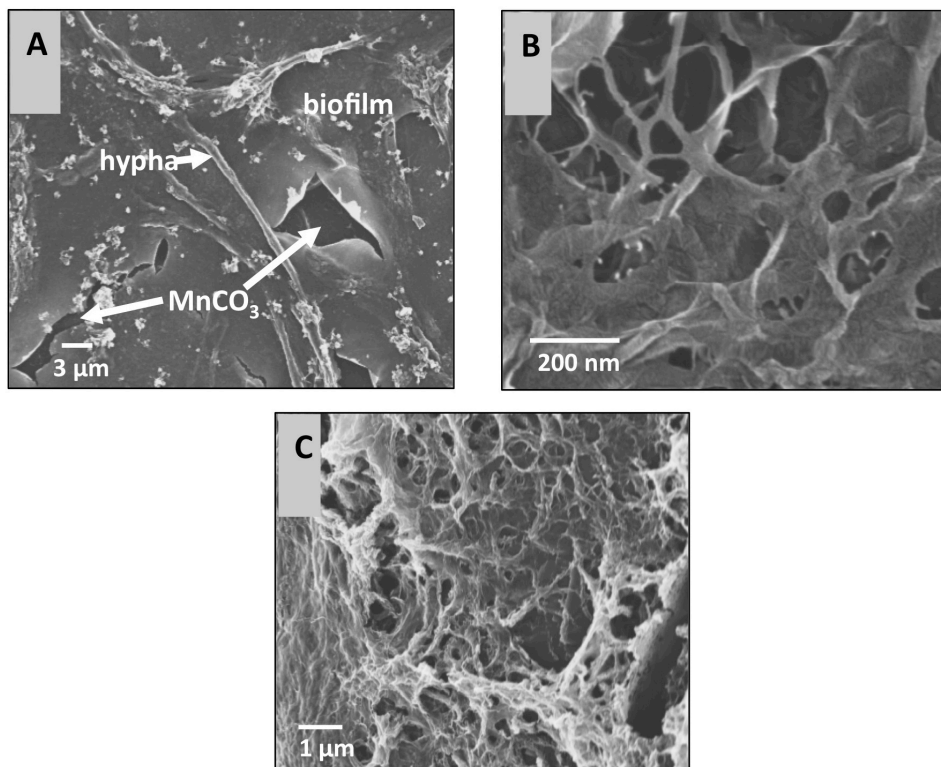


Figure S2.3. SEM images showing organic coatings on rhodochrosite crystals after reaction with (A-B) *Pithomyces chartarum* DS1bioJ1b and (C) *Pleosporales* sp. AP3s5JAC2b.

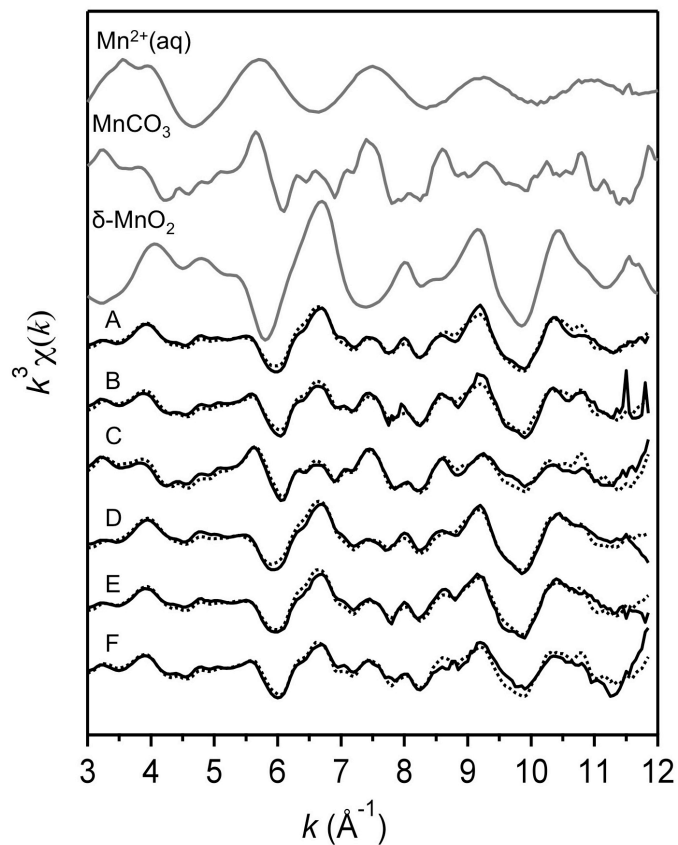


Figure S2.4. Bulk EXAFS of Mn oxides formed following Mn(II) oxidation of MnCO_3 by fungal species A – F (see Table 2.1 for species name). Three reference compounds needed to reconstruct the mycogenic oxides by linear combination fitting (LCF) are included in gray. Data are shown in solid lines and fits in dotted lines. Fitting results and parameters are listed in Table 2.1.

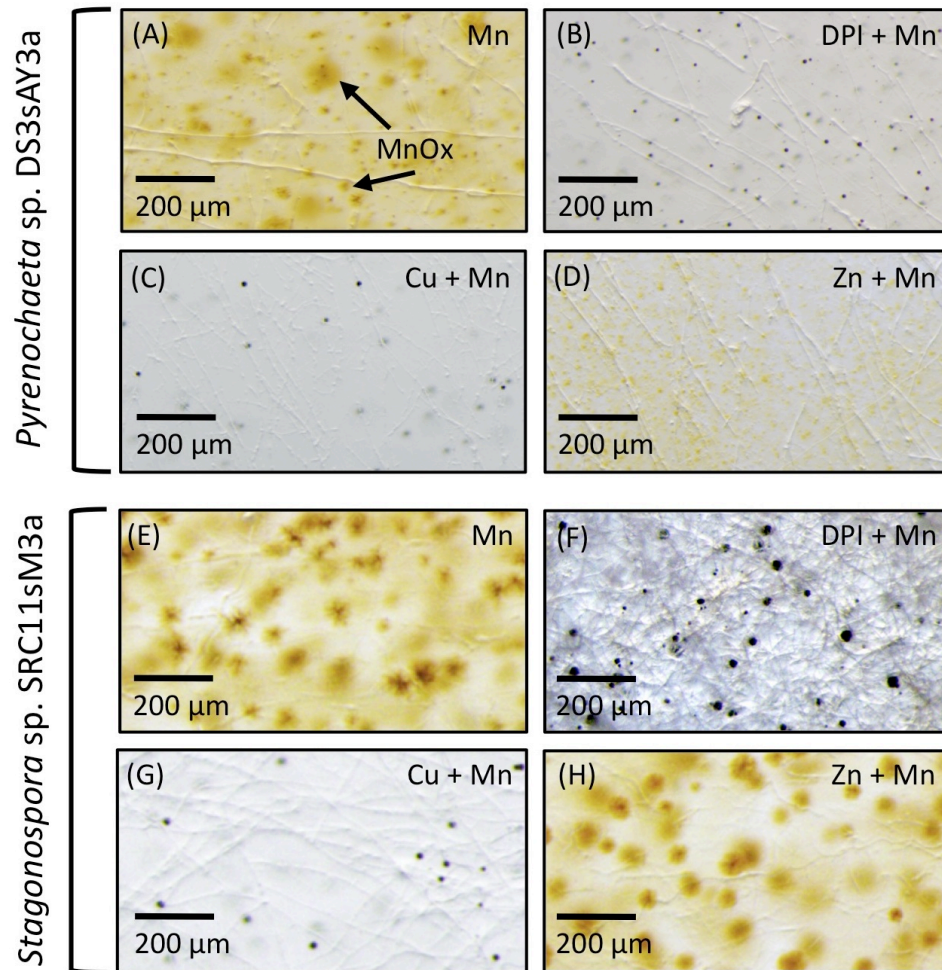


Figure S2.5. Stereomicroscope images showing the impact of chemical/enzyme inhibitors on Mn oxide formation by *Pyrenochaeta sp. DS3sAY3a* (A-D) and *Stagonospora sp. SRC11sM3a* (E-H). All images depict fungal hyphae and Mn oxides on AY agar plates after approximately 2 weeks of growth. (A, E) AY agar controls amended with 200 μM Mn(II). Brown color indicates mycogenic Mn oxides. (B, F) Cells grown with 200 μM Mn(II) and 25 μM (B) or 10 μM (F) DPI, an inhibitor of NADPH oxidases. (C, G) Cells grown with 200 μM Mn(II) and 200 μM Cu(II), a scavenger of superoxide. (D, H) Cells grown with 200 μM Mn(II) and 200 μM Zn(II). Zn(II) imparts a similar level of toxicity as Cu(II) but does not react with superoxide.

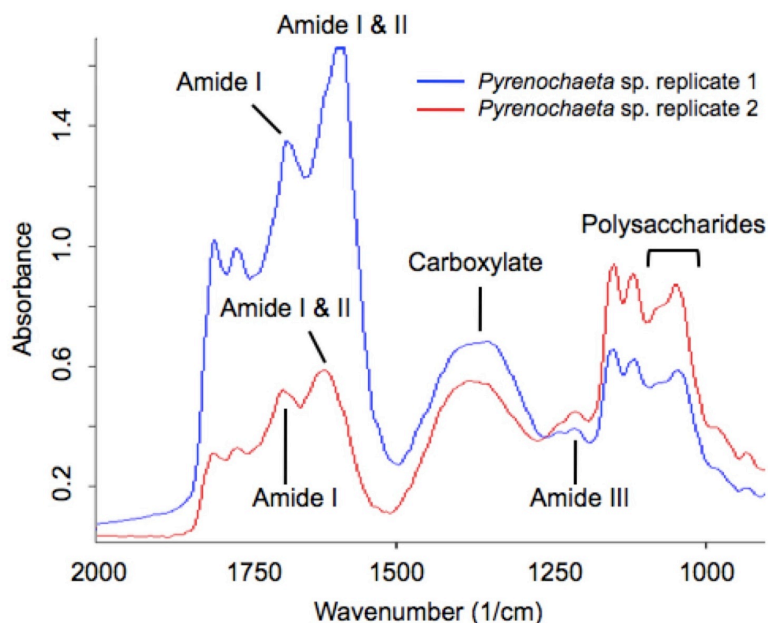


Figure S2.6. Mycogenic Mn oxide samples were analyzed with micro-Fourier transform infrared spectroscopy (μ FTIR). Mn oxide clusters in cultures of *Pyrenochaeta* sp. DS3sAY3a. The Mn oxides were not associated with any cellular materials. Clusters were gently removed from the medium with sterile wooden inoculation sticks, washed six times in distilled water, and dissolved with 20 mM ascorbic acid to liberate organics from Mn oxides prior to analysis. Samples were analyzed on a μ -FTIR at Bruker Optics, Inc. (Billerica, MA) in reflectance mode. These preliminary μ -FTIR data are promising in that they indicate the presence of organics directly associated with cell-free Mn oxide clusters.

APPENDIX 2

Supplemental Material for Chapter 3

Mechanisms of manganese(II) oxidation by filamentous ascomycete fungi vary with species and time as a function of secretome composition

This material was submitted to the journal *Applied and Environmental Microbiology*.
(Zeiner C.A., Purvine S.O., Zink E., Wu S., Paša-Tolić L.,
Chaput D.L., Santelli C.M., Hansel C.M.)

Supplementary Methods

Several chemical assays were used to supplement LC/MS/MS characterization of the fungal secretomes.

Proteinaceous nature of the Mn oxidizing factor. (A) Boiling. Secretome samples from all 3 fungi and 3 time points were boiled at 100°C in 2 mL tubes for 30 minutes, followed by Mn(III/IV) oxide quantification with LBB in 96-well plates. Alternatively, secreted metabolites were heated using a procedure modified from Thomson et al. (2006) (Thompson et al., 2006), as follows. *Stagonospora* sp. was grown on a 0.2 µm cellulose acetate filter (Whatman) on agar plates containing unamended AY medium. After the fungal mycelia had reached the edge of the filter (approximately 8 days of growth), the filter and associated mycelia were removed with sterile forceps, and the agar plates containing secreted metabolites were either (i) heated by floating in a 70°C water bath for 30 minutes, or (ii) left untreated at 20°C as a control. After incubation, all treatments were flooded with 200 µM Mn(II), incubated for 1 hour at 20°C, and evaluated for the formation of Mn oxides by flooding with LBB. The blue color produced upon reaction of LBB with biogenic Mn(III/IV) oxides was used as a qualitative indicator of Mn oxide presence or absence.

(B) Protease addition. Secretome samples from all 3 fungi and 3 time points were incubated with 1 mg mL⁻¹ proteinase K (fungal, Sigma) at 20°C for 2 hours, followed by Mn(III/IV) oxide quantification with LBB in 96-well plates.

For Mn oxide quantification in both (A) and (B), the mass of fungal protein and concentration of Mn(II) were optimized on a sample-specific basis to ensure Mn oxidative capacity of the secretome would not be limited by the amount of Mn(II) provided. Protein and Mn(II) concentrations were generally 10-25 µg mL⁻¹ and 100-250 µM, respectively.

Superoxide dismutase assay. Secretome samples were evaluated for the effect, if any, of the reactive oxygen species superoxide (O₂⁻) on Mn oxide formation. Samples from all 3 fungi and 3 time points were incubated with 50 kU L⁻¹ superoxide dismutase (bovine, Sigma) at 20°C for 1 hour, followed by Mn(III/IV) oxide quantification as above.

o-phenanthroline assay. Concentrated +Mn secretome samples from *Pyrenochaeta* sp. (culture aged 17 days) were evaluated for inhibition of enzymatic Mn oxide formation by o-phenanthroline, a copper chelating compound, as follows. Secretome samples were either (i) incubated with 75 µM o-phenanthroline dissolved in 8% ethanol at 20°C for 2 hours, (ii) incubated with 8% ethanol only as a solvent control, or (iii) left untreated as a positive control. Samples were then dropped onto agar plates containing AY medium supplemented with 200 µM Mn(II), incubated for 1 hour at 20°C, and evaluated for the formation of Mn oxides by flooding with LBB.

References

Thompson, I.A., Huber, D.M., and Schulze, D.G. (2006) Evidence of a multicopper oxidase in Mn oxidation by *Gaeumannomyces graminis* var. *tritici*. *Phytopathology* **96**: 130-136.

Supplementary Figures

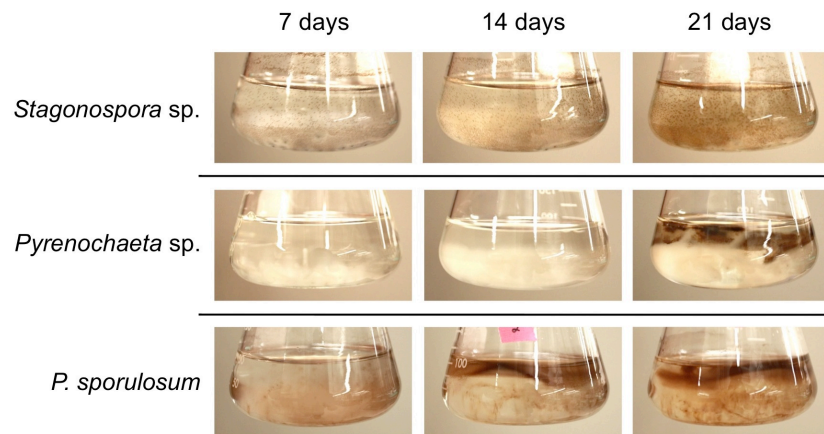


Figure S3.1. Fungal cultures of *Stagonospora* sp., *Pyrenochaeta* sp., and *P. sporulosum* in liquid AY + Mn medium at time of secretome harvest. Dark brown color indicates presence of biogenic Mn oxides. Images are representative of 4 biological replicates.

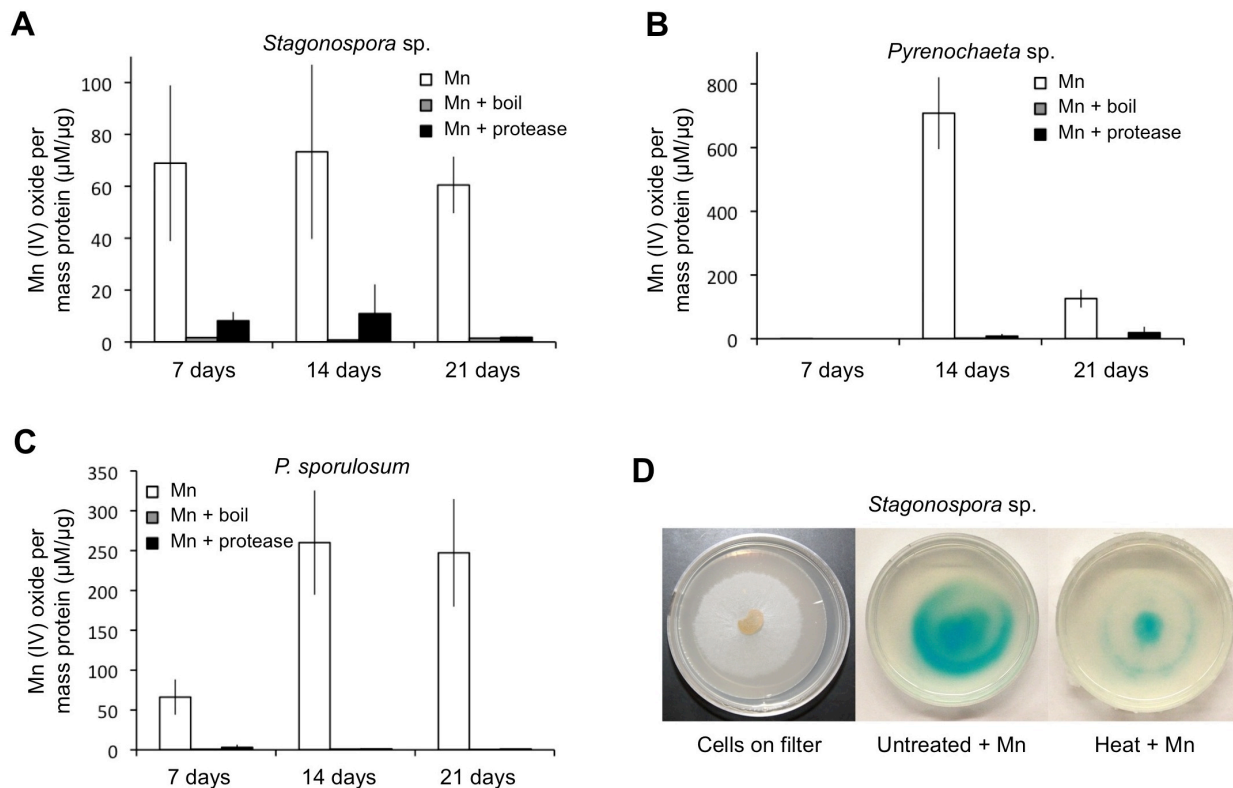


Figure S3.2. (A-C) Mn(II) oxidation normalized to protein mass in the untreated secretome (white bars), after boiling at 100°C for 30 minutes (gray bars), and after incubation with 1 mg mL⁻¹ proteinase K for 2 hours (black bars). All error bars represent +/- 1 standard deviation over 4 biological replicates. (D) *Stagonospora sp.* mycelium growing on a 0.2 µm filter on solidified AY medium without Mn(II) (left). Cells and filter were removed, and metabolites in agar either untreated (center) or heated at 70°C for 30 minutes (right). Plates in center and right images were then flooded with 200 µM Mn(II) for 1 hour and stained with LBB. Blue color indicates presence of Mn(III/IV) oxides.

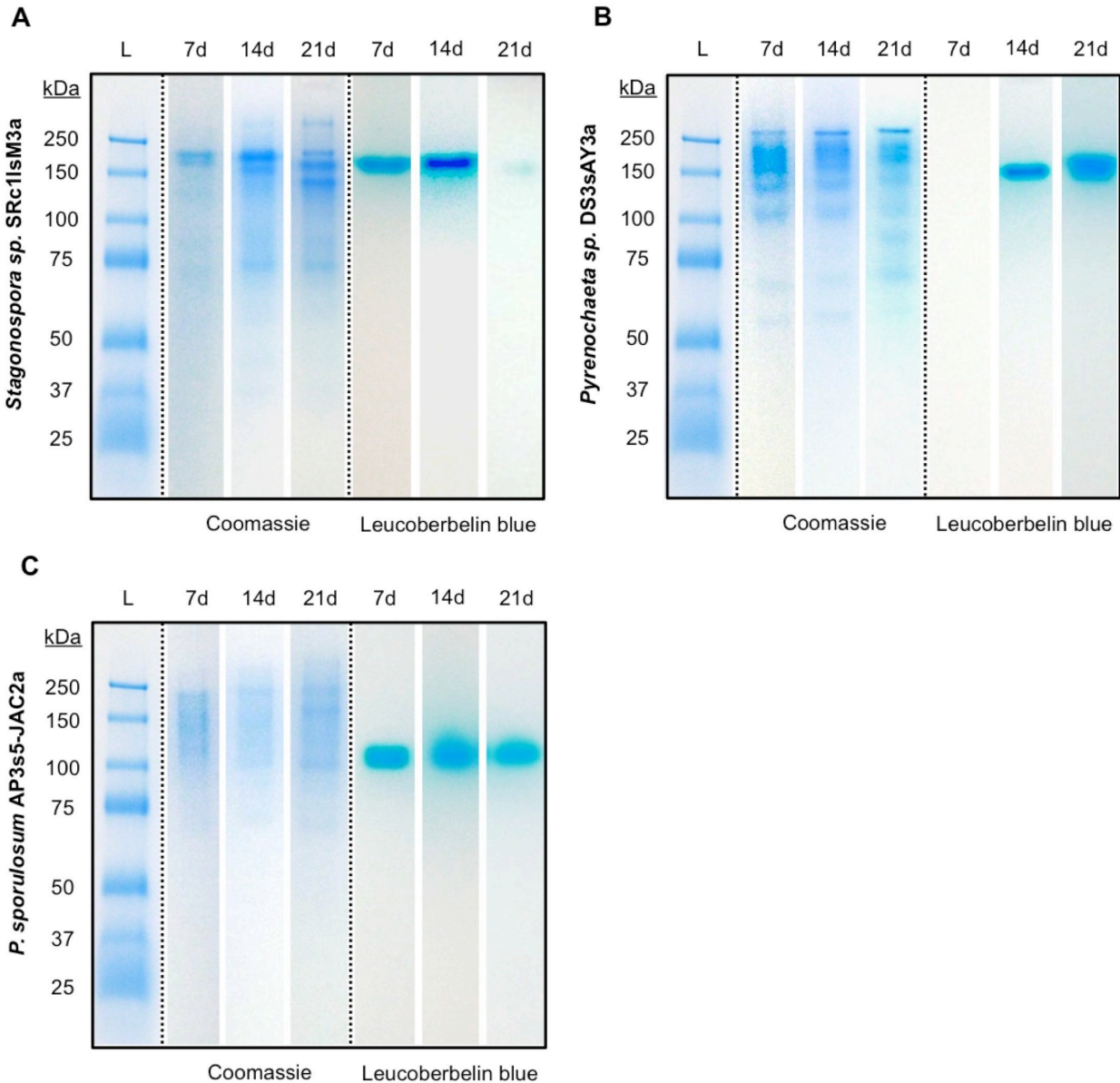


Figure S3.3. Native PAGE of secretome samples from all 3 time points for *Stagonospora sp.* (A), *Pyrenochaeta sp.* (B), and *P. sporulosum* (C). (L) Pre-stained blue molecular mass markers with sizes in kDa to left of images. (Center panels) Gel stained with Coomassie G-250 for 1 hour. (Right panels) Replicate gel of the same secretome samples after incubation with 400 μM Mn(II) for 2 hours followed by staining with Leucoberbelin blue, which turns blue in the presence of Mn(III/IV) oxides. Images shown are representative of 4 biological replicates.

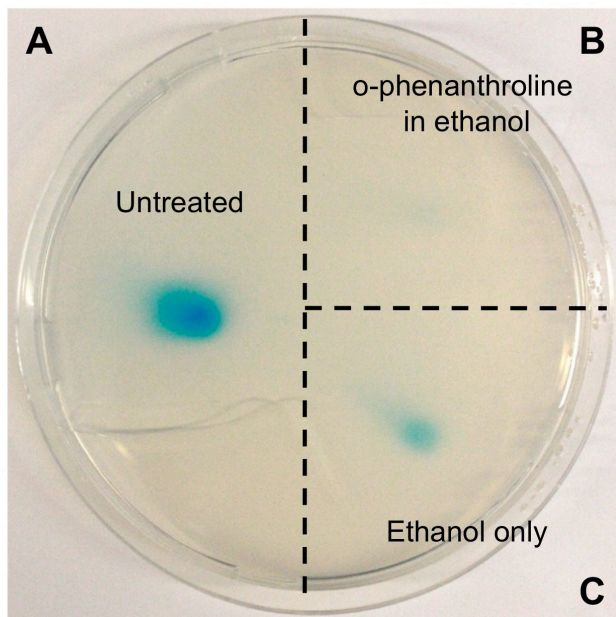


Figure S3.4. (A) *Pyrenochaeta* sp. secretome sample dropped onto solidified AY medium supplemented with 200 μM Mn(II). Secretome from 500 mL culture aged 17 days. (B) Same secretome sample incubated with 75 μM *o*-phenanthroline in 8% ethanol for 2 hours prior to dropping sample on plate. (C) Same sample incubated with 8% ethanol only prior to dropping on plate. Entire plate was stained with LBB; blue color indicates presence of Mn(III/IV) oxides.

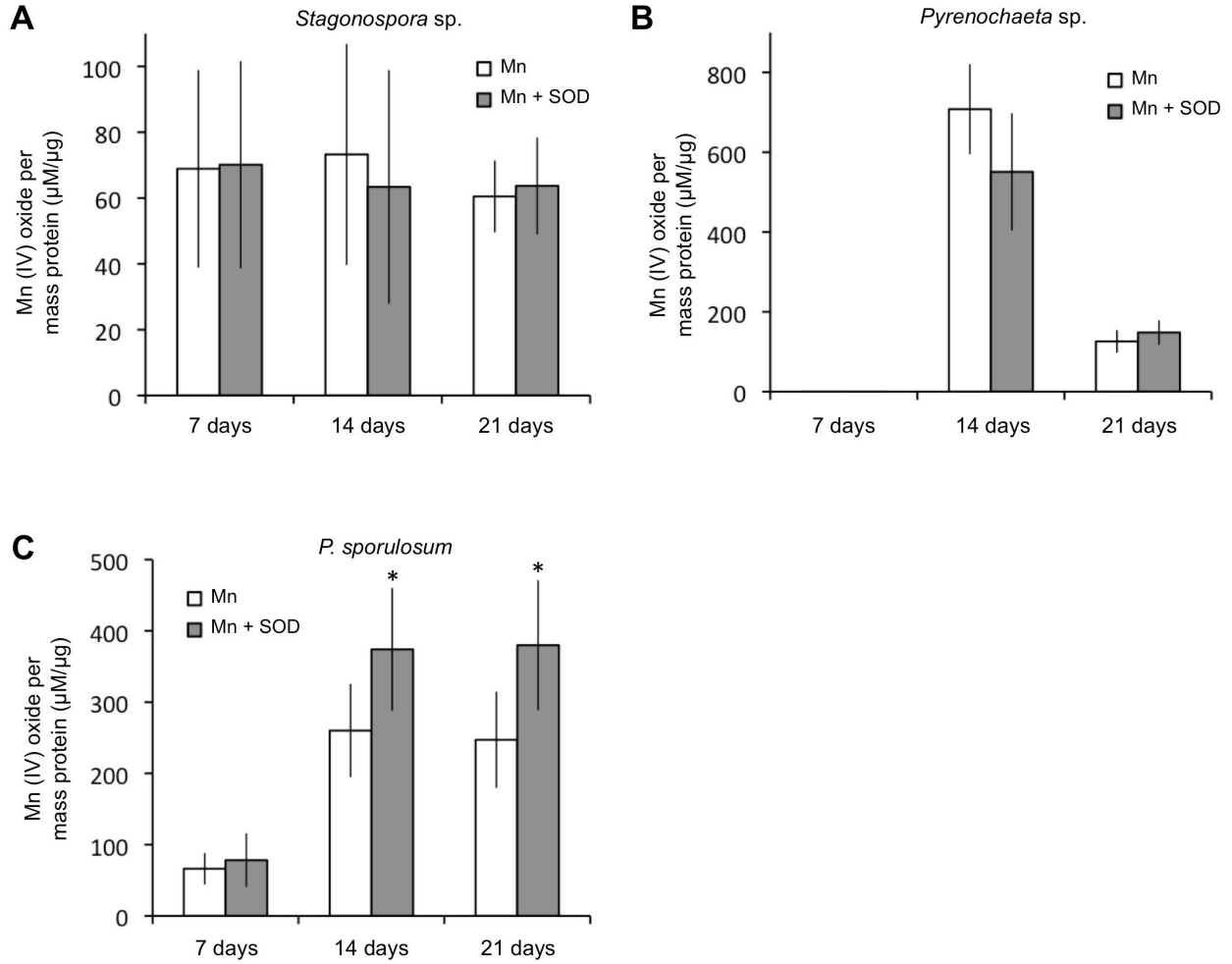


Figure S3.5. Mn(II) oxidation normalized to protein mass in the unamended cell-free secretome (white bars) and in the presence of 50 kU L⁻¹ superoxide dismutase (gray bars) for (A) *Stagonospora* sp., (B) *Pyrenochaeta* sp., and (C) *P. sporulosum*. All error bars represent +/- 1 standard deviation over 4 biological replicates. * The Mn+SOD treatment is significantly different from the Mn treatment by a paired t-test with P<0.05.

APPENDIX 3

Supplemental Material for Chapter 4

Comparative analysis of secretome profiles of four manganese(II)-oxidizing ascomycete fungi

This material is currently in preparation for journal submittal.
(Zeiner C.A., Purvine S.O., Zink E., Wu S., Paša-Tolić L.,
Chaput D.L., Santelli C.M., Hansel C.M.)

Supplementary Tables

Tables S4.1 through S4.5 were submitted electronically.

APPENDIX 4

Supplemental Material for Chapter 5

Quantitative iTRAQ-based secretome analysis reveals species-specific and temporal shifts in carbon utilization strategies among manganese(II)-oxidizing ascomycete fungi

This material is currently in preparation for journal submittal.
(Zeiner C.A., Purvine S.O., Zink E., Wu S., Paša-Tolić L.,
Chaput D.L., Santelli C.M., Hansel C.M.)

Supplementary Tables

Tables S5.1 through S5.5 were submitted electronically.